Université catholique de Louvain

Institute of Condensed Matter and Nanosciences

Molecular Chemistry, Materials and Catalysis

Histidine Brace Containing Ligand Scaffolds for Developing Biomimetics of Lytic Polysaccharide Monooxygenases

Dissertation submitted for the Degree of Doctor in Sciences

by

Xiao MU

Members of the Jury

Prof. Yann Garcia (UCLouvain, President)

Dr. Victor Maurizot (Université de Bordeaux, France)

Prof. Pedro Fardim (KU Leuven)

Prof. Tom Leyssens (UCLouvain)

Dr. Koen Robeyns (UCLouvain)

Prof. Olivier Riant (UCLouvain, Co-Promoter)

Prof. Michael Singleton (UCLouvain, Promoter)

This thesis is dedicated to the people who always support me but who will never get the opportunity to see it.

My dearest mother

Acknowledgments

During these four years of Ph.D. journey, I have received a lot of invaluable helps from many people. It is my great honor to take this opportunity to express my special thanks to them. Without their support and encouragement, I cannot finish my thesis.

First of all, I would like to express my heartfelt thanks to my supervisor professor Michael Singleton, who gives me the opportunity for this project, allows me to have great flexibility at work, and provides me patient and helpful guidance, valuable suggestions and constant encouragement in my study and life. Without his support and help, this thesis could not have reached its present form. I am also thankful to my co-supervisor professor Olivier Riant who gave helpful suggestions during the synthesis of scaffold ligands.

Besides my supervisor, I would like to thank all the jury members, Prof. Yann Garcia, Dr. Victor Maurizot, Prof. Pedro Fardim, Prof. Tom Leyssens, Dr. Koen Robeyns, for accepting to be my jury members and taking the time to read this thesis. Thanks for your kindness, patience and advice towards me and this work.

I would like to express a special thanks to Fabio Lucaccioni, Audrey Dejean and Catherine Francart for their thoughtful support in work and daily affairs.

Of course, I also should give my thanks to all my colleagues: Jérémie Bourotte, Akin Aydogan, Jérôme Savary, Cuilian Liu, Yang Fu, François Kerff, Maëlle Bottin, Corentin Pochet, Ugo Gilbert, Louis Smal, Jiajun Bi, Hu Wang, Yan Yu Sarah Lam, Oscar Mauricio Bautista Aguilera.

I would like to express a special acknowledgment to my friends both in here and China. I appreciate your comfort and encouragement to me and being patient listeners to my stories.

Last, thanks to my family. Mom and Dad, I am thankful for your support with gentle love in silence. My sister, thank you for your companionship on the road of growth. My husband, Yazhou, thank you for your constant support and thank you for bringing me to another loving family.

Authors' Contributions

The Author and the supervisor Prof. Michael Singleton have designed this project.

The Author carried out the experiments, recorded the analytical data and interpreted the results that are presented in this thesis with the following exceptions:

The elemental and mass spectroscopic experiments were recorded by Mr. Raoul Rozenberg (UCLouvain).

Crystallographic data was collected by Dr. Koen Robeyns (UCLouvain) and Dr. Brice Kauffmann (Université de Bordeaux, France).

List of abbreviations

°	Degree
ºC	Celsius degree
α	Alpha
β	Beta
Δ	Delta
ΔE_p	Peak to peak separation
δ	Delta
Å	Ångström
A	Ampere
Ac	Acetyl
BDE	Bond dissociation energy
Bn	Benzyl
Boc	*tert*-Butyloxycarbonyl
B_2Pin_2	Bis(pinacolato)diboron
BPO	Benzoyl peroxide
CDH	Cellobiose dehydrogenase
Cp	Cyclopentadienyl
CV	Cyclic voltammetry
DCM	Dichloromethane
DIAD	Diisopropyl azodicarboxylate
DIPEA	Di-iso-propylethylamine
DMAD	Dimethylacetylene dicarboxylate
DMF	Dimethylformamide

DMSO	Dimethylsulfoxide
Et	Ethyl
Et_3N	Triethylamine
Et_2O	Diethyl ether
EPR	Electron paramagnetic resonance
Eq.	Equivalent
Gln	Glutamine
GMC	Glucose-methanol-choline
HAA	Hydrogen atom abstraction
HRMS	High resolution mass spectrometry
Hz	Hertz
*i*Bu	*Iso*-butyl
IR	Infrared spectroscopy
kJ	Kilo Joule
LPMO	Lytic polyscaccharide monooxygenases
M	Molar
MS	Mass spectrometry
MS 4 Å	Molecular sieves 4 Ångström
NBS	N-Bromosuccinimide
NMR	Nuclear magnetic resonance spectroscopy
Ph_2O	Diphenyl ether
Phe	Phenylalanine
PQQ	Pyrroloquinoline quinone
PyBOP	Benzotriazol-1-yl-oxytripyrrolidinophosphonium hexafluorophosphate
RT	Room temperature
SCS	Second coordination sphere
*t*Bu	*Tert*-butyl
TFA	Trifluoroacetic acid

THF	Tetrahydrofuran
Thp	Tryptophan
Thr	Threonine
UV-vis	Ultraviolet–visible spectroscopy

Abstract

Lytic polysaccharide monooxygenases (LPMOs) have attracted considerable attention due to their ability to enhance enzymatic degradation of recalcitrant polysaccharide biomass via an oxidative cleavage mechanism. LPMOs are copper-containing monooxygenases and the active site copper ion is coordinated by a histidine brace motif, an N_3 coordination consisting of an N-terminal histidine imidazole, NH_2 and a second histidine imidazole. Beyond this, many variations of the second coordination sphere are observed in different species of this family and the importance of these variations is still uncertain. Understanding the factors that contribute to the high oxidative capabilities of the enzyme can facilitate the design of future catalysts for biomass conversion. The aim of the research described herein is to design both small molecule and scaffold based models to mimic structural features of the LPMO active site and to study the effects of the first and second coordinate sphere on the properties and reactivity of copper.

First, the small molecule ligands (**L1**-**L4**) containing two imidazole groups connected by an aliphatic amide linker were designed and synthesized successfully. The crystal structure of ligand **L4** further supported the formation of the amide compounds. The amide ligands were used to coordinate with $CuCl_2$ to form the Cu(II) complexes **1**-**4** in the presence of Et_3N as the base to perform the deprotonation of the amide bond, while no crystal structure of these small molecule complexes could be obtained. The UV-vis spectrophotometric titration, Job's plot analysis and MS data suggest that the stoichiometries between $CuCl_2$ and the ligands in MeOH and H_2O were 1:1.

The FTIR data indicate the participation of the amide for Cu(II) coordination, and the ligand could provide the N_3 coordination environment to copper as we expected. When ligand **L1** was used to directly coordinate $CuCl_2$ without prior deprotonation, the complex **$Cu_2(L1)_2$** forms, for which the crystal structure showed two ligands **L1** bond to two Cu(II) metals. The UV-vis spectrum of this complex is different than that for complex **1** suggesting different structures for the two complexes.

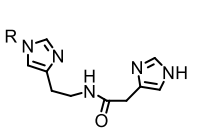

ligand **L1** R = H
ligand **L2** R = CH_3

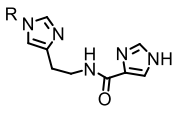

ligand **L3** R = H
ligand **L4** R = CH_3

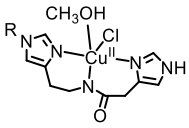

complex **1** R = H
complex **2** R = CH_3

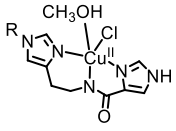

complex **3** R = H
complex **4** R = CH_3

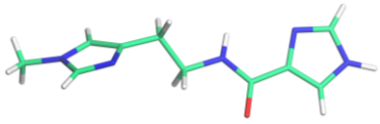

The crystal structure of ligand **L4**

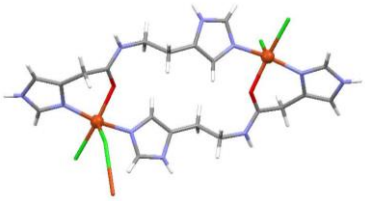

The crystal structure of Cu(II) complex **$Cu_2(L1)_2$**

P-nitrophenyl-β-D-glucopyranoside was used as a model substrate to study the oxidative reactivity of the complexes, using H_2O_2 as oxygen source in either carbonate buffer (100 mM, pH=10.5) solution or H_2O (with Et_3N). In both solvents, the concentration of p-nitrophenolate produced during the assays was higher in the presence of the Cu(II) complexes **1**, **2** than with Cu(II) salt ($CuCl_2$, $CuSO_4$). In all cases, complexes **3** and **4** containing the small chelate rings were found to be less reactive than the larger ligands.

In the second part of this work, the ability of conformationally stable and predictable folded aromatic oligoamides as ligand scaffolds was studied. These molecules can represent a powerful tool to design first and second coordination spheres. Based on this idea, two scaffold ligands, **L5** and the

more flexible ligand **L6**, containing imidazole/histamine functionalized quinoline units and diazaanthracene were designed and synthesized successfully. The crystal structure of precursor **4.058** of ligand **L6** showed the compact conformation corresponding to our initial idea and a curved shape which could provide adequate space to coordinate with Cu(II) metal.

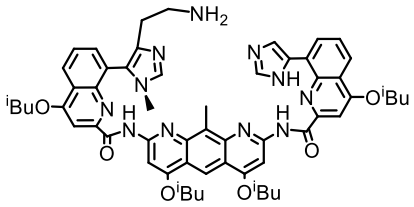

ligand **L5**

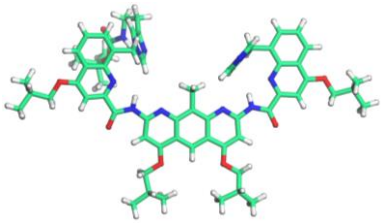
The crystal structure of precursor compound **4.058** of ligand **L6**

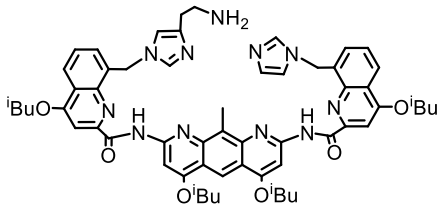

ligand **L6**

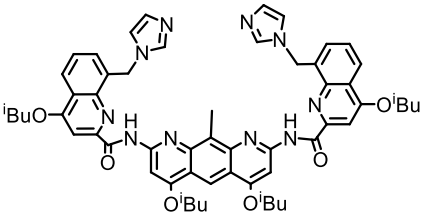

ligand **L7**

The UV-vis spectra of the reaction of Cu(II) salts with ligands **L5** and **L6** suggest that the scaffolds do coordinate a Cu(II) center. However, additional structural studies are needed to validate the exact coordination environment of Cu and see if it matches with the active site of LPMO.

Table of contents

Chapter I

Introduction

1. The composition of biomass for second generation biofuels production

Nowadays, the growth of the global economy, tourism and population has led to a continuously increasing demand for energy. This increase has resulted in the reduction of non-renewable energy sources, such as petroleum, which is becoming a major issue within our current industrial stage. Therefore, it is necessary to develop renewable energy sources for the future. One area of research towards alternative energy sources that has attracted considerable attention in recent years has been the biofuel and biotechnology industry.[1,2] Biofuels can be produced from the fermentation of plant polysaccharides, which can be obtained from first or second-generation sources.[3]

The first-generation biofuels are produced directly from the food chain (starch

[1] Simpson-Holley M., Higson A., Evans G., *Chem. Eng.*, **2007**, 795, 46-49.

[2] Molino A., Larocca V., Chianese S., Musmarra D., *Energies.*, **2018**, 11(4), 811.

[3] Naik S. N., Goud V. V., Rout P. K., Dalai A. K., *Renew. Sust. Energ. Rev.*, **2010**, 14(2), 578-597.

containing crops), such as wheat, corn, or sugarcane.[2, 4] While second-generation biofuels are produced from nonfood crops or biomass, including the waste from food crops, agricultural residue, wood chips, and waste cooking oil (Figure 1.1).[5] Because the use of land and food sources for producing the first-generation biofuels constitutes potential risks related to food shortages, second-generation biofuel processes are becoming increasingly favored. Increasing the efficiency of these processes for the production of renewable energy and materials from biomass is of global importance and crucial to establish a sustainable bio-based economy.[6,7]

[4] Laursen W., *Chem. Eng.*, **2005**, (774-75)32-34.

[5] Dahman Y., Dignan C., Fiayaz A., *In Biomass, Biopolymer-Based Materials, and Bioenergy*, **2019**, 241-276.

[6] Sheldon R. A., *Green Chem.*, **2014**, 16, 950–963.

[7] Himmel M. E., Ding S. Y., Johnson D. K., Adney W. S., Nimlos M. R., Brady J. W., Foust T. D., *Sci.*, **2007**, 315(5813), 804–807.

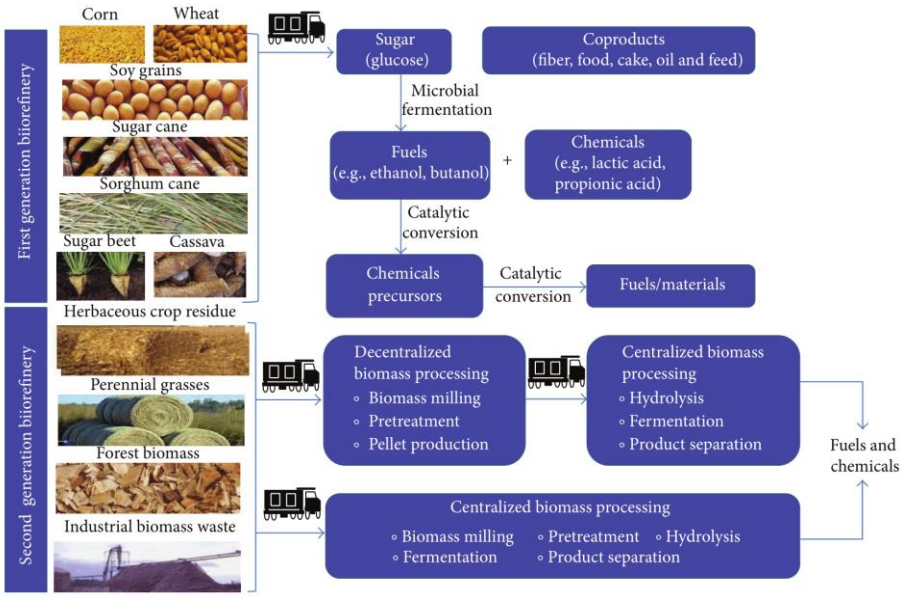

Figure 1.1 Different feedstocks used in the first and second generation biorefinery for producing biofuels, biochemicals, food and feed.[8]

Biomass used as a source of fuel normally consists of plant materials and animal waste. Second generation biofuel feedstocks include lignocellulosic biomass or woody crops, agricultural residues or waste, and dedicated non-food energy crops grown on marginal land unsuitable for food production.[9] Among these feedstocks, lignocellulosic biomass offers the largest inexpensive and renewable source of potentially degradable carbohydrates and is the most abundant biopolymer on earth with yields from agriculture and

[8] Balan V., *Int. Sch. Res. Notices.*, **2014**, 463074.

[9] Begum S., Dahman Y., *Biofuel Bioprod. Biorefin.,* **2015**, 9(5), 529-544.

other sources.[10,11]

2. Lignocellulosic biomass structure

Lignocellulosic biomass forms the cell wall of plants and primarily consists of cellulose, hemicellulose, and lignin.[12] Both cellulose and hemicellulose are complex of polysaccharides. Cellulose is a long homopolymer and involves very long glucan chain, which is composed of thousands of glucose molecules, coupled by β-1,4 glycosidic linkages (Figure 2.1). The glucan chains interact with each other by an extensive network of inter- and intramolecular hydrogen bonds involving the three hydroxyl groups of each glucose monomer, which are responsible for various crystalline arrangements with different degrees of crystallinity and limits the accessibility of hydrolytic enzymes to the glycosidic linkages.[13]

Hemicellulose is a heterogeneous group of polysaccharides, which is comprised of different sugar units, such as pentoses, hexoses and sugar acids. The most common hemicellulosic polysaccharides have four main types that include xyloglycans, xyloglucans, mannoglycans and mixed-linked β-glucans, which all have β-1,4-linked saccharide backbones, and a variety of

[10] Ezeilo U. R., Zakaria I. I., Huyop F., Wahab R. A., *Biotechnol. Biotechnol. Equip.*, **2017**, 31(4), 647-662.

[11] Allen S. A. A., REE A. G., Ayodeji S. A. M., Deborah S. A. E., *Mngmt*., **2016**, 1(3), 128-144.

[12] Klemm D., Heublein B., Fink H. P., Bohn A., *Angew. Chem. Int. Ed. Engl.*, **2005**, 44, 3358-3393.

[13] a) Chang M. C., *Curr. Opin. Chem. Biol.*, **2007**, 11(6), 677-684. b) Himmel M. E., Ding S. Y., Johnson D. K., Adney W. S., Nimlos M. R., Brady J. W., Foust T. D., *Sci.*, **2007**, 315(5813), 804-807.

modifications are found on the side chains of hemicellulose.[14] Compared to cellulose, hemicellulose has a lower degree of polymerization and it has a more branched structure.

Excluding the above two, lignin is the only plant cell wall polymer which does not belong to the family of polysaccharides. This highly complex polymer is formed by three different phenylpropane-based monomer units, coumaryl, coniferyl and sinapyl alcohol connected through carbon-carbon and carbon-oxygen bonds.[15] The lignin matrix fills the space between and interconnected cellulose and hemicellulose, which makes the entire structure of cell wall rigid.

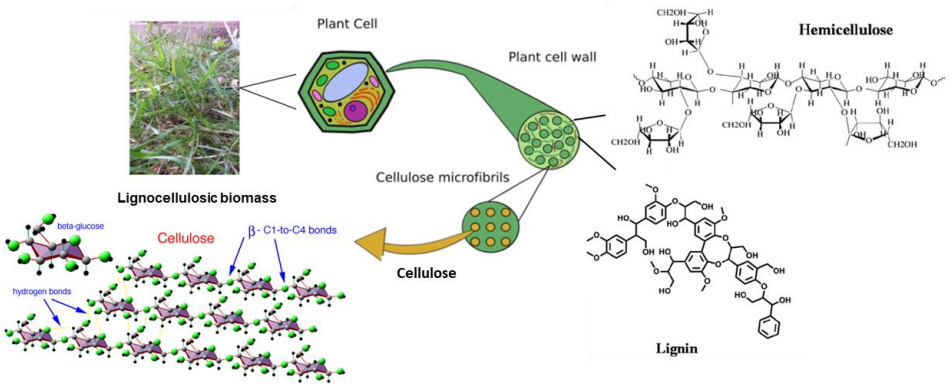

Figure 2.1. The compositions of lignocellulosic biomass and molecular structures of cellulose

Among these, cellulose is the major structural polysaccharide of plant cell walls and is the most abundant and readily accessible source of renewable organic carbon on earth, which makes it an ideal resource for biofuel

[14] Ebringerova A., *Macromol. Symp.,* **2006**, 232,1−12.

[15] Ralph J., Lundquist K., Brunow G., Lu, Christensen J. H. et al. *Phytochem. Rev*., **2004**, 3,29−60.

production.[16,17]

3. Lignocellulosic biomass recalcitrance and classic degradation

Biomasses from plants are naturally recalcitrant and have evolved to protect themselves against invading microorganism. For example, the half-life of cellulose, is estimated at 22 million years which places it among the most stable and abundant polymers in nature.[18] In the structure of lignocellulosic biomass, crystalline cellulose are covered with a heterogeneous hemicellulose polymer that is wrapped by an amorphous lignin polymer that makes biomass more recalcitrant. Between lignin and hemicelluloses, there are additionally bridges called lignin-carbohydrate complexes which also play a major role in biomass recalcitrance.[19]

In order to increase the accessibility of converting lignocellulosic biomass to fuels, energy, or other chemicals, the recalcitrance must be overcome. Therefore, an efficient pretreatment step is required. Broadly, pretreatment methods include physical pretreatment, chemical pretreatment, and biological pretreatment.[20] After these pretreatments, the resulting product can be

[16] Sundarraj A. A., Ranganathan T. V., *Drug Inven. Today,* **2018**, 10, 89-94.

[17] Klemm D., Heublein B., Fink H. P., Bohn A., *Angew. Chem. Int. Ed*., **2005**, 44(22), 3358-3393.

[18] Wolfenden R., Lu X., Young G. *J. Am. Chem. Soc.*, **1998**, 120, 6814−6815.

[19] Buranov A. U., Mazza G., *Ind. Crop. Prod.*, **2008**, 28, 237–259.

[20] a) Nanda S., Mohammad J., Reddy S. N., Kozinski J. A., Dalai A. K., *Biomass Conv. Biorefinery*, **2014**, 4(2), 157-191. b) Jordan D. B., Bowman M. J., Braker J. D., Dien B. S., Hector R. E., Lee C. C., Wagschal K., *Biochem.*

converted to biofuels by chemical means or by fermentation with enzymes or microorganisms.

Physical pretreatment is used to reduce the particle size and increase the accessible surface area of lignocellulosic biomass and to decrease the crystallinity and degree of polymerization present in the cellulose. Different types of physical processes such as mechanical processing and extrusion can be used to improve the enzymatic digestibility of lignocellulosic biomass.

The chemical pretreatment of lignocellulosic biomass can be beneficial for enzymatic conversion to fermentable sugars (Figure 3.1). Before treating with an enzyme, a pretreatment with acidic, steam or basic conditions of the biomass is essential. The acids generally used in the acid treatment include mineral acids such as H_2SO_4, HCl, HNO_3 and organic acids like fumaric, maleic and acetic acids.[21] Acid pretreatment can hydrolyze the hemicelluloses, especially xylan, present in lignocelluloses. Hemicelluloses can be degraded to xylose, mannose, acetic acid and glucose, which increase the pore size of biomass and its accessibility.[22] Steam pretreatment is a physico-chemical method. The lignocellulosic biomass can be treated with steam at a high temperature for few minutes to promote subsequent enzymatic hydrolysis of cellulose and hemicellulose to monomeric hexose and pentose sugars. This method can generate acetic acid in situ from hydrolysis of acetyl groups from hemi- cellulose which can increase the overall sugar yield. Alkaline pretreatment employs various compounds such as NaOH, KOH

J., **2012**, 442(2), 241-252. c) Laser M., Larson E., Dale B., Wang M., Lynd L. R., *Biofpr,* **2009**, *3*(2), 247-270.

[21] Balan V., *Int. Sch. Res. Notices*., **2014**.

[22] Mosier N., Wyman C., Dale B. et al., *Bioresour. Technol.*, **2005**, 96(6), 673–686.

and ammonia. Alkaline pretreatment can remove acetyl groups and various uronic acid substitutions in hemicelluloses, decrease crystallinity of cellulose, break lignin-carbohydrate bonds, and solubilize lignin to increase the accessibility of lignocellulosic biomass to hydrolytic enzymes. [23] The thermochemical pretreatments have a fast process with low residence time and a broad range of feedstock, but it is a non-specific type of biomass deconstruction and there are also unfavorable effects of the pretreatment, such as generating some compounds that can inhibit enzymes.

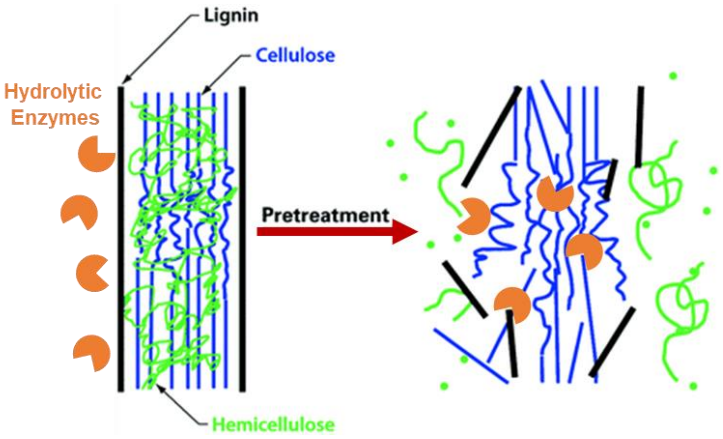

Figure 3.1 Schematic representation pretreatment enhances accessibility of lignocellulose to enzymes. (Modified from Ji Xiao-Jun, et al. *Biotechnology in China III: biofuels and bioenergy*. **2011**. 199-224.)

Biological approaches rely on enzymes. Because of their efficiency, there is a deep interest in understanding enzymatic degradation of cellulose and similar polysaccharides, such as chitin (its structure is similar to cellulose). [24] Glycoside hydrolases known as cellulases have received considerable

[23] Zheng Y., Pan Z., Zhang R., *Int. J. Agric. Biol. Eng.*, **2009**, 2, 51- 68.

[24] Eijsink V.G.H. et al., *Trends Biotechnol.,* **2008**, 26, 228–235

attention. Traditionally, degradation of cellulose, involves three main types of enzymes: endo-active cellulases, exo-active cellulases and β-glucosidases. The endo-active cellulases catalyse random cleavage of internal glycosidic bonds of the cellulose chain, while exo-active cellulases attack the chain ends to release cellobiose. β-glucosidases can only work on small cello-oligosaccharides and cellobiose to release glucose monomers.[25] However, this degradation method has a problem, which is that endo-active and exo-active cellulases have a low level of synergy, which make the degradation of polysaccharides slow and industrially ineffective. Besides, if these enzymes carry out the hydrolysis of glycosidic bonds, polysaccharide chains need to be isolated from the bulk of the crystal which in turn requires energy. Currently the inefficiency of the production of second-generation biofuels has limited the industrial production to only a few test-scale plants.[26] Therefore, there remains a drive to improve these problems.

Besides people have thought for a long time, that hydrolysis by glycoside hydrolases was the only type of enzyme activity in biological cellulose degradation. In 1950 Reese and co-workers published a paper discussing the relative activities of cellulolytic and non-cellulolytic organisms on cellulose derivatives.[27] They found that some non-cellulolytic organisms can degrade smaller oligosaccharides and did not have the ability to use native cellulose as the substrate. Based on these results, they proposed the process of

---

[25] Merino S., Cherry J., *Adv. Biochem. Eng. Biotechnol.*, **2007**, 108, 95-120.

[26] a) Payne C. M., Knott B. C., Sandgren M., Sta hlberg J., Beckham G. T., *Chem. Rev.*, **2015**, 115, 1308-1448. b) Mancini E., Mansouri S. S., Gernaey K. V., Luo J., Pinelo M., *Crit. Rev. Environ. Sci. Technol.*, **2020**, 50(18), 1829-1873. c) Carvalho D. J., Moretti R. R., Colodette J. L., Bizzo W. A., *Energy Convers. Manag.*, **2020**, 203, 112267.

[27] Reese E. T., Siu R. G., Levinson H. S., *J. Bacteriol.*, **1950**, 59, 485.

converting native cellulose to small soluble molecules is carried out by two enzyme systems: first step, C_1, converting the native cellulose to smaller oligosaccharides; then the second step, C_x, further degrading the substrate into oligomeric and monomeric molecules. It was the first realization that crystalline polysaccharides needed enzymatic pretreatment to increase solubilization. Later, the above mentioned work by Eriksson et al. in 1974 reported that cellulose can be degraded by an enzyme secreted from *Sporotrichum pulverulentum* fungus that uses oxygen from the atmosphere, indicating the process was an oxidation reaction.[28] Reese and Eriksson's papers indicated that some enzymes could boost the activity of canonical cellulases through an oxidative mode of action on cellulose substrate, but were largely ignored until 2010, when Vaaje-Kolstad et al. identified a bacterial metalloenzyme that could cleave the glycosidic bonds of chitin by an oxidative mechanism.[29] Soon after, similar enzymes were found that acted on cellulose to cleave the substrate by oxidation.[30] Collectively, these enzymes, later named lytic polysaccharide monooxygenases (LPMOs), provide new avenues toward the more efficient enzymatic conversion of lignocellulosic biomass.

---

[28] Eriksson K. E., Pettersson B., Westermark U., *FEBS Lett.,* **1974**, 49, 282−285.

[29] Vaaje-Kolstad G., Westereng B., Horn S. J., Liu Z. L., Zhai H., Sorlie M., Eijsink V. G. H., *Science*, **2010**, 330, 219−222.

[30] a) Forsberg Z., Vaaje-Kolstad G., Westereng B., Bunæs A.C., Stenstrøm Y., MacKenzie A., Sørlie M., Horn S.J., Eijsink V.G.H., *Protein Sci.*, **2011**, 20,1479-1483. b) Quinlan R. J., Sweeney M. D., Lo Leggio L., Otten H., Walton P. H., *Proc. Natl. Acad. Sci. U. S. A.*, **2011**, 108, 15079−15084. c) Westereng B., Ishida T., Vaaje-Kolstad, G., Wu M., Eijsink V.G. H., Igarashi K., Samejima M., Stahlberg J., Horn S. J., Sandgren M., *PLoS One,* **2011**, 6, 27807.

4. Lytic polysaccharide monooxygenases

The LPMOs have been found to play a vital role in the degradation of recalcitrant polysaccharides through oxidation in nature. Through the cooperation between LPMOs and classic cellulases, the LPMOs can boost the activity of classical glycoside hydrolase enzymes. As shown in Figure 4.1, LPMOs can create more new chain ends (more details shown after) in crystalline cellulose areas which can be utilized by progressive cellulases. This offers great promise for further improvements in lignocellulose deconstruction processes. As these enzymes can be used optimally to allow the production of second-generation biofuels.

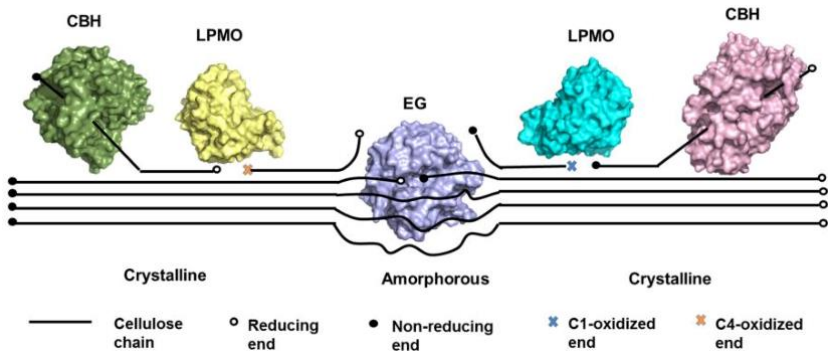

Figure 4.1 Schematic illustration of the cooperation between LPMOs and classic cellulases in cellulose degradation. (Liu B., Ph.D. diss., 2019.) (CBH: cellobiohydrolase; EG: endoglucanase)

4.1 The classification and function of the LPMOs

Henrissat and co-workers in 1991 initiated an amino acid sequence-base classification of glycosyl hydrolases that resulted in the Carbohydrate Active enzymes (CAZy) database.[31] Later, the database was divided into six major

[31] Henrissat B., *Biochem. J.*, **1991**, 280, 309−316.

classes: Glycoside Hydrolases(GH), Glycosyl Transferases, Polysaccharide Lyases, Carbohydrate Esterases, Auxiliary Activities(AA) and Carbohydrate-Binding Modules(CBM).[32]

Initially, LPMOs were assumed to be solely hydrolytic and were classified as belonging to the glycoside hydrolase 61 (GH 61) and carbohydrate-binding module 33 (CBM 33) families.[33] However, the exact role of LPMOs was demonstrated later, in 2010 by Vaaje-Kolstad et al.,[28] who showed that LPMOs belonging to the CBM 33 family were in fact oxidative enzymes. It was observed that LPMOs employed a common mechanism, different from the traditional glycoside hydrolases, so in 2013 the enzymes were reclassified to Carbohydrate-Active Enzymes (CAZymes) – in the auxiliary activity (AA) class.[34] The first discovered members of the LPMOs family are enzymes AA9 (formerly GH61) and AA10 (formerly CBM33).[28,33] However, many additional members AA11, AA13, AA14, AA 15 and AA 16 have since been reported.[30b,35]

---

[32] Lombard V., Golaconda Ramulu H., Drula E., Coutinho P.M., Henrissat B., *Nucleic Acids Res.*, **2014**, 42, D490−D495.

[33] Harris P. V., Welner D., McFarland K. C., Re E., Navarro Poulsen J.C., Brown K., Salbo R., Ding H., Vlasenko E., Merino S. and Xu F., *Biochem.*, **2010**, 49(15), 3305-3316.

[34] Levasseur A., Drula E., Lombard V., Coutinho P. M., Henrissat B., *Biotechnol. Biofuels*, **2013**, 6(1), 41.

[35] a) Hemsworth G. R., Henrissat B., Davies G. J., Walton P. H., *Nat. Chem. Biol.*, **2014**, 10(2), 122. b) Vu V. V, Beeson W. T., Span E. A., Farquhar E. R., Marletta M. A. *Proc. Natl. Acad. Sci. U.S.A.*, **2014**, 111, 13822–13827. c) Leggio L. Lo et al., *Nat. Commun.*, **2015**, 6, 5961. d) Couturier M, Ladevèze S, Sulzenbacher G, Ciano L, Fanuel M, Moreau C, et al. *Nat. Chem. Biol.*,

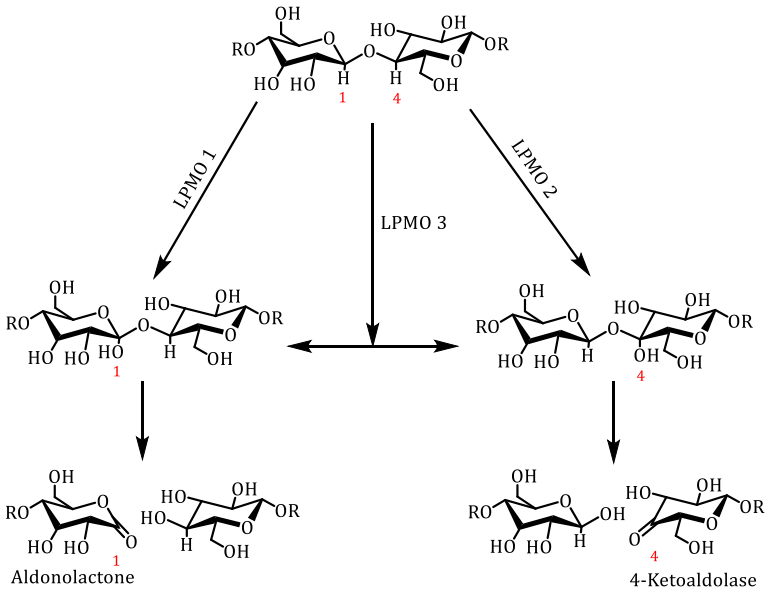

Figure 4.2 Hydroxylation-induced cleavage of glycosidic bond by three types of cellulose active LPMOs[36]

Reactivity studies showed that LPMOs use molecular oxygen and an electron donor to catalyze the oxidative O_2-dependent cleavage of insoluble polysaccharides. The emergence of different regioselectivities has been demonstrated for these enzymes. Depending on the type of LPMO, the oxidative cleavage can occur at different positions of the glycoside linkage: some oxidize only the C1 atom producing an aldonolactone at the reducing

---

2018, 14, 306-310. e) Sabbadin F., Hemsworth G. R., Ciano L., Henrissat B., Dupree P., Tryfona T., et al., *Nat. Commun.*, **2018**, 9, 756. f) Filiatrault-Chastel C., Navarro D., Haon M., Grisel S., Herpoël-Gimbert I., Chevret D., Berrin J. G., *Biotechnol. Biofuels*, **2019**, 12(1), 55.

[36] Ezeilo U. R., Zakaria I. I., Huyop F., et al. *Biotechnol. Biotechnol. Equip.*, **2017**, 31(4), 647-662.

end, others oxidize only the C4 atom producing a 4-ketoaldose at the non-reducing end, whereas still others can oxidize both C1 and C4 (Figure 4.2).[37]

AA9 family members are fungal LPMOs that act on cellulose, hemicellulose and glucose derivative units. This family was known to selectively oxidize at C1, selectively oxidize at C4 or oxidize at both C1 and C4. The AA10 family were found mainly to be produced by bacterial and some viruses and can oxidize either chitin or cellulose at the C1 position or both C1 and C4. AA11 and AA13 are fungal LPMOs oxidizing chitin and starch, respectively. But families are only known to oxidize at C1. The AA 14 are a fungal family and showed activity on recalcitrant xylan coating cellulose fibers through oxidation at C1. The AA 15 family revealed the existence of LPMOs of animal origin (invertebrates), active on both cellulose and chitin by oxidizing at the C1 position. Finally, the discovery in 2019 of the AA 16 family, encountered in fungi, showed they were oriented toward interactions with cellulosic substrates and oxidized the C1 position.[35f]

4.2 The structure and active site of the LPMOs

The multiple structures of LPMOs enzymes available show that the enzyme families share a common core immunoglobulin-like or fibronectin type III-like β-sandwich structure (Figure 4.3). The β-sandwich structure consists of 8-10 β-stands. Loops connecting these β-stands constitute the flat substrate binding surface. Unlike canonical glycoside hydrolase enzymes which have substrate binding grooves or tunnels, LPMOs position their active site at the center of a flat surface that provides the possibility to interact with substrates. In AA9 LPMOs, the region located between β-stand 1 and β-stand 2 of the core β-sandwich, is called L2. A similar L2 region occurs in AA10 LPMOs

[37] Liu B., Kognole A. A., Wu M., Westereng B., Crowley M. F., Kim S., Sandgren M., *The FEBS journal.*, **2018**, 12(285), 2225-2242.

between β-stand 1 and β-stand 3. The L2 region includes a variable number of loops and short helices. Some LPMOs have an insertion between β-stand 3 and β-stand 4, referred to as L3, that interacts with the L2 loop. On the opposite side of L2, in AA9 and AA13 LPMOs, there are LS (loop short) and LC (long C-terminal loop).[38] Depending on the substrate specificity, these loops comprise various hydrophilic and aromatic residues that are involved in the substrate binding of LPMOs. For example, AA9 LPMOs contain multiple aromatic amino acids, notably tyrosine, which are expected to take part in the binding of cellulose.[39] Within the AA10 family, the aromatic amino acid composition was shown to also influence the different substrate affinity. The amino acids Gln, Thr are presumed to be a determinant of chitin activity, whereas in cellulose-active, the corresponding sites are Phe and Trp.[40]

[38] Zhou X., Zhu H., *Bioresour. Bioprocess.*, **2020**, *7*(1), 1-19.

[39] Li X., Beeson IV W. T., Phillips C. M., Marletta M. A., Cate, J. H. *Structure*, **2012**, 20(6), 1051-1061.

[40] Frandsen K. E., Simmons T. J., Dupree P., Poulsen J. C. N., Hemsworth G. R., Ciano L., Marmuse L., *Nat. Chem. Biol.*, **2016**, 12(4), 298.

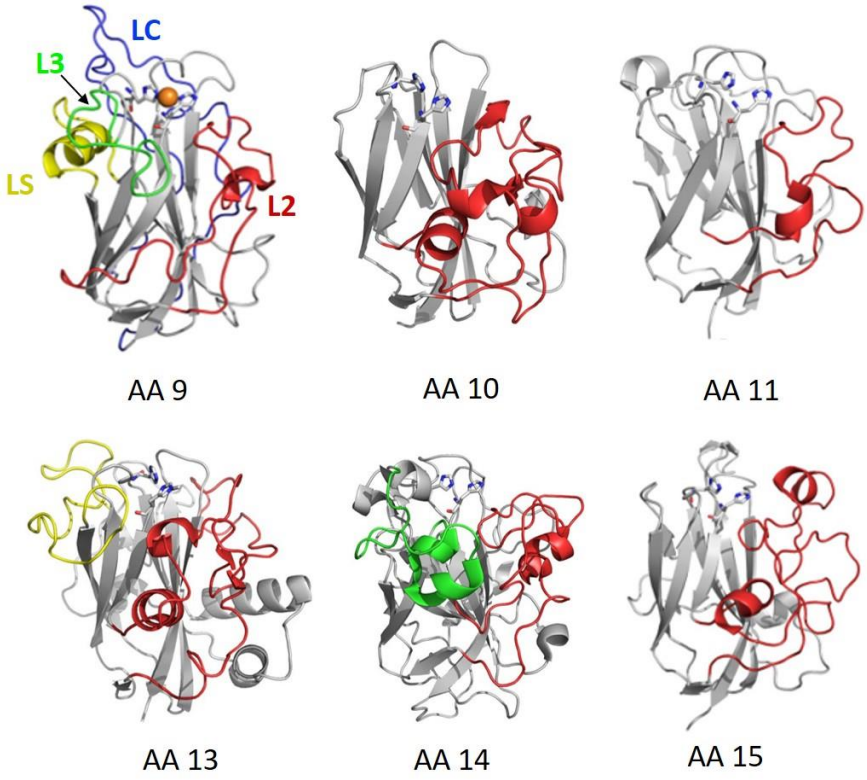

Figure 4.3 Structures of LPMOs from each CAZy family are shown: *Neurospora crassa* AA9 (NcLPMO9C) (PDB: 4d7u),[41] *Serratia marcescens* AA10 (CBP21) (PDB: 2bem),[42] Aspergillus oryzae AA11 (AoLPMO11) (PDB: 4mah),[35a] Aspergillus oryzae AA13 (AoAA13) (PDB: 4opd),[35c] Pycnoporus coccineus AA14 (PcAA14B) (PDB: 5no7),[35d] Thermobia domestica AA15 (TdAA15A) (PDB: 5msz)[35e] (*Bioresour. Bioprocess.*, **2020**, 7(1), 1-19)

[41] Borisova, Anna S., et al. *J. Biol. Chem.*, **2015**, 290(38), 22955-22969.

[42] Vaaje-Kolstad G., Houston D. R., Riemen A. H., Eijsink V. G., Van Aalten D. M., *J. Biol. Chem.*, **2005**, 280(12), 11313-11319.

Early crystallographic and spectroscopic studies of the different LPMOs showed that all contained a similar solvent-exposed mononuclear copper active site (Figure 4.4A).[43,44,45] The copper ion is coordinated in a T-shaped N_3 coordination environment consisting of the imidazole N and primary amine of an N-terminal histidine and an additional imidazole group coming from a second histidine residue. This equatorial coordination is described as the histidine brace motif [46] and is similar to the active site reported for particulate methane monooxygenase (pMMO), another powerful oxidative enzyme.[47]

Photoreduction of the Cu(II) to Cu(I) has been a common phenomenon in X-ray crystal structures and some spectroscopic techniques such as X-ray absorption spectroscopic can be used to determine LPMOs coordination

[43] Quinlan R. Jason, et al., *Proc. Natl. Acad. Sci. U. S. A.*, **2011**, 108(37), 15079-15084.

[44] a) Hemsworth G. R., Taylor E. J., Kim R. Q., et al., *J. Am. Chem. Soc.*, **2013**, 135(16), 6069-6077. b) Aachmann F. L., Sørlie M., Skjåk-Bræk G., et al., *Proc. Natl. Acad. Sci. U.S.A.*, **2012**, 109(46), 18779-18784. c) Beeson W. T., Phillips C. M., Cate J. H. D., et al., *J. Am. Chem. Soc.*, **2011**, 134(2), 890-892.

[45] a) Wu M., Beckham G. T., Larsson A. M., et al., *J. Biol. Chem.*, **2013**, 288, 12828-12839. b) Beeson W. T., Vu V. V., Span E. A., et al., *Annu. Rev. Biochem*, **2015**, 84, 923-946.

[46] Hemsworth G. R., Johnston E. M., Davies G. J., et al., *Trends Biotechnol.*, **2015**, 33(12), 747-761.

[47] a) Ro S. Y., Schachner L. F., Koo C. W., Purohit R., Remis J. P., Kenney G. E., Rosenzweig A. C., *Nat. Commun.*, **2019**, 10(1), 1-12. b) Ross M. O., MacMillan F., Wang J., Nisthal A., Lawton T. J., Olafson B. D., Hoffman B. M., *Sci.*, **2019**, 364(6440), 566-570. c) Cao L., Caldararu O., Rosenzweig A. C., Ryde U., *Angew. Chem.*, **2018**, 130(1), 168-172.

geometries. Reduced LPMOs show three-coordinate structures consistent with Cu(I) coordination preferences. Oxidized LPMOs contain additional ligands coordinating the Cu (II) in a distorted octahedral or trigonal bipyramidal geometry. These additional ligands can come from the solvent. For example, Quinlan et al.[48] first got the structure of TaAA9. X-ray crystallography showed that reduced TaAA9 exhibit Cu(I) coordinated by three nitrogen (Cu-N distances ranging from 1.9-2.4 Å) from the histidine brace. And the Cu (II) structures were resolved with an H_2O molecule as an additional ligand.[49] The first use of reduced-intensity X-ray collection strategies to obtain the structure of the Cu(II) active site of Enterococcus faecalis AA10 found the Cu coordinated by the three nitrogen of the histidine brace and two water ligands forming a trigonal bipyramidal structure.[50]

Comparison of the active sites in LPMO families show that this histidine brace is a common feature, however, there are several distinct differences across the families as well, shown in Figure 4.4B, notably in the second coordination sphere. These include:

-Firstly, in the axial direction, all the families have a tyrosine (Tyr) residue near the copper ion, except most AA10, which have a phenylalanine (Phe)

---

[48] Quinlan R. J., Sweeney M. D., Leggio L. L., Otten H., Poulsen J. C. N., Johansen, K. S., Tryfona, T., *Proc. Natl. Acad. Sci. U. S. A.*, **2011**, 108(37), 15079-15084.

[49] Kjaergaard C. H., Qayyum M. F., Wong S. D., Xu, F., Hemsworth G. R., Walton D. J., Hodgson K. O., *Proc. Natl. Acad. Sci. U.S.A.*, **2014**, 111(24), 8797-8802.

[50] Gudmundsson M., Kim S., Wu M., Ishida T., Momeni M.H., Vaaje-Kolstad G., Lundberg D., Royant A., Ståhlberg J., Eijsink V. G. H. et al., *J. Biol. Chem.* **2014**, 289, 18782−18792.

residue,[51] although tyrosine also occurs.[55] In here, the hydroxyl group of the tyrosine can contribute a long range interactions to the octahedral coordination of the Cu(II) ion. Additionally, in the solvent exposited axial position, AA10, AA11 and AA13 have an alanine (Ala) molecule which can restrict access and may prevent binding dioxygen at this position.[45a]

-Furthermore, fungal LPMOs, AA9 and AA13, show an unusual methylation of the second nitrogen atom of the N-terminal histidine. Based on the recent research result of Petrović et al., this modification has been proposed to protect the active site from self-inactivation from H_2O_2 reactivity.[52]

-Additional ligands, such as water molecules, have been shown to be weakly coordinated depending on the hydrogen bonding patterns present. For example, the first coordination sphere of AA9 could be considered a distorted octahedral as a result of the water molecules and a long-range interaction with the tyrosine.[41]

[51] Beeson W. T., Vu V. V., Span E. A., Phillips C. M., Marletta M. A., *Annu. Rev. Biochem.*, **2015**, 84, 923-946.

[52] Petrović D. M., Bissaro B., Chylenski P., Skaugen M., Sørlie M., Jensen M. S., Eijsink V. G., *Protein Sci.*, **2018**, 27(9), 1636-1650.

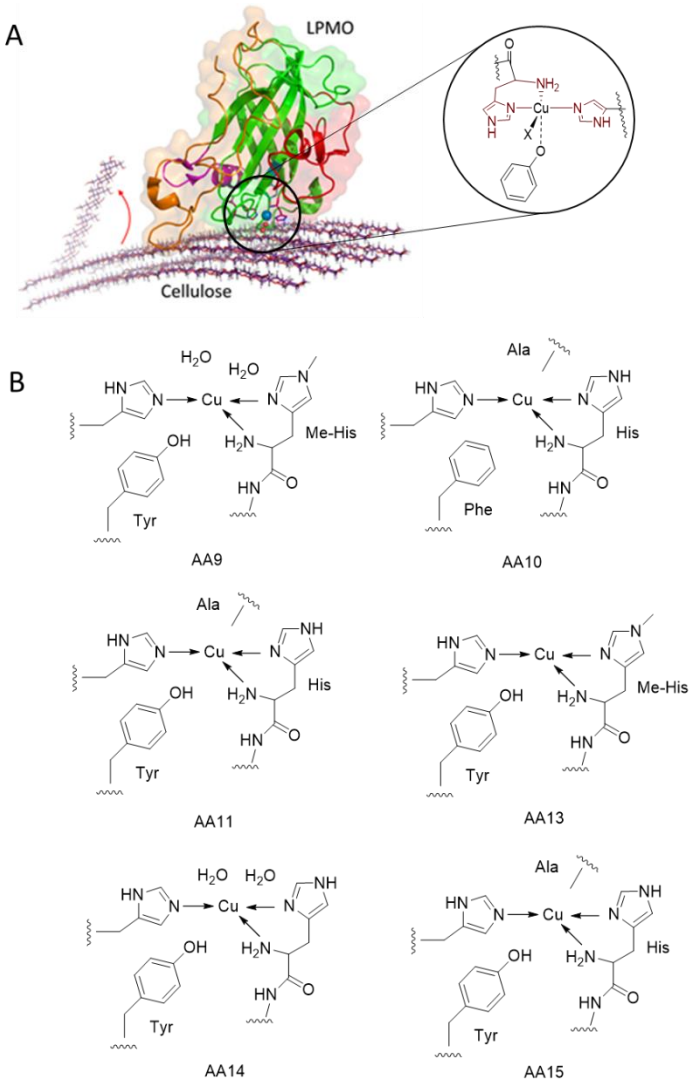

Figure 4.4 A) The mono-copper active site structure of LPMOs and hypothetical interaction with the flat surface of cellulose; B) Schematic representations of the copper active sites observed in AA9, AA10, AA11, AA13, AA14, AA15 structures

4.3 The second coordination sphere of the LPMOs

The nature and the number of the donating atoms in the metal coordination sphere dictate its geometry and influence the catalytic reactivity. However, the presence of non-coordinated groups around the metal can have an equally important contribution to reactivity. These groups which are not directly bound to the metal but are important to its properties and reactivity are described as the “second coordination sphere (SCS)” (Figure 4.5). SCS interactions can include any number of non-covalent interactions, but also aspects like site isolation.

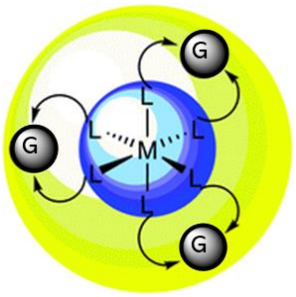

Figure 4.5 Schematic representations of interaction in the first-sphere and second-sphere of coordination (first-sphere = blue, second-sphere = yellow).

In LPMOs, multiple groups have been proposed to contribute to reactivity through second coordination sphere interactions including a conserved hydrogen-bonding (H-bonding) network, which based on structural studies and bioinformatic analysis, is present in all LPMO active sites.[53]

In fungal LPMOs AA9 family, a case study of MtPMO3* as the example, the active site of MtPMO3* shares the first coordination sphere features of other LPMOs, including the histidine brace (H1 and H75), axial tyrosine

[53] Shook R. L., Borovik A. S., *Inorg. Chem.*, **2010**, 49(8), 3646-3660.

residue(Y169), and N-terminal histidine methylation (Figure 4.6A).[54] The secondary coordination sphere comprises residues that form a network of H-bonds around the first coordinating ligands. These include T74, which H-bonds with the N-terminal amino group of H1 as well as ligands in the axial solvent-facing position; H161, which is positioned to H-bond with equatorial solvent-facing ligands; and Q167, which also H-bonds which equatorial solvent ligands and with Y169. Point mutation studies have implied that histidine and glutamine residues, H161 and Q167, are involved in stabilizing bound oxygen, and H161 appears to play a role in proton transfer. Additionally, Q167 can potentially increase the long-range effect of Y169 to the copper via a hydrogen-bonding interaction.

In the bacterial LPMO AA10 family, the structures of cellulose-active (C1 position) AA10 (Figure 4.6B) shows that the H-binding residues R212, E217 and F219 closely resemble those of H161, Q167, and Y169 in the AA9 family. A similar structure also appears on another kind of AA10 (Figure 4.6C) which oxidize C1/C4 position of cellulose.[55] However, this kind of H-binding network is not found in chitin-active bacterial LPMOs (Figure 4.6D),[50] where only the conserved E64 might form a weak H-binding interaction with a coordination water ligand.[56] Highly conserved H-bonding residues are also found in AA11-AA15, and the position of H-bonding residues and the presence of the active site tyrosine are very similar to the AA9 LPMOs.

---

[54] Span E. A., Suess D. L. M., Deller M. C., et al., *ACS Chem. Biol.*, **2017**, 12(4), 1095-1103.

[55] Forsberg Z., Mackenzie A. K., Sørlie M., Røhr Å. K., Helland R., Arvai A. S., Eijsink V. G., *Proc. Natl. Acad. Sci. U. S. A.*, **2014**, 111(23), 8446-8451.

[56] Beeson W. T., Vu V. V., Span E. A., Phillips C. M., Marletta, M. A., *Annu. Rev. Biochem.*, **2015**, 84, 923-946.

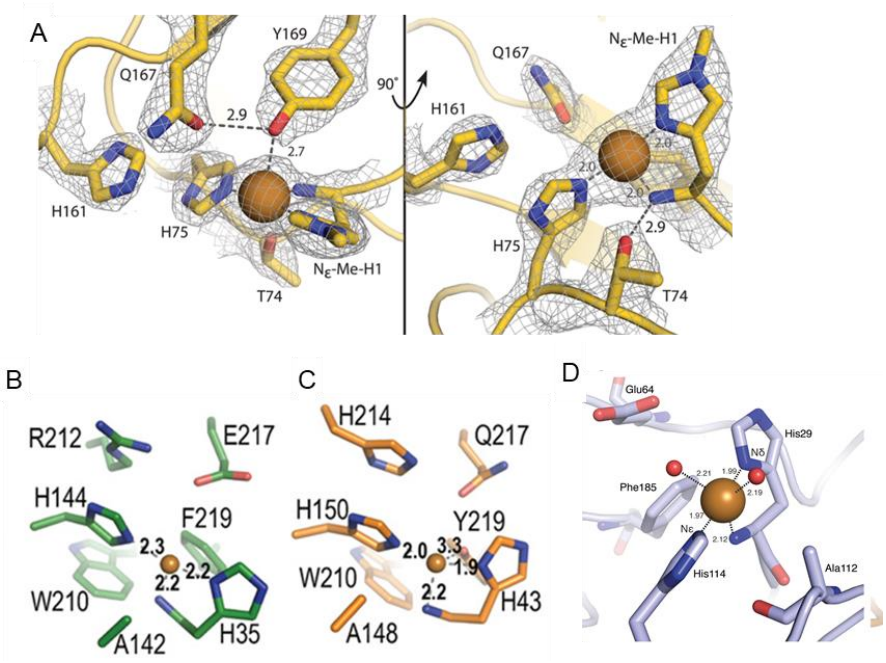

Figure 4.6 A) MtPMO3* active site showing first (N-Me-H1, H75, Y169) and secondary (T74, H161, Q167) sphere residues (*ACS Chem. Biol.*, **2017**, 12(4), 1095-1103); Cartoon representation of B. ScLPMO10C (PDB: 4OY7), C. ScLPMO10B (PDB: 4OY6), D. EfaCBM33A (PDB: 4ALC)

The H-bonding network in LPMOs appear to modulate both the first sphere geometry and electronic properties of the copper center, and can also play an important role in stabilizing different metal-oxygen intermediates and help to precisely deliver the required protons to the correct oxygen atom of the O-O moiety for the cleavage of O-O bond.[57] Of particular interest in the H-binding residues is a conserved glutamine found in proximity to active site of all

[57] a) Makris T. M., Von Koenig K., Schlichting I., et al., *Biochem.*, **2007**, 46(49), 14129-14140. b) Denisov I. G., Makris T. M., Sligar S. G., et al., *Chem. Rev.*, **2005**, 105(6), 2253-2278.

LPMOs. Mutation of the glutamine led to the release of $O_2^{\bullet-}$ and a decrease in product formation, suggesting that this residue stabilizes a Cu-superoxo intermediate. Additionally, this residue could provide the protons necessary to reduce oxygen to hydrogen peroxide. Besides, in chitin-active bacterial LPMOs, molecular dynamics suggest this residue serves as a gate to control co-substrate access to the active site.[58]

4.4 The proposed mechanisms of the LPMOs

LPMOs are known to be active on recalcitrant polysaccharide substrates through a difficult oxidation reaction. Because the bond dissociation energy (BDE) of glycosidic C-H bonds in polysaccharide is near 100 kcal/mol, it gives a high reaction barrier for hydrogen atom abstraction (HAA).[59] Due to the sequence variation within LPMOs families, different LPMOs can act on different substrates and have different regioselectivities (oxidize C1/C4). However, this has been ascribed to difference in surface (substrate binding) residues. Thus, the structural variations of the active site are not thought to influence the binding to the different polysaccharides. It may be that these active site changes could lead to different LPMOs employing slightly different mechanisms or that the changes result in different oxidation strengths. While the general transformation that the enzymes perform is understood, there is still much debate on the specifics of the mechanism. For example, the order of substrate binding, O_2/H_2O_2 reduction, and hydrogen abstraction is still

[58] Bissaro B., Isaksen I., Vaaje-Kolstad G., Eijsink V. G. H., Røhr Å. K., *Biochem.*, **2018**, 57, 1893–1906.

[59] Gao J., Thomas D. A., Sohn C. H., Beauchamp, J. L., *J. Am. Chem. Soc.*, **2013**, 135(29), 10684-10692.

uncertain.[60]

Depending on results with synthetic complexes and computational studies, both O_2 and H_2O_2 have been proposed, utilizing different mechanisms to generate oxidizing species for substrate hydroxylation. Here a common ground is that one electron was used to reduce the active-site Cu from Cu(II) to Cu(I) which increases the binding affinity to the polysaccharide substrate and co-substrate (O_2 or H_2O_2) activation.

4.4.1 The O_2 reaction mechanism

In the O_2 based mechanism, when there is an absence of polysaccharides and a presence of reductant, LPMOs also can act as oxidases, which are able to reduce O_2 to H_2O_2. This is not unexpected for a solvent-exposed active site in combination with high concentrations of reductant.

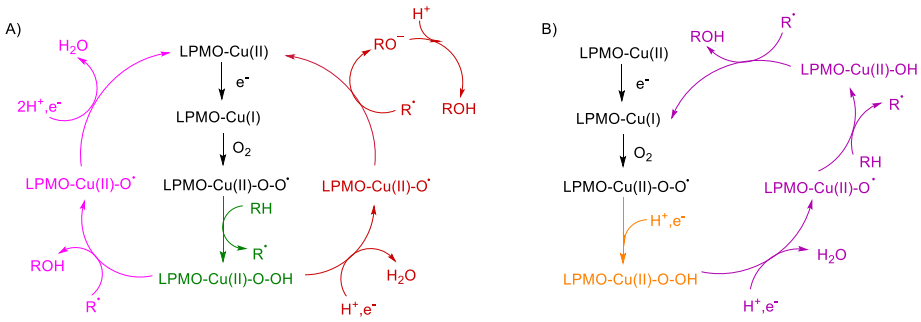

Figure 4.7 Proposed LPMOs mechanisms in which O_2 is the direct oxidant of the polysaccharide substrate. A) Shows Cu-superoxide is responsible for the H atom abstract from substrate; B) Shows utilizing Cu-oxyl to abstract H atom from substrate

[60] a) Vaaje-Kolstad G., Westereng B., Horn S. J., *Sci.*, **2010**, 330(6001), 219-222. b) Bissaro B., Røhr Å. K., Müller G., et al., *Nat. Chem. Bio.*, **2017**, 13(10), 1123.

So, this mechanism based on O_2, requires the precisely timed delivery of two electrons, the availability of two protons, O_2 and a polysaccharide substrate. Based on those, there are two kinds of mechanisms, differing in the oxidation state of the initial and final enzyme forms.

For the first one, Phillips et al. and Beesson et al.[61] have suggested a pathway involving a Cu-superoxo active species, Figure 4.7A. The catalytic cycle starts with the reduction of LPMO-Cu(II) to LPMO-Cu(I) and the subsequent formation of a Cu(II)-superoxo intermediate [Cu(II)-O-O$^{\bullet}$] via activation of oxygen by the reduced LPMO-Cu(I). The superoxo intermediate subsequently abstracts a H atom from the polysaccharide substrate to produce a substrate radical (R$^{\bullet}$) and a Cu(II)-hydroperoxo species [Cu(II)-O-OH] which is an import intermediate (in green). At this point there is the possibility to either have the addition of a proton and an electron to give water and a Cu(II)-oxyl radical [Cu(II)-O$^{\bullet}$] (red pathway). This mechanism is similar to that proposed by Klinman in the Cu enzymes peptidylglycine α-hydroxylating monooxygenase (PHM) and dopamine β-monooxygenase (DβM).[62] The Cu(II)-oxyl radical then recombine with the substrate radical (R$^{\bullet}$) and protonation gives the oxidized product and the starting Cu(II) state. An alternative path shows that an initial HO$^{\bullet}$ transfer from the Cu(II)-hydroperoxo species to the substrate radical (R$^{\bullet}$) (pink pathway) to give a [Cu(II)-O$^{\bullet}$] which is reduced and protonated to return to the starting Cu(II) state, also similar with the PHM.[63]

---

[61] a) Phillips C. M., Beeson IV W. T., Cate J. H., Marletta M. A., *ACS Chem. Biol.*, **2011**, 6(12), 1399-1406. b) Beeson W. T., Phillips C. M., Cate J. H., Marletta M. A., *J. Am. Chem. Soc.*, **2011**, 134(2), 890-892.

[62] a) Klinman J.P., *J. Biol. Chem.*, **2006**, 281, 3013–16. b) Evans J.P., Ahn K., Klinman J.P., *J. Biol. Chem.*, **2003**, 278,49691–98

[63] Chen P., Solomon E.I., *J. Am. Chem. Soc.*, **2004**, 126, 4991-5000.

When superoxide is bound to copper it can adopt one of two geometries: end on or side on. Depending on the computational analyses, the end-on intermediate has lower barriers for H atom abstraction as compared to the side-on one.[64] The end-on one has also been found in a previous study of copper enzymes PHM.[64] This intermediate was stabilized through intra- and intermolecular hydrogen bonds. In fungal LPMOs, it is stabilized by a conserved glutamine residue.[65] However, Cu(II)-O-O$^{\bullet}$ is frequently dismissed as the oxidant in LPMOs, because it is proposed that it is less able to perform H atom abstraction from a glycosidic C-H bond.

The second mechanism based on O_2 involves a Cu oxyl radical [Cu(II)-O$^{\bullet}$] for initial H atom abstraction from the substrate instead of a superoxo intermediate, Figure 4.7 B.[66] The starting point of this mechanism is similar. After O_2 activation, the superoxo intermediate [Cu(II)-O-O$^{\bullet}$] is reduced to the oxyl radical [Cu(II)-O$^{\bullet}$], a potentially stronger oxidative species. The oxyl radical abstracts a H atom from the substrate to give a Cu(II)-OH and a substrate radical (R$^{\bullet}$). Then the OH group from Cu(II)-OH is transfered to the substrate R$^{\bullet}$ to give the ROH and the active Cu(I) state to restart another catalytic cycle.[67]

---

[64] a) Cowley R. E., Tian L., Solomon E. I., *Proc. Natl. Acad. Sci. U. S. A.*, **2016**, 113, 12035−12040. b) Bertini L., Breglia R., Lambrughi M., Fantucci P., De Gioia L., Borsari M., Bruschi M., *Inorg. Chem.*, **2018**, 57(1), 86-97.

[65] Span E. A., Suess D. L. M., Deller M. C., Britt R. D., Marletta M. A., *ACS Chem. Biol.*, **2017**, 12, 1095-1103.

[66] Kim S., Ståhlberg J., Sandgren M., et al., *Proc. Natl. Acad. Sci. U. S. A.*, **2014**, 111(1): 149-154.

[67] Beeson W. T., Vu V. V., Span E. A., Phillips C. M., Marletta M. A., *Annu. Rev. Biochem.*, **2015**, 84, 923-946.

In this path, the first proton and electron reduce Cu(II)-O-O• to Cu(II)-O-OH, which is an important intermediate observed in engineered proteins and synthetic complexes.[68] Second proton-coupled electron transfer to Cu(II)-O-OH then forms Cu(II)-O• through heterolytic cleavage of the O-O bond. Tolman and co-workers [69] reported that Cu(III)-OH species was isoelectronic with protonated Cu(II)-O• and have observed through synthetic complexes that, Cu(III)-OH species are able to cleave a C-H bond in cyclohexane. LPMOs could use this highly valent species to provide suitable reactivity for the catalytic route. The N-terminal amine of the histidine brace has been proposed to be deprotonated to stabilize the Cu(III)-OH species.

4.4.2 The H_2O_2 reaction mechanism

While the above based O_2 mechanisms are the most widely discussed, recently a report published by Bissaro et al. argues that hydrogen peroxide is the direct oxidant employed by LPMOs rather than molecular dioxygen.[70] In this report, the experiments with labeled hydrogen peroxide ($H_2{}^{18}O_2$) in the presence of 10-times molar of O_2 showed that the oxygen atom which was

---

[68] a) Mann S. I. et al., *J. Am. Chem. Soc.*, **2017**, 139, 17289-17292. b) Peterson R. L. et al., *J. Am.Chem. Soc.*, **2013**, 135, 16454-16467. c) Concia A. L. et al., *Inorg. Chem.*, **2017**, 56, 1023-1026.

[69] a) Donoghue P. J., Tehranchi J., Cramer C. J., Sarangi R., Solomon E. I., Tolman W. B., *J. Am. Chem. Soc.*, **2011**, 133(44), 17602-17605. b) Dhar D., Tolman W.B., *J. Am. Chem. Soc.*, **2015**, 137, 1322–1329. c) Dhar D., Yee G. M., Spaeth A. D., Boyce D. W., Zhang H., Dereli B., Tolman W. B., *J. Am. Chem. Soc.*, **2016**, 138(1), 356-368.

[70] a) Bissaro B., Røhr Å. K., Skaugen M., Forsberg Z., Horn S. J., Vaaje-Kolstad G., Eijsink V., *BioRxiv*, **2016**, 097022. b) Bissaro B, Røhr Å K, Müller G, et al., *Nat. Chem. Biol.*, **2017**, 13(10), 1123.

introduced into polysaccharide came from H_2O_2. There are two possible mechanistic pathways based on H_2O_2. They all require an initial reduction from LPMO-Cu(II) to LPMO-Cu(I), to enter the catalytic cycle and each turnover returns the Cu(I) state of LPMOs.

One plausible pathway is breaking the O-O bond in H_2O_2 through one electron transfer from LPMO-Cu(I) to form an •OH radical and a Cu(II)-OH species (Figure 4.8 upper path). This radical is stabilized by H-binding interactions with LPMOs. Calculations by Wang et al.[71] suggest that the highly reactive •OH radical subsequently abstracts a hydrogen atom from Cu(II)-OH species to form Cu(II)-O• species, rather than directly abstracting a hydrogen from substrate. Then the Cu(II)-O• species abstracts a H atom from the polysaccharide substrate followed by •OH transfer to return to the Cu(I) state while giving ROH.

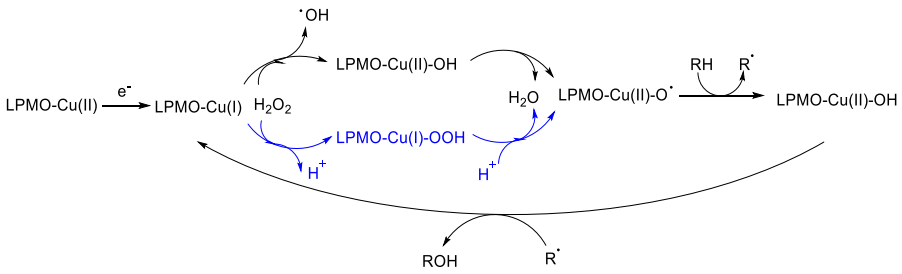

Figure 4.8 Proposed LPMOs mechanisms in which H_2O_2 is the direct oxidant of the polysaccharide substrate

Another possible pathway (Figure 4.8 bottom path) is that LPMO-Cu(I) binds H_2O_2 to form LPMO-Cu(I)-OOH, then homolytic cleave peroxide with protonation of the distal oxygen to give off H_2O and form Cu(II)-O• species.

---

[71] Wang B., Johnston E. M., Li P., Shaik S., Davies G. J., Walton P. H., Rovira C., *ACS Catal.*, **2018**, 8(2), 1346-1351.

This would abstract a H atom from substrate to give Cu(II)-OH and substrate radical (R•). Rebound of the hydroxyl with substrate radical would produce the product ROH and Cu(I) active state of the enzyme.

In this mechanism based on H_2O_2 as a cosubstrate, it is worth noting, that LPMOs may be able to tolerate low concentrations of H_2O_2 while high concentrations lead to enzyme inactivation.[72] Another point, the formation of •OH radical through the reaction of H_2O_2 with reduced transition metals is via the Fenton reaction, usually involving iron, which is important in the degradation of lignocellulosic material by brown-rot fungi.[73] The formation of powerful oxidative species brings the risk of autocatalytic damage to the enzymes. So, how the reactivity of •OH radical is controlled creates an additional potential challenge for understanding the enzyme. For here, substrate binding is proposed to be very important, LPMOs need to find a way to control •OH radical within the confinement of an enzyme-substrate complex.[71,73]

4.4.3 Electron transfer

For all of the reaction mechanisms of LPMOs, we can see that LPMOs depend on a source of electrons. The catalytic cycles require the delivery of one or two electrons to the copper center depending on the use of H_2O_2 or O_2 as cosubstrate. In all the reactions, the reduction of LPMO-Cu(II) to LPMO-Cu(I) is generally accepted as a necessary step preceding catalysis. The standard reduction potentials reported for fungal LPMOs range from 155 to 330 mV vs

[72] Bissaro B., Røhr Å. K., Müller G., Chylenski P., Skaugen M., Forsberg Z., Eijsink V. G., *Nat. Chem. Biol.*, **2017**, 13(10), 1123.

[73] Cragg S. M., Beckham G. T., Bruce N. C., Bugg T. D. H., McGeehan J. E., McQueen-Mason S. J., Schnorr K., Walton P. H., Watts J. E. M., Zimmer, M. *Curr. Opin. Chem. Biol.*, **2015**, 29, 108−119.

the standard hydrogen electrode (SHE),[41,74,75] and those for bacterial LPMOs have been reported in the range about 220-370 mV vs SHE.[44a,44b,55] In order to activate the LPMOs catalysis, the electron donor must have a reduction potentials that is close to or below the reduction potentials of the LPMOs copper active site (200-300mV).

The electron donors can be a plethora of reductants including small organic molecules such as ascorbic acid, reduced glutathione,[28] cysteine,[76] a wide range of plant biomass or fungal phenolic compounds, [77] lignin and oxidoreductases.

Several small molecule reductants have been used in vitro. Ascorbic acid is an important biological cofactor and has been used as an electron donor for the activity of LPMOs. Ascorbic acid is a weak acid, (pKa is 4.17).[78] Normally, at physiological pH, it exists mainly in the form of ascorbate monoanion. The ascorbate monoanion species is a good electron donor, which can donate one electron to form the neutral ascorbyl radical or donate one electron and a

---

[74] Quinlan R. J., Sweeney M. D., Lo Leggio L., Otten H., Poulsen J.-C., Johansen K. S., Krogh K. B., Jørgensen C. I., Tovborg M., Anthonsen A.,et al., *Proc. Natl. Acad. Sci.*, **2011**, 108, 15079–15084.

[75] Garajova S., Mathieu Y., Beccia M. R., Bennati-Granier C., Biaso F., Fanuel M., Henrissat B., *Sci. Rep.*, **2016**, *6*, 28276.

[76] Frommhagen M., Koetsier M. J., Westphal A. H., Visser J., Hinz, S. W. A., Vincken, J. P., van Berkel W. J. H., Kabel M. A., Gruppen H., *Biotechnol. Biofuels.*, **2016**, 9, 186.

[77] Kracher D., Scheiblbrandner S., Felice A. K. G., Breslmayr E., Preims M., Ludwicka K., Haltrich D., Eijsink V. G. H., Ludwig R., *Sci.*, **2016**, 352, 1098-1101.

[78] Warren J. J., Mayer J. M., *J. Am. Chem. Soc.,* **2010**, 132, 7784−7793.

proton to form the ascorbyl radical anion.[79] Carme Rovira and co-workers[80] used quantum mechanics/molecular mechanics (QM/MM) metadynamics simulations to study this process with LPMOs. They found that LPMOs-Cu(II) in the presence of an ascorbate molecule can lead to the Cu(II) being reduced to Cu(I) and the ascorbate being oxidized to an ascorbyl radical.

Lignin is a major structural component of plant cell walls and has been identified as an additional potential electron source for LPMOs. It has been demonstrated that the interaction of the bulk insoluble lignin fraction extracted from pretreated biomass with LPMOs can have the ability to provide electrons to the active site of the enzyme through long-range electron transfer mediated by low-molecular-weight soluble lignin present in plant cell walls.[81,82]

The most studied enzymatic electron donor is cellobiose dehydrogenase (CDH). CDHs are bi-modular redox enzymes belongs to the superfamily of glucose-methanol-choline (GMC) oxidoreductase, so far only identified in fungi. The CDH consists of a flavin adenine dinucleotide (FAD)-binding domain and a cytochrome domain (CYT) connected by a flexible linker

[79] Olsson M. H. M., Søndergaard C. R., Rostkowski M., Jensen, J. H., *J. Chem. Theory Comput.,* **2011**, 7, 525−537.

[80] Wang B., Walton P. H., Rovira, C., *ACS Catal.*, **2019**, *9*(6), 4958-4969.

[81] Westereng B., Cannella D., Wittrup Agger J., Jørgensen H., Larsen Andersen M., Eijsink V. G., Felby C., *Sci. Rep.,* **2016**, 5, 18561-18570.

[82] Muraleedhara, M. N., Zouraris D., Karantonis A., Topakas E., Sandgren M., Rova U., Karnaouri A., *Biotechnol. Biofuels.***, 2018**, 11(1), 1-15.

allowing mobility between the two domains.[83,84,85] Some CDHs have a carbohydrate-binging module (CBM) domain that also allows binding to cellulose.[86] The FAD-binding domain is rapidly reduced by cellobiose and then shuttles the two electrons to CYT domain which are proposed to reduce the LPMOs Cu active site and participate in the catalytic cycle.[87]

The interactions between CDH and LPMOs have been studied. While evidence suggests that CDH can supply electrons, the exact timing/transfer is still uncertain. In the O_2 activated mechanism two electrons are needed, one proposal is that the second electron is initially provided by oxidizing the tyrosine through a copper-hydroperoxo species. In this part, the CDH would donate two electrons, one used to reduce Cu(II) to Cu(I) and another to then quench the tyrosine radical. This delivery of the electrons is likely to occur through a protein-based electron transfer pathway. It has been proposed that CDH can interact directly with the active site. Because the active site of LPMOs is on a flat protein surface, the copper center could possibly accept electrons through a patch of surface residues including His-1, Ala-80, His-83

---

[83] Tan T. C., Kracher D., Gandini R., Sygmund C., Kittl R., Haltrich D., Hallberg B. M., Ludwig R., Divne C. S., *Nat. Commun.*, **2015**, 6, 7542.

[84] Zamocky M., Ludwig R., Peterbauer C., Hallberg B. M., Divne C., Nicholls P., Haltrich D., *Curr. Protein Pept. Sci.*, **2006**, 7, 255-280.

[85] Harada H., Onoda A., Uchihashi T., Watanabe H., Sunagawa N., Samejima M., Igarashi K., Hayashi T., *Chem. Sci.,* **2017**, 8, 6561-6565.

[86] Henriksson G., Johansson G., Pettersson G., *J. Biotechnol.,* **2000**, 78, 93-113.

[87] Kracher D., Zahma K., Schulz C., Sygmund C., Gorton L., Ludwig R., *FEBS J.*, **2015**, 282, 3136−3148.

and Tyr-204 (Figure 4.9 A).[88] However, these residues are also on the substrate binding surface of LPMOs which is likely to be occupied by cellulosic substrates.

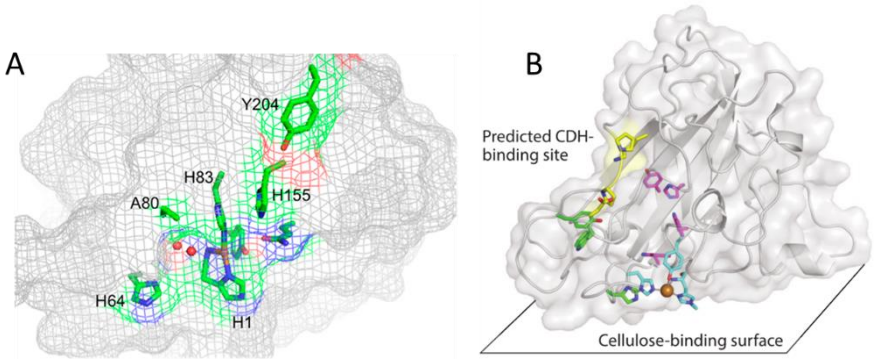

Figure 4.9 A) Crystal structure of NcLPMO9C showing the surface residues (PDB: 4D7U) (*Chem. Rev*, **2017**, 118(5), 2593-2635).B) Cartoon representation of the Neurospora crassa PMO3 (NcPMO3) (PDB: 4EIS) Proposed CDH binding surface showed yellow. Putative electron transfer pathways showed green and magenta. (*Annu. Rev. Biochem.*, **2015**, 84, 923-946.)

An alternative model exploits the aromatic residues in the copper site to form a through protein electron transfer connecting the active site of LPMOs to a CDH-binding site on a solvent exposed surface of LPMOs. Figure 4.9 B shows several conserved residues proposed as a potential electron transfer pathway linking the conserved histidine of the active site H-bonding network to the

[88] Courtade G., Wimmer R., Røhr Å. K., Preims M., Felice A. K., Dimarogona M., Eijsink V. G., *Proc. Natl. Acad. Sci. U. S. A.*, **2016**, 113(21), 5922-5927.

CDH-binding site on the opposite side of the protein.[89]

So, there is strong evidence that CDHs are the most common electron donor for fungal LPMOs, but the exact mode of interplay still needs to be fully elucidated, such as direct source of the second electron in the O_2-based LPMOs mechanism. Additionally, the electron transfer in bacterial LPMOs may differ from that in the fungal enzymes, but there is not enough evidence to date for a bacterial CDH. Extracellular oxidoreductases and other redox-active enzymes may serve as electron donors for bacterial LPMOs. One recent study has identified two genes in the saprophytic bacterium Cellvibrio japonicus, which have been implicated in redox function coupled to LPMOs activity.[90]

Recently, another enzyme family was researched, that is pyrroloquinoline quinone (PQQ)-dependent pyranose dehydrogenase (PDH) from Coprinopsis cinereal (CcPDH). The PQQ has been proposed to activate cellulose active AA9 LPMOs.[91] PQQ do not belong to the superfamily of glucose-methanol-choline (GMC) oxidoreductase, which includes CDH. PQQ has a similar domain architecture to CDH, but the flavin domain is replaced by PQQ-dependent sugar dehydrogenase domain.[92] The cytochrome domain of PQQ possesses similar biophysical properties with those of CDH. However, PQQ

---

[89] Li X., Beeson W. T., Phillips C. M., Marletta M. A., Cate J.H.D., *Structure*, **2012**, 20,1051-1061.

[90] Gardner J. G., Crouch L., Labourel A., Forsberg Z., Bukhman Y. V., Vaaje‐Kolstad G., Keating D. H., *Mol. Microbiol.*, 2014, 94(5), 1121-1133.

[91] Várnai A., Umezawa K., Yoshida M., Eijsink V. G. H., *Appl. Environ. Microbiol.*, **2018**, 84, e00156.

[92] Matsumura H., Umezawa K., Takeda K., Sugimoto N., Ishida T., Samejima M., Ohno, H., Yoshida M., Igarashi K., Nakamura N., *PLoS One*, **2014**, 9, e104851- e104859.

prefers to catalyze the two-electron oxidation of monosaccharide substrates. The fungal PQQ are able to reduce LPMOs and drive oxidative activity, but the mechanism of electron transfer is unknown.

LPMOs reactions may also be promoted by photocatalytic systems providing electrons. Canella and co-workers reported the photosynthetic pigments could be used to provide electrons to LPMOs. They found that a bacterial LPMOs was exposed to low intensity light in the presence of plant derived pigments and reducing agents, which can speed up LPMOs catalytic rates and enhance the reaction with the substrate.[93] Although the photoexcited pigment molecule can deliver an electron to LPMOs, this proposal is controversial. While the mechanism for photocatalytic reduction of LPMOs need more research, it should be noted that the use of photocatalytic systems in an industrial saccharification have significant consequences for the design and operation of the reactor.

Some research on O_2 driven LPMOs reactions showed that higher concentrations of reductant can lead to higher catalytic rates and of course higher consumption of O_2. But it should be noted that high concentrations of reductant can also lead to inactivation of LPMOs.[94,95,96] Because the rate of LPMOs reduction is in the milliseconds range, but the reported apparent

---

[93] Cannella D., Mollers K. B., Frigaard N. U., Jensen P. E., Bjerrum M. J., Johansen K. S., Felby C., *Nat. Commun.*, **2016**, 7, 11134−11142.

[94] Müller. G., Chylenski P., Bissaro B., Eijsink V. G. H., Horn S. J., *Biotechnol. Biofuels*, **2018**, 11, 209.

[95] Loose J. S. M., Forsberg Z., Kracher D., Scheiblbrandner S., Ludwig R., Eijsink V. G. H., Vaaje-Kolstad G., *Protein Sci.*, **2016**, 25, 2175-2186.

[96] Gusakov A. V., Bulakhov A. G., Demin I. N., Sinitsyn A. P., *Carbohydr. Res.*, **2017**, 452, 156-161.

catalytic rate is in the minute range,[77] there is an obvious discrepancy. Normally, in the O_2 driven reaction mechanism of LPMOs, the delivery of the second electron may be the rate limiting step. However, the H_2O_2 driven mechanism does not require delivery of a second electron.[97]

For now, many studies are looking at the correlation between LPMO reactivity and electron donors. However, the binding site of the reductant and the delivery mechanism of electrons to the active site still need further study to help better understand the mechanism of LPMO reactivity.

5. Mimic the active site of LPMO to research the mechanisms and activity

Despite the insight gained so far (described above), many questions remain for the LPMO catalytic mechanism, including what is the nature of the copper oxygen species involved in the H-atom transfer step, what is the source for electrons, as well as the catalytic pathway and the order of proton/electron transfers. While the above mentioned studies provide some detail, multiple functional groups both in and surrounding the enzyme active site have also been implicated in the mechanism. Both the axial tyrosine and the primary amine have been hypothesized to participate in the reaction through H-atom transfer to the Cu oxygen intermediates or through stabilization of certain Cu intermediates. Moreover, groups further away from the Cu site have also been reported to be important for reactivity through second coordination sphere interactions.

Because the networks of interactions in the SCS of the enzyme are often

[97] Chylenski P., Bissaro B., Sørlie M., Røhr Å. K., Várnai A., Horn S. J., Eijsink V. G., *ACS Catal.*, **2019**, 9(6), 4970-4991.

extensive, modification of these groups in the enzyme can result in secondary structural changes that influence reactivity unexpectedly. Thus, distinguishing the role of a specific group is often difficult. Even for the more local structures of the active site, the complexity of the enzyme can make it difficult to draw direct conclusions about the effects a certain modification brings, for example the N-histidine methylation. There are many unknown aspects about the geometric and electronic features of the histidine brace, the mechanism of the enzyme, and SCS interactions in LPMOs. One tool for better understanding some of these aspects are small molecule mimics or model complexes, where the effect of a specific modification can be better isolated from changes the rest of the molecule. Moreover, their smaller size can also make the study of reaction intermediates easier as well. For example, hypothesized Cu oxygen intermediates can be synthesize, isolated, and used as spectroscopic probes or proof of existence for proposed species in the catalytic cycle.

6. Different Cu-O intermediates based on copper monooxygenase model complexes

The high bond dissociation energy (BDE) of glycosidic C-H bonds in cellulose makes understanding the oxidative power of the mononuclear copper center in LPMOs an intriguing challenge. The high BDE requires that a powerful oxidant is generated during the reaction. Depending on the proposed mechanism discussed above, Cu(II)-O-O$^{\bullet}$ or Cu(II)-O$^{\bullet}$ intermediates are proposed to perform hydrogen atom abstraction (HAA) with O_2 or H_2O_2 as cosubstrate. Small molecule copper complexes have found evidence for both of these intermediates.

Still, mononuclear Cu-O_2 has the tendency to form more stable dicopper peroxide complexes through interaction with the Cu(I) starting material,

making the development of these model complexes a challenge. In order to prevent the dimerization, ligands often rely on bulky and strongly electron donating substituents to stabilize the mononuclear Cu-O_2 species. [98] Nevertheless, a number of copper oxygen species have been reported. These are described below.

6.1 Copper(II)-superoxide: Cu(II)-O-O$^{\bullet}$

Cu(II)-O-O$^{\bullet}$ is a key reactive intermediate in several copper monooxygenases, PHM, DβM, and LPMO, and is proposed to be responsible for attacking a substrate C-H bond.

When oxygen binds to Cu(I) center, electron transfer leads to a Cu(II)-O-O$^{\bullet}$. The geometry of the oxygen in copper(II)-superoxide can be either in an end-on or side-on fashion. Crystal structures of these two coordination modes have been reported (Figure 6.1.1A and B).[99,100] An X-ray crystal structure of PHM (PDB: 1SDW) complexed with substrate and O_2 demonstrate existence of a mononuclear copper active center having an end-on bound O_2 with a distorted tetrahedral geometry.[101] The crystal structure of Neurospora crassa LPMO (PDB: 5TKH) also showed that O_2 directly coordinates to the copper

[98] a) Itoh S., *Acc. Chem. Res.*, **2015**, 48(7), 2066-2074. b) Lewis E. A., Tolman W. B., *Chem. Rev.*, **2004**, 104(2), 1047-1076.

[99] Fujisawa K., Tanaka M., Moro-oka Y., Kitajima N., *J. Am.Chem.Soc.*, **1994**, 116(26), 12079-12080.

[100] Würtele C., Gaoutchenova E., Harms K., Holthausen M. C., Sundermeyer J., Schindler S., *Angew. Chem. Int. Ed.*, **2006**, 45(23), 3867-3869.

[101] Prigge S. T., Eipper B. A., Mains R. E., Amzel L. M., *Sci.*, **2004**, 304, 864-867.

center in an end-on mode.[102] Therefore, it has been proposed that mononuclear enzymes normally prefer end-on coordination.

The end-on copper(II)-superoxide species share similar features in their UV-vis spectra with a stronger peak around 410-420 nm and a broad low-energy absorption around 600-800 nm, and in resonance Raman spectra, exhibit stretching frequencies of v(O-O) at 1100-1130 cm^{-1} and v(Cu-O) at 460-480 cm^{-1}.[103] Schindler and co-workers monitored this species by UV-vis and Resonance Raman spectroscopy at low temperature using a tripodal tetradentate tren ligand with a sterically bulky and strongly electron donating substituent, tetramethylguanidine (TMG).[104] Subsequently, they got the crystal structure (Figure 6.1.1A) of an end-on copper(II)-superoxide complex generated by the same ligand.[100]

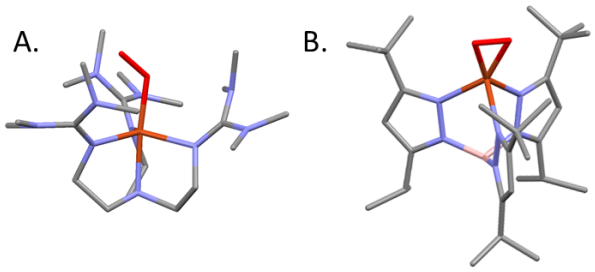

Figure 6.1.1 Crystal structure of copper(II)-superoxide complex, A) end-on coordination; B) side-on coordination

[102] O'Dell W. B., Agarwal P. K., Meilleur F., *Angew. Chem. Int. Ed.,* **2017**, 56, 767-770.

[103] Elwell C. E., Gagnon N. L., Neisen B. D., Dhar D., Spaeth A. D., Yee G. M., Tolman W. B., *Chem. Rev.*, **2017**, 117(3), 2059-2107.

[104] Schatz M., Raab V., Foxon S. P., Brehm G., Schneider S., Reiher M., Schindler S., *Angew. Chem. Int. Ed.*, **2004**, 43(33), 4360-4363.

After Schindler's report, a good number of well-characterized mononuclear copper(II)-superoxide (end-on) complexes (shown in Figure 6.1.2) have been developed using supporting ligands containing strongly electron donating groups, hydrogen bonding interactions, or sterically bulky substituents to stabilize the superoxide moiety. Among these different ligands, with sterically bulky substituents groups, such as tetramethylguanidine (TMG, Figure 6.1.1A) and hexaisoprophylter-phenyl[105] (HIPT, Figure 6.1.2G) can prevent formation of dicopper(II) peroxide species, in favor of mononuclear copper(II)-superoxide. The strongly electron donating groups and hydrogen bonding interaction can influence the stability and ability of copper(II)-superoxide.

Normally, copper(II)-superoxide complexes can abstract a hydrogen atom to cleave phenolic O-H bonds, as well as weak C-H bonds. This may be due to the electron richness of the metal center. Reactivity studies with different complexes showed that in complexes containing a more weakly donating thioether ligand, the copper(II)-superoxide [106] (Figure 6.1.2F) was more capable of performing hydrogen atom abstraction from phenol and N-methyl-9,10-dihydroacridine (C-H) substrates than a complex with TMPA (Figure 6.1.2A).[107]

Non-covalent interactions can also affect oxidative reactivity. In researching a series of TMPA ligand based copper(II)-superoxide complexes (Figure 6.1.2

---

[105] Kobayashi Y., Ohkubo K., Nomura T., Kubo M., Fujieda N., Sugimoto H., Fukuzumi S., Goto K., Ogura T., Itoh S., *Eur. J. Inorg. Chem.*, **2012**, 2012, 4574-4578.

[106] Kim S., Lee J. Y., Cowley R. E., Ginsbach J. W., Siegler M. A., Solomon E. I., Karlin K. D., *J. Am. Chem. Soc.*, **2015**, 137, 2796−2799.

[107] Maiti D., Fry H. C., Woertink J. S., Vance M. A., Solomon E. I., Karlin K. D., *J. Am. Chem. Soc.*, **2007**, 129, 264-265.

A-D), gradual strengthening of ligand derived intramolecular hydrogen bonds can enhance the corresponding copper(II)-superoxide stability and reactivity toward hydrogen atom abstraction of phenolic O-H bonds.[108] The copper(II)-superoxide complex (Figure 6.1.2A) without H-bonding did not exhibit reactivity toward the hydrogen atom abstraction of 4-methoxyphenol where the BDE (O-H) is 87.6 kcal/mol in DMSO. However, complex B (in Figure 6.1.2) with weak H-bonding exhibited exceeding slow reactivity and complex C (in Figure 6.1.2) reacted considerably faster. Complex D (in Figure 6.1.2) exhibited the highest reactivity. Additionally, the species E (in Figure 6.1.2) could react with substrates containing O-H BDE of up to 91.5 kcal/mol (p-methylphenol) and BDE of C-H up to 79.7 kcal/mol in dihydroanthracene.

However, these superoxide complexes shown in Figure 6.1.2 have tripodal tetradentate (N4) structure, which are different from the tridentate (N3) coordination environment found in the enzymatic system (PHM, LPMOs).

[108] a) Bhadra M., Lee J. Y. C., Cowley R. E., Kim S., Siegler M. A., Solomon E. I., Karlin K. D., *J. Am.Chem.Soc.*, **2018**, 140(29), 9042-9045. b) Diaz D. E., Quist D. A., Herzog A. E., Schaefer A. W., Kipouros I., Bhadra M., Karlin K. D. *Angew. Chem. Int. Ed.*, **2019**, 58(49), 17572-17576.

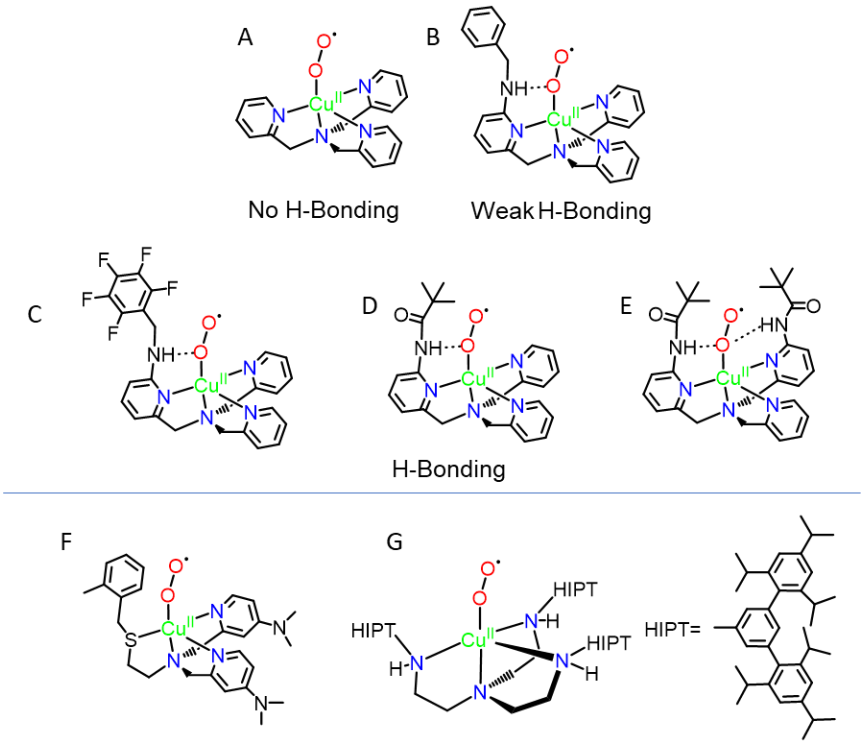

Figure 6.1.2 Well characterized copper(II)-superoxide complexes (end-on coordination)

Itoh and coworkers reported the first example of copper(II)-superoxide complexes using a tridentate ligand (L^{Pye}, in Figure 6.1.3).[109, 110] The mononuclear copper(II)-superoxide complex (B, in Figure 6.1.3) was obtained through reaction of O_2 with the copper(I) starting materials (A, in Figure 6.1.3).

[109] Kunishita A., Kubo M., Sugimoto H., Ogura T., Sato K., Takui T., Itoh S., *J. Am. Chem. Soc.*, **2009**, 131, 2788−2789.

[110] Kunishita A., Ertem M. Z., Okubo Y., Tano T., Sugimoto H., Ohkubo K., Fujieda N., Fukuzumi S., Cramer C. J., Itoh S., *Inorg. Chem.*, **2012**, 51, 9465−9480.

The proposed copper(II)-superoxide complex (B, in Figure 6.1.3) that formed was able to abstract an H atom intramolecularly from a benzylic C-H in the ligand to generate complex C, which then rebound with the C-centered radical to form the final Cu-alkoxide product (D, in Figure 6.1.3). This ligand geometry and reaction with substrate mimics the structure and the reactivity of enzymes such as PHM and DβM, which also exhibit aliphatic C-H bond hydroxylation reactivity. Recently, the same group used a similar tridentate (N3) ligand L^{Pym} (Figure 6.1.3) with a shorter pyridylmethyl sidearm than their previous ligand (L^{Pye}) to generate another mononuclear copper(II)-superoxide complex. This superoxide complex exhibited different reactivity inducing a catalytic C-C bond formation reaction between carbonyl compounds (substrate) and the solvent molecule (acetone) to give β-hydroxyketones (aldol) (bottom, in Figure 6.1.3).[111]

[111] Abe T., Hori Y., Shiota Y., Ohta T., Morimoto Y., Sugimoto H., Itoh S., *Chem. Commun.*, **2019**, 2(1), 1-7.

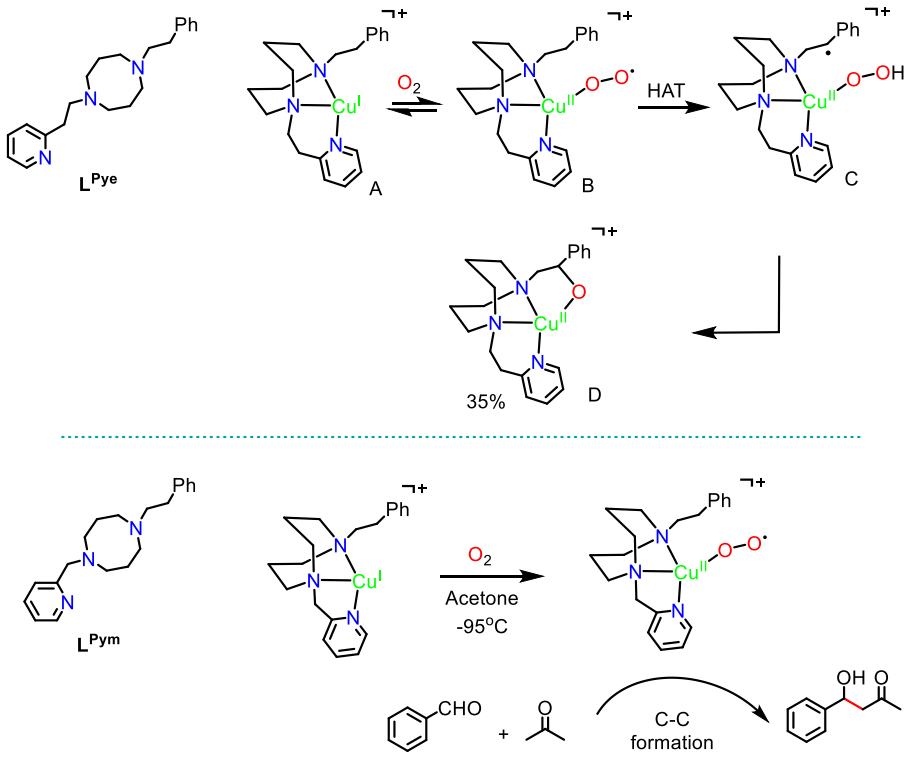

Figure 6.1.3 Structure of tridentate ligand L^{Pye} and L^{Pym}; proposed mechanism for intramolecular hydroxylation by L^{Pye} derived copper(II)-superoxide complex (upper) and the generation of L^{Pym} derived copper(II)-superoxide complex (bottom)

Another kind of tridentate (N3) ligand was designed by Tolman and coworkers.[112] They reported the synthesis of a copper(II)-superoxide complex from addition of KO_2 and 18-crown-6 to a copper(II) complex supported by a dianionic pyridine dicarboxamide ligand (shown in Figure 6.1.4A). This superoxide complex [K(18-crown-6)][$LCuO_2$] was stable in a DMF/THF

[112] Donoghue P. J., Gupta A. K., Boyce D. W., Cramer C. J., Tolman W. B., *J. Am. Chem. Soc.*, **2010**, 132(45), 15869-15871.

solution at -80°C, but when warmed to -60°C decomposed. Then McDonald and coworkers synthesized the same complex and reported that it had nucleophilic reactivity.[113] This complex was reported to convert acyl chlorides to the carboxylic acid and with certain aldehydes to undergo aldehyde deformylation (shown in Figure 6.1.4B).

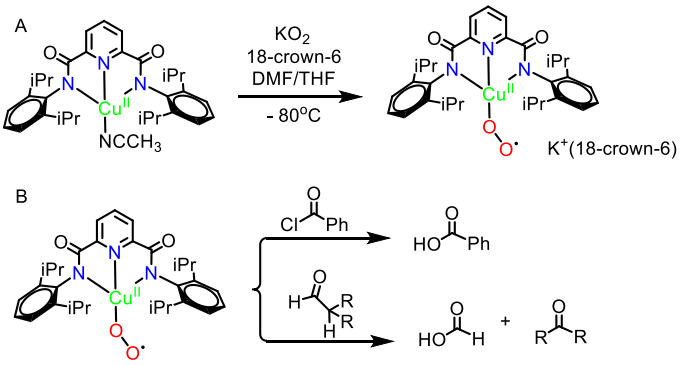

Figure 6.1.4 (A) Synthesis of copper(II)-superoxide complex (ligand: N,N ' -bis(2,6-diisopropylphenyl)-2,6-pyridi-nedicarboxamide); (B) Nucleophilic reactivity of this superoxide specie

Because the copper(II)-superoxide complex supported by a dianionic pyridine dicarboxamide ligand, described above was not stable, Tolman and coworkers sought an improved method for synthesis of this superoxide complex to enhance the solubility and stability. They used Kryptofix222 (Krypt) instead of above 18-crown-6, first mixing the KO_2 and Krypt in CH_3CN to yield homogeneous [K(Krypt)]-[O_2] which was added to the copper(II) complex supported by a dianionic pyridine dicarboxamide ligand to generate the

[113] Pirovano P., Magherusan A. M., McGlynn C., Ure A., Lynes A., McDonald A. R., *Angew. Chem. Int. Ed.*, **2014**, 53(23), 5946-5950.

copper(II)-superoxide complex [K(Krypt)][LCuO$_2$] (shown in Figure 6.1.5).[114] This paper enabled reexamination of this superoxide complex's reactivity with 2-phenylpropionaldehyde (2-PPA). The study revealed that the copper(II)-superoxide reacts with wet 2-PPA through deprotonation of the acidic benzylic C-H bond and decomposition of $[CuOOH]^{2+}$ to form a $[LCu\text{-}OH]^{-}$ intermediate, which then deprotonates 2-PPA to yield the product copper(II) enolate complex.

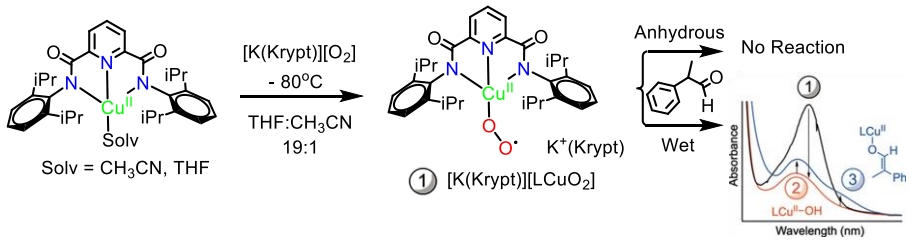

Figure 6.1.5 Synthesis and reactivity of [K(Krypt)][LCuO$_2$]

The mononuclear copper(II)-superoxide (end-on) complex exhibit similar structural features and reactivity to a putative reactive intermediate of the copper monooxygenases (such as PHM, DβM, LPMOs). These superoxide complexes have been developed using N3-tridentate ligand (L^{Pye}, L^{Pym}, dianionic pyridine dicarboxamide ligand). The notable feature of L^{Pye}-copper(II)-superoxide complex is the reactivity for aliphatic hydroxylation, which is an important example of a functional model of copper monooxygenases such as PHM and DβM that oxidize C-H bond with BDE < 90 kcal/mol. However, the BDE of glycosidic C-H bonds is higher, which creates a formable barrier. A more powerful oxidant is needed to overcome the barrier. Multiple computational studies on LPMOs have also proposed that

[114] Bailey W. D., Gagnon N. L., Elwell C. E., Cramblitt A. C., Bouchey C. J., Tolman W. B., *Inorg. Chem.*, **2019**, 58(8), 4706-4711.

copper(II)-superoxide is not powerful enough to perform HAA from the glycosidic bond in polysaccharide substrates.[115]

6.2 Copper(II)-hydroperoxide: Cu(II)-O-OH

During early investigations into the biochemistry and mechanism of action of some enzymes (PHM, DβM or LPMOs), mononuclear copper(II)-hydroperoxide was also an important intermediate proposed for oxidation. The copper(II)-hydroperoxide can be formed by the delivery of a hydrogen atom from substrate to copper(II)-superoxide or through proton coupled electron transfer (PCET) to the copper(II)-superoxide.[116] Another way is that copper(II)-hydroperoxide can also be generated by addition of H_2O_2 and a base to Cu(II) precursors complexes.[117] As with many other Cu-oxygen species, the ligand structure (such as coordination geometry or sterics) or secondary coordination sphere (hydrogen binding interaction) can influence the formation, stability and reactivity of copper(II)-hydroperoxides.

The first example of an isolated copper(II)-hydroperoxide species has been characterized by X-ray crystallography from Masuda group (Figure 6.2.1A).[118] This specie was supported by a tripodal tetradentate (N4) amino-pyridyl ligand (called bppa in the original paper) framework. From the X-ray structure of this species, there are two hydrogen-bonding interaction between the amide

[115] Hedegård E. D., Ryde U., *Chem. Sci.*, **2018**, 9, 3866-3880.

[116] Maiti D., Lee D.-H., Gaoutchenova K., Würtele C., Holthausen M. C., Narducci Sarjeant A. A., Sundermeyer J., Schindler S., Karlin K. D., *Angew. Chem. Int. Ed.*, **2008**, 47, 82−85.

[117] Osako T., Nagatomo S., Tachi Y., Kitagawa T., Itoh S., *Angew. Chem., Int. Ed.*, **2002**, 41, 4325−4328.

[118] Wada A., Harata M., Hasegawa K., Jitsukawa K., Masuda H., Mukai M., Kitagawa T., Einaga H., *Angew. Chem. Int. Ed.*, **1998**, 37, 798−799.

substituent N-H groups and the proximal oxygen of the peroxide (shown in Figure 6.2.1B). Therefore, the stability of this species was attributed to the two hydrogen bonds and steric shielding by the tert-butyl substituents, which let the usually thermally unstable copper(II)-hydroperoxide species survive at room temperature.

Another similar complex (shown in Figure 6.2.1C) was synthesized, they used the ligand with a single benzylamine substituent on a pyridyl arm to replace the original tert-butyl group.[119] There is only one H-binding interaction between the N-H of secondary amine and the proximal O atom. The hydroperoxide species can be formed with one equiv. H_2O_2 in the presence of Et_3N, the reaction can be reversed by treatment with $HClO_4$. This species was stable at -90°C but decayed to a (trans-1,2-peroxo)dicopper(II) when warmd to -50°C. This example highlights that the H-binding interaction between N-H and proximal peroxide O atom is important to the stability for copper(II)-hydroperoxide species.

[119] Kim S., Saracini C., Siegler M. A., Drichko N., Karlin K. D., *Inorg. Chem.*, **2012**, *51*(23), 12603-12605.

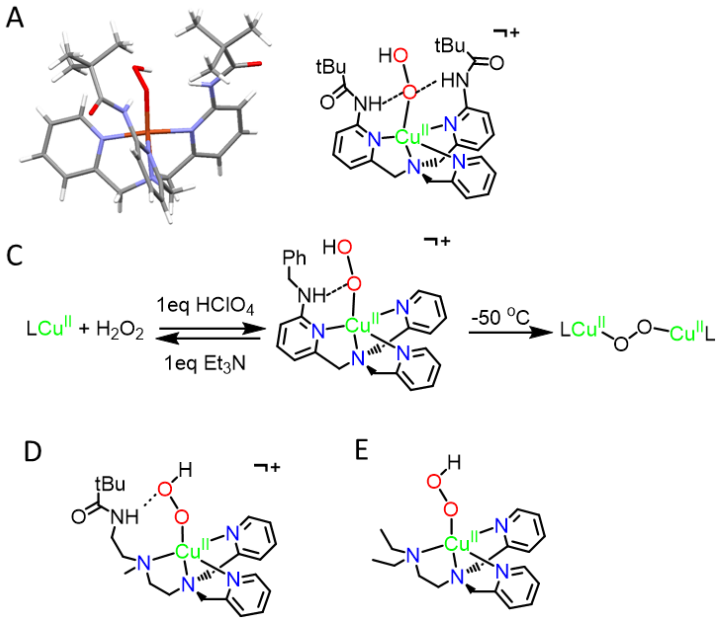

Figure 6.2.1 Crystal structure (A) and molecule structure (B) Masuda's $[(bppa)Cu^{II}OOH]^{+}$ complex stabilized by two H-bonds to the proximal O atom; (C) Reactivity of $[(BA)Cu^{II}OOH]^{+}$ complex; (D and E) $Cu(^{II})$-OOH complex illustrating H-bond to the distal O atom and with no H-bond

Another comparative study on two N4 ligands was also reported by Masuda and coworkers (Figure 6.2.1 D and E).[120] They found that the hydroperoxide species with H-bonding to the distal O atom could decompose faster than the one without this distal H-binding interaction. That means that the H-bonding with the distal O atom can activate the copper(II)-hydroperoxide species, as have been suggested in DβM.

[120] Yamaguchi S., Nagatomo S., Kitagawa T., Funahashi Y., Ozawa T., Jitsukawa K., Masuda H., *Inorg. Chem.*, **2003**, 42(22), 6968-6970.

Recently, Borovik, Ward, and coworkers[121] used biotin-streptavidin (Sav) technology to insert a bis(2-pyridylethyl)amine copper(II) complex into a streptavidin host and then generated the stable copper(II)-hydroperoxide complex in the presence of H_2O_2 (shown in Figure 6.2.2A), which could persist for over a day at room temperature. The stability was achieved because the Sav host provided a local environment around the copper(II)-hydroperoxide species and also formed a network of H-bonds with the hydroperoxide ligand. Residue N49 could form an H-bond with the distal O atom (O4) of hydroperoxide moiety. A second H-bond was very special and was formed between the proximal O atom (O3) of the hydroperoxide moiety and O1 which came from a water molecule held in place by interaction with a nearby amino acid residue, S112. They also researched how mutation of N49 or S112 to alanine would alter the local environment to possibly modulate the stability and reactivity of the copper(II)-hydroperoxide specie. When N49 was mutated to alanine, there was only one H-bond to the proximal O3 atom of hydroperoxide moiety. The resulting complex had the same stability as when two H-bonds were present, and the copper(II)-hydroperoxide species was also unreactive toward weak C-H substrates. However, with the engineered alanine residue at position S112, the structural water molecule containing O1 was removed and it cannot form an H-bond with S112. So, only a single H-bond to the distal O4 atom was found. This destabilizes the copper(II)-hydroperoxide species and reduces the half-life to 20 min. However, this copper(II)-hydroperoxide species can perform benzylic C-H activation of an exogenously added 4-chlorobenzylamine substrate.

[121] Mann S. I., Heinisch T., Ward T. R., Borovik A. S., *J. Am. Chem. Soc.*, **2017**, 139(48), 17289-17292.

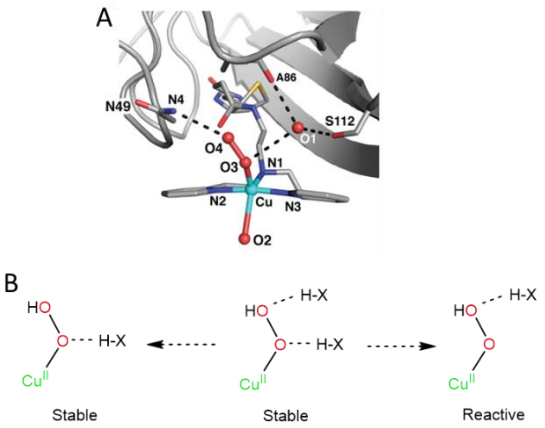

Figure 6.2.2 (A) The molecular structure of engineered protein active site designed by Borovik group and the H-binding network around copper(II)-hydroperoxide complex (PDB: 6ANX)(*J. Am. Chem. Soc.*, **2017**, 139(48), 17289-17292); (B) Overall proposed effects of H-bonds on the stability or reactivity of copper(II)-hydroperoxide specie.

The Masude, Karlin and Borovik studies show that modulation of the H-bonds around copper(II)-hydroperoxide specie can influence the stability and reactivity of this species (Figure 6.2.2 B). A single H-bond to the proximal O atom or together with another H-bond to distal O atom of hydroperoxide moiety was essential to form a stable copper(II)-hydroperoxide species. With only one H-bond to the distal O atom, an unstable and reactive copper(II)-hydroperoxide specie that can oxidize a substrate can be produced. For LPMOs, there are also some H-bonds involving the second coordination sphere, which can participate in the activation of a copper(II)-hydroperoxide intermediate.

The Tolman group provided an indirect way to implicate the presence of another kind of copper(II)-hydroperoxide intermediate in the mechanism of

LPMOs.[122] They reported the characterization of formally Cu(III)-OOR complexes (Figure 6.2.3A) with pincer ligand containing a T-shaped core. These complexes could be supposed to serve as model for possible copper(III)-hydroperoxide intermediate in LPMOs. As shown in Figure 6.2.3B, this copper(III)-hydroperoxide intermediate is equivalent to a copper(II)-hydroperoxide generated from the protonation of the copper(II)-superoxide. In order to stabilize these intermediate, the terminal NH_2 group could undergo deprotonation. Recently two mononuclear Cu(II) complexes were designed as models for LPMOs.[123,124] They found that the Cu(II) complexes could react with H_2O_2 under aqueous conditions to form a mononuclear copper(II)-hydroperoxide species characterized by UV-Vis.

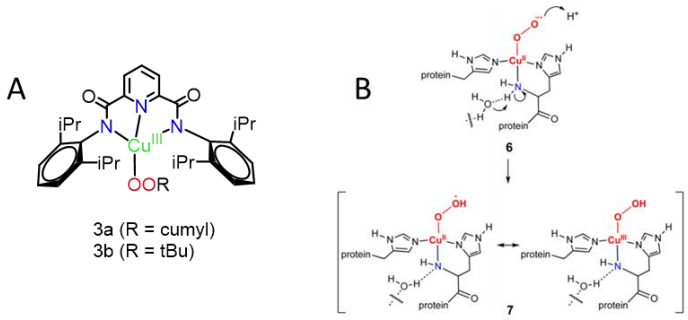

Figure 6.2.3 A copper(III)-alkylperoxo species (A) as the model for possible intermediate (B) in LPMOs (*J. Am. Chem. Soc.*, **2017**, 139(30), 10220-10223)

[122] Neisen B. D., Gagnon N. L., Dhar D., Spaeth A. D., Tolman W. B., *J. Am. Chem. Soc.*, **2017**, 139(30), 10220-10223.

[123] Concia A. L., Beccia M. R., Orio M., Ferre F. T., Scarpellini M., Biaso F., Guigliarelli B., Réglier M., Simaan A. J., *Inorg. Chem.*, **2017**, 56, 1023−1026.

[124] Muthuramalingam S., Maheshwaran D., Velusamy M., Mayilmurugan R., *J. Catal.*, **2019**, 372, 352-361.

Some papers reported the oxidative capabilities of copper(II)-hydroperoxide species, such as the intramolecular aryl hydroxylation (shown in Figure 6.2.4A)[125] and the N-dealkylation reaction (model function of PHM) (shown in Figure 6.2.4B).[126,127,128] However, experimental and DFT analyses suggest that copper(II)-hydroperoxide species cannot directly perform these activation reactions. One hypothesis is that the O-O bond in the copper(II)-hydroperoxide species would be cleaved to form a putative Cu(II)-O$^{\bullet}$ species as the oxidizing intermediate. Another hypothesis is that Cu-O bond homolysis yields Cu(I) and a hydroperoxyl radical. Then a Fenton-like reaction occurs in the presence of a Cu(I) complex and H_2O_2 to form a copper(II)-hydroxide and a hydroxyl radical. The hydroxyl radical (•OH) would be responsible for substrate C-H attack and N-dealkylation.

[125] Maiti D., Lucas H. R., Sarjeant A. A. N., Karlin K. D., *J. Am. Chem. Soc.*, **2007**, 129, 6998−6999.

[126] Maiti D., Narducci Sarjeant A. A., Karlin K. D., *J. Am. Chem. Soc.*, **2007**, 129, 6720−6721.

[127] Maiti D., Narducci Sarjeant A. A., Karlin K. D., *Inorg. Chem.*, **2008**, 47, 8736−8747.

[128] Kim S., Ginsbach J. W., Lee J. Y., Peterson R. L., Liu J. J., Siegler M. A., Sarjeant A. A., Solomon E. I., Karlin K. D., *J. Am. Chem. Soc.*, **2015**, 137, 2867−2874.

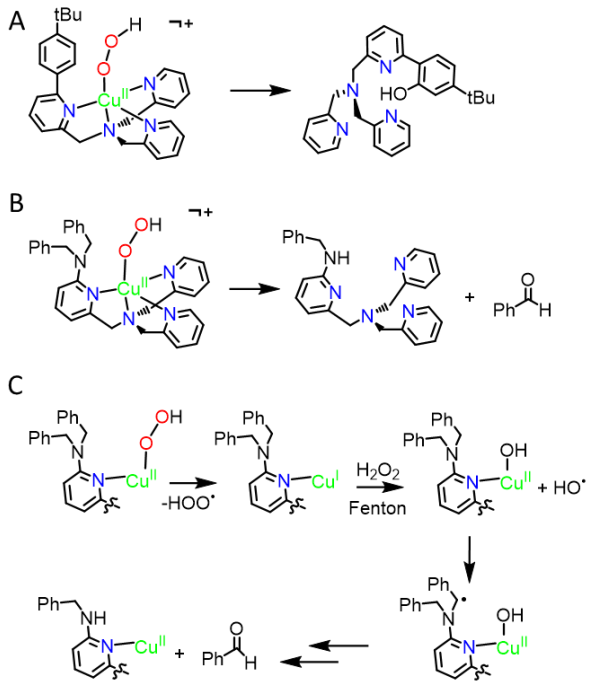

Figure 6.2.4 Examples of aryl hydroxylation(A) or N-dealkylation reactions(B) of copper(II)-hydroperoxide specie; (C) Hypothesized mechanism for intramolecular for N-dealkylation by the species in B

The stability and oxidase activity of copper(II)-hydroperoxide species can be influenced by coordination geometry and sterics. Besides, the H-bond with different O atom (distal or proximal) in hyperoxide moiety also have great influence on the activity of this species. Delivery of one or two electrons and a proton would reduce copper(II)-hydroperoxide to a Cu(II)-O• specie, which could be another possible oxidizing intermediate.

6.3 Copper(II)-oxyl: Cu(II)-O•

In the proposed mechanisms for reactivity of LPMOs, with either O_2 or H_2O_2 as cosubstrate, all can converge on a copper(II)-oxyl intermediate. Oxygen

can react with the Cu(I) complex to form Cu(II)-O• with the addition of two protons and two electrons via homolytic O-O bond cleavage of Cu(II)-hydroperoxide. Or Cu(I) complex can react with H_2O_2 to generate Cu(II)-O• without addition of protons and electrons. In this proposed mechanism, the Cu(II)-O• are responsible for HAA from substrate. It is an important intermediate not only for LPMOs but also for another copper enzymes DβM,[129] PHM[130] or pMMO.[131]

For now, the copper(II)-oxyl species have not been observed experimentally in solution, synthetic models or enzymes. Some studies have indicated that copper(II)-oxyl species in the gas phase can attack the strong C-H bond of methane.[132,133,134] There is some indirect evidence for the existence of copper(II)-oxyl species in some synthetic system. For example, Karlin and coworkers[114] proposed that the intramolecular oxidation of an aliphatic C-H bond on the ligand to copper was supported by the copper(II)-oxyl species (Figure 6.3.1A). And they suggested that the copper(II)-oxyl intermediate was formed through homolytic O-O bond cleavage of copper(II)-hydroperoxide or

[129] Kamachi T., Kihara N., Shiota Y., Yoshizawa K., *Inorg. Chem.*, **2005**, 44, 4226-4236.

[130] Crespo A., Martí M. A., Roitberg A. E., Amzel L. M., Estrin D. A., *J. Am. Chem. Soc.*, **2006**, 128, 12817-12828.

[131] Cao L., Caldararu O., Rosenzweig A. C., Ryde U., *Angew. Chem. Int. Ed.*, **2018**, 57, 162-166.

[132] Dietl N., Van Der Linde C., Schlangen M., Beyer M. K., Schwarz H., *Angew. Chem. Int. Ed.,* **2011**, 50, 4966−4969.

[133] Dietl N., Schlangen M., Schwarz H., *Angew. Chem. Int. Ed.*, **2012**, 51, 5544−5555.

[134] Rijs N. J., González-Navarrete P., Schlangen M., Schwarz H., *J. Am. Chem. Soc.*, **2016**, 138 (9), 3125−3135.

through the reaction of Cu(I) complex precursor and the iodosobenzene as the O atom donor. The Itoh group[135] also reported that the copper(II)-oxyl was formed through thermal O-O bond homolysis of a copper(II)-cumylperoxide complex and the copper(II)-oxyl species induced C-H bond activation in exogenous substrates (Figure 6.3.1B).

Recently Diaz et al.[136] reported that the reaction of a series of copper(I) complexes and N,N-dimethylaniline N-oxides (DMAOs) (shown in Figure 6.3.1C), as the oxygen surrogates, and proposed the formation of copper(II)-oxyl species as a putative key intermediate in the reactivity of copper monooxygenases. And this species could hydroxylate strong C-H bonds (BDE 90 kcal/mol) to form the product p-cyano-N-methylaniline. These examples are all the indirect evidence to support the formation of the copper(II)-oxyl intermediate and capable of C-H bond oxidation.

[135] Kunishita A., Ishimaru H., Nakashima S., Ogura T., Itoh S., *J. Am. Chem. Soc.*, **2008**, 130, 4244−4245

[136] Diaz D. E., Bhadra M., Karlin K. D., *Inorg. Chem.*, **2019**, 58(20), 13746-13750.

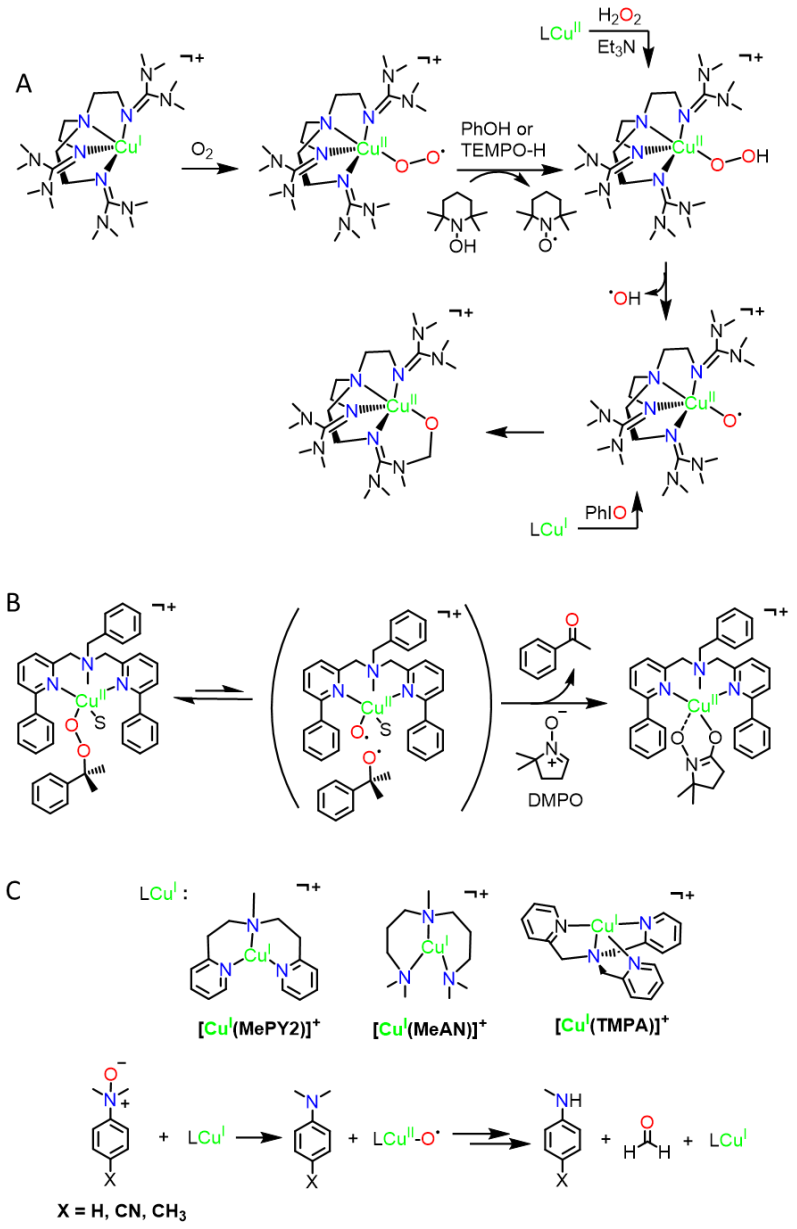

Figure 6.3.1 Chemical systems which have provided indirect evidence for the formation of copper(II)-oxyl specie

Although the copper(II)-oxyl species have not been observed experimentally in solution, protonation of a copper(II)-oxyl species would generate a copper(III)-OH (conjugate acid of copper(II)-oxyl species). This has been studied and characterized in recent works from the Tolman group[69a-c,137,138]and shown to be able to oxidize some strong C-H bonds.[139,140] They synthesized a series of copper(III)-OH intermediates through 1-electron oxidation of the corresponding copper(II)-OH precursors bearing an electron donating tridentate dianionic ligand (Figure 6.3.2A). They also studied the reactivity of copper(III)-OH species showing that this species can perform HAA from substrates with C-H bond BDE ranging from 76 kcal/mol (9,10-dihydroanthracene) to 99 kcal/mol (cyclohexane). Therefore, the copper(III)-OH species was considered as a viable alternative in the proposed mechanisms for oxidation in LPMOs (shown in Figure 6.3.2B). Those also can be envisioned for other copper oxygenase such as PHM, DβM or pMMOs. In the future, not only copper(II)-oxyl but also copper(III)-OH species requires considerable research. Recently, the Garcia-Bosch group[141] got the crystal structure of a mononuclear copper(II)-OH complex ($[L^{3-}CuOH]^{2-}$, shown in

---

[137] Spaeth A. D., Gagnon N. L., Dhar D., Yee G. M., Tolman W. B., *J. Am. Chem. Soc.*, **2017**, 139, 4477-4485.

[138] a) Gagnon, N., Tolman, W. B., *Acc. Chem. Res.*, **2015**, *48*(7), 2126-2131. b) Ciano L., Davies G. J., Tolman W. B., Walton P. H. B., *Nat. Catal.*, **2018**, 1(8), 571-577.

[139] Dhar D., Yee G. M., Markle T. F., Mayer J. M., Tolman W. B., *Chem. Sci.*, **2017**, 8, 1075-1085.

[140] Mandal M., Elwell C. E., Bouchey C. J., Zerk T. J., Tolman W. B., Cramer C. J., *J. Am. Chem. Soc.*, **2019**, 141(43), 17236-17244.

[141] Wu T., MacMillan S. N., Rajabimoghadam K., Siegler M. A., Lancaster K. M., Garcia-Bosch I., *J. Am. Chem. Soc.*, **2020**, *142*(28), 12265-12276.

Figure 6.3.2C) which was supported by a tridentate redox-active ligand and stabilized through intramolecular H-bonds between the H-donors of the ligand and the hydroxide anion. This $[L^{3-}CuOH]^{2-}$ complex could undergo two reversible oxidation processes to produce two metastable "high-valent" copper(II)-OH species ($[L^{2-}CuOH]^{1-}$ and $[L^{-}CuOH]$) by adding stoichiometric amounts of $1e^-$ oxidants (ferrocenium). The copper(II)-OH in higher oxidation states could react with the phenolic O-H in a series of 4-substitued-2,6-di-tert-butylphenols via two consecutive $1H^+/1e^-$ processes, differing from the $1H^+/1e^-$ reactivity of the above mentioned copper(III)-OH systems.

Besides, in LPMOs, the deprotonated N-terminus or the N-methylated histidine of the active site can increase electron density to stabilize the copper-oxyl intermediate. In particular, in fungal LPMOs the Try residues also have a proposed role in stabilizing the copper(II)-oxyl. Computational and UV-Vis studies have suggested that by treating the reduced AA9LPMOs with H_2O_2 a Cu(II)-Tyr radical species is formed (shown in Figure 6.3.2D).[142] This species is inactive for oxidation of saccharide substrates, but it offers a new perspective into the oxidative reaction mechanism of LPMOs.

[142] a) Paradisi A., Johnston E. M., Tovborg M., Nicoll C. R., Ciano L., Dowle A., Walton P. H., *J. Am. Chem. Soc.*, **2019**, 141(46), 18585-18599. b) Singh R. K., Blossom B. M., Russo D. A., Singh R., Weihe H., Andersen N. H., Bjerrum M. J., *Chem. Eur. J.*, **2020**, 26(2), 454-463.

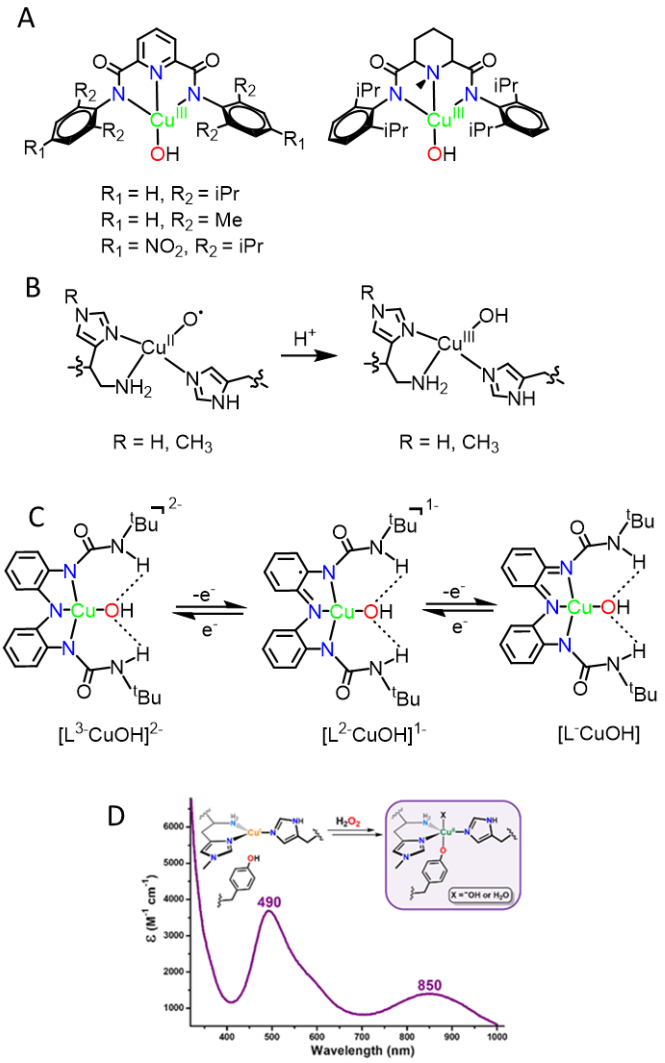

Figure 6.3.2 (A) Copper(III)-OH complexes designed by Tolman group; (B) Copper(II)-oxyl and its conjugate acid Copper(III)-OH as reactive intermediates in the active site of LPMOs; (C) The reduction/oxidation of three oxidation states of Copper(II)-OH complexes ;(D) Proposed copper(II)-Try radical species in the active site of LPMOs (*J. Am. Chem. Soc.*, **2019**, 141(46), 18585-18599.)

In this part, we described several reports that estimate and predict the possible Cu(II) active intermediate in copper monooxygenases through computational and experimental method. Still, large differences in the ligands from the active site of LPMO and the range of different species observed makes it difficult to draw direct conclusions from the models for potential intermediates (Cu-superoxide, Cu-oxyl) of LPMOs.

7. Small molecule models relevant to LPMOs

As we discussed above, the details of the mechanism and the potential intermediates in the key C-H activation step need to be determined. Although Cu(II)-superoxide and Cu(II)-oxyl species have been suggested as the reactive intermediates, synthetizing models may be a useful way to prove which are plausible. In this regard, a large number of small molecule copper complexes exist that can bind to oxygen in a variety of different structures.[143] Much early work by Tolman, Karlin, Itoh, Stack, and others have shown the variety of ligands that can be used for O_2 activation and the variety of structures that can form.[69b,144]

For example, the Stack group reported the synthesis of dicopper(III) bis(μ-oxide) complex **2** ligated by propylenediamine through a ligand substitution strategy (core capture) from complex **1** (shown in Figure 7.1A). The same strategy was used to show that the histamine with mixed imidazole and primary amine ligation could stabilize the dicopper(III) bis(μ-oxide) species (**3, 4** in Figure 7.1 A) at low temperature, which was more compatible with the histamine ligation in copper enzymes. And they found that the imidazole and NH_2 binding resulted in strong donation to copper center and improved the

[143] a) Mirica L. M., Ottenwaelder X., Stack T. D. P., *Chem. Rev.*, **2004**, 104(2), 1013-1046. b) Lewis E. A., Tolman W. B., *Chem. Rev.*, **2004**, 104(2): 1047-1076. c) Wendlandt A. E., Suess A. M., Stahl S. S., *Angew. Chem. Int. Ed.*, **2011**, 50(47), 11062-11087.

[144] a) Liu J. J., Diaz D. E., Quis, D. A., Karlin K. D., *Isr. J. Chem.*, **2016**, 56(9-10), 738-755. b) Itoh S., *Acc. Chem. Res.*, **2015**, 48(7), 2066-2074. c) Citek C., Lin B. L., Phelps T. E., Wasinger E. C., Stack T. D. P., *J. Am. Chem. Soc.*, **2014**, 136(41), 14405-14408.

energetic stabilization of Cu(III) species.[145] After they reported the direct oxygenation of a histamine-copper(I) complex and formation of a mixture of dinuclear with trinuclear Cu(III) species. These Cu(III) species also could be synthesized by using a bisimidazole ligand (shown in Figure 7.1B).[146] It should be noted that this work was aimed at modeling other metalloenzymes but is nevertheless relevant to LPMO.

[145] a) Citek C., Gary J. B., Wasinger E. C., Stack T. D. P., *J. Am. Chem. Soc.*, **2015**, 137(22), 6991-6994. b) Citek C., Lin B.-L., Phelps T. E., Wasinger, E. C., Stack, T. D. P., *J. Am. Chem. Soc.*, **2014**, 136, 14405−14408.

[146] a) Gary J. B., Citek C., Brown T. A., Zare R. N., Wasinger E. C., Stack, T. D. P., *J. Am. Chem. Soc.*, **2016**, 138(31), 9986-9995. b) Keown W., Large T. A., Chiang L., Wasinger E. C., Stack T. D. P., *Chem. Comm.*, **2019**, 55(51), 7390-7393.

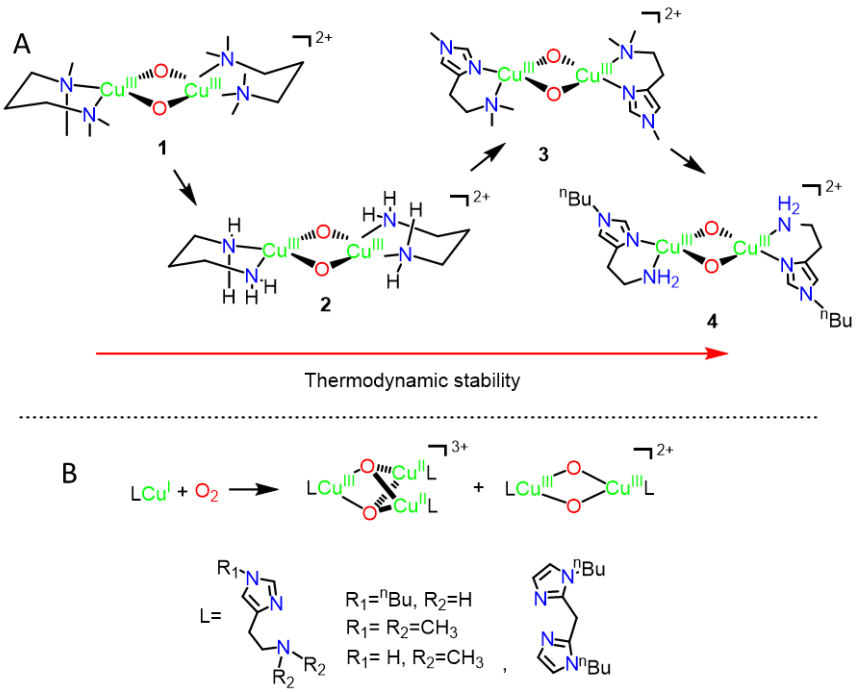

Figure 7.1 A) Histamine ligation core capture synthetic methodology with the rank ordered thermodynamic stability of dicopper(III) bis(μ-oxide) species; B) Direct oxygenation of copper(I)-histamine or copper(I)-imidazole yields mixtures of dinuclear and trinuclear species

In fact, little work has been focused on LPMOs. Despite the simplicity of the active site (two imidizaoles and a primary amine), it is difficult to replicate due to the coordination preferences of the metal and controlling the specific binding of each ligand. Nevertheless, aims to model the N_3 coordination have been made. Castillo et al.[147] synthesized Cu(II) complex based on the bis(benzimidazole)amine (2BB) ligand containing a secondary and a tertiary

[147] Castillo I., Neira A. C., Nordlander E., Zeglio E., *Inorganica Chim. Acta*, **2014**, 422, 152-157.

amine which coordination environment similar to the active site of LPMOs, but no oxidative reactivity was reported in this paper. Recently, they used the same 2BB ligand to prepare copper complexes [(2BB)Cu^{I}]OTf and [(2BB)$Cu^{II}(H_2O)_2$]$(OTf)_2$ as bioinspired models of LPMOs.[148] These copper complexes could interact with O_2, H_2O_2 and KO_2, and then oxidatively cleave cellobiose as a model polysaccharide substrate (Figure 7.2). During the reaction, the spectroscopic studies indicated that a proposed dicopper(II) side-on peroxide complex was generated. These intermediates are less relevant to LPMOs. Also, with regards to the histidine brace, it should be noted that the imidazole units are connected through the 2-postion rather than the 4 or 5-position and it contains a secondary amine rather than a primary amine.

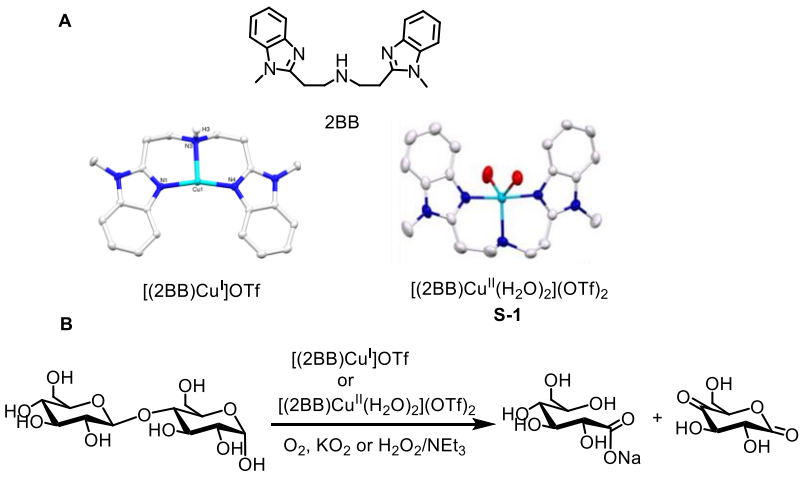

Figure 7.2 (A) Structure of ligand 2BB and the copper complex; (B) Cellobiose degradation by 2BB copper complex.

[148] Neira A. C., Martínez-Alanis P. R., Aullón G., Flores-Alamo M., Zerón P., Company A., Castillo I., *OACS omega*, **2019**, 4(6), 10729-10740.

Concia et al.[149] showed that tridentate complexes with both ligands L^{AM} and L^{IM}, which contain three N-atoms have been characterized as the first functional models for LPMOs (Figure 7.3). These complexes react with H_2O_2 in the presence a base (Et_3N) in water to form stable Cu(II)-hydroperoxo species with UV/Vis absorption bands 305nm and 375nm. More importantly, both complexes can react with a model substrate (p-nitrophenyl-β-$_D$-glycopyranoside) of cellulose at room temperature. But further studies are needed to verify the correlation of the Cu(II)-hydroperoxo species with the oxidative cleavage activity. P-nitrophenyl-β-$_D$-glycopyranoside was also employed as the model substrate to research other copper complex models for LPMOs.

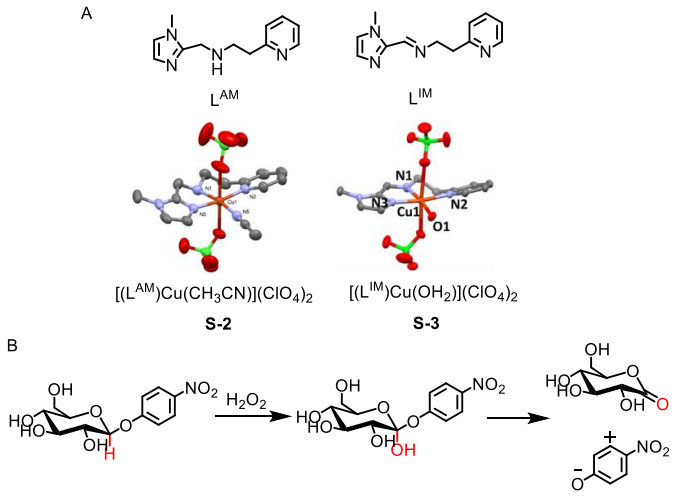

Figure 7.3 (A) The ligands (L^{AM}, L^{IM}) of modeling LPMOs and the crystal structure of [(L^{AM})(MeCN)Cu(II)](ClO_4)$_2$; (B) Oxidative cleavage of p-nitrophenyl-β-D-glycopyranoside

[149] Concia A. L., Beccia M. R., Orio M., et al., *Inorg. Chem.*, **2017**, 56(3), 1023-1026.

Mayilmurugan et al.[150] synthesized three copper(II) complexes (Figure 7.4A) based on the ligand including 1,4-diazepane backbone and pyridine unit to mimic N3 coordination environment of LPMOs. Most recently, the Itoh group[151] designed and synthesized a ligand (N-(2-(1H-imidazol-4-yl)-benzyl)histamine) (LH_3) and its copper(II) complex $Cu^{II}(LH_3)(tfa)_2$ (Figure 7.4B). This complex could meet the structural requirements of the 'histidine brace' in LPMOs and was the first ligand where the imidazole units are connected through the 4-position of the rings, similar to the enzyme.

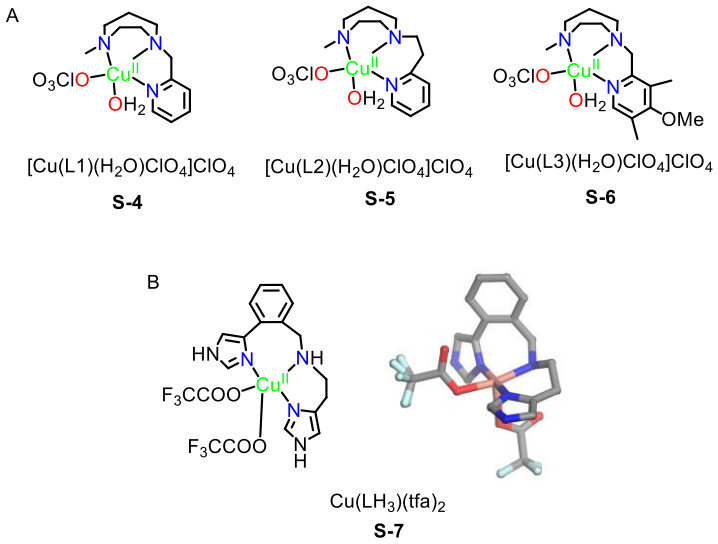

Figure 7.4 Structure of copper(II) complexes synthesized by Mayilmurugan group (A) and Itoh group (B)

[150] Muthuramalingam S., Maheshwaran D., Velusamy M., Mayilmurugan R., *J. Catal.*, **2019**, 372, 352-361.

[151] Fukatsu A., Morimoto Y., Sugimoto H., Itoh S., *Cheml. Comm.*, **2020**. DOI : 10.1039/D0CC01392G.

The physicochemical properties of these model complexes discussed above are summarized in Table 1. Except for complex **S-1**, the typical d-d band of these complexes in the UV-vis absorption spectrum all appear at around 600-660 nm, similar to the position of this band in LPMOs. The electron paramagnetic resonance (EPR) spectrum of all these complexes were also very close to those of LPMOs and other copper complexes in an N_3 coordination. Cyclic voltammetric measurements of the complexes showed a quasi-reversible redox couple at a range of potentials. However, to date, only the model complex **S-7** from the Itoh group was within the range of redox potentials of LPMOs so far been reported. They propose that this is due to the fact that in this model the twist angle of the two imidazole rings was 75°, which is very close to the average value (72°) of the reported copper(II) sites in LPMOs. Still, it should be noted that no substantial evidence was provided for this claim. Despite the advances in these model complexes, the development of new systems that can not only mimic the structure but also reproduce the physicochemical features of active site of LPMOs remain important.

Table 1. Comparison of the physicochemical properties of the Cu(II) model complexes for LPMOs

Complex[a]	Twist angle of trans-positioned imidazolyl group, °	UV-vis absorption of d-d band	Redox potetential	EPR parameters			
		λ_{max}, nm (ε,$M^{-1}cm^{-1}$)	E(Cu(II)/Cu(I)), mV vs SHE	$g_{\parallel}$	$g_{\perp}$	$A_{\parallel}$	$A_{\perp}$
Cu(II) active sites in LPMOs	43-86	615-650(37-113)	155-370	2.23-2.28	2.05-2.12	116-186	0.5-50
S-1	15	722(82)	76	2.021	2.157		
S-2	33	660(56)	5	2.258	2.068	172	
S-3	24	660(60)	5	2.270	2.064	170	
S-4		635(139)	8 (vs. NHS)	2.28	2.08	168	154
S-5		630(199)	41 (vs. NHS)	2.28	2.07	163	149
S-6		600(112)	112 (vs. NHS)	2.29	2.02	160	141
S-7	75	662(83)	323	2.266	2.062	158.9	12.61

a. The schematic structures of the complexes **S-1--S-7** are shown in figures **7.2-7.4**.

8. Using foldamer scaffolds to develop multi-layered coordination environments for mimic active site of LPMOs

Several small molecule copper complexes (as we discussed last part) have been synthesized and reported with the aim to replicate the active site of LPMOs and give some spectroscopic support for potential intermediates in the LPMO catalytic cycle. However, despite their structural similarity, these complexes have not been able to fully model the “histidine brace” coordination of the active site of LPMOs, especially the terminal NH_2 in the “histidine brace” motif, and the second coordination sphere interactions. But these also are important to the reactivity of LPMOs.

The amino acid residues in the second coordination sphere may not only have effects on the mechanism of substrate oxidation, but also the H-bonding formed by residues can be important to stabilize bound dioxygen (more details are shown in section 4.3). Additionally, the deprotonation of NH_2 in the “histidine brace” could help to stabilize the Cu(III) intermediate in the enzymatic active site. Finally, the twist angles of the two imidazoles in “histidine brace” could also influence the redox potentials thus affecting the reactivity. Taken together, it is necessary to develop suitable model complexes that can mimic not only the active site structure, but that can also allow these structural features and the second coordination sphere to be controlled or tuned in order to better study and understand the physicochemical features of active site of LPMOs.

However, the construction of such complex mimics containing both modifiable first and second coordination sphere is more challenging because of the increased difficulties in design and preparation. In the “histidine brace” active site of LPMOs, the histamine and imidazole groups are fixed in a particular position by the surrounding protein structure. This directs the formation a

specific complex between these components and copper. The specific arrangement of these functional groups must be carefully considered when designing the structure of model because an unsuitable position or arrangement of these functional groups will influence the cooperation with copper and the reactivity of the complexes. A scaffold approach could be one choice to develop better models of the “histidine brace”, which position the histamine and imidazole units.

Several examples wherein scaffolds could facilitate the construction of artificial molecules to mimic naturally metalloenzyme active sites have been reported (Figure 8.1).[152,153] The scaffold could be simply defined as a platform on which a metal-binding motif can be assembled, enforcing specific binding geometries, and/or allowing for multidentate ligands to be oriented in a specific fashion about the metal center.[154] The orientation (*cis*, *trans*, fluctional) information on a scaffold molecule can be used at the binding site of molecule, but also the scaffold can be modified and equipped with highly functionalized substituents to alter the binding affinity and specificity. For example, Holm et al.[155] used the trisubstituted benzene scaffold to synthesize [Fe_4S_3] clusters, and Lippard et al.[156] utilized the triptycene scaffold to model the bimetallic core of methane monooxygenase. Besides, there are a lot of reports to use anthracene as a scaffold in coordination chemistry for the assembly of trans-

[152] Shima S., Chen D., Xu T., Wodrich M. D., Fujishiro T., Schultz K. M., Hu X., *Nat. Chem.*, **2015**, *7*(12), 995.

[153] Sallmann M., Limberg C., *Acc. Chem. Res.*, **2015**, *48*(10), 2734-2743.

[154] Manes Taylor A., Michael J. Rose., *Coord. Chem. Rev.,* **2017**, 353, 295-308.

[155] Zhou J., Hu Z., Münck E., Holm R. H., *J. Am. Chem. Soc.*, **1996**, 118(8), 1966-1980.

[156] Li Y., Cao R., Lippard S. J., *Org. Lett.*, **2011**, 13(19), 5052-5055.

spanning diphosphine ligands for catalysis.[157] For example, the Rose group[158] synthesized an asymmetric anthracene scaffold that can support a facial set of biomimetic donors to model the active site of mono-iron hydrogenase and exhibit H_2 activation and hydride transfer activity.

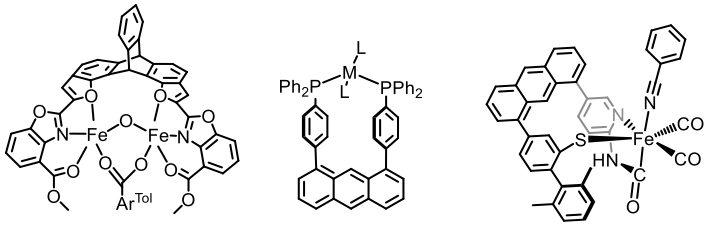

Figure 8.1 Examples of scaffold-based ligand metal complexes

Therefore, one option for modelling the active site of LPMOs would be the use of scaffold molecules to organize ligands in a specific orientation. This could allow the groups in the active site of LPMOs to be placed in a precise orientation and could allow better control of binding geometries when a primary amine is used. Specifically, a scaffold molecule that could position one histamine group and one imidazole *trans* to each other could provide the exact binding site. However, this requires a large enough spacing of the coordination sites to also accommodate the metal center. Additionally, through modifying the scaffold molecule, it could also be possible to incorporate hydrogen bond

[157] a) Kaganovsky L., Cho K. B., Gelman D., *Organometallics*, **2008**, 27(19), 5139-5145. b) Kaganovsky L., Gelman D., Rueck-Braun K., *J. Organomet. Chem.*, **2010**, 695(2), 260-266.

[158] Kerns S. A., Magtaan A. C., Vong P. R., Rose M. J., *Angew. Chem. Int. Ed.*, **2018**, 57(11), 2855-2858.

donor and acceptor groups or other functionalities that can mimic the SCS.[159]

However, major limitations of using the scaffolds include the size required and the need for a defined conformation. Because metal complexes usually are large, and the scaffold must be large and rigid with groups well placed. This can be synthetically challenging. Potential scaffold molecules include cavitands such as cyclodextrins[160] or calixarenes[161] or self-assembled cages. For example, Otte group[162] reported that an imidazole-functionalized cage was synthesized to coordinate with Cu(I) (shown in Figure 8.2A), and could catalyze the oxidation of benzylic alcohols to benzaldehydes. Additionally, cyclodextrins and calixarenes have been used as scaffolds, though the metal is often located outside of the cavity with its binging site pointing towards it. Recently, the Sollogoub and Riant groups synthesized cyclodextrin complexes where Cu(I) was encapsulated in a cyclodextrin capped with an N-heterocyclic carbene (shown in Figure 8.2B). This cyclodextrin complex could catch the isolated monomeric CuH moiety (Figure 8.2C). Moreover, it could control the chemoselective reductions of α,β-unsaturated ketones, Cu(I) α-cyclodextrin complexes promoted the 1,2-addtition exclusively and 1,4-addition was more favorable in presence of β-cyclodextrins macrocycle complexes.[163] Still,

---

[159] a) Rebilly J. N., Colasson B., Bistri O., *Chem. Soc. Rev.*, **2015**, 44(2), 467-489. b) Badetti E., dos Santos N. A. C., Scaramuzzo F. A., Bravin C., Wurst K., Licini G., Zonta C., *RSC Adv.*, **2018**, 8(35), 19494-19498.

[160] Tabushi I., Kuroda Y., *J. Am. Chem. Soc.*, **1984**, 106(16), 4580-4584.

[161] Parrot A., Collin S., Bruylants G., Reinaud O., *Chem. Sci.*, **2018**, 9(24), 5479-5487.

[162] Bete S. C., Würtele C., Otte M., *Chem. Comm.*, **2019**, 55(30), 4427-4430.

[163] a) Xu G., Leloux S., Zhang P., Meijide Suárez J., Zhang Y., Derat E., Ménand M., Bistri‐Aslanoff O., Roland S., Leyssens T., Riant O., Sollogoub

readily modifying cavitands or controlling the precise self-assembly of cages remains a challenge.

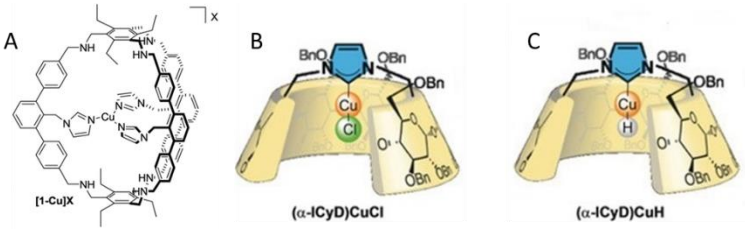

Figure 8.2 A) The molecular structure of Cu(I) cage complex; B) and C) Developed structure of the Cu(I) α-cyclodextrins macrocycle complexes

One way around these problems of scaffolds is to use a biomimetic approach, folding. This is the approach selected by nature to create well defined cavities, to position chemical groups in space with atomic precision, and to achieve high binding affinity and selectivity. This is what endows biopolymers with extraordinary functions such as enzyme catalysis in proteins and genetic information storage in nucleic acids.[164,165] Inspired by these, in the last decades, significant attention has been devoted to non-natural backbones which have the propensity to fold. These synthetic oligomers or polymers could be connected together to form large well-defined structures and have a strong conformational preferences as found in biopolymers. This class of molecules was termed foldamers. Foldamers are artificial folded molecular architectures or more precisely, oligomers that adopt stable higher-ordered

M., *Angew. Chem. Int. Ed.*, **2020**, 59(19), 7591-7597. b) Wen Z., Zhang Y., Roland S., Sollogoub M., *Eur. J. Org. Chem.*, **2019**, (15), 2682-2687.

[164] Anfinsen C. B., *Sci.*, **1973**, 181(4096), 223-230.

[165] Watson J. D., Crick F. H., *Nature*, **1953**, *171*(4356), 737-738.

structures in solution through non-covalent interactions.[166] When designing and developing foldamers, aromatic rich sequences have found significant use as potential backbones (Figure 8.3), and examples include oligo-phenylene-ethynylenes, [167] aryl-oligomers based on aza-heterocycles(pyridines, pyrimidines, pyridazines), [168] aromatic tertiary amide/imide/urea oligomers[169] and aromatic oligoamides.[170] Among these, aromatic oligoamide foldamers have been growing as an important class of foldamers, because of their remarkable properties, such as folded structures with high stability, folding modes with predictability and tunability, and ease of synthesis.[171]

---

[166] Hecht S., Huc I., eds., *John Wiley & Sons*, **2007**.

[167] Nelson J. C., Saven J. G., Moore J. S., Wolynes P. G., *Sci.*, **1997**, *277*(5333), 1793-1796.

[168] Bassani D. M., Lehn J. M., Baum G., Fenske D., *Angew. Chem. Int. Ed.*, **1997**, 36(17), 1845-1847.

[169] Tanatani A., Kagechika H., Azumaya I., Fukutomi R., Ito Y., Yamaguchi K., Shudo K., *Tetrahedron Lett.*, **1997**, 38(25), 4425-4428.

[170] a) Hamuro Y., Geib S. J., Hamilton A. D., *J. Am. Chem. Soc.*, **1996**, 118(32), 7529-7541. b) Berl V., Huc I., Khoury R. G., Krische M. J., Lehn J. M., *Nature*, **2000**, 407(6805), 720-723. c) Zhu J., Parra R. D., Zeng H., Skrzypczak-Jankun E., Zeng X. C., Gong B., *J. Am. Chem. Soc.*, **2000**, 122(17), 4219-4220.

[171] Guichard G., Huc I., *Chem. Comm.*, **2011**, 47(21): 5933-5941.

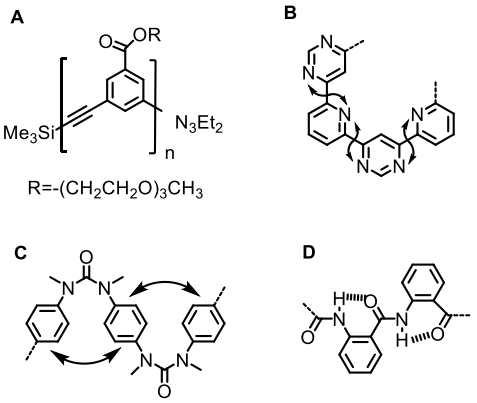

Figure 8.3 Examples of foldamer backbones. Phenylacetylene oligomers (A); Aza-aromatic oligomers (B); Tertiary aromatic ureas. Arrows represent intramolecular repulsive and attractive interactions

In the case of aromatic oligoamide foldamers, the oligomers consist of heterocyclic (or functionalized) aromatic units connected through amide bonds. The conjugation across the amide bond and adjacent aryl rings results in a rigid planar or close to planar system because the rotation of aryl-amide bonds is restricted compared with alkyl-amide bonds. The hydrogen bonds and specific electrostatic interactions between the endo- or exocyclic heteroatoms on the aromatic ring and the oxygen or N-H of the amides (in Figure 8.4 A) can give a preferred relative orientation on the amide oligomer backbones and forces the structures into well-defined conformations with different curvatures. This has led to the development of diverse monomers with heterocyclic amino acid, diacid or diamine (Figure 8.4 B). These monomers all have the endocyclic nitrogen atoms which are necessary to keep conformational stability.[172]

[172] Ferrand Y., Huc I., *Acc. Chem. Res.*, **2018**, 51(4), 970-977.

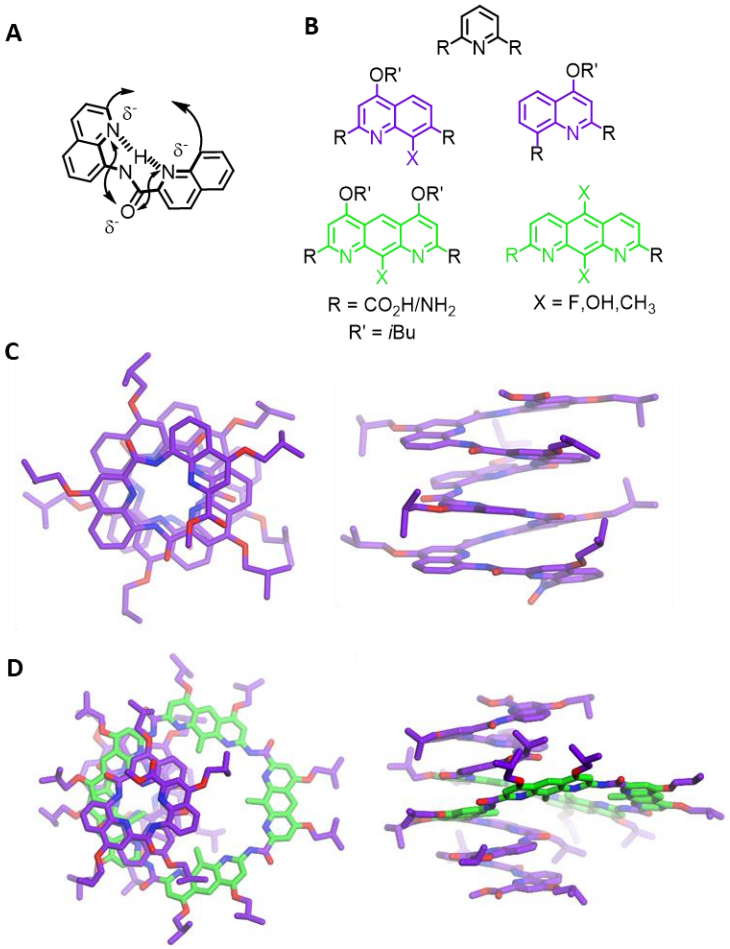

Figure 8.4 A) Interactions in aromatic oligoamide folding, hydrogen bonds (dotted lines) and electrostatic repulsions (arrows); B) Examples of aromatic amine/acid monomers; C) Example of crystal structures of a folded helical loop using quinoline as monomer; D) Example of crystal structures of a folded helical loop using quinoline and anthracene as monomers

Extending these to multiple monomers can lead to highly stable secondary structures and several groups have shown the power of these foldamers in the design of complex molecular structures including systems for molecular

recognition of guest molecules.[173] As shown in Figure 8.4 C.D, in the secondary structures, the local curvature and diameter depend on the monomer unit size, with large monomers giving larger diameters (low curvature). Therefore, with larger monomers, the secondary structures can become large enough to incorporate multiple convergent functional groups, which can allow binding the metal atom.[174] The ease of synthesis and often high yielding reactions with aromatic oligoamide foldamers also adds to their attractive aspects. Moreover, the functional groups can be easily exchanged through variation of the oligomer sequences. Such as, the R' group (Figure 8.4) can be changed and modified to provide more solubility and the X group in diazaanthracene can be varied to provide different potential steric interactions or electron donor groups. These properties of aromatic oligoamides are ideal for developing and modifying traditional scaffolds for coordination chemistry and biomimetics.

[173] a) Zhang D. W., Zhao X., Li Z. T., *Acc. Chem. Res.*, **2014**, 47(7), 1961-1970. b) Lautrette G., Wiche B., Kauffmann B., Ferrand Y., Huc I., *J. Am. Chem. Soc.*, **2016**, 138(32), 10314-10322. c) Juwarker H., Suk J. M., Jeong K. S., *Chem. Soc. Rev.*, **2009**, 38(12), 3316-3325.

[174] a) Singleton M. L., Pirotte G., Kauffmann B., et al., *Angew. Chem. Int. Ed.*, **2014**, 53(48), 13140-13144. b) Mateus P., Wicher B., Ferrand Y., et al., *Chem. Commun.*, **2017**, 53(67), 9300-9303.

Chapter II

Objectives

LPMOs plays an important role in the oxidative degradation of the carbohydrate polymer components of lignocellulosic biomass. Understanding how the geometric and electronic features of the active site ("histidine brace") and second coordination sphere contribute to the reactivity of the enzymes can help to better understand how nature designs such powerful catalysts. One approach for studying metalloenzymes is through the development of model complexes or biomimetics, molecules that replicate or mimic certain structural features. By replicating or mimicking certain features of the natural system, these model complexes can help better understand the relationship between different structural and reactive or electronic properties.[1] Developing good models or biomimetics is thus important.

A handful of small molecule models of LPMO have been described that mimic the N_3 coordination to copper, however few of these complexes are able to replicate the reactivity or properties of LPMO. This may be for several reasons, for example, the 2-position of imidazole was used to connect with the amine group rather than the 4-position of imidazole as in the active site of LPMOs or the use of a secondary amine group rather than the primary amine

[1] Halime Z., Kieber-Emmons M.T., Qayyum M.F., Mondal B., Gandhi T., Puiu S.C., Chufán E. E., Sarjeant A.A.N., Hodgson K. O., Hedman B., Solomon E.I., Karlin K.D., *Inorg. Chem.*, **2010**, 49, 3629.

coordination found in the enzyme. These structures also did not explore the influence of the imidazole methylation on the reactivity or properties. Most recently, the Itoh group have also suggested that the torsion angle between the two heterocyclic rings could also influence the electronic properties, though to study this aspect additional models with different torsion angles are needed.

Therefore, the main aim of this thesis is to design new small molecule models with two imidazole groups that better match the first coordination sphere features (especially the connection of the 4-position of the imidazoles with the alkyl amine group) and that can be used to study the effect that imidazole orientation (chelate ring size, torsion angles) and methylation patterns have on the properties and reactivity of the metal. Additionally, as small molecule models just mimic the first coordination sphere of LPMOs, they ignore the additional layers of functional group present in the enzyme, which could provide second coordination sphere interaction influencing the reactivity of enzyme. Because of this, we also set out to develop molecular systems to mimic both first and second coordination spheres in LPMOs and replicate the exact binding histidine brace motif. This work is divided into the specific aims shown below:

1. Based on the ideas proposed by Itoh and co-workers, new small molecule N_3 ligands were designed and their synthesis targeted. These models with two imidazoles and a secondary amine can be used to look at the role of the first coordination sphere. Varying the chelate ring size should lead to changes in the torsion angle between the imidazoles as a result of the five or six membered rings. Additionally, the N-methylated and non-methylated imidazole derivatives can be compared. This should lead to a better understanding of how these structural modifications influence the properties and reactivity of copper.

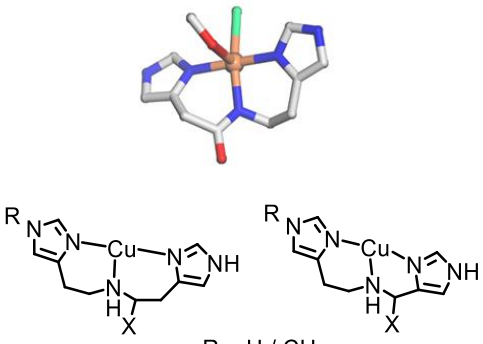

2. Show that organic scaffolds, including conformationally stable and predictable aromatic oligoamides, can be used to design novel ligands that contain a histidine brace like binding site. As an initial approach, these can be constructed from two types of monomers, quinolines and diazaanthracene. The quinolines can be functionalized by imidazole or histamine through two different strategies to mimic the first coordination sphere (histidine brace motif). These monomers could be connected to a central diazaanthracene unit that would act as a spacer to provide the appropriate distance between the imidazoles. Because the histamine and imidazole groups would be held in place by the scaffold, this approach could allow easily incorporating the primary amine group and also second coordination sphere interactions.

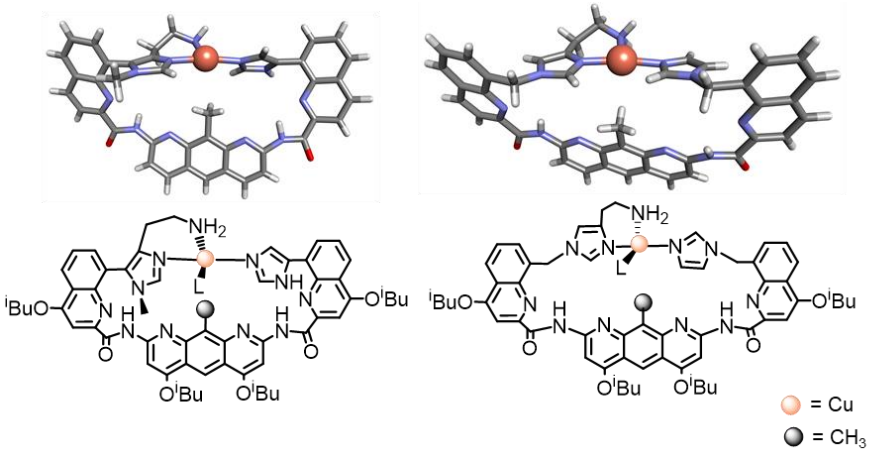

3. Finally, using the p-nitrophenyl-β-D-glycopyranoside assay reported by Conica et al for the study of LPMO models,[2] study the reactivity of the new model complexes using UV to monitor the oxidation reaction via the formation of p-nitrophenolate.

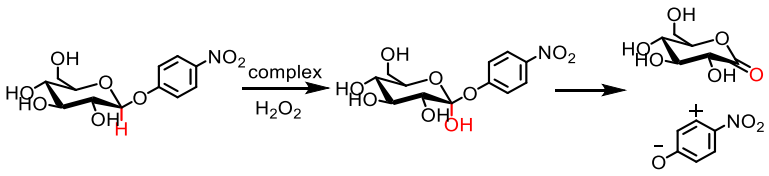

[2] Concia A. L., Beccia M. R., Orio M., Ferre F. T., Scarpellini M., Biaso F., Simaan A. J., *Inorg. Chem.*, **2017**, 56(3), 1023-1026.

Chapter III

Small Molecule Models Relevant to LPMOs

A full understanding of how the structural and electronic properties of the LPMO active site influence the reactivity of the enzyme is complicated by the large size of the protein. Small molecule models of the active site can be a useful tool for elucidating some of these aspects. Indeed, in the field of metalloenzyme biomimetics, the design of small metal complexes that match structural features of the active site (first coordination sphere) have been of significant importance for understanding mechanisms or interpreting spectroscopic data of biological molecules.[1] In this chapter we will discuss the design and work towards new small molecule model complexes of LPMO.

As mentioned in chapter I (section 7), a handful of small molecule models of the active site of LPMOs were reported,[2] Figure 1. Although these ligands

[1] Rebilly J. N., Colasson B., Bistri O., et al., *Chem. Soc. Rev.*, **2015**, 44(2), 467-489.

[2] a) Concia A. L., Beccia M. R., Orio M., Ferre F. T., Scarpellini M., Biaso F., Simaan A. J., *Inorg. Chem.*, **2017**, 56(3), 1023-1026. b) Scarpellini M., Neves A., Hörner R., Bortoluzzi A. J., Szpoganics B., Zucco C., Passos W. A., *Inorg. Chem.*, **2003**, 42(25), 8353-8365. c) Ferre F. T., Resende J. A., Schultz J., Mangrich A. S., Faria R. B., Rocha A. B., Scarpellini M., *Polyhedron*, **2017**, 123, 293-304.

support the N_3 coordination to copper and contain some aspects of the active site of LPMOs, there are a number of limitations with these reported systems.

In these cases, most imidazole units in Figure 1 complexes **1-6** were methylated limiting the study of the effect of this modification. Additionally, the connectivity between the imidazole and the amine group was through the 2-position of the imidazole in most of the small molecule ligands (**1 - 6** in Figure 1). This could have important electronic effects on the reactivity. Notably, a 2-position C-H would be oriented towards the nearby equatorial site and could provide an electrostatic interaction important for substrate binding or reactivity. Based on these results, the Itoh group recently designed and synthesized complex **7**, where the substituent position of imidazole was at the 4-position and the twist angle of the two imidazole rings were at 75°, similar to the average value of 72° in LPMOs. In their work, they suggested that this twist angle of the two heterocyclic donor groups was highly important for the electronic properties of the complex model. Though due to the limited number of similar complexes for comparison, this remains largely conjecture. Additionally, it should be noted that their model did not look at the effect of imidazole methylation.

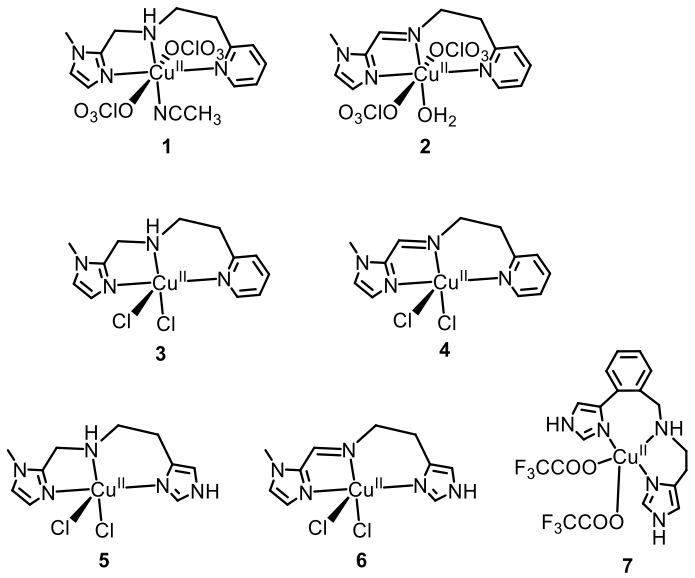

Figure 1. Schematic structures of Cu(II) complexes bearing T-shaped N3 tridentate ligand containing imidazolyl groups

As the observed twist angle in the Itoh complex is derived largely by the nature of the chelate rings, variations in this parameter could be interesting to study their effects on twist angle deviation and electronic properties. Indeed, the size of the chelate ring alone also has been shown to be important for the metal based properties. In another study, Itoh and co-workers looked at ligand effects on the structure and reactivity of copper(I) complexes using bis (pyridine-2-ylalkyl)amine ligands, shown in Figure 2.[3,4] They found that the electron-donor ability of pyridine and the dioxygen activation ability increases with decreasing chelate ring size and steric bulk, from **L4^{R}** to **L1^{R}**.

[3] Osako T., Terada S., Tosha T., Nagatomo S., Furutachi H., Fujinami S., Itoh S., *Dalton Trans.*, **2005**, (21), 3514-3521.

[4] Itoh S., Tachi Y., *Dalton Trans.*, **2006**, (38), 4531-4538.

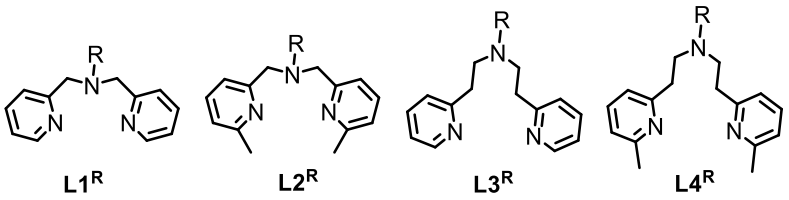

Figure 2. Examples of bis(pyridine-2-ylalky)amine tridentate ligands (**L1^{R}**, **L2^{R}**, **L3^{R}**, **L4^{R}**)

For the design of models to mimic the active site of LPMOs, it is necessary to take into account factors including different chelate ring sizes, the twist angles of two heterocyclic groups, methylation and the position by which the imidazole is connected. A series of molecules to systematically explore these modifications will be important for understanding their individual effects.

1. Small molecule complexes design

Based on the aspects discussed above, we designed a new series of small molecule complexes with different sizes for the chelate rings, either methylated or non-methylated in histamine, shown in Scheme 1.

For the initial ligand designs, **3.001**, **3.002** and **3.003**, **3.004**, we planned to react the corresponding imidazole aldehydes directly with histamine or 1-methylhistamine followed by reduction of the imine intermediate with sodium borohydride. In parallel, it was envisaged that the new ligands **3.009**, **3.010** **3.011**, and **3.012**, containing amide bonds, could also be readily obtained and offer both an alternative route to **3.001-3.004** and a separate series of ligands with potentially strong donor abilities.

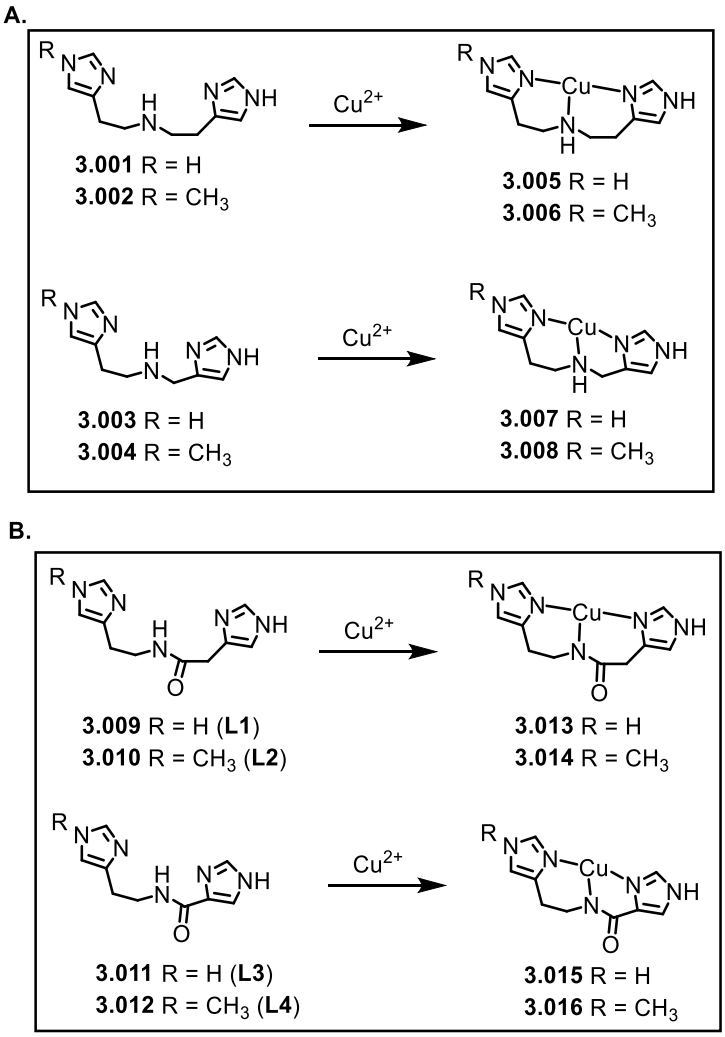

Scheme 1: A. Initial design ligands and corresponding complexes;
B. The new design ligands and corresponding complexes

2. Synthesis of initial designed ligands

2.1 Schiff base approach

The synthetic strategy of the initially designed ligands is shown in Scheme 2, the imidazole acetaldehyde (**3.019**) and imidazole carbaldehyde (**3.020**) were directly reacted with histamine or methylated histamine, to form four different Schiff bases. These were then subsequently subjected to reduction with sodium borohydride.

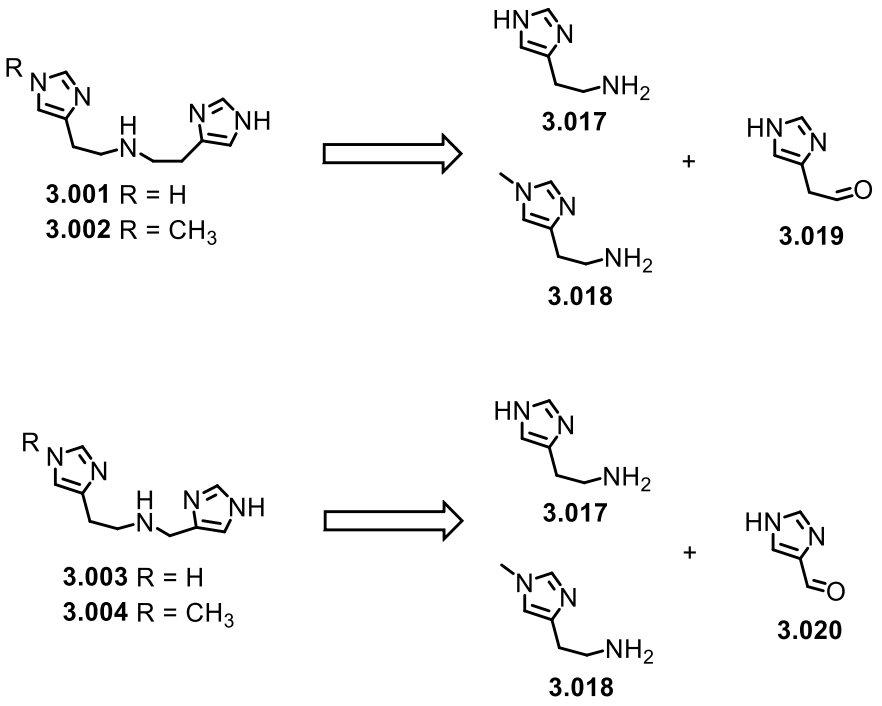

Scheme 2: The retro synthesis of the initial designed ligands

To reach ligand **3.001** and **3.002**, monomer **3.018** and **3.019** were first synthesized. As shown in Scheme 3, the synthesis of methylated histamine **3.018** started from histamine. Histamine dihydrochloride **3.021** was reacted

with carbonyl diimidazole (CDI) to give cylic urea **3.022**. Then **3.022** was methylation by methyl iodide, followed by hydrolysis, to give 1-methylated histamine **3.018**.

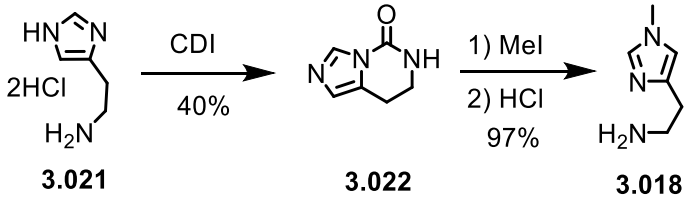

3.021 **3.022** **3.018**

Scheme 3: Synthesis of **3.018**

The synthetic approach of **3.019** is shown in Scheme 4. First, imidazole carbaldehyde **3.020** was protected with triphenylmethyl groups to form **3.023**. Then the reaction between trityl-protected imidazole aldehyde **3.023** and phosphonate **3.024** was tested with various bases. Unfortunately, none of them gave the desired product. Similarly, the Wittig reaction also was tested using different bases and solvents, but the result was the same. This led us to put the synthesis of **3.001** and **3.002** on hold while the synthesis of the other ligands was attempted.

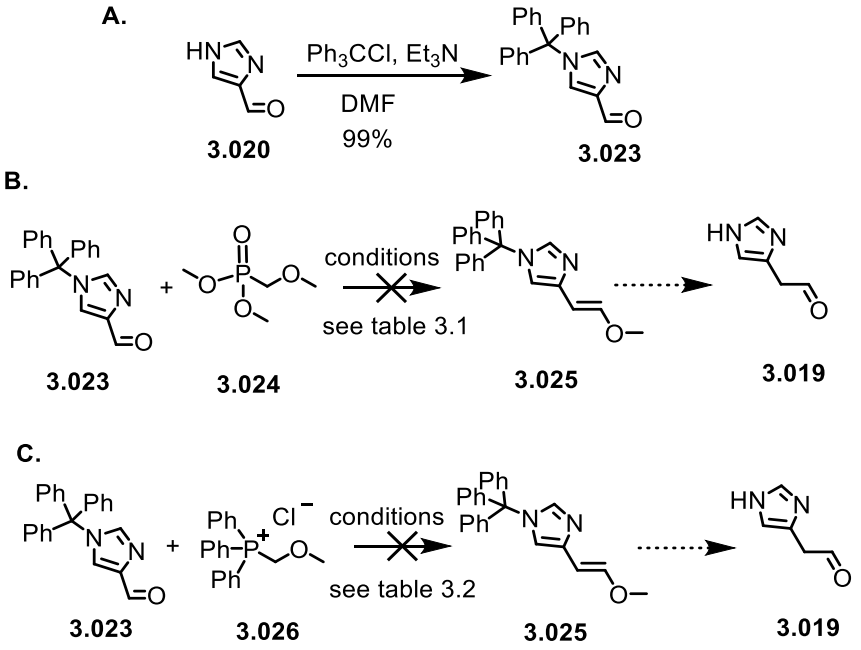

Scheme 4: A. Tritylation of aldehyde **3.020**. B. Horner-Emmons reaction towards **3.019**. C. Witting reaction towards **3.019**

Table 3.1 Reaction conditions attempted for Horner-Emmons reaction

Entry	Conditions	Solvent	Result
1	NaHMDS, -78ºC	THF	Starting material
2	KHMDS, -78ºC	THF	Starting material
3	LDA, -78ºC	THF	Starting material
4	tBuOK, -78ºC/0 ºC	THF	Starting material
5	NaH, -78ºC/0 ºC	THF	Starting material

Table 3.2 Reaction conditions attempted for Witting reaction

Entry	Conditions	Solvent	Result
1	NaH, RT	THF	Starting material
2	tBuOK, 0 °C	THF/Toluene	Starting material
3	n-BuLi, -78°C	THF	Starting material

For ligands **3.003** and **3.004**, the synthetic route that we designed began with the commercially available imidazole carbaldehyde **3.020**. Based on other literature procedures, in order to form the imine between **3.020** and **3.017** or **3.019**, the histamine and 1-methylated histamine hydrochloride salts needs to be neutralized,[5] prior to imine formation and then reduction with sodium borohydride. The reaction with histamine **3.017** was tested with various bases (Scheme 5) for the neutralization and different acids/catalysts and solvents for the imine formation, unfortunately all of the reactions failed and no imine formation was observed by NMR.

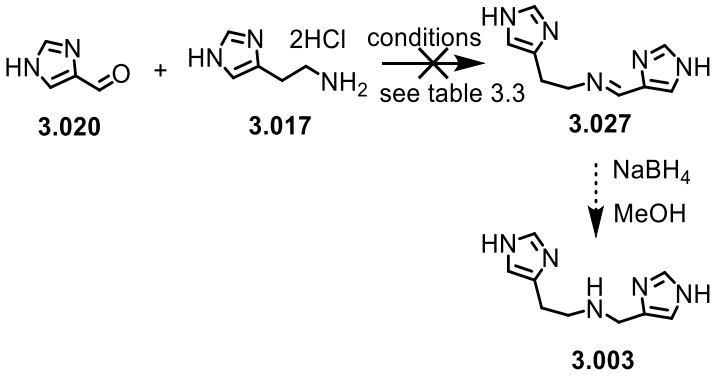

3.020 **3.017** **3.027** **3.003**

Scheme 5: Attempted conditions for the formation of Schiff base

[5] Hagiwara H., Nishi K., Matsumoto N., Sunatsuki Y., Kojima M., Iijima S., *Bull. Chem. Soc. Jpn.*, **2011**, 84(3), 306-311.

Table 3.3 Reaction conditions attempted for the formation of Schiff base

Entry	Conditions	Solvent	Result
1	NaOH, AcOH, RT/Reflux	EtOH	No product
2	NaOH, TFA, RT/Reflux	EtOH	No product
3	NaOH, AcOH, RT/Reflux	MeOH	No product
4	NaOH, TFA, RT/Reflux	MeOH	No product
5	NaOH, MS3Å, 50°C	MeOH	No product
6	KOH, AcOH/TFA, RT/Reflux	MeOH	No product
7	NaOH, PTSA/AcOH, Reflux	MeOH	No product

Based on these unpromising results and the limited reactivity of the imidazole carboxaldehyde for the formation of imidazole acetaldehyde **3.019**, we supposed that this is because the imidazole carboxaldehyde **3.020** is not sufficiently reactive. As such, we did not test the reaction with the more synthetically expensive **3.018** and instead looked into another synthetic pathway.

2.2 Alkylation approach

The second route we designed to synthesize the ligands is shown in Scheme 6 and starts from bromo- and chloro-ethylimidazlole **3.029** or chloro-methylimidazole **3.033**. These halogenated derivatives could then be used to alkylate N-Boc protected histamine or 1-methylhistamine.

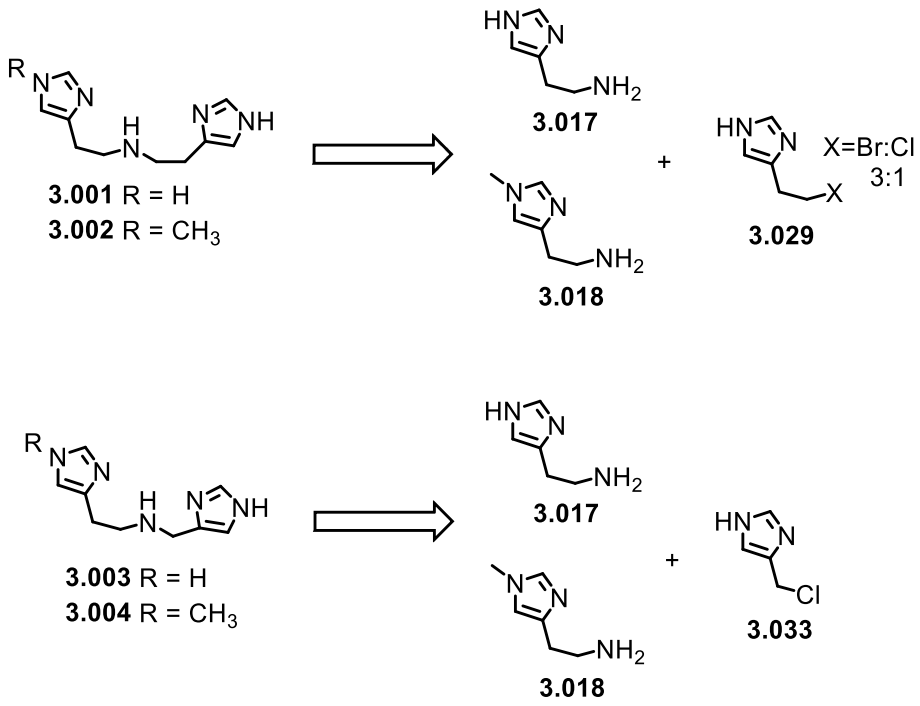

Scheme 6: The retro synthesis of the initial designed ligands

In this synthetic sequence, halogenation of histamine dihydrochloride **3.017** is accomplished by dissolution in sulfuric acid and potassium bromide, followed by addition of sodium nitrite. This provided the corresponding bromo- and chloro-enthylimidazoles **3.029** in 50% yield, about 3:1 bromo-/chloro-mixture as described in literature.[6] The chloride in this case comes from the HCl of the hydrochloride salt. To avoid over alkylation, the primary amine of 1-methylhistamine **3.018** was protected with a Boc group to give compound **3.030**, and the histamine **3.017** was first fully protected with Boc groups at both the primary amine and imidazole nitrogen, leading to compound **3.027**,

[6] Shapiro J. A., Wencewicz T. A., *ACS Infect. Dis.*, **2016**, *2*(2), 157-168.

which was then selectively deprotected on the nitrogen of imidazole ring in the presence of potassium carbonate in methanol to get the product **3.028**.[7] For the next reaction, the bromo- and chloro-ethylimidazole **3.029** was reacted with the Boc amine in the protected 1-methylhistamine **3.030** in the presence of DMF at 80 °C. Different conditions were tried for this reaction (Scheme 7), but none of these gave the desired product.

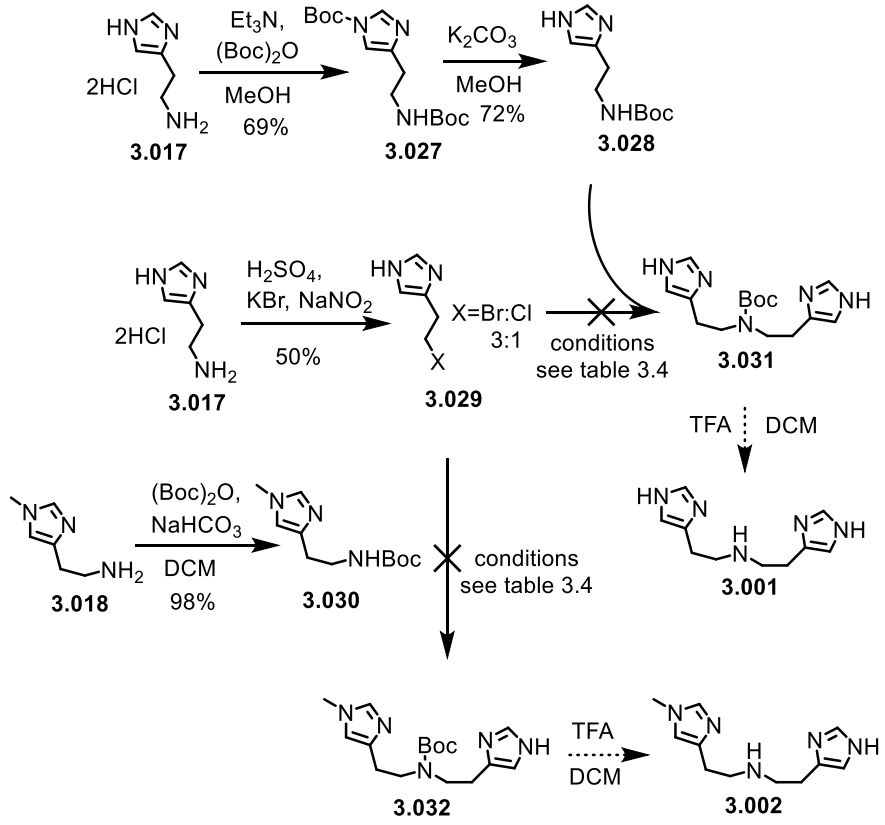

Scheme 7: The second synthetic route of the monomers and ligand **3.001** and **3.002**

[7] Abdo M. R., Joseph P., Boigegrain R. A., Liautard J. P., Montero J. L., Köhler S., Winum J. Y., *Bioorg. Med. Chem.*, **2007**, *15*(13), 4427-4433.

Table 3.4 Reaction conditions attempted for compound **3.031/3.032**

Entry	Conditions	Solvent	Result
1	80ºC	DMF	No product
2	NaH, RT	DMF	No product
3	K_2CO_3, KBr, RT/60ºC	MeCN	No product

A similar approach using a benzyl protecting group, instead of a Boc group, was also applied. As shown in Scheme 8, reductive amination of benzaldehyde with histamine **3.017** afforded the desired compound **3.033**.[8] Although various conditions were tested in the next coupling step, unfortunately, none led to the desired product **3.034** (Scheme 8).

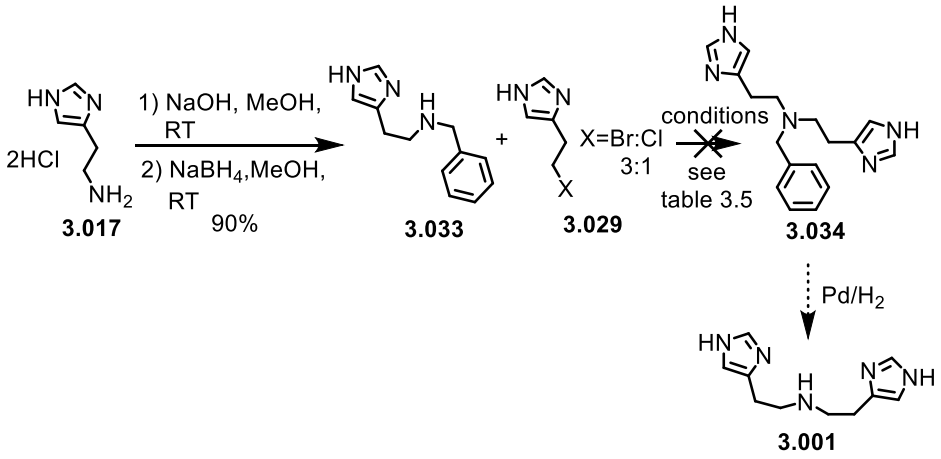

Scheme 8: Benzyl protection and coupling

[8] Shimasaki Y., Kiyota H., Sato M., Kuwahara S., *Tetrahedron*, **2006**, *62*(41), 9628-9634.

Table 3.5 Reaction conditions attempted for compound **3.034**

Entry	Conditions	Solvent	Result
1	80ºC	DMF	No product
2	NaH, RT	DMF	No product
3	K_2CO_3, KBr, RT/60ºC	MeCN	No product
4	K_2CO_3, KBr, RT/60ºC	DMF	No product

For the ligand **3.003** and **3.004**, in order to get the chloromethyl-imidazole monomer **3.033**, the synthesis started from imidazole carbaldehyde **3.020** treated with $NaBH_4$ reduction to result in the hydroxymethyl imidazole **3.035**.[9] Then **3.035** was prepared by chlorination with thionyl chloride to the chloromethyl imidazole **3.033**. After, the coupling was tested with both, no methylation histamine **3.028** and methyl-histamine **3.030** in the presence of chloromethyl imidazole **3.033** were observed. As far as the conditions we tested, the reaction did not react at all (Scheme 9).

[9] a) Matziari M., Bauer K., Dive V., Yiotakis A., *J. Org. Chem.*, **2008**, 73(21), 8591-8593. b) Madsen C., Jensen A. A., Liljefors T., Kristiansen U., Nielsen B., Hansen C. P., Frølund B., *J. Med. Chem.*, **2007**, 50(17), 4147-4161.

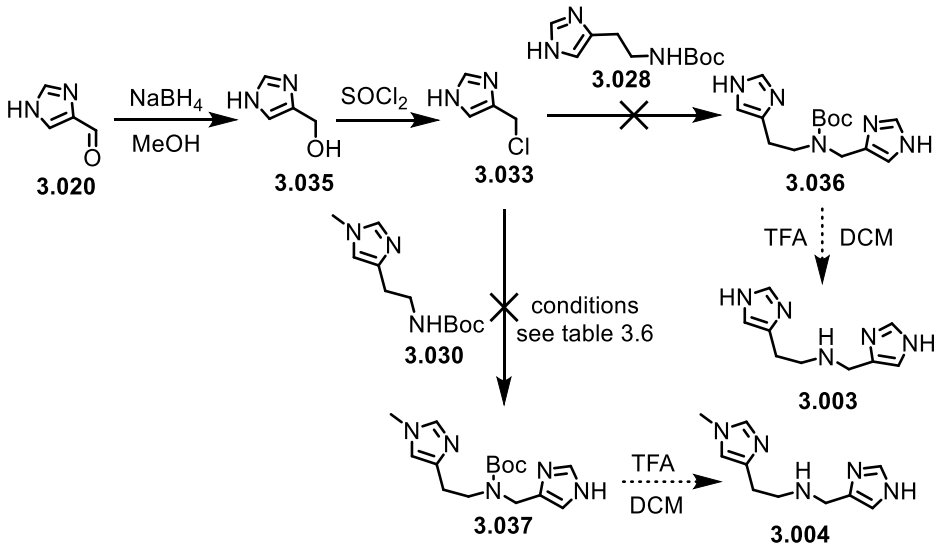

Scheme 9: The second synthetic route of the ligand **3.003** and **3.004**

Table 3.6 Reaction conditions attempted for compound **3.037**

Entry	Conditions	Solvent	Result
1	80°C	DMF	No product
2	NaH, RT	DMF	No product
3	K_2CO_3, RT	DMF	No product
4	Cs_2CO_3, RT	DMF	No product

2.3 Amide bond approach

As none of the above approaches gave the final products, we decided to modify the ligands. The new synthetic route was based on amide coupling between commercially available 4-imidazoleacetic acid hydrochloride **3.038**, 4-Imidazolecarboxylic acid **3.039** and histamine **3.017**, 1-methylated histamine **3.018**, respectively (Scheme 10).

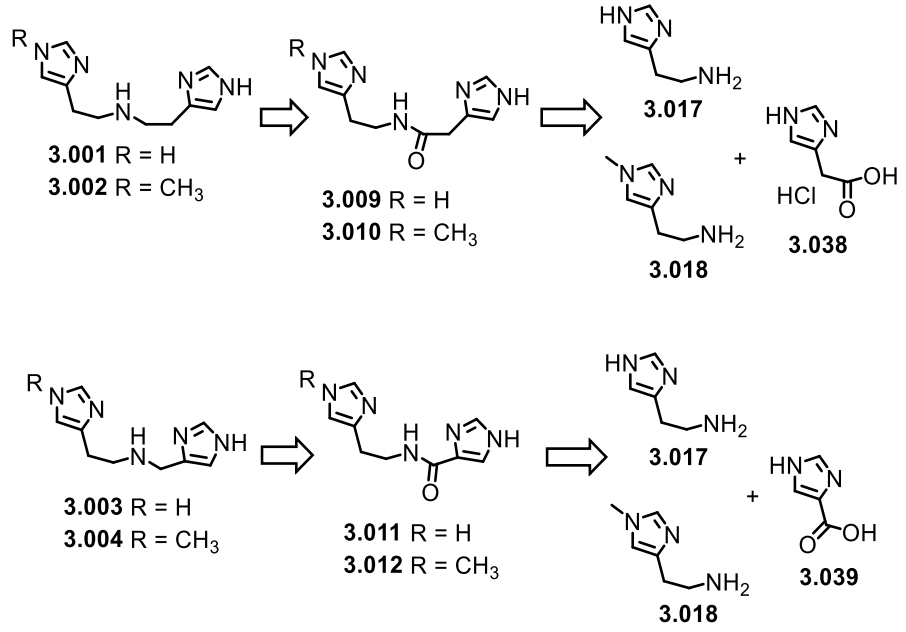

Scheme 10: The retro synthesis of the initial designed ligands

For the synthesis of long chain ligands **3.001** and **3.002**, this pathway started with neutralization of the hydrochloric acid salt of histamine using DIPEA as the base. Then the coupling reactions between 4-imidazoleacetic acid hydrochloride **3.038** and histamine **3.017** or 1-methylated histamine **3.018** were performed with PyBOP and DIPEA to give the carboxamide derivatives **3.009** and **3.010**. From these derivatives, it could also be possible to obtain the amine ligands, targeted in **2.1** and **2.2**, via reduction of the amide bond, (Scheme 11). However, none of our attemps at this reduction yielded positive results.

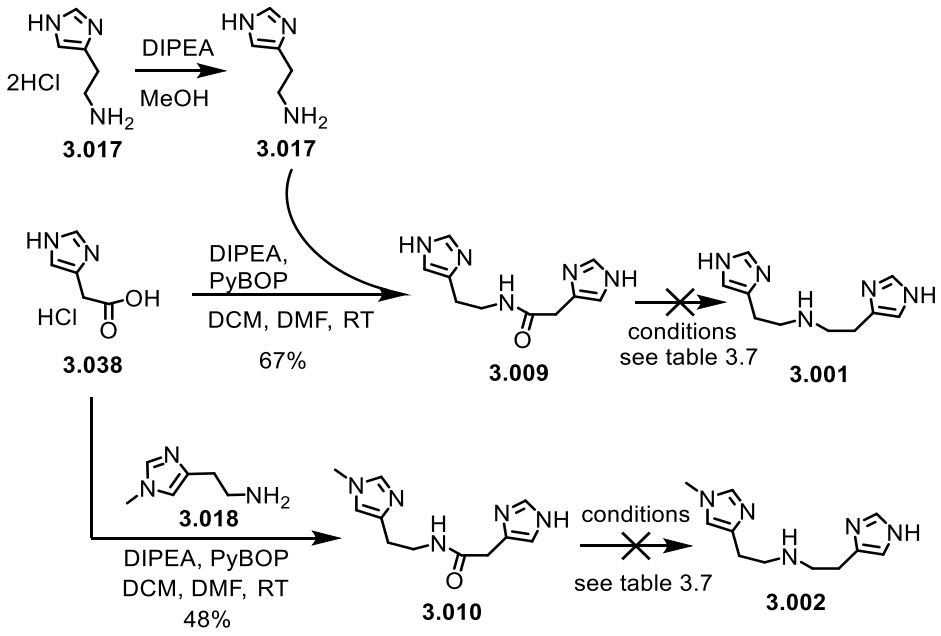

Scheme 11: Attempts of synthesizing ligand **3.001** and **3.002**

Table 3.7 Reaction conditions attempted for compound **3.001/3.002**

Entry	Conditions	Solvent	Result
1	LAH, Reflux	THF	No product
2	LAH, Reflux	1,4-dioxane	No product
3	BH_3-THF, Reflux	THF	No product
4	$NaBH_4$, AcOH, Reflux	1,4-dioxane	No product
5	$NaBH_4$, TFA, Reflux	1,4-dioxane	No product

As shown in Scheme 12, the synthesis of short chain ligands **3.003** and **3.004** followed the same procedure as describe above for ligands **3.009** and **3.010**. By this route, the corresponding amide derivatives **3.011** and **3.012** were obtained.

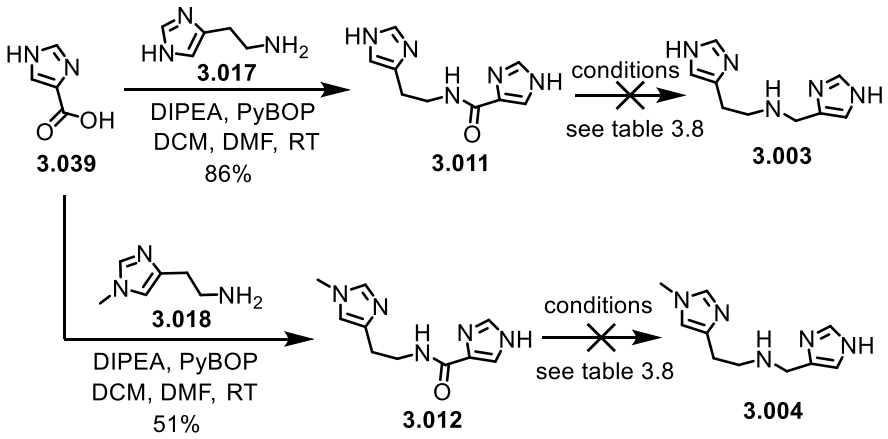

Scheme 12: Attempts of synthesizing ligand **3.003** and **3.004**

Table 3.8 Reaction conditions attempted for compound **3.003/3.004**

Entry	Conditions	Solvent	Result
1	LAH, Reflux	THF	No product
2	LAH, Reflux	1,4-dioxane	No product
3	$NaBH_4$, TFA, Reflux	1,4-dioxane	No product

3. The copper complexes with amide ligands

As discussed in section **2**, the intially designed ligands (**3.001**-**3.004**) containing secondary amines in the chain could not be synthesized successfully despite multiple approaches.

However, during these attempts, the carboxamide derivatives (**3.009**-**3.012**) were obtained. These ligands also display different chelating ring sizes and methylation patterns making their copper complexes also interesting to study for comparison to LPMO. For these ligands, the amides can serve as an excellent binding moiety for metal ions. In the past few years, due to the strong σ-donor and π-donor abilities in the deprotonated carboxamidate nitrogens,

deprotonated carboxamide ligands have attracted more and more attention for the design of metal complexes, especially for unusal higher oxidation states.[10]

Futhermore, there are several examples using carboxamidate ligands to synthesize models of various metalloenzymes including some relevant to LPMOs. Tolman's group has synthesized a pyridine-dicardoxamidate ligand, Figure 3, and used it to get a solvent (THF) coordinated copper complex. Exchange of the THF ligand for hydroxide followed by oxidation, gave a high valent intermediate complex (Cu^{III}-OH) able to abstract a hydrogen atom from dihydroanthracene. [11] Additionally, the end-on copper-superoxide was prepared using the same ligand in the presence of Ktyptofix222 and KO_2 (Figure 3).[12] (more details are shown in Chapter I) These could be notably relevant to proposals of LPMOs.

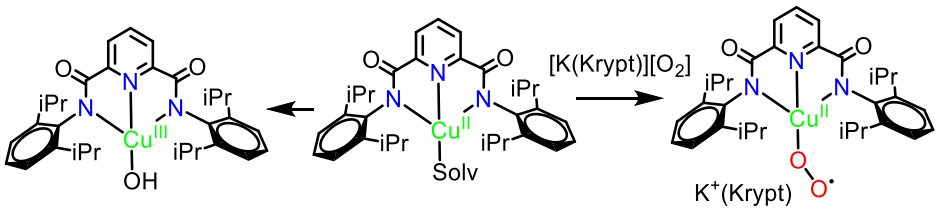

Figure 3. Molecular structure of the copper-solv complex and the corresponding copper(III)-hydroxide and copper(II)-superoxide

Base on these previous studies, we decided to use the carboxamide derivatives (**3.009** - **3.012**) as ligands **L1 - L4** to prepare the corresponding

[10] Panda C., Sarkar A., Gupta S. S., *Coord. Chem. Rev.*, **2020**, 417, 213314.

[11] Dhar D., Tolman W. B., *J. Am. Chem. Soc.*, **2015**, 137(3), 1322-1329.

[12] Bailey W. D., Gagnon N. L., Elwell C. E., Cramblitt A. C., Bouchey C. J., Tolman W. B., *Inorg. Chem.*, **2019**, 58(8), 4706-4711.

copper complexes and study how the chelating ring size and the methaltion of histamine influence the reactivity.

As shown in Figure 4, a single crystal structure of **L4** was obtained by slow diffusion of THF into a methanol solution of **L4**. In the solid state, an intramolecular H-bond between the amide and imidazole (NH···N, 2.47 Å, <= 105.86°) is present, which holds the amide and imidazole in the same plane. The other similar carboxamide ligands (**L1**, **L2** and **L3**) could not be crystallized with the same method.

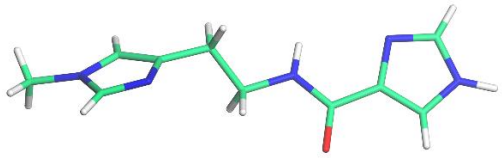

Figure 4. X-ray crystal structure of ligand **L4**
(green: C, blue: N, red: O, white: H)

3.1 Synthesis of complexes

In order to synthesize the copper(II) complexes, the four carboxamide ligands (**L1, L2, L3, L4**) were treated with triethylamine in methanol. Then $CuCl_2 \cdot 2H_2O$ in methanol was added and stirred overnight at room temperature. Through this approach, the corresponding complexes **1**, **2**, **3** and **4** could be formed (Figure 5). The same procedure was also performed without triethylamine for ligand **L1** with $CuCl_2$ to form complex $\mathbf{Cu_2(L1)_2}$. Louloudi and co-workers reported previously that **L1** can react with $Cu(ClO_4)_2$ in MeOH in the presence of triethylamine to form a bimetallic complex $[Cu_2(ClO_4)_4(\mathbf{L1})]$.[13]

[13] Zois D., Vartzouma C., Deligiannakis Y., Hadjiliadis N., Casella L., Monzani, E., Louloudi M., *J. Mol. Catal. A-Chem.*, **2007**, 261(2), 306-317.

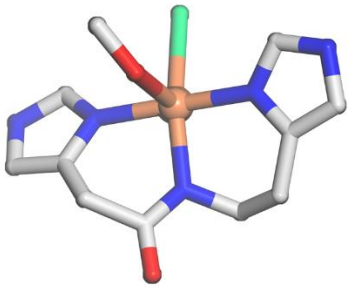

Figure 5. The proposed model structure based on DFT (PBE1PBE/ Lanl2dz, 6-311G*) calculations of copper(II) complex **1** (gray: C, blue: N, red: O, green: Cl, orange: Cu). Hydrogen atoms were omitted for clarity.

3.2 Characteristics of complexes in solid state

Despite several attempts to obtain crystals of complexes **1**-**4** with the deprotonated ligands and $CuCl_2$, no crystals of sufficient quality for X-ray crystal structure determination were obtained. However, the Cu(II) complex $\mathbf{Cu_2(L1)_2}$, formed when no base was used, gave green colored single crystals by diffusion of Et_2O into methanol solution of the complex. The crystal structure of complex $\mathbf{Cu_2(L1)_2}$ is shown in Figure 6. The copper(II) center exhibits a square pyramidal coordination geometry comprised by the two nitrogen atoms of the imidazoles, one oxygen atom of amide carbonly in **L1**, and two chloride anions. One of the chloride ions on each copper in the $\mathbf{Cu_2(L1)_2}$ unit, is found briding to another molecule in the crystal latice, resulting in a 1-D coordination polymer.

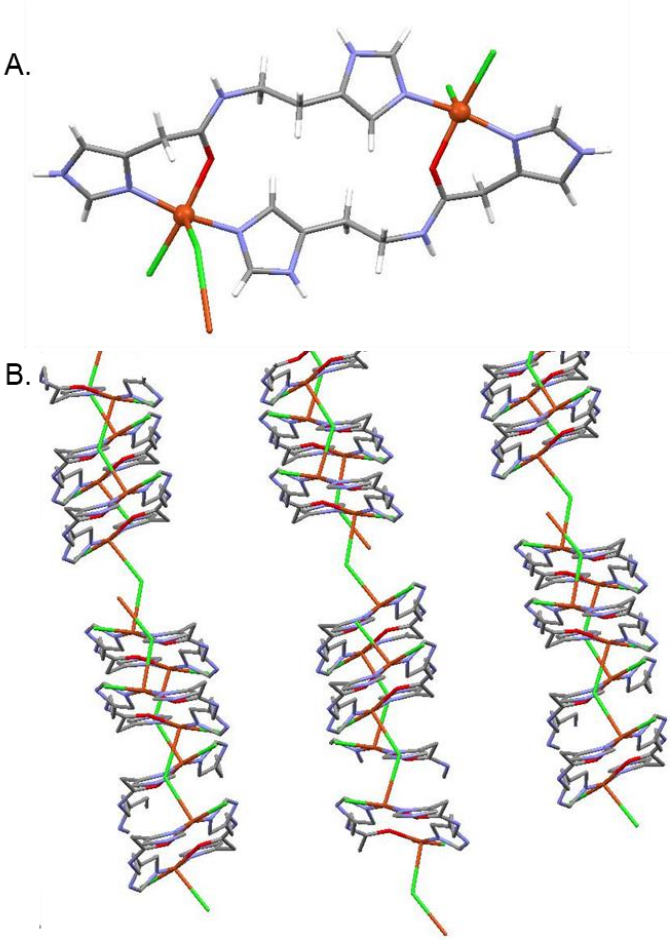

Figure 6. Single (A) and packing (B) X-ray structure of complex **$Cu_2(L1)_2$**. The hydrogen atoms are omitted for clarity in B.

3.3 Spectral characteristics of complexes in solution state

The paramagnetic nature of copper(II) limits the usefulness of NMR spectroscopy for studying the copper(II) complexes. Reactions and metallations were instead followed by UV-vis spectroscopy.

For our complexes, the stoichiometry of complexation in solution between

Cu(II) and free amide ligands **L1**, **L2**, **L3** and **L4** were determined through UV-vis titration and Job's plot analysis.[14] These were tested in both MeOH and H_2O.

The long alkyl chain ligands **L1** and **L2**, were first reacted with $CuCl_2$ and Et_3N in MeOH for forming complex **1** and complex **2**, respectively. In the UV-vis titration data (shown in Figure 7A and Figure 9A, respectively), with the increasing concentration of Cu(II), there is an increase in the absorbance at around 620 nm indicating the formation of a new species in solution. This corresponds to the Cu d-d transitions and is consistent with other N3 complexes described in the literature.[15] From the inset figure in Figure 7A and Figure 9A, we can find that the absorbance at 620nm in the titration spectra increases with the addition of Cu(II) and reaches a maximum value at around one equvalent of metal salt, suggesting the ligand and Cu(II) fit for 1:1 binding stoichiometry. The binding stoichiometry was further elucidated by using Job's plot analysis shown in Figure 7B and Figure 9B, respectively. The absorbance change at 620 nm was plotted against the molar fraction of the ligand. The maximum change in absorbance occurred with a molar fraction of 0.5, indicating a 1:1 binding stoichiometry, consistent with the results of the UV-vis titration.

Additionally, similar UV-vis spectral titration (Figure 8A and Figure 10A) and Job's plot (Figure 8B and Figure 10B) were run for ligands **L1**, **L2** and $CuCl_2$ in H_2O. The results were similar to when MeOH was used as the solvent, all showed the binding stoichiometry was 1:1.

---

[14] MacCarthy P., *Anal. Chem.*, **1978**, 50(14), 2165-2165.

[15] Muthuramalingam S., Maheshwaran D., Velusamy M., Mayilmurugan R., *J. Catal.*, **2019**, 372, 352-361.

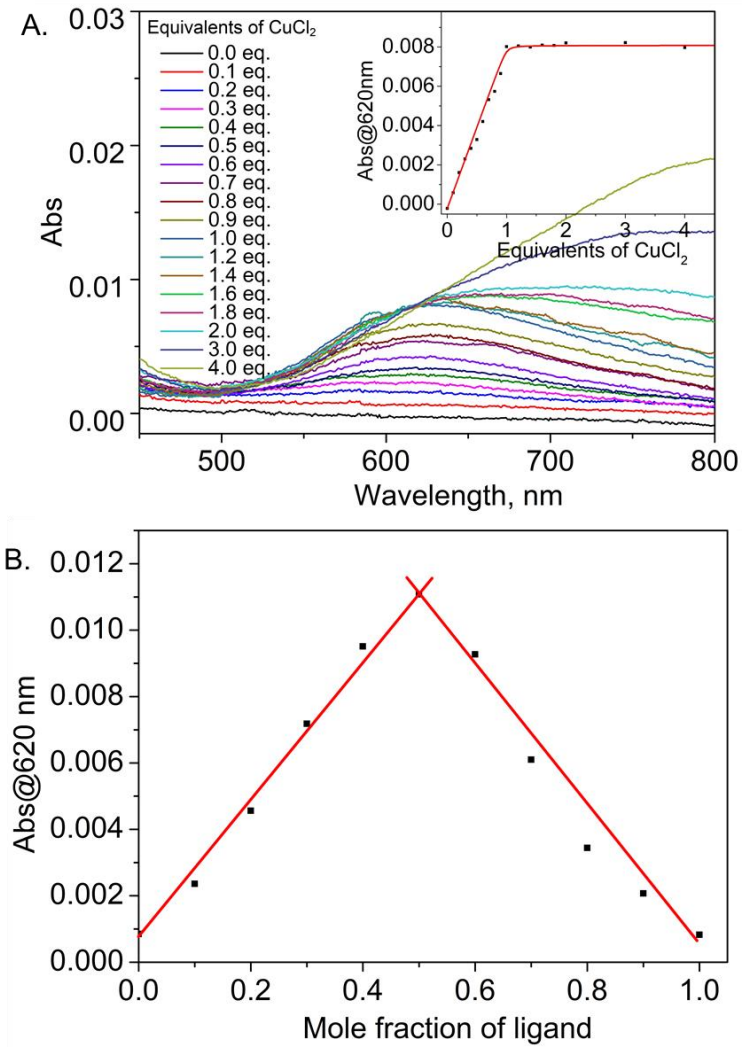

Figure 7. (**A**) UV-vis spectral titration of ligand **L1** (0.1 mM) with $CuCl_2$ (0 - 0.4 mM) in MeOH at room temperature (inset: absorbance at 620 nm vs equivalents of $CuCl_2$ added); (**B**) Job's plot for ligand **L1**-$CuCl_2$ complex formation in MeOH

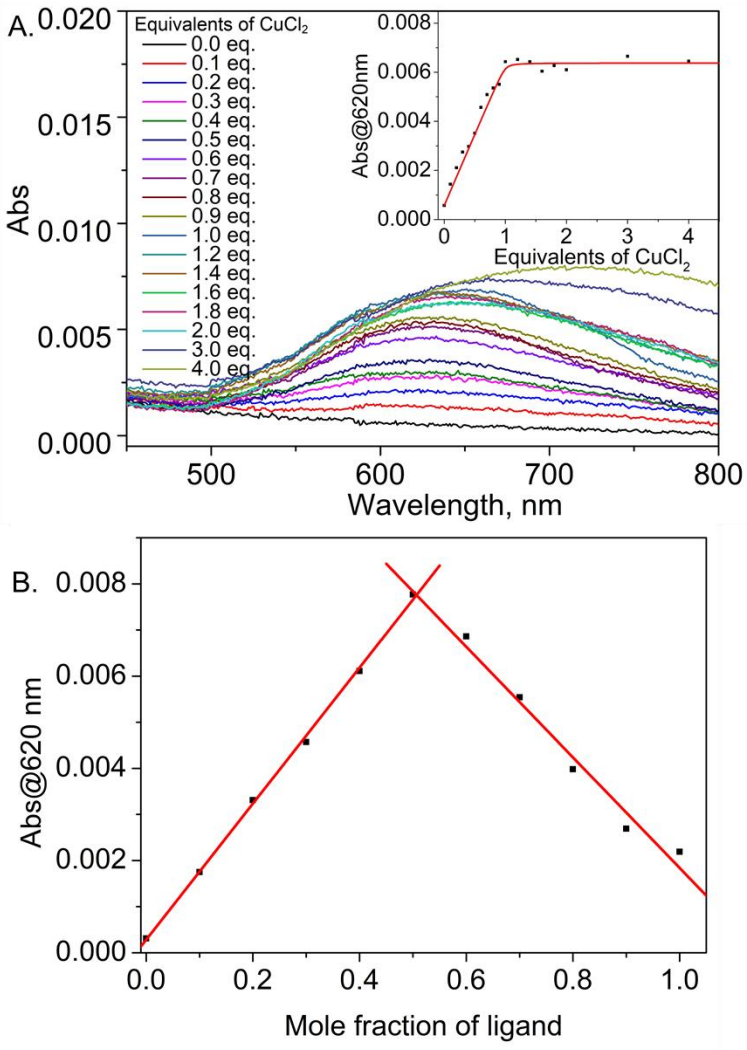

Figure 8. (**A**) UV-vis spectral titration of ligand **L1** (0.1 mM) with $CuCl_2$ (0 - 0.4 mM) in H_2O at room temperature (inset: absorbance at 620 nm vs equivalents of $CuCl_2$ added); (**B**) Job's plot for ligand **L1**-$CuCl_2$ complex formation in H_2O

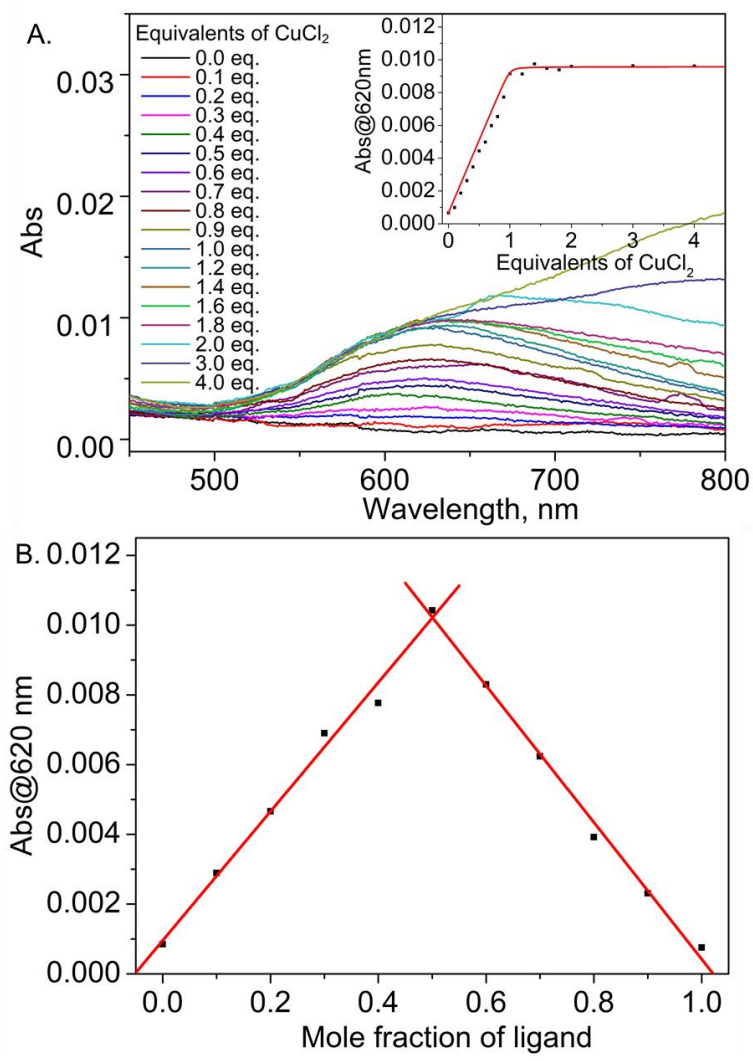

Figure 9. (**A**) UV-vis spectral titration of ligand **L2** (0.1 mM) with $CuCl_2$ (0 - 0.4 mM) in MeOH at room temperature (inset: absorbance at 620 nm vs equivalents of $CuCl_2$ added); (**B**) Job's plot for ligand **L2**-$CuCl_2$ complex formation in MeOH

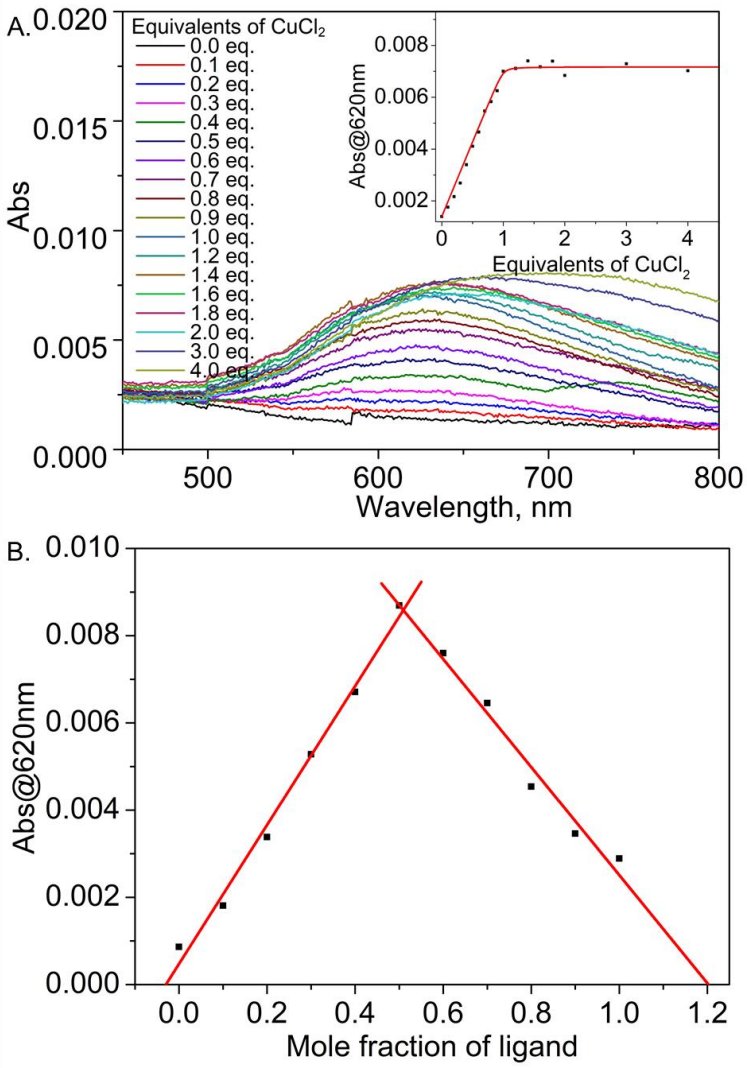

Figure 10. (**A**) UV-vis spectral titration of ligand **L2** (0.1 mM) with $CuCl_2$ (0 - 0.4 mM) in H_2O at room temperature (inset: absorbance at 620 nm vs equivalents of $CuCl_2$ added); (**B**) Job's plot for ligand **L2**-$CuCl_2$ complex formation in H_2O

Interestingly, different results have been reported in the literature. When Louloudi and co-workers coordinated $Cu(ClO_4)_2$ with **L1** in MeOH, a new peak appeared at 689 nm (in MeOH) in the UV-Vis spectra. The Mass and FTIR data indicated a bimetallic [$Cu_2(ClO_4)_4$(**L1**)] (2:1 stoichiometry) and that metal coordination to the amide and both imidazole nitrogens occured.[16] The difference in their results versus ours may be due to the stronger coordination ability of Cl^- versus ClO^{4-}. Still, it should be noted that no titrations were described in their work.

It should be noted that 1:1 binding observed simply indicates that the ligand and metal are present in equal amounts in the complex. This could also result from 2:2 or higher equal stoichiometries. Indeed, as a 2:2 structure was observed in the solid state for **L1** with $CuCl_2$, higher stoichiometries cannot entirely be ruled out. However, the UV-vis spectra of complex **1** and **Cu_2(L1)$_2$**, Figure 11, show a notable difference. There is an obvious absorption peak around 290 nm in the spectrum of complex **Cu_2(L1)$_2$** and the position of the d-d transition changes to around 680nm compared to in complex **1**. These differences suggest that the coordination geometry of complex **1** is different from complex **Cu_2(L1)$_2$** potentially supporting the suspected 1:1 stoichiometry in complex **1**.

[16] Zois D., Vartzouma C., Deligiannakis Y., Hadjiliadis N., Casella L., Monzani, E., Louloudi M., *J. Mol. Catal. A-Chem.*, **2007**, 261(2), 306-317.

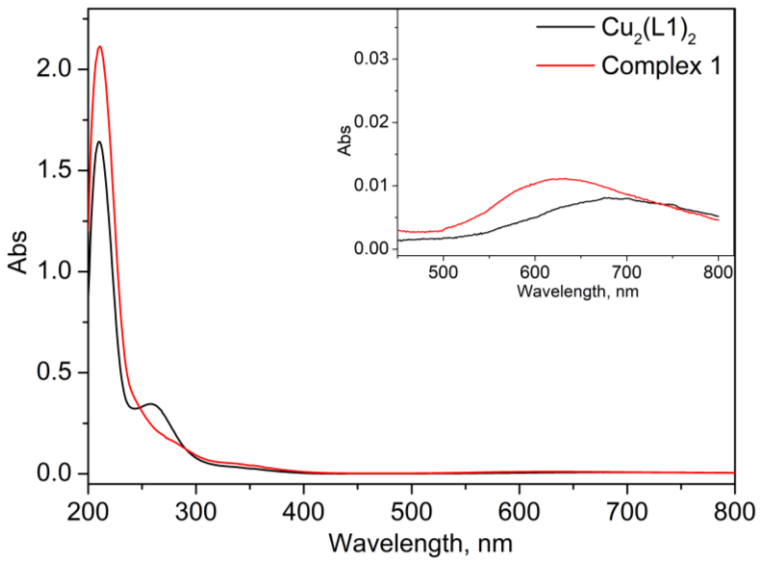

Figure 11. The comparison of UV-vis spectrum of complex **1** and **$Cu_2(L1)_2$** (in MeOH, 0.125 mM) (inset: zoom the part 450nm to 800nm)

Similar spectroscopic studies were used to elucidate the formation of complexes **3** and **4**. Complexation between Cu(II) and the free short alkyl chain ligands **L3** and **L4** in the presence of Et_3N, was also studied by means of UV-vis spectral titration (Figure 12A, 13A and Figure 14A, 15A) and Job's plot (Figure 12B, 13B and Figure 14B, 15B) in MeOH and H_2O. In the UV-vis spectral titration, an absorbance at around 620 nm also appeared for these complexes. These results also all suggested similar phenomenon as for the long chain ligand-Cu(II) complexes, i.e. 1:1 binding stoichiometry.

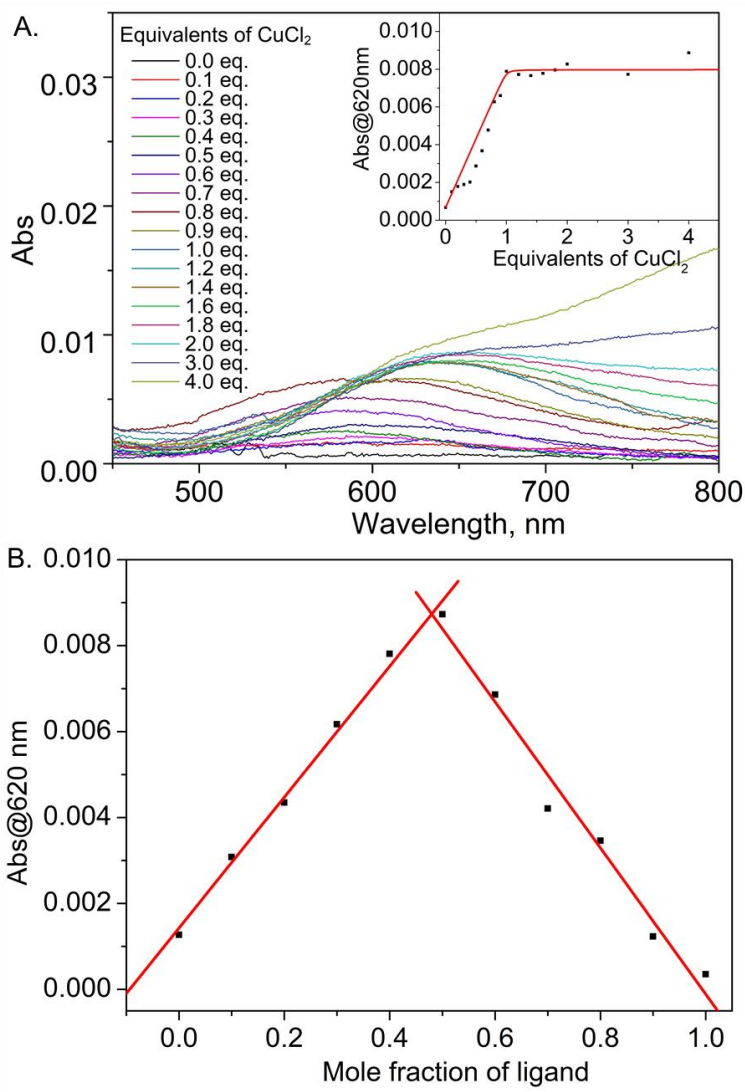

Figure 12. (**A**) UV-vis spectral titration of ligand **L3** (0.1 mM) with $CuCl_2$ (0 - 0.4 mM) in MeOH at room temperature (inset: absorbance at 620 nm vs equivalents of $CuCl_2$ added); (**B**) Job's plot for ligand **L3**-$CuCl_2$ complex formation in MeOH

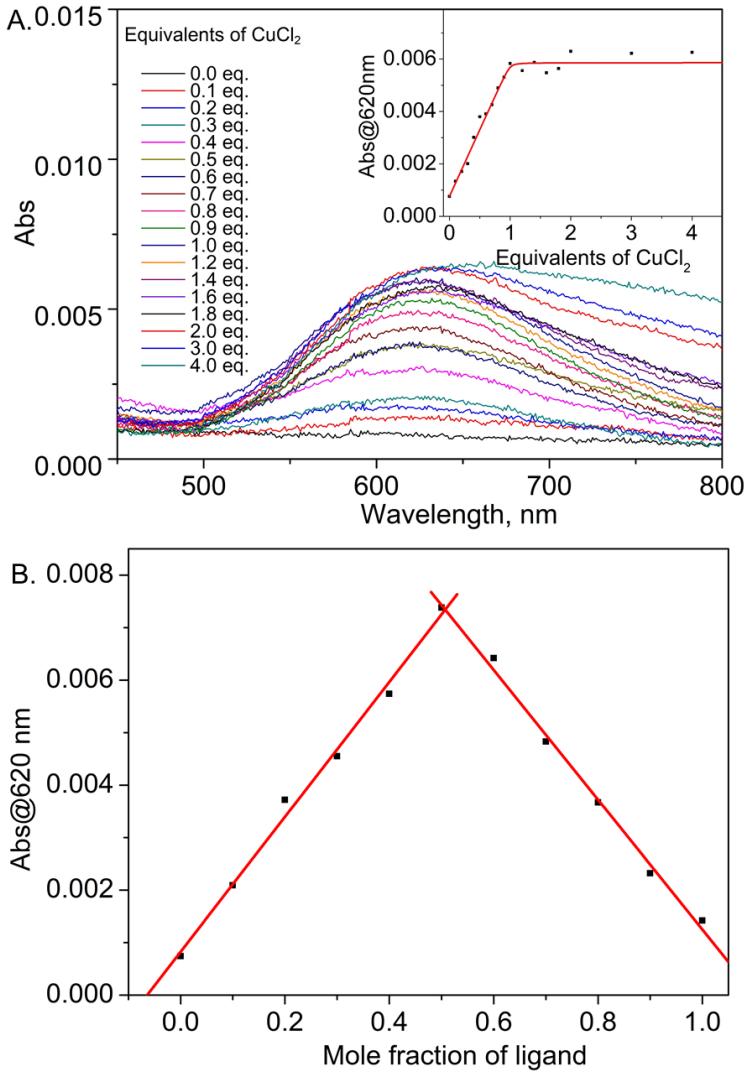

Figure 13. (**A**) UV-vis spectral titration of ligand **L3** (0.1 mM) with $CuCl_2$ (0 - 0.4 mM) in H_2O at room temperature (inset: absorbance at 620 nm vs equivalents of $CuCl_2$ added); (**B**) Job's plot for ligand **L3**-$CuCl_2$ complex formation in H_2O

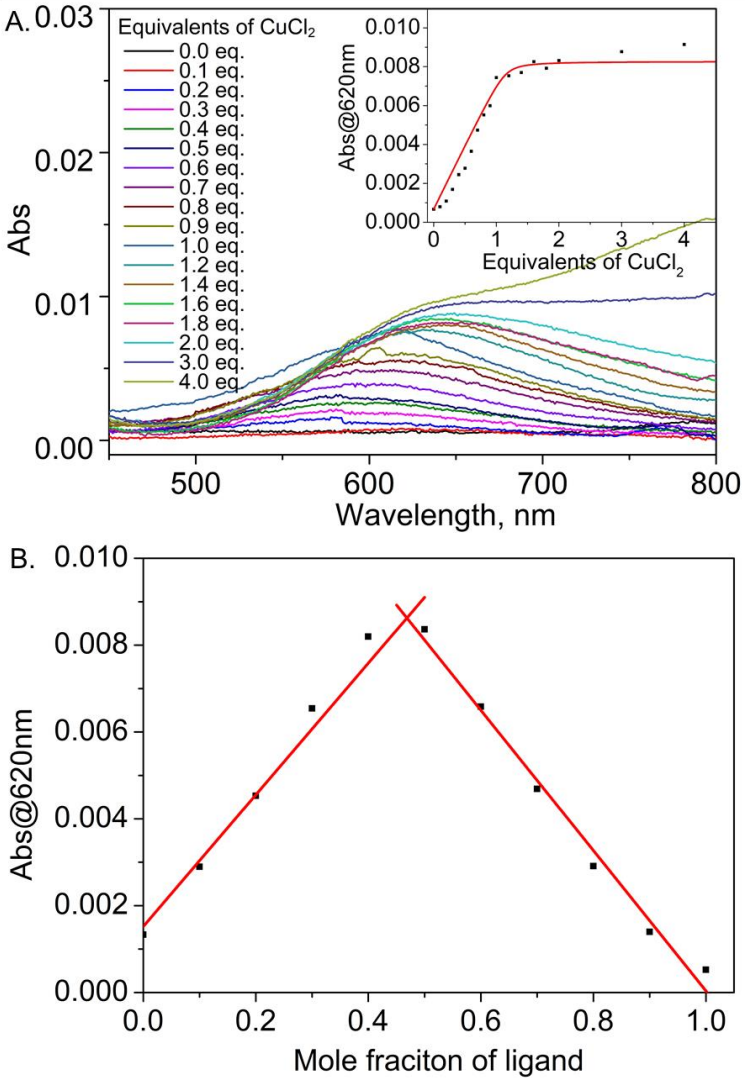

Figure 14. (**A**) UV-vis spectral titration of ligand **L4** (0.1 mM) with $CuCl_2$ (0 - 0.4 mM) in MeOH at room temperature (inset: absorbance at 620 nm vs equivalents of $CuCl_2$ added); (**B**) Job's plot for ligand **L4**-$CuCl_2$ complex formation in MeOH

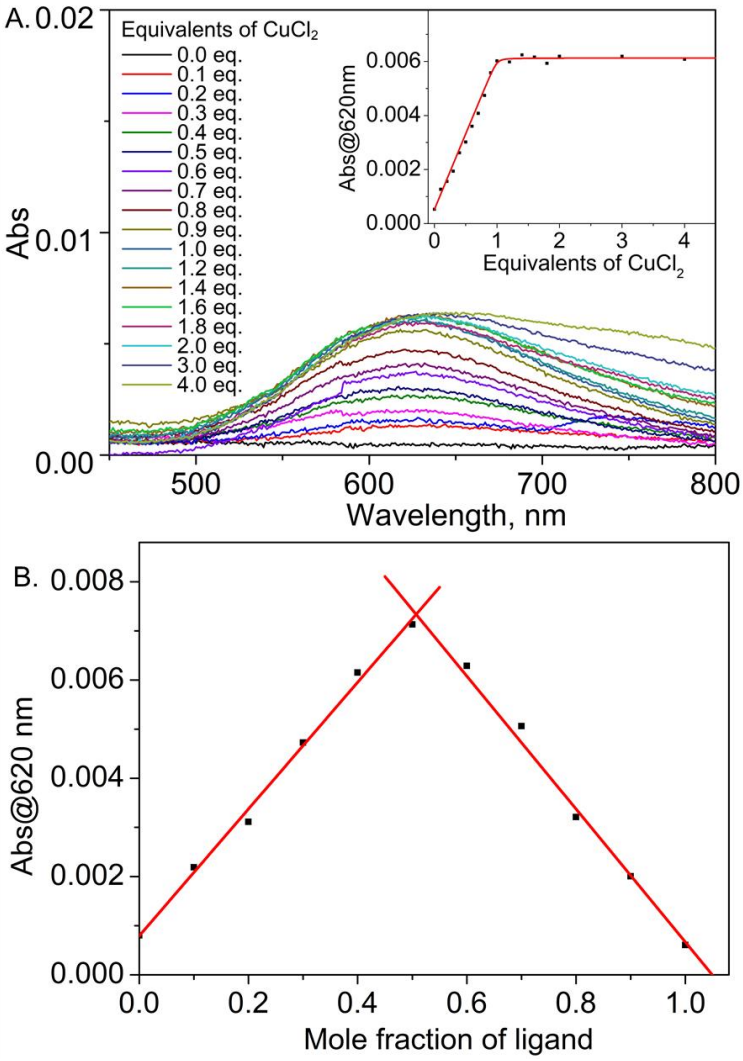

Figure 15. (**A**) UV-vis spectral titration of ligand **L4** (0.1 mM) with $CuCl_2$ (0 - 0.4 mM) in H_2O at room temperature (inset: absorbance at 620 nm vs equivalents of $CuCl_2$ added); (**B**) Job's plot for ligand **L4**-$CuCl_2$ complex formation in H_2O

In the (**L1**, **L2**)-Cu(II) systems, the Job's plot conclusions are also supported by changes in the UV studies. The inset figure in UV-vis titration spectrum, Figure 14, shows a saturation in the absorption changes occurred with equimolar amounts of the ligands and Cu(II). However, for the short chain ligands (**L3**, **L4**), while coordination with Cu(II) in H_2O fit reasonably well with the 1:1 binding stoichiometry, with MeOH as solvent greater variation was observed, possibly indicating the contribution of other stoichiometries in the overall equilibrium. This difference between the pairs of ligands could be due to the longer chains in ligands (**L1**, **L2**) permitting better coordination of the copper than for short chain ligands (**L3**, **L4**). Additionally, this shows that the solvent also could have a stronger influence on the coordination of copper by the short ligand.

Overall, the UV-vis absorption spectra of complexes **1** - **4** showed a single similar d-d transition absorption band in around 620 nm in both MeOH and H_2O.[17] The energies of the d-d transition of these complexes are very close to the LPMOs, which is around 650 nm.[18]

3.4 Mass spectrometry and FTIR spectra characteristics of complexes

Further evidence for the complexes were obtained by mass spectrometry on the Cl^- salts of these compounds. For complex **1** (Figure 16A), there are two mass peaks appearing at 281.0331 and 317.0100 corresponding to the formation of $[Cu(\mathbf{L1}\text{-}H)]^{1+}$ and $[Cu(\mathbf{L1}\text{-}H)]^{1+}\bullet HCl$, respectively, which match

[17] Muthuramalingam S., Maheshwaran D., Velusamy M., Mayilmurugan R., *J. Catal.*, **2019**, 372, 352-361.

[18] a) Garajova S., Mathieu Y., Beccia M. R., Bennati-Granier C., Biaso F., Fanuel M., Henrissat B., *Sci. Rep.*, **2016**, 6, 28276. b) Vu V. V., Ngo S. T., *Coord. Chem. Rev.*, **2018**, 368, 134-157.

well with the simulated spectra. Similar species [Cu(**L2**-H)]$^{1+}$ and [Cu(**L2**-H)]$^{1+}$•HCl were found at 295.0488 and 331.0255 in the mass spectra of complex **2** (Figure 16B). Likewise, in the mass spectra of complex **3** (Figure 16C), the main peak appeared at 267.0173 consistent with the formation of the species [Cu(**L3**-H)]$^{1+}$. Finally, based on the isotopic patterns, the mass analysis of complex **4** also suggests that species [Cu(**L4**-H)]$^{1+}$ was formed (Figure 16D).

Thus, the mass spectra results corroborate the UV-Vis studies indicating that the ligands **L1**, **L2**, **L3** and **L4** coordinate the Cu(II) with a 1:1 stoichiometry.

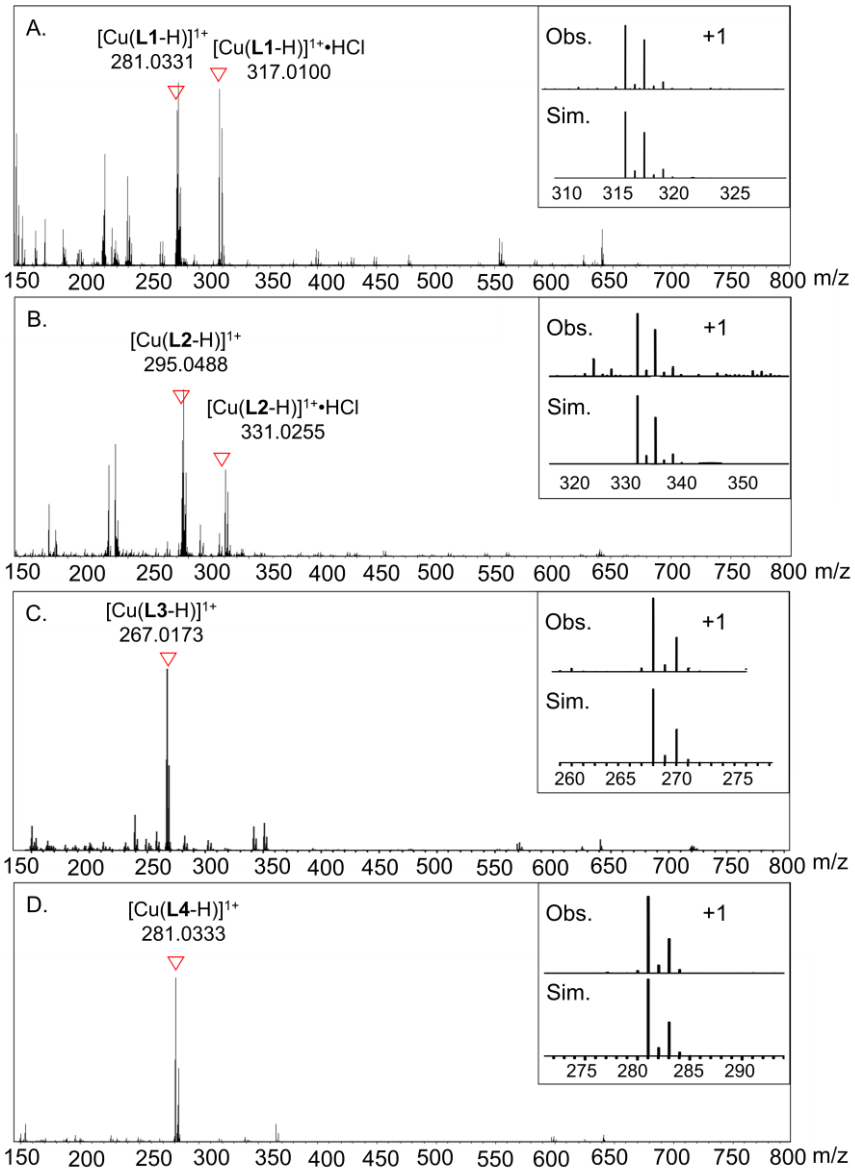

Figure 16. Portion of the mass spectra for **L1** (A), **L2** (B), **L3** (C) and **L4** (D) coordinated with $CuCl_2$. Insets show the comparison of the observed isotopic bundles with the simulated spectra

Complexation involving the amide was also supported by the FTIR spectra, upon complexation, the carbonyl ($C=O_{amide}$) stretching band in all ligands undergoes a bathochromic shift relative to the free ligands (Figure 17). Such changes could be expected from the deprotonation of the amide group upon coordination to Cu(II).[19] This would also match with the chemical formula suggested by the mass spectral studies.

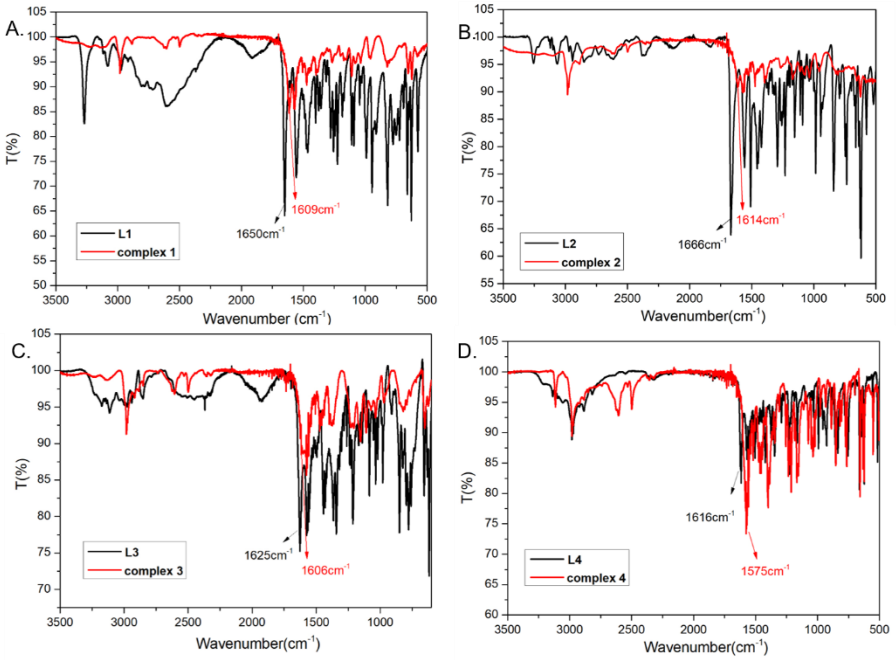

Figure 17. Comparison of the FTIR spectra for ligands and corresponding the complex A) ligand **L1** and complex **1**; B) ligand **L2** and complex **2**; C) ligand **L3** and complex **3**; D) ligand **L4** and complex **4**

[19] a) Wagler T. R., Fang Y., Burrows C. J., *J. Org. Chem.*, **1989**, *54*(7), 1584-1589. b) Martí I., Ferrer A., Escorihuela J., Burguete M. I., Luis S. V., *Dalton. Trans.*, **2012**, 41(22), 6764-6776.

4. Oxidative cleavage of p-nitrophenyl-β-D-glucopyranoside

In order to study the reactivity of the complexes, p-nitrophenyl-β-D-glucopyranoside was used as the model saccharide substrate. Hydrogen peroxide (H_2O_2) is a powerful oxidant, and its use as a cosubstrate in the reactions of LPMOs has been the center of many recent studies,[20] for this reason we employed H_2O_2 as the oxygen source. Upon oxidative to cleavage of the glycosidic bond in the model substrate, yellow p-nitrophenolate is released (absorption band is at 400nm) allowing the reaction to be monitored by UV-vis (Figure 18).

[20] Paradisi A., Johnston E. M., Tovborg M., Nicoll C. R., Ciano L., Dowle A., Walton P. H., *J. Am. Chem. Soc.*, **2019**, *141*(46), 18585-18599.

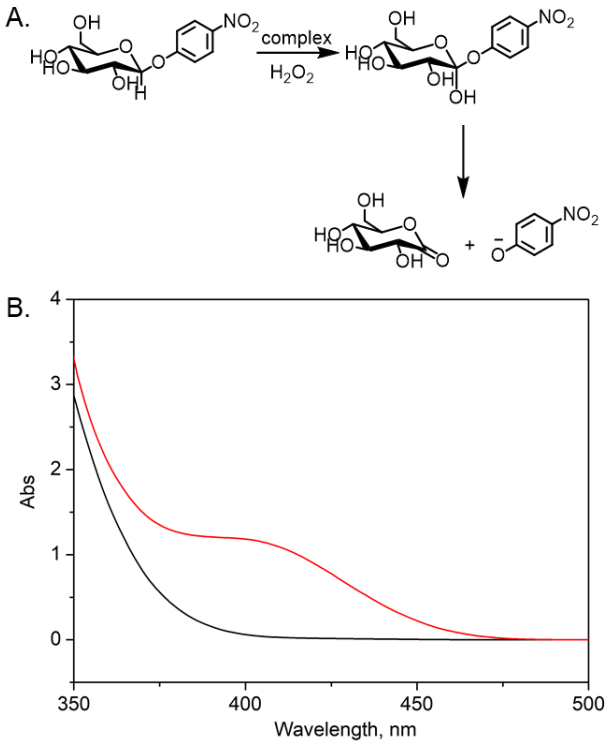

Figure 18. (A) The oxidative cleavage of p-nitrophenyl-β-D-glucopyranoside. (B) The comparison of the spectral before (black) and after (red) the formation of p-nitrophenolate.

For the initial conditions of the assay, carbonate buffer solution (100 mM, pH = 10.5) was used as the solvent. The reaction of p-nitrophenyl-β-D-glucopyranoside (S) (20 mM) with aqueous hydrogen peroxide (20 mM) in the presence of the complexes (0.05 mM) was carried out for 24h at room temperature. In addition to the complexes, $CuCl_2$ or $CuSO_4$ salts were used for control reactions. The calculated concentration of produced p-nitrophenolate for different conditions is shown in the Figure 19. After long reaction times 24h, about 630 μM p-nitrophenolate was produced using 0.05 mM complex **1** and **2** with long alkyl chain ligands, which was slightly higher

than that obtained in the presence of the Cu(II) salt alone ($CuCl_2$, $CuSO_4$). However, the produced p-nitrophenolate in the presence of complex **3** and **4** was actually less than for both Cu(II) salts. In the absence of H_2O_2 and presence of complexes **1-4**, the p-nitrophenolate was only detected in low amounts (about 30 µM).

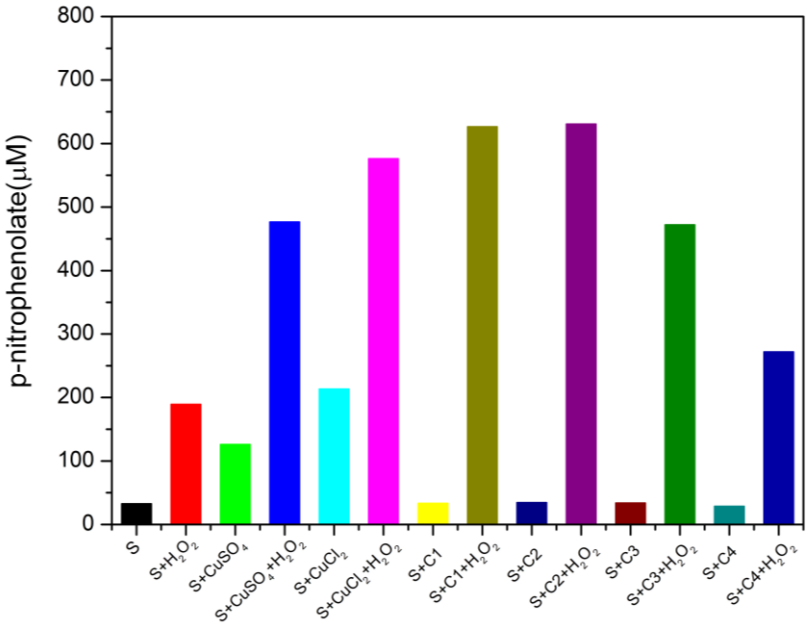

Figure 19. Concentration of p-nitrophenolate obtained after 24h of reaction with complex **1-4** in carbonate buffer solution (100 mM, pH = 10.5)

Mayilmurugan et al[15] reported this assay could also be performed in aqueous solution using Et_3N as base, but they did not report the quantity of p-nitrophenolate produced in the absence of the complexes (i.e. only with Cu salts or H_2O_2). Using these conditions, we also studied the reaction with aqueous hydrogen peroxide (20 mM) in the presence of the complexes (0.05 mM) and triethylamine (20 mM) for 24 hours at room temperature. And at same time, the Cu(II) salts ($CuCl_2$, $CuSO_4$) as controls were used to perform

this reaction. The calculated concentration of produced p-nitrophenolate is shown in Figure 20. The resulting concentration of p-nitrophenolate were all higher for the Cu(II) complexes **1-4** than with the Cu(II) salts. The Cu(II) complex **1** could produce the most p-nitrophenolate compared to all the tested Cu(II) complexes. However, the control reaction mixture with just H_2O_2 and substrate also yielded a similar concentration of p-nitrophenolate with Cu(II) complex **1**. While unexpected, we cannot rule out the possibility that trace metal impurities on the flask may have contributed to this reactivity. These reactivity assays need to be repeated more times.

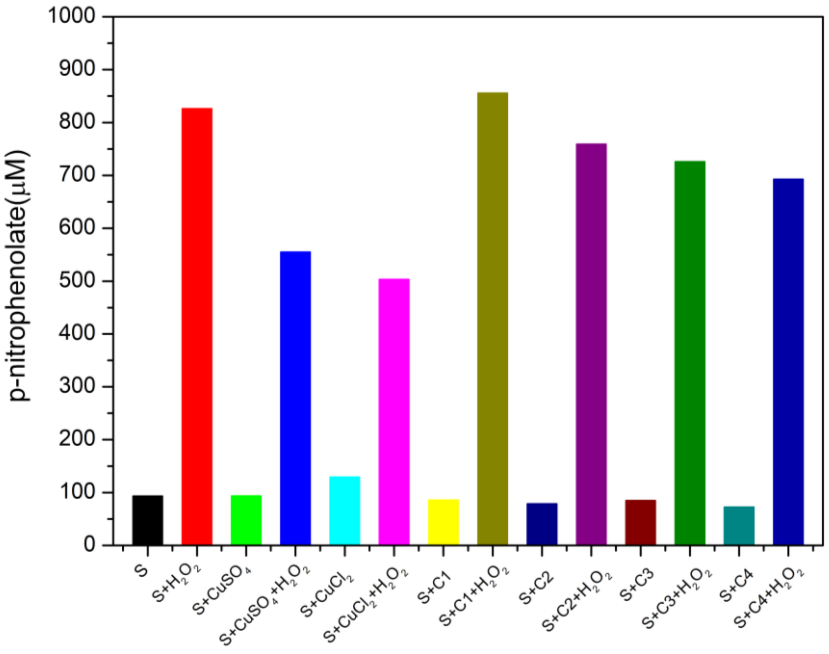

Figure 20. Concentration of p-nitrophenolate obtained after 24h of reaction with complex **1-4** in aqueous solution

Overall, the reactivity assay in different conditions indicate that the methylation of the imidazoles in the ligand do not have a great influence on the reactivity of the Cu(II) complexes. By contrast, the chelating ring size does appear to have a significant influence on the reactivity of the Cu(II) complexes. The long chain is more advantageous to the reactivity, which is probably because the T-shape coordinated geometry of complex, similar to the active site of LPMOs, is easier to form in the presence of long chain ligand. Therefore, additional effects of chelate ring size are worth continued study.

5. Conclusions

In this chapter, we initially designed the small molecule ligands **3.001-3.004** (Scheme 1) containing secondary amines to connect the imidazole or 1-methyled imidazole. However, several attempts to synthesize these ligands such as a Schiff base approach, an alkylation approach, and an amide bond approach, did not yield the target ligands.

Still, in synthesizing the amide intermediates, the derivatives **3.009-3.012** were obtained. These ligands **L1-L4**, which could still be used to study the effects of different size chelate rings and methylation patterns on the reactivity of the complexes. In addition to NMR characterization, the crystal structure of ligand **L4** further supported the formation of the amide compounds.

In the presence of Et_3N in MeOH, the amide derivatives were used as ligands to synthesize Cu(II) complexes **1-4**. The UV-vis spectrophotometric titration and Job's plot between $CuCl_2$ and ligands all showed that the Cu(II) complexes displayed 1:1 stoichiometries in MeOH and H_2O. The position of d-d transitions in the complexes is also almost identical to LPMOs. The FTIR and MS data also suggest the deprotonation of ligand amides and the formation of our proposed complexes.

At the same time, ligand **L1** could also be used to directly coordinate $CuCl_2$ without prior deprotonation. This led to the complex **$Cu_2(L1)_2$**, for which the crystal structure showed two ligands **L1** bound to two Cu(II) metals. The chlorides present on the copper are connected to neighboring molecules in the crystal forming long one dimensional chains. However, the UV-vis spectrum of this complex is different than for complex **1** suggesting different structure.

P-nitrophenyl-β-D-glucopyranoside and hydrogen peroxide were used as model substrate and oxygen source respectively in two different reactivity assays. We studied the reaction in carbonate buffer (100 mM, pH=10.5) solution and in aqueous solution (with Et_3N). While control studies suggest that the H_2O_2 may be able to react directly with the p-nitrophenyl-β-D-glucopyranoside in the presence of H_2O_2 and Et_3N in aqueous solution, it is also possible that trace metals may have assisted in this reactivity. Nevertheless, in both the carbonate buffer (100 mM, pH=10.5) and aqueous solutions, the concentration of p-nitrophenolate produced during the assays was higher in the presence of the Cu(II) complexes **1**, **2** than with Cu(II) salt ($CuCl_2$, $CuSO_4$). In all cases, complexes **3** and **4** containing the small chelate rings were found to be less reactive than the larger ligands.

Chapter IV

Scaffold Based Models Relevant to LPMOs

Although small molecule models can mimic certain features of the active site of LPMOs through N_3 coordination to copper atom, other features, such as the primary amine group, are more challenging to incorporate using only small molecules. Moreover, small molecules largely only model the first coordination sphere of LPMOs and generally ignore the additional layers of interactions present. Incorporating groups that can provide these types of second coordination sphere interactions is also important for elucidating other factors that can control reactivity. In the enzyme, the collection of these effects and the control over the coordination site results from the active site being found in a conformationally controlled protein environment that has evolved over time to place all of the functional groups in precise locations. Replicating this idea with synthetic systems is challenging, and yet a modular and conformationally controlled organic scaffold containing histamine and imidazole groups could be a powerful tool for better understanding these enzymes. Aromatic oligoamide foldamers are one possibility for the design of these scaffolds. The connection of heterocyclic aromatic rings through amide bonds leads to an almost coplanar arrangement of the aromatic groups, with the conformations around the amide dictated by the electrostatic interactions between the amide group and substituents on the aromatic rings. Together, these features can give highly stable secondary structures with predictable folding. Importantly, with longer oligomers or large aromatic monomers, the

structures can be made large enough to incorporate multiple convergent functional groups for binding of metal atoms.

Based on this idea, we set out to design novel aromatic oligoamide scaffolds that can function as multi-layered models of LPMO, Figure 1. The initial scaffold skeleton was designed using two types of monomers, quinolines and diazaanthracenes. To replicate the N_3 coordination found in LPMO, the 8-position of the quinolines was functionalized by imidazole or histamine via two different strategies. As the scaffold holds these groups in close proximity, it should be possible to control the imidazole and primary amine coordination of the copper to obtain complex **4.001** (Figure 1B) and complex **4.004** (Figure 1C). Since the sequence is connected together by amide bonds, it should also be possible to use modified monomers to look at incorporation of additional second coordination sphere interactions such as the long range axial tyrosine Cu interaction present in the enzyme.

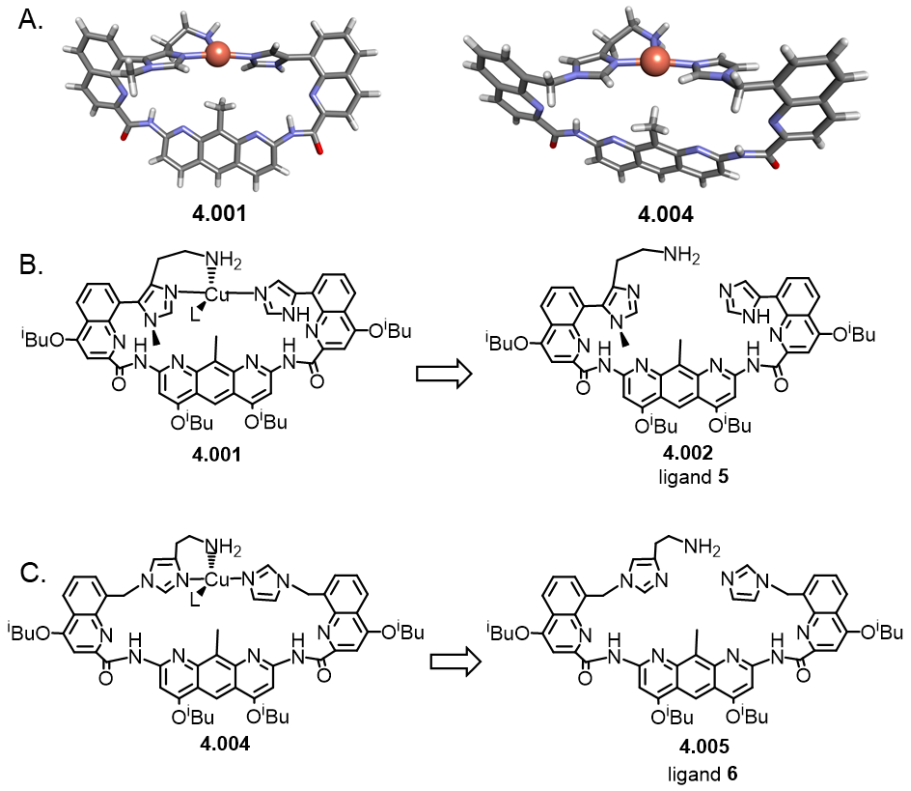

Figure 1. (A) The model of designed scaffold. (B)(C) The molecular structure of designed ligands.

1. The initial scaffold design

In the initially designed scaffold, quinolines would be first directly connected to the 4-position of imidazole or 5-position of histamine, then coupled to a central diazaanthracene monomer. The specific interactions in the oligoamide sequence will lead to a folded structure that should orient all of the ligands in a convergent fashion. Based on the biological studies, the resulting “histidine brace” motif should have very high affinity for Cu to mimic the active site of

LPMOs. A retro synthesis for the target ligands, is given in Scheme 1. For the synthesis of the quinolines, imidazole and histamine parts, the initial idea was to use 8-bromo-quinolines and directly couple it with either a 4(5)-halo-imidazole or 5-halo-histamine. Then these functionalized quinolines would be connected to a central diazaanthracene monomer via amide bonds.

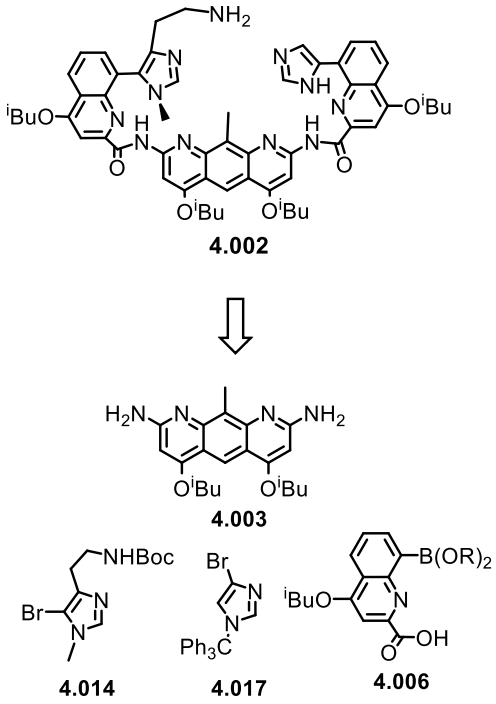

Scheme 1. The retro synthesis of the target initial designed ligand

2. Sythesis of initial designed ligand

2.1 Monomer synthesis

The monomer precusors (quinoline, imidazole, histamine and diazaanthrance) were synthesized successfully. The central 2,7-diamino-1,8-diazaanthracene monomer **4.003** can be obtained in seven steps starting from 2,6-diaminotoluene **4.007** as shown in scheme 2. The synthesis initially follows reported procedures, i.e. initial Michael addition of 2 equiv. of dimethyl acetylenedicarboxylate (DMAD) to the appropriate 1-functionalized 2,6-diaminobenzene **4.008**. Thermal cyclization in refluxing diphenyl ether at 260 ^{o}C and then alkylation of the resulting 4,5-dihydroxy-9-methyl-1,8-diazaanthracenes **4.009** under Mitsunobu conditions gives product **4.010**.[1] This intermediate can then be converted to the corresponding bishydrazide by using a mixture of hydrazine/MeOH under reflux conditions to give **4.011** in very good yield. In the presence of nitrosyl tetrafluoroborate ($NOBF_4$), the intermediate **4.012** was obtained and a Curtius rearrangement was performed in refluxing toluene and ^{t}BuOH to give the Boc-protected amine **4.013**. Finally, the Boc-protecting group was removed using TFA to get the final monomer **4.003**.

[1] a) Berni E., Dolain C., Kauffmann B., Léger J. M., Zhan C., Huc, I., *J. Org. Chem.*, **2008**, 73(7), 2687-2694. b) Singleton M. L., Castellucci N., Massip S., Kauffmann B., Ferrand Y., Huc I., *J. Org. Chem.*, **2014**, 79(5), 2115-2122.

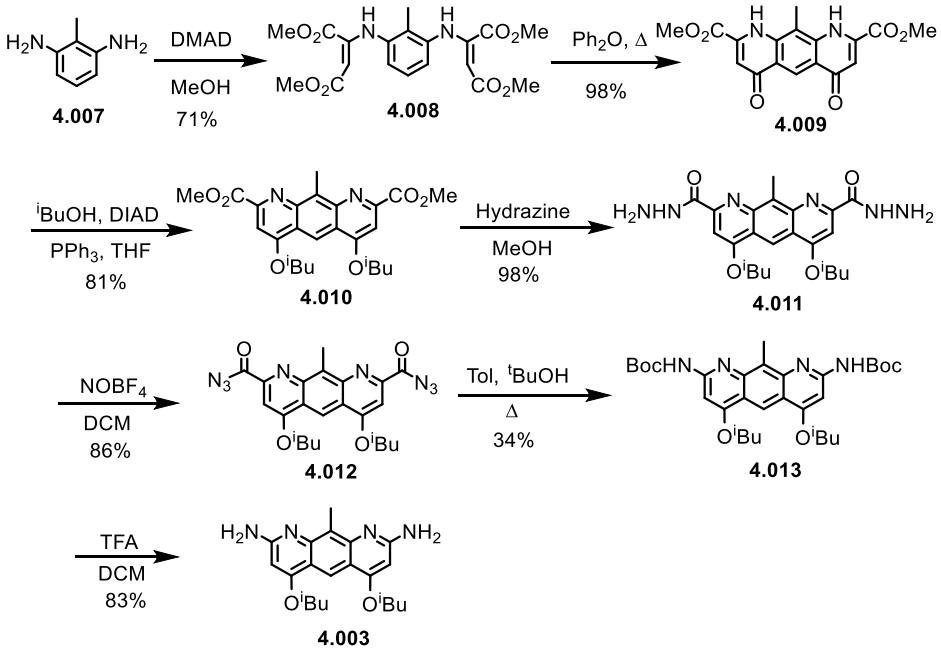

Scheme 2. The synthetic route of the central 2,7-diamino-1,8-diazaathracene monomer

For imidazole/histamide building blocks both the iodo and bromo derivatives were synthesized, Scheme 3. The N-Boc-protected intermediate **3.030** undergoes regio-selective halogenation exclusively at C-5 using NBS in acetonitrile to provide product **4.014**.[2] For the imidazole unit **4.017**, imidazole was first protected using a triphenylmethyl group and then treated with NBS to form 4-bromo-1-trityl-imidazole **4.017**. [3] The synthesis of 4(5)-

[2] Saulnier M. G., Frennesson D. B., Wittman M. D., Zimmermann K., Velaparthi U., Langley D. R., Greer A., *Bioorg. Med. Chem. Lett.*, **2008**, 18(5), 1702-1707.

[3] a) Aldabbagh F., Bowman W. R., *Tetrahedron*, **1999**, 55(13), 4109-4122. b) Palmer B. D., Denny W. A., *J. Chem. Soc. Perkin Trans. I*, **1989**, (1), 95-99.

iodoimidazole **4.019** was performed according to literature procedures via polyiodination of imidazole and reductive deiodination with Na_2SO_3 in refluxing aqueous ethanol, providing the product in good overall yield.[4] The subsequent protection of N1 was accomplished with trityl chloride to afford imidazole **4.020**. Finally, the 8-bromoquinoline monomer **4.024** was prepared by introduction of the isobutyl chain to the quinolinone **4.023** under Mitsunobu conditions.

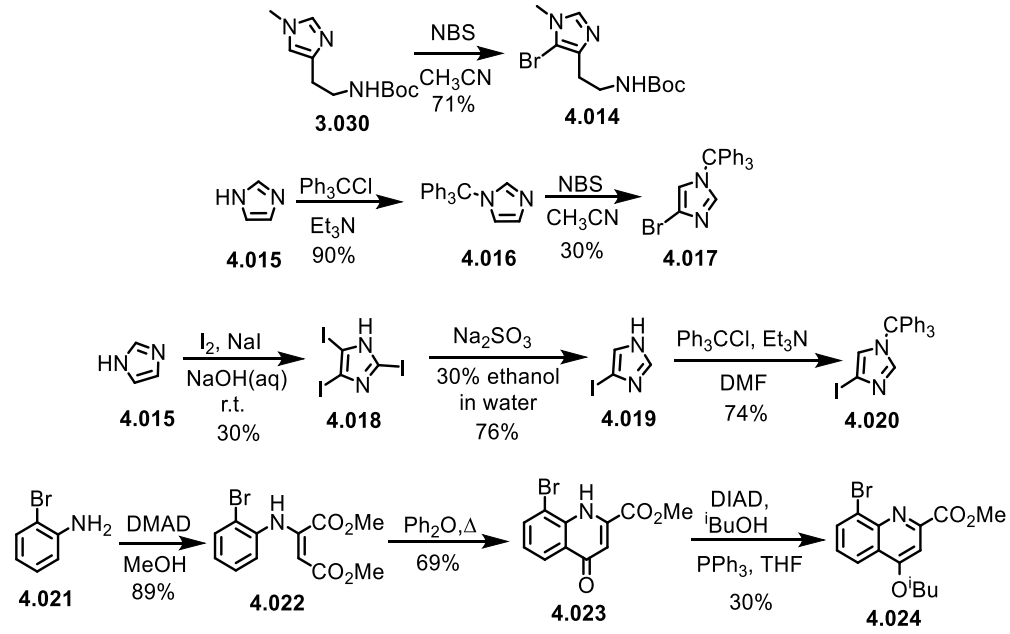

Scheme 3. The synthetic route of monomers (imidazole, histamine and quinoline derivatives)

[4] Iddon B., Lim B. L. *J. Chem. Soc. Perkin Trans. I*, **1983**, 735-739.

2.2 Cross coupling reaction between quinoline and imidazole

After successfully obtaining the monomers, the initial plan to access the quinoline-imidazole structure **4.025** was by direct cross coupling of 8-bromoquinoline monomer with imidazole or histamine. This work was done in collaboration with a post-doctoral researcher in the Singleton group, Dr Yan Yu Sarah Lam.

First, a one-pot borylation/Suzuki cross coupling was attempted in the presence of catalyst $Pd(dba)_2$ and SPhos as shown in Scheme 4 , which unfortunately did not work.

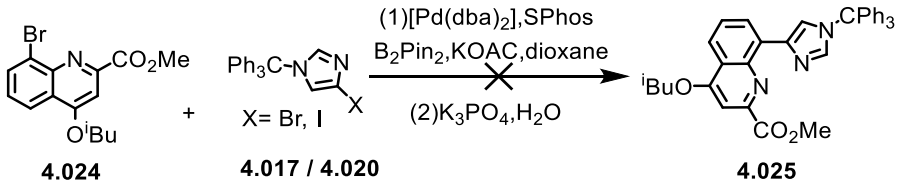

Scheme 4. The one-pot reaction for quinoline coupling with imidazole

Several attempts using Suzuki or Stille cross-coupling were also attempted. To achieve these cross-coupling reactions, conversion of 8-bromoquinoline into the boron or tin derivatives was necessary.

a. Suzuki coupling reaction attempts

In order to obtain the corresponding boronic acid derivative of the 8-bromoquinoline moiety, several conditions were tried (Scheme 5). The first two attempts, condition a and b in Scheme 5, used different Grignard reagents for the halogen exchange to obtain the quinoline boronic acid but failed. The palladium catalyzed borylation was also tried and led to a new product, however, characterization indicated this to be the quinoline homocoupling product. After these attempts, we believe the quinoline substrate might be causing problems for this reaction and so we decided to functionalize the

imidazole with the boronic acid instead.

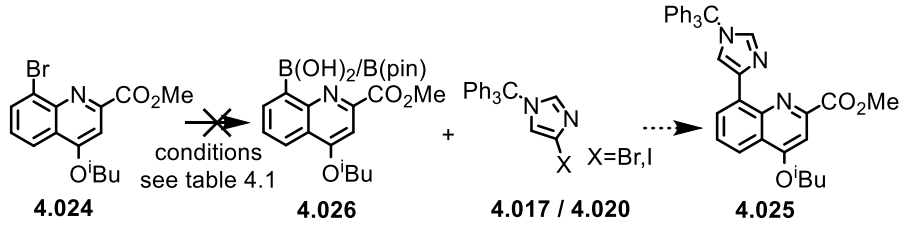

Scheme 5. The attempts of coupling quinoline and imidazole

Table 4.1 Reaction conditions attempted for compound **4.026**

Entry	Conditions	Solvent	Result
1	iPrMgCl, $B(OC_4H_9)_3$, -78°C	THF	No product
2	iPrMgCl·LiCl, $B(OC_4H_9)_3$, -78°C	THF	No product
3	B_2Pin_2, KOAC, $Pd(dppf)Cl_2·CH_2Cl_2$, 60°C	DMSO	No product
4	B_2Pin_2, KOAC, $Pd(dppf)Cl_2·CH_2Cl_2$, Reflux	1,4-dioxane	No product
5	B_2Pin_2, K_3PO_4, $Pd(dppf)Cl_2·CH_2Cl_2$, Reflux	1,4-dioxane	Quinoline homocoupling

Starting from the bromo-imidazole, the halogen/metal exchange reactions were tried with same conditions as above (Scheme 6), however this also failed to give the desired product. Some literature showed that iodo-imidazole should be a better substrate.[5] However, while we could obtain the iodo-imidazole the introduction of the boronic acid to replace the iodine group was

[5] a) Liu P., Hamill T. G., Chioda M., Chobanian H., Fung S., Guo Y., Lin L. S., *ACS Med. Chem. Lett.*, **2013**, 4(6), 509-513. b) Mathieu V., Van Den Berge E., Ceusters J., Konopka T., Cops A., Bruyère C., Kiss R., *J. Med. Chem.*, **2013**, 56(17), 6626-6637.

not successful.

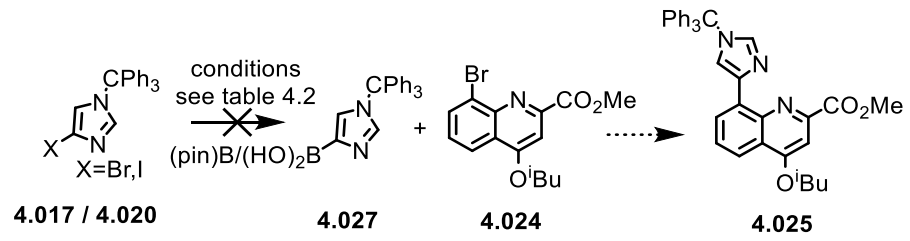

4.017 / 4.020 **4.027** **4.024** **4.025**

Scheme 6. The attempts of coupling quinoline and imidazole

Table 4.2 Reaction conditions attempted for compound **4.027**

Entry	Conditions	Solvent	Result
1	iPrMgCl, $B(OC_4H_9)_3$, -78°C	THF	No product
2	iPrMgCl·LiCl, $B(OC_4H_9)_3$, -78°C	THF	No product
3	B_2Pin_2, KOAC, $Pd(dppf)Cl_2 \cdot CH_2Cl_2$, 60°C	DMSO	No product
4	B_2Pin_2, KOAC, $Pd(dppf)Cl_2 \cdot CH_2Cl_2$, Reflux	1,4-dioxane	No product

a. Stille coupling reaction attempts

The difficulty in installing the boronic acid led us to try the Stille coupling (Scheme 7) as the starting materials were easier to obtain. An initial approach using halogen/metal exchange was not successful. However, palladium coupling with a distannane afforded the desired quinoline tin derivative in moderate yield. Unfortunately, attempts at coupling this molecule with the imidazoles did not yield the desired products.

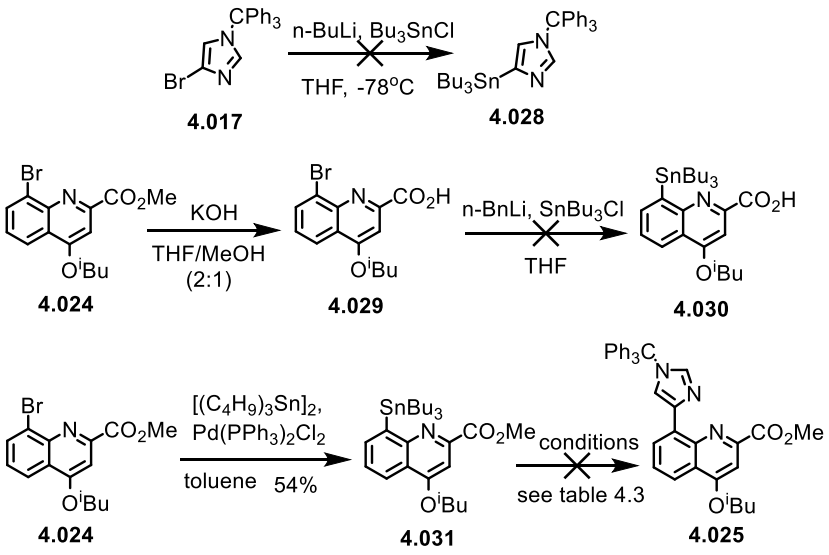

Scheme 7. The tried stille reactions

Table 4.3 Reaction conditions attempted for compound **4.025**

Entry	Conditions	Solvent	Result
1	bromoimidazole, $Pd(PPh_3)_2Cl_2$, CuI, CsF,	DMF	No product
2	bromoimidazole, $Pd(PPh_3)_2Cl_2$, CuI, CsF,	1,4-dioxane	No product
3	iodide imidazole, $Pd_2(dba)_3$, PPh_3, 90°C	DMF	No product
4	iodide imidazole, $Pd(PPh_3)_4$, $CuBr{\cdot}CH_3SCH_3$, 90°C	DMF	No product

The failure of the initial proposed direct cross coupling routes pushed us to modify the synthetic strategy. Rather than attaching the imidazole to quinoline, the quinoline unit was unit was built onto the imidazole. This was done by generating the imidazole functionalized aniline precursor **4.033** followed by synthesis of the quinoline unit as shown in Scheme 8.

The synthesis started from bromo-aniline. This was borylated in one step to obtain aniline boronic ester **4.032**, which was coupled with trityl protected iodo-imidazole to give compound **4.033**. In the presence of DMAD, compound **4.034** was obtained through alkylating. The thermal cyclization was accomplished with good yield and the trityl group was found to be stable at high temperature. However, the subsequent introduction of the isobutoxy side chain failed under the same Mitsunobu conditions used for forming 8-bromoquinoline. We suspect this was probably due to the higher steric hindrance around the reaction center when compared with its 8-bromo analogue. Therefore, the alkylation into quinoline **4.035** was accomplished by heating with isobutyl bromide in the presence of a weak base. This allowed the 8-imidazole-functionalized quinoline **4.036** to be obtained and after saponification, compound **4.037** was ready for coupling with the central diazaanthracene monomer.

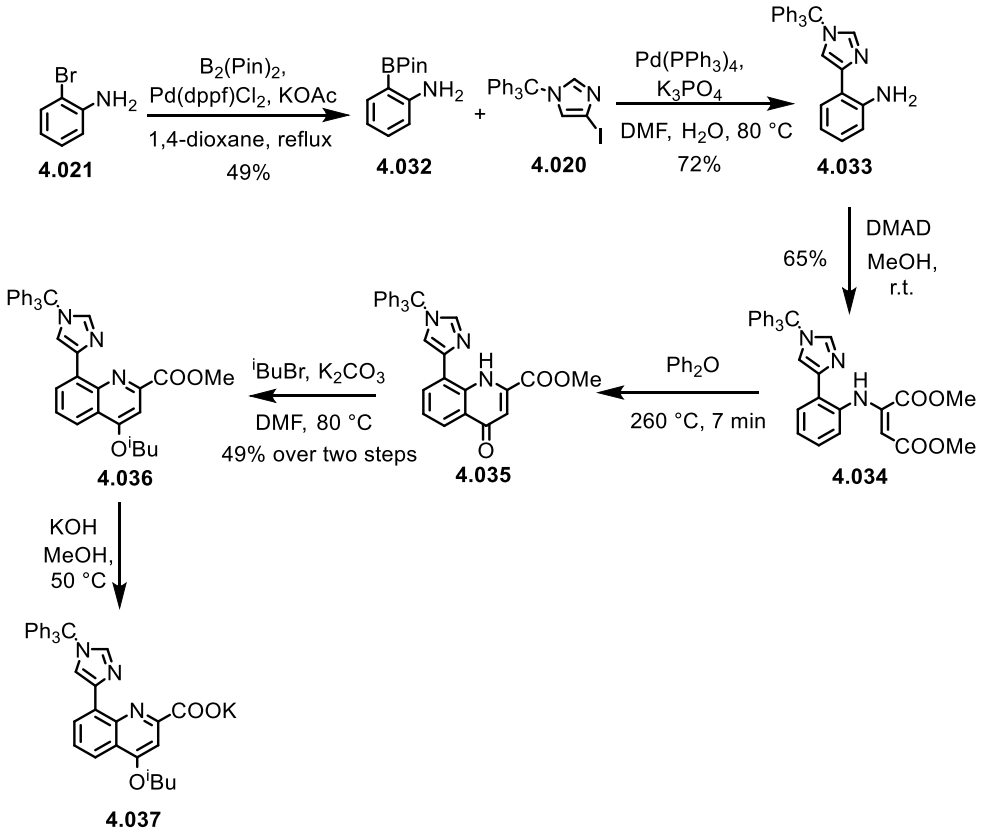

Scheme 8. Synthesis of 8-imidazole-functionalized quinoline

The same strategy was adopted to prepare the 8-histamine-functionalized quinoline **4.042** and shown to be feasible (Scheme 9). The Suzuki coupling reaction between bromohistamine **4.014** and aniline boronic ester **4.032** was successful using modified conditions for the product **4.038**,[6] which after reaction with DMAD cyclized in boiling diphenylether. Surprisingly, the thermal unstable Boc protecting group on primary amine could be retained under the

[6] Cerezo V., Afonso A., Planas M., Feliu L., *Tetrahedron*, **2007**, *63*(42), 10445-10453.

high temperature conditions by carefully controlling the reaction time and running the reaction in small batches. Therefore, the desired cyclized product **4.040** was obtained. The subsequent alkylation was conducted with isobutyl bromide and the saponification reaction was performed to get the monomer **4.042** for use in the next coupling.

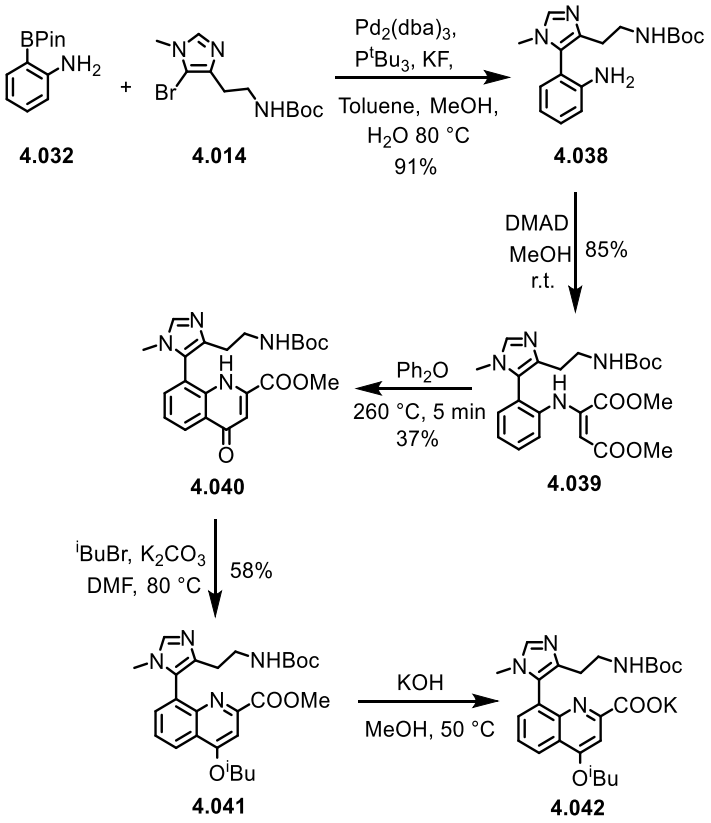

Scheme 9. Synthesis of 8-histamine-functionalized quinoline

2.3 Oligomers synthesis

With all of the monomers synthesized, the coupling for oligomer formation could procede. The 8-imidazole-functionalized quinoline monomer **4.037** could be coupled to the central diazaanthracene monomer **4.003** using PyBOP to give compound **4.043** which needed purification by column. This dimer could then be reacted with 8-histamine-functionalized quinoline **4.042** to obtain the scaffold motif **4.044** of our target LPMO mimic (Scheme 10).

Next the two acid labile protecting groups in the scaffold motif, Boc and trityl groups, were cleaved using TFA in the presence of triisopropylsilane as a cation scavenger. As the trityl residue in the crude product was difficult to remove, the highly polar unprotected trimer was reprotected with a Boc group to assist purification and permit product **4.045** to be obtained. Finally, the Boc group was removed by treatment with HCl. The crude product **4.046** was furnished with reasonable purity and could be directly used as ligand **L5** for metal binding without further purification.

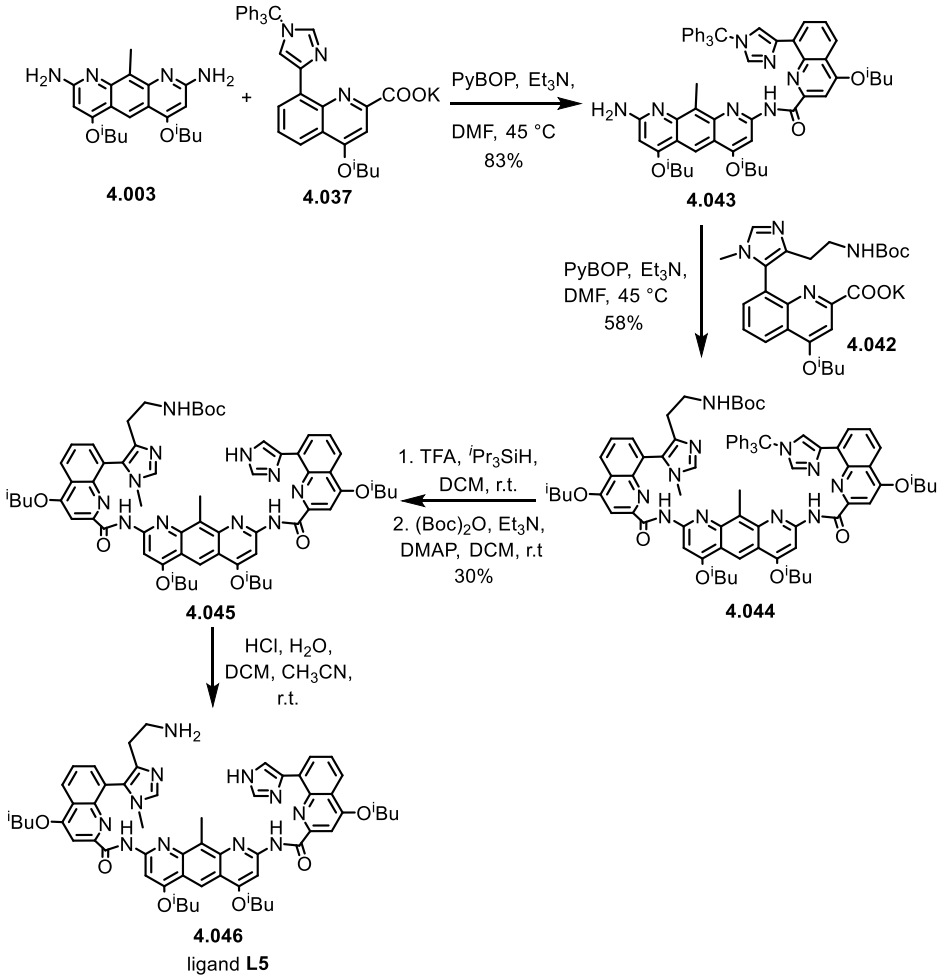

Scheme 10. The synthetic route of coupling monomers and removing the protecting groups

3. The second scaffold design

In order to study the influence of flexibility on the ability of the scaffold ligand to coordinate copper and its influence on reactivity, another more flexible scaffold **4.004** was also envisaged. This could still potentially provide the

appropriate binding site. Additionally, this design avoids some of the complicated synthetic steps described above. For this scaffold, the 8-bromomethyl quinoline derivative **4.047** was used and directly substituted with imidazole or histamine to give the monomers (Scheme 11). Once obtained, these monomers can be connected to the diazaathracene monomer **4.003** to give the scaffold ligand **4.005**. While the added flexibility of the methylene linker in quinoline leads to less pre-organization, this can nevertheless still potentially allow metal binding.

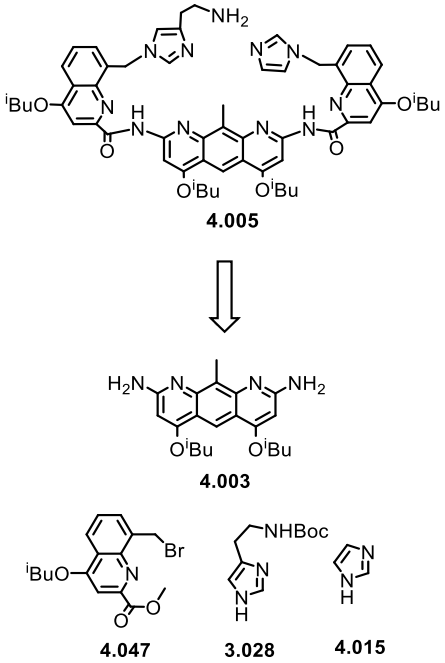

Scheme 11. The retro synthesis of the second designed complex

4. Synthesis of second designed ligand

In the second design, the 8-bromomethyl quinoline **4.047** was synthesized through halogenation of methyl quinoline which was obtained using the quinoline synthesis route described in the initial design. Then imidazole **4.015** was directly coupled with the 8-bromomethyl quinoline **4.047** in the presence of NaH. Fortuitously, the product **4.051** was obtained where the methyl ester group on quinoline was also removed during the reaction, as shown in Scheme 12. Compound **4.051** could then be directly used to couple with the central monomer diazaathracene.

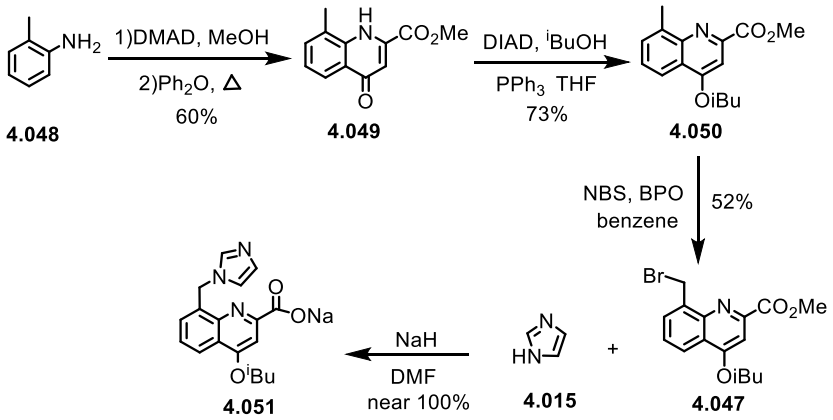

Scheme 12. The synthetic route of the quinoline-imidazole monomer

The same strategy, as shown in Scheme 13, was used to couple 8-bromomethyl quinoline **4.047** with Boc protected histamine **3.028**. However, the obtained product was found to be a mixture of the 1- and 3-alkylated histamine-quinoline regioisomers (**4.052** and **4.053**) which were difficult to separate.

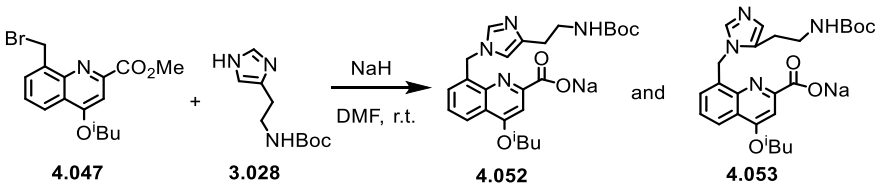

Scheme 13. The synthesis of quinoline-histamine with regioisomers

A new strategy for exclusive formation of 1-alkylated histamines that avoids the problem of regioisomers has been described.[2] This is via cyclization of histamine dihydrochloride with N,N'-carbonyldiimidazole (CDI) to provide a cyclic urea **3.022**, for which the second imidazole nitrogen atom can be functionalized by 8-bromomethyl quinoline **4.047** selectively through nucleophilic substitution. Subsequently, the quinoline-functionalized urea compound **4.054** can be ring-opened by reacting with ^{t}BuOH and DIPEA, which liberates the imidazole and provides a Boc-protected amine.[7] Then saponification of the qunoline methyl ester using KOH as base gave monomer **4.056** in good yield (Scheme 14).

[7] a) Shelton K. L., DeBord M. A., Wagers P. O., Southerland M. R., Taraboletti A., Robishaw N. K., Paruchuri S., *Tetrahedron*, **2016**, 72(38), 5729-5743. b) Guillen F., Brégeon D., Plaquevent J. C., *Tetrahedron Lett.*, **2006**, 47(8), 1245-1248.

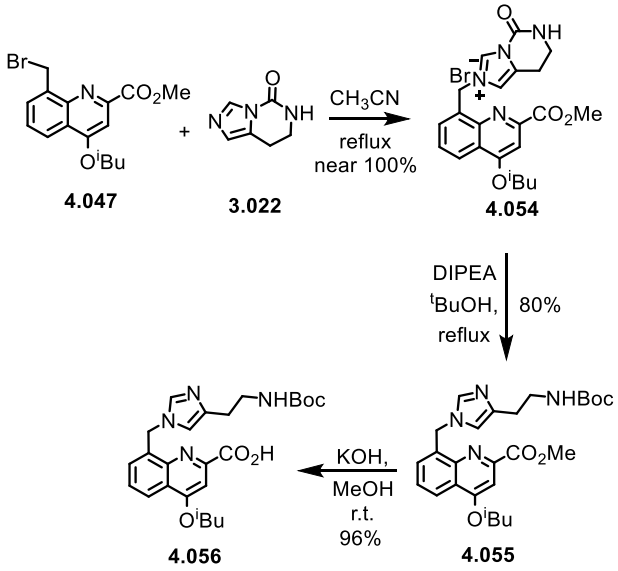

Scheme 14. The synthesis of quinoline-histamine monomer

After synthesizing all three monomers, we proceeded to couple them together to complete the synthesis of the target scaffold motif (Scheme 15). Two successful amide coupling were accomplished by using PyBOP as the coupling agent and Et_3N as the base. Finally, the compound **4.005** was obtained after removing the Boc protecting group with TFA. And the compound **4.005** (ligand **L6**) was used for coordination with copper salts.

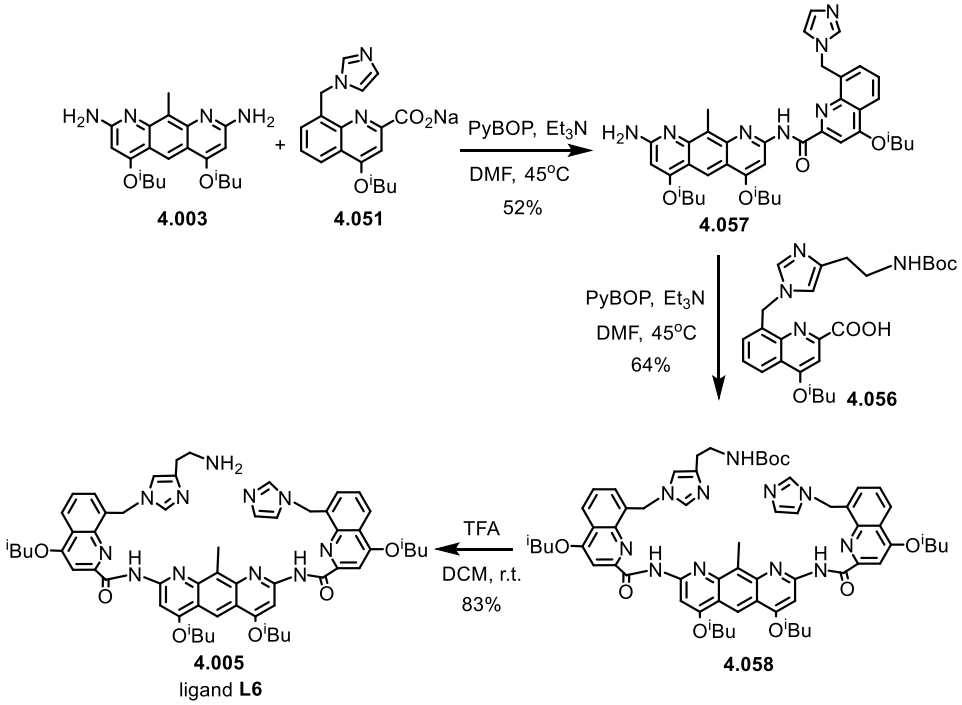

Scheme 15. Coupling of monomers

In course of the synthesis of ligand **L6**, we also observed a secondary product after the first coupling with diazaanthracene that resulted from coupling with two equivalents of **4.051**. This could be prevented by mono-protection of the diamino diazaathracene **4.003**, however, this monoprotection was not found to be efficient. However, as the doubly coupled product can also be interesting for study, it was also synthesized directly using a similar procedure, with two equivalents of **4.051** to give compound **4.059** as the ligand **L7** to study metal binding, shown in Scheme 16.

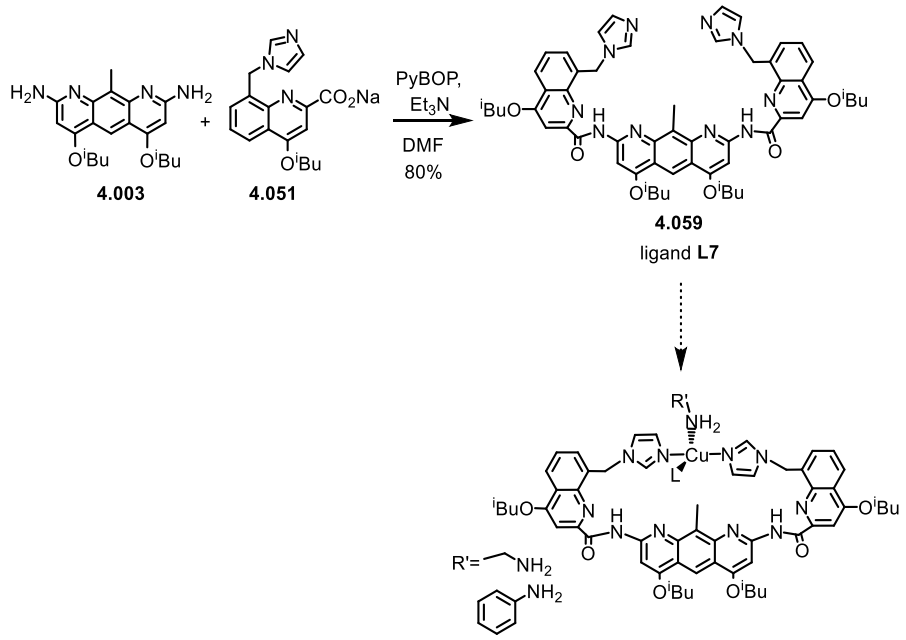

Scheme 16. The synthetic route of the ligand **L7**

Compound **4.058** was characterized by X-ray crystallography. After several attempts, the single crystal of compound **4.058** was obtained by slow diffusion of n-hexane into a DCM solution of the compound. Top and side views of crystal structure are shown in Figure 2A and B. In the solid state, intermolecular hydrogen bonding between the amide hydrogen and both adjacent quinoline or diazaanthrances is observed. This makes the trimer structure adopt the curved shape predicted for the target scaffold skeleton. From the top view, there was the cavity between histamine and imidazole moieties, which could provide enough space for metalation. Modelling studies also suggest that the flexible chains could permit the histamine and imidazole units to adopt a histidine brace like coordination motif.

Due to the π-π interaction between diazaanthrance and quinoline units, compound **4.058** was found to pack in large extended stacks, Figure 2 C and D.

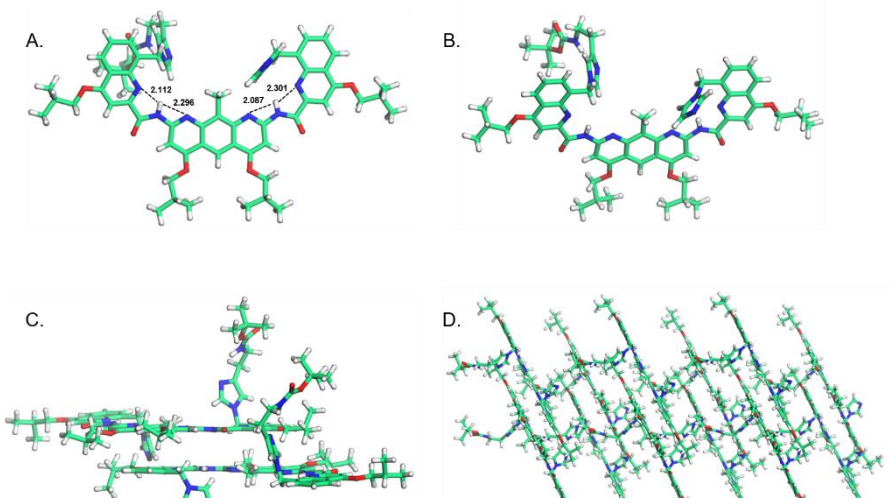

Figure 2. Side (A), top (B) and association(C) view of crystal structure of compound **4.058** (green: C, blue: N, red: O, white: H)

5. Study the scaffold ligands with metal binding

The scaffold ligands **L5-L7** were only found to be soluble in DCM and $CHCl_3$, which limited the choice of solvents for the metallation. Therefore, the scaffold ligand **L5** was metallated by reaction with three kinds of Cu(II) salts, Cu(II) tetrafluoroborate, Cu(II) perchlorate and Cu(II) chloride in a biphasic DCM and H_2O mixture solution. The UV-vis spectra of DCM solutions of these three Cu (II) complexes were taken. The results are shown in Figure 3. A new absorbance maxima appeared at around 380nm versus the free ligand **L5**. Additionally, in the spectra of complexes formed from Cu(II) tetrafluoroborate and Cu(II) perchlorate, a shoulder around 605nm was observed, whereas an

obvious peak at around 695nm was shown in the spectrum of the complex formed from Cu(II) chloride. These peaks at around 605nm and 695nm likely correspond to the d-d transition of Cu(II).[8] These data suggest that the coordination of the scaffold ligand **L5** with Cu(II) was possible. However, additional characterization studies are necessary to verify the nature of the complexes.

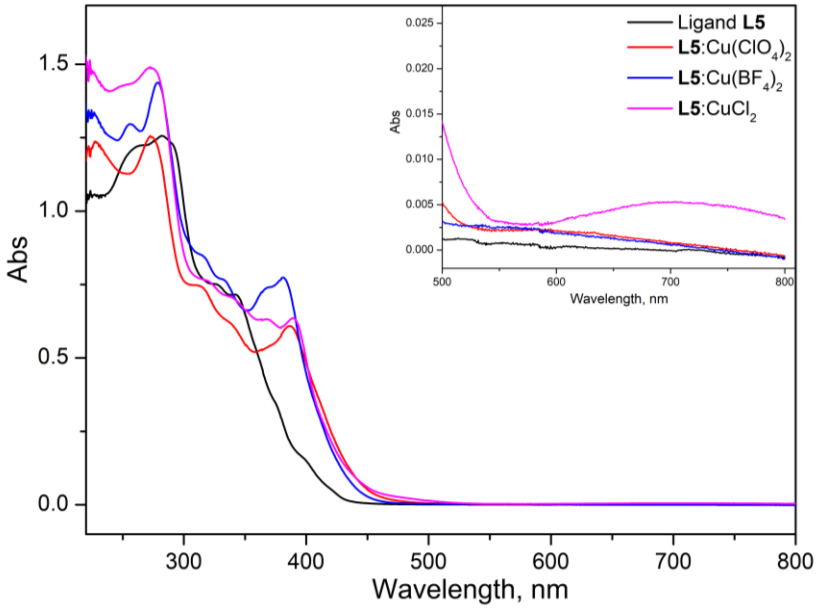

Figure 3. UV-vis spectra for ligand **L5** in the presence of different Cu(II) metals in DCM solution. (inset: zoom of the absorbance part at 500 – 800nm)

Ligand **L6** was metallated using the same conditions of ligand **L5** by reacting with Cu(II) chloride. However, by UV-vis monitoring there were no obvious

[8] a) Muthuramalingam S., Maheshwaran D., Velusamy M., Mayilmurugan R., *J. Catal.*, **2019**, 372, 352-361. b) Fukatsu A., Morimoto Y., Sugimoto H., Itoh S., *Chem. Comm.*, **2020**, *56*(38), 5123-5126.

changes compared to the free ligand.

Ligand **L6** could be dissolved in DCM, while the Cu(II) salts are normally dissolved in polar solvents, such as H_2O, MeOH and MeCN. Therefore, we tried the metallated reaction between ligand **L6** and other Cu(II) salts, Cu(II) perchlorate and Cu(II) triflate in the mixed solvent systems DCM/MeOH or DCM/MeCN = 10:1. The UV-vis spectra of DCM/MeOH solution of the two Cu(II) complexes were shown in Figure 4. In the spectra of the complex formed from Cu(II) perchlorate, there was a new obvious peak at around 372nm and a small shoulder that appears at around 650nm with respect to the free ligand. These changes were not observed when Cu(II) triflate was used as the copper source.

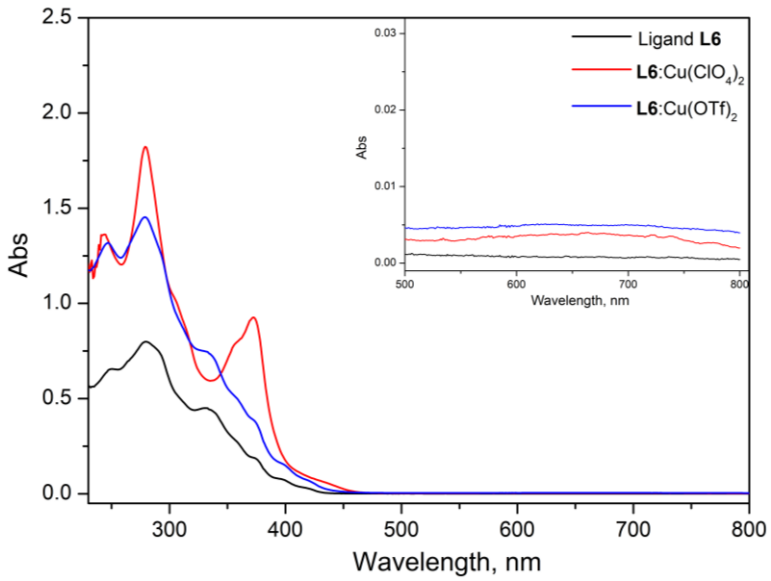

Figure 4. UV-vis spectra for ligand **L6** in the presence of $Cu(ClO_4)_2$ and $Cu(OTf)_2$ in DCM:MeOH = 10:1 solution. (inset: zoom of the absorbance part at 500 – 800nm)

In a DCM/MeCN solvent mixture, the peak at 372nm and small shoulder at 650nm were also observed in the UV-vis spectra of complexes formed from both Cu(II) perchlorate and Cu(II) triflate (Figure 5). These data could give us evidence that our scaffold ligand **L6** coordinated to the Cu(II) center in both complexes in DCM/MeCN solution, and that the same coordination could be possible with Cu(II) perchlorate in DCM/MeOH solution.

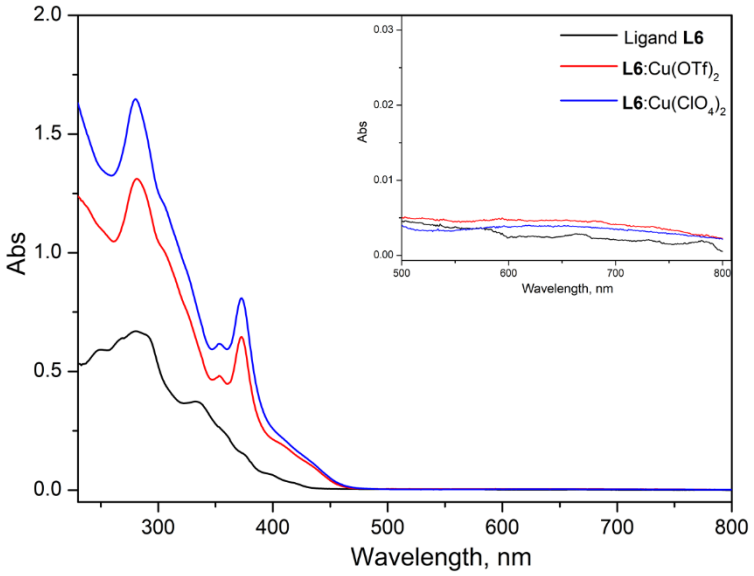

Figure 5. UV-vis spectra for ligand **L6** in the presence of $Cu(OTf)_2$ and $Cu(ClO_4)_2$ in DCM:MeCN = 10:1 solution. (inset: zoom of the absorbance part at 500 – 800nm)

6. Conclusions

A modular and conformationally controlled scaffold could be a powerful tool to design both first and second coordination spheres together in the same complexes. The easy synthesis of aromatic oligoamide foldamers, combined with their predictability and stability makes them ideal for use as scaffold. Therefore, in this chapter, we designed two scaffold ligands **L5** and the more flexible ligand **L6** with imidazole/histamine functionalized quinoline units connected to a central diazaanthracene unit. For the synthesis of ligand **L5**, the best approach started from the aniline boronic ester which could be coupled directly with a 4-halo-imidazole or 5-halo-histamine followed by building up of the quinoline moiety. These units could then be reacted with the central diazanthrance monomer to form ligand **L5**.

The methodology used for the synthesis the quinolines connected to imidazole/histamine allows them to be obtained in moderate yields and in gram scale. This is actually higher than for similar compounds reported in the literature and provides a more functionalized scaffold. As these types of structural motifs have been reported to have interesting biological activities, including inhibition of parasital growth and good selectivity over the activity of human histone deacetylases in cells,[9] this new synthetic approach can be of more general interest. More specifically, this method could also provide easy access to the quinoline-imidazole/histamine compound to be used for medicinal chemistry studies.

When we synthesized the ligand **L6**, the benzyl position of methyl quinoline could be readily brominated, allowing direct alkylation of the imidazole or

[9] Ontoria J. M., Paonessa G., Ponzi S., Ferrigno F., Nizi E., Biancofiore I., Bresciani A., *ACS Med. Chem. Lett.*, **2016**, 7(5), 454-459.

histamine endocyclic nitrogens. Ligand **L6** was then successfully obtained by coupling of the central diazaanthracene monomer and the imidazole/histamine functionalized quinoline moieties. The crystal structure of ligand **L6** precursor, compound **4.058**, indeed showed the expected compact curved shape of the trimer and it was observed that the scaffold provides adequate space to coordinate with Cu(II).

Finally, the UV-vis studies suggested that ligand **L5** could be metallated by reaction with Cu(II) salts, $Cu(BF_4)_2$, $Cu(ClO_4)_2$ and $CuCl_2$ in DCM solution. Ligand **L6** also appears to be able to coordinate to Cu(II) in DCM/MeOH = 10:1 mixtures when $Cu(OTf)_2$ and $Cu(ClO_4)_2$ are used. Nevertheless, additional characterization and structural studies are necessary to validate the nature of the complexes.

Chapter V

Conclusions and Perspectives

1. Conclusions

Despite significant research done on LPMO, many questions about its specific active site structure and reactivity persist. Notably, the role of certain first and second coordination sphere features is unclear from the biological studies. A major goal of the research described in this thesis was the design and synthesis of new model complexes of the LPMO active site, specifically the histidine brace. For this, the work was split into two parts.

First, a series of small molecule copper complexes were designed using the simple ligands (**L1-L4**) containing two imidazole groups connected by an aliphatic amide linker (Figure 1A). These were designed in order to look at the effect that orientation of the imidazoles (chelate ring size, torsion angles) and imidazole methylation patterns have on the properties and reactivity of the metal site. While no crystal structure of the small molecule complexes could be obtained, UV-vis spectrophotometric titration, Job's plot analysis, and MS data suggest that the stoichiometries between $CuCl_2$ and the ligands in MeOH and H_2O, were 1:1. As would be expected with an N_3 coordination of Cu by the ligand, FTIR indicate the participation of the amide for Cu(II) ligation. The catalytic activity of the Cu(II) complexes **1-4** were evaluated for the cleavage of the glycosidic bond of a model saccharide substrate, p-nitrophenyl-β-D-

glucopyranoside (Figure 1 B, C) in the presence of H_2O_2 and in two different solutions, carbonate buffer (100mM, pH=10.5) solution and aqueous solution (with Et_3N). The concentration of p-nitrophenolate produced during the assays was higher in presence of Cu(II) complexes **1**, **2** than Cu(II) salts ($CuCl_2$, $CuSO_4$) in all cases. The methylation of the imidazole in the ligands did not have obvious influence on the reactivity, however, the complexes **3** and **4** with small chelate rings were less reactive than the larger ligands.

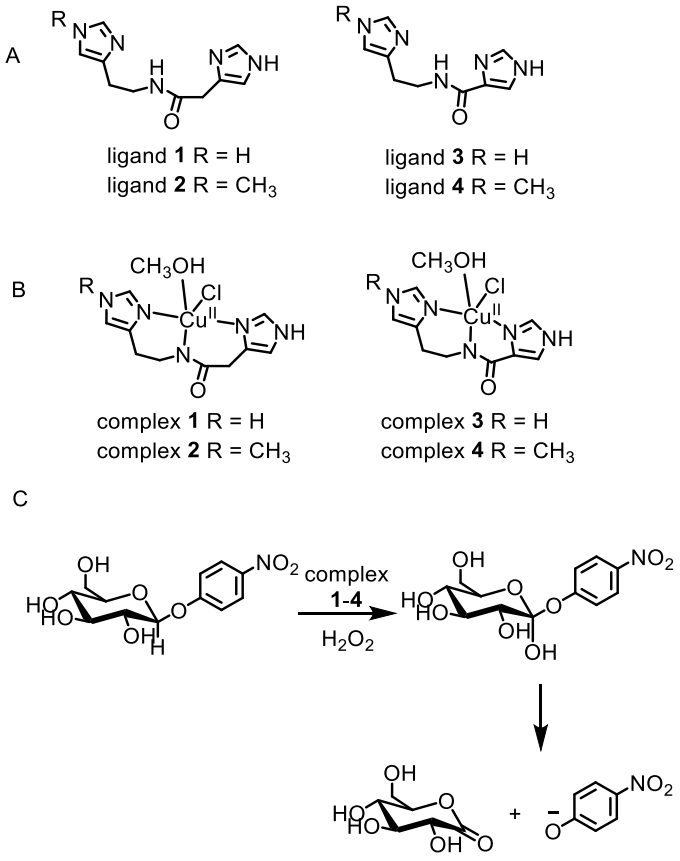

Figure 1. A) The structure of small molecule ligands. B) The proposed structure of small molecule complexes. C) The oxidative cleavage of p-nitrophenyl-β-D-glucopyranoside

In the second part of the work, we looked at developing molecular systems that could model both the first and second coordination spheres in LPMOs. Conformationally stable and predictable folded aromatic oligoamide scaffolds were used to engineer multi-layered coordination environment that could potentially replicate the exact binding motif found in the histidine brace and be modified for studying second coordination sphere interactions. Two scaffold motifs, ligands **L5** and **L6**, were designed and consisted of a central diazaanthracene unit and two quinolines functionalized with imidazole or histamine (Figure 2). For these last two monomers, the new routes to obtain them represent important approaches for synthesizing imidazole functionalized quinolines. This structure represents a potentially interesting motif for medicinal chemistry studies or interaction with biomolecules.[1] Still, to date, only a few approaches for obtaining this motif have been described, with most giving only low yields of the products.

The crystal structure of **L6** showed the formation of the expected curved conferred by intramolecular electrostatic interactions between the endocyclic nitrogen of the heteroaromatics and the internal amide bonds. The resulting structures could hold the imidazole and histamine in the desired oriented to mimic the “histidine brace” motif in the LPMOs active site with incorporation of the primary amine group, something that has not yet been achieved by other model complexes. The UV-vis spectra of the reaction of Cu(II) salts with ligands **L5** and **L6** suggest that the scaffolds do coordinate a Cu(II) center. However, additional structural studies are needed to validate the exact coordination environment of Cu and see if it matches with the active site of LPMO. In course of the synthesis of ligand **L6**, ligand **L7** could also be isolated, coming from reaction of two equivalents of **4.051** with the diamino

[1] Ontoria J. M., Paonessa G., Ponzi S., Ferrigno F., Nizi E., Biancofiore I., Bresciani A., *ACS Med. Chem. Lett.*, **2016**, 7(5), 454-459.

diazaanthracene **4.003**. This ligand can also be interesting to use for studying metal binding.

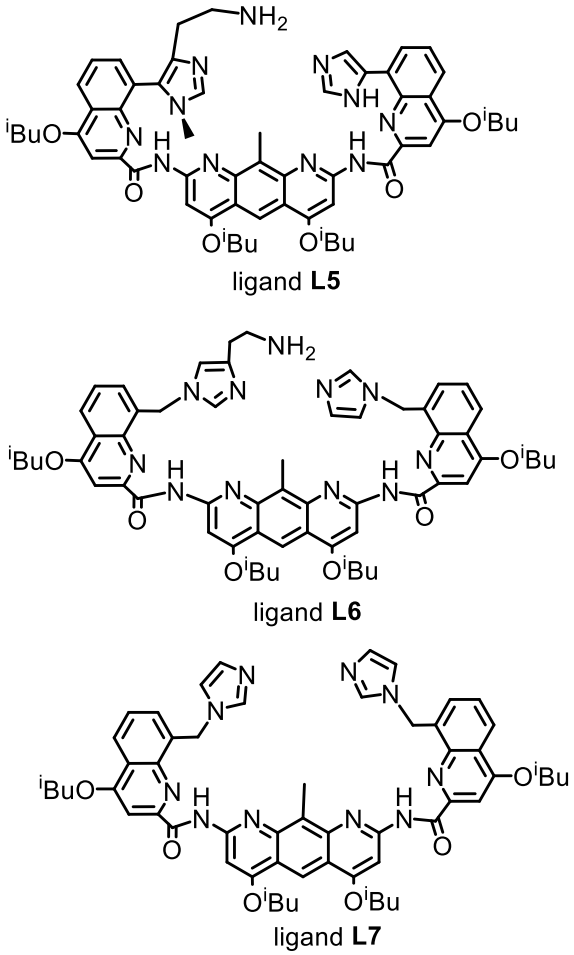

Figure 2. The molecular structures of the scaffold ligands

In all, a large amount of synthetic work has gone into the ligand development and a range of new molecules and synthetic procedures have been obtained. Initial work has been performed for coordination of the ligands to Cu(II) salts, and while optimization is still needed, it shows the potential of these structures

in coordination chemistry and for modeling LPMO. Notably, the reactivity studies using small molecule Cu(II) complexes do show that the complexes possess some catalytic activity. However, more work towards confirming the structure of the Cu(II) complexes and studying the electronic properties, and reactivity of the complexes needs to be done.

2. Perspectives

2.1 Small molecule models

Although the small molecule ligands could coordinate Cu(II) with a 1:1 stoichiometry as indicated by the UV-vis studies, obtaining the solid state structures will be necessary for comparison of the structural parameters vs properties with previously reported complexes. Therefore, obtaining the crystal structures of the Cu(II) complexes is an important goal. With this, the corresponding electronic properties of the Cu(II) complexes, based on cyclic voltammetry and EPR, can be rationalized to better understand the role of the active site “histidine brace” of LPMOs. Additionally, it will be useful to perform the catalytic reactivity assays with additional verification of the products formed, notably the aldonic acid formed during the oxidation reaction of p-nitrophenyl-β-D-glycopyranoside.

It will also be important to look at other methods for obtaining the amine linked ligands. Based on literature, the Cu(II) complex **5.002** was proposed to be obtained based on spectroscopic determintion.[2] For the synthesis of their imine, they used a one pot synthesis/metallation procedure. The presence of the metal likely drives the equilibrium for imine formation towards the product.

[2] Casella L., Gullotti M., Pallanza G., Buga M., *Inorg. Chem.*, **1991**, 30(2), 221-227.

Using this approach could help form the imine containing Cu(II) complex with imidazolecarboxaldehyde and methyl histamine. Then through reducing in the presence of $NaBH(OAc)_3$, or another hydride source, the secondary amine Cu(II) complex can be produced, Figure 3. A similar reaction sequence could be done with histimine or methylhistidine.

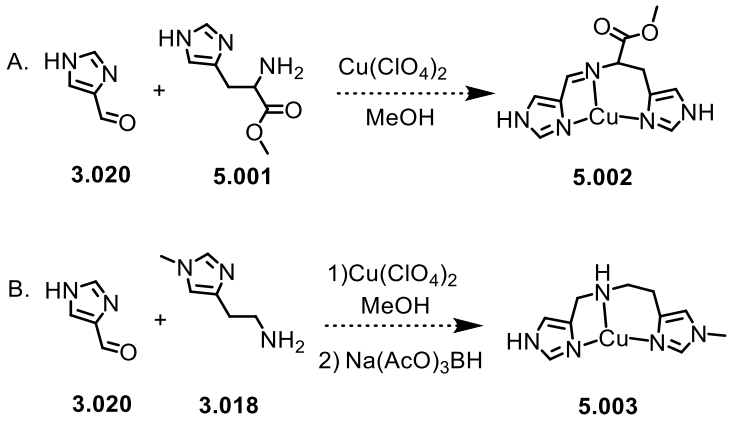

Figure 3. The proposed synthetic routes for imine and secondary amine Cu(II) complexes (A. reported in literature; B. designed in our lab)

2.2 Scaffold based models

For the scaffold models, three scaffold ligands **L5**, **L6** and **L7** have been synthesized successfully. The UV-vis spectra of the reaction of Cu(II) salts with ligands **L5** and **L6** suggest that the scaffolds do coordinate a Cu(II) center. However, additional optimization of the conditions for metallation and additional structural studies are needed to validate the exact coordination environment of Cu and see if it matches with the active site of LPMO. This will require notably, the growing the crystals of the corresponding Cu(II) complexes. Additionally, in order to study how the second coordination sphere structural changes affect the electronic nature and stability of copper active site, the ligands will need to be modified. Specifically the central

diazaanthracene unit could be used to provide different long range axial interactions (Figure 4).

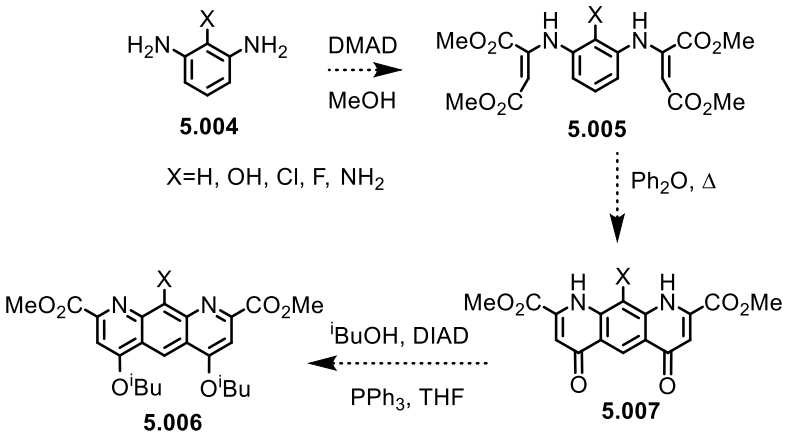

Figure 4. The derivatization of diazaanthracene units.

Because the solubility of scaffold ligands **L5** and **L6** have impeded trying a large number of conditions for the metalation with copper salts. It can be interesting to increase solubility. The side chains in quinoline and diazaanthracene monomers could also be changed to more soluble groups such as tetraethylene glycol chains[3] or water solubilizing groups.[4] Both of these can facilitate metalation by allowing both the salt and ligand to be in the same (more polar) solvent. Additionally, our group recently found that by performing a Diels-Alder reaction on the central anthracene unit to obtain triptycene unit, the solubility is significantly enhanced. Moreover, this could also provide an additional site for the incorporation of second coordination

[3] Hu X., Dawson S. J., Mandal P. K., Hatten X., Baptiste B., Huc I., *Chem. Sci.*, **2017**, 8(5), 3741-3749.

[4] Hu X., Dawson S. J., Nagaoka Y., Tanatani A., Huc I., *J. Org. Chem.*, **2016**, 81(3), 1137-1150.

sphere functionalities (Figure 5).

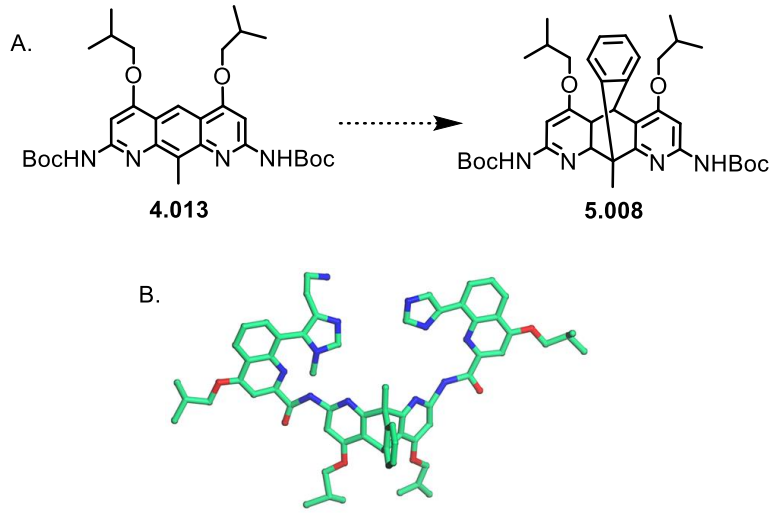

Figure 5. A) The Diels-Alder reaction on the central anthracene unit to obtain triptycene unit, B) The proposed structure of scaffold ligand with triptycene center monomer

The studying of the oxidation reactivity of the copper complexes based on scaffold ligands will also be very important. The p-nitrophenyl-β-D-glycopyranoside could also be used as the model saccharide substrate for these complexes. However, other saccharide substrates such as cellobiose, or molecules containing stronger C-H bonds such as cyclohexane could give an important indication of the strength of the reactive oxygen species. Such studies would also need to be performed with spectroscopic monitoring to see if the nature of the reactive oxygen species can be determined.

Finally, the scaffold ligands developed in this chapter represent a potentially important tool for use more generally in coordination chemistry as their modular nature can allow easy modification for studying second coordination sphere interactions. With the new imidazole based monomers, this approach

could be extended to the modeling of a range of biological metalloenzyme active sites.

Chapter VI

Experimental Section

1. Instrumentation

^{1}H and ^{13}C nuclear magnetic resonance spectra were recorded on a Bruker Avance II 300 MHz spectrometer (^{1}H 300 MHz and ^{13}C 75 MHz). ^{1}H chemical shifts are reported in ppm downfield from internal tetramethyl silane (δ = 0 ppm), Chloroform-*d* (δ = 7.26 ppm), DMSO-d_6 (δ = 2.50 ppm) or Methanol-d_4 (δ = 3.31 ppm). ^{13}C chemical shifts are reported in ppm using Chloroform-*d* (δ = 77.16 ppm), DMSO-d_6 (δ = 39.52 ppm) or Methanol-d_4 (δ = 49 ppm). If necessary, the structures were determined by two-dimensional analysis (COSY, HMQC and HMBC). ^{1}H NMR spectra are described as follows: chemical shift (multiplicity, coupling constant (Hz), integration). ^{13}C spectra are described as follow: chemical shift. Multiplicity is designed as: s = singlet; d = doublet; t = triplet; q = quartet; qui = quintet; sex= sextet; sep = septet; b = broad; m = multiplet.

High-resolution mass spectra were recorded by Mr. Raoul Rozenberg using VARIAN MATT-44, FINNIGAN MAT-TSQ 7000 and THERMOFISCHER ORBITRAP spectrometers from Mass Spectrometry Service of Université catholique de Louvain (Belgium).

X-ray diffraction analysis of compounds **3.012** and **4.005** was recorded by Dr. Koen Robeyns at the Institute of Condensed Matter and Nanosciences of

UCLouvain. X-ray analysis of compound **$Cu_2(L1)_2$** was recorded by Dr. Brice Kauffmann at the European Institute of Chemistry and Biology in Pessac, France.

Infrared spectra were recorded by transmittance on PerkinElmer spectrum two and reported in wavenumber(cm^{-1}). The samples were analyzed directly as solid.

UV-vis spectra were recorded using VWR UV-1600PC spectrophotometer.

2. Procedure

Unless otherwise noticed, all manipulations were performed under an argon atmosphere using standard glassware. Diethyl ether and tetrahydrofuran were distilled on sodium/benzophenone under an argon atmosphere. Dichloromethane, triethylamine and toluene were distilled on calcium hydride under an argon atmosphere. Solvents used for work-ups were of technical grade. Commercial reagents were purchased from Acros, Sigma-Aldrich, ABCR, TCI, Merck or Fluorochem and used as received unless stated otherwise.

Thin layer chromatography (TLC) was performed on Merck Millipore F_{254} silica gel 60 plates (200 µm thickness, aluminium supported). The plates were visualized using ultra-violet light (254 nm) and stained using an alkaline potassium permanganate, vanillin or ninhydrin solution. Flash chromatography was performed with the stated solvents using Sigma-Aldrich silica gel 60 (70 – 230 mesh).

Synthesis of 7, 8-dihydroimidazo[1,5-c] pyrimidin-5(6H)-one (3.022)

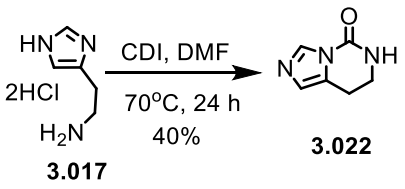

3.017 **3.022**

A solution of histamine dihydrochloride **3.017** (3 g, 16.3 mmol) and carbonyl diimidazole (2.67 g, 16.4 mmol) in DMF (30 mL) was stirred at 70 °C for 24h. All DMF was removed in vacuo, yielding the crude oil which was dissolved in saturated $NaHCO_3$ solution. The aqueous solution was extracted with DCM, and the combined extracts were dried (Na_2SO_4) and evaporated. The residual solid was recrystallized from acetonitrile to afford product (0.9 g, 40%) as a white solid.

Formula: $C_6H_7N_3O$ **Molecular Weight:** 137.14 g/mol

^{1}H NMR (300 MHz, DMSO-*d*$_6$) δ 8.20 (s, 1H), 8.05 (d, *J* = 0.9 Hz, 1H), 6.80 (q, *J* = 1.1 Hz, 1H), 3.40 – 3.33 (m, 2H), 2.88 (td, *J* = 6.5, 1.2 Hz, 2H) ppm.

^{13}C NMR (75 MHz, DMSO-*d*$_6$) δ 148.8, 134.5, 127.7, 125.1, 39.1, 19.7 ppm.

The characteristic data corresponded with reported literature values.[1]

[1] Durmus S., Garrison J. C., Panzner M. J., Tessier C. A., Youngs W. J., *Tetrahedron*, **2005,** 61(1), 97-101.

Synthesis of 2-methyl-5-oxo-5,6,7,8-tetrahydroimidazo[1,5-c] pyrimidin-2-ium (3.040)

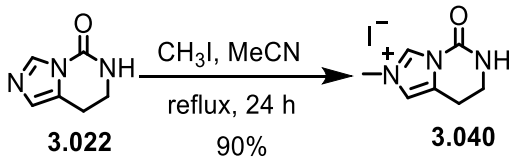

3.022 **3.040**

To a suspension of **3.022** (1.0 g, 7.29 mmol) in acetonitrile (50 mL) were added 3 equivalents of CH_3I (1.36 mL, 21.87 mmol). The reaction mixture was heated under reflux for 24 h, at which point TLC showed the absence of starting material. The solution was cooled and evaporated to dryness in vacuo to give the pure product (1.83 g, 90%)

Formula: $C_7H_{10}N_3O^+I^-$ **Molecular Weight:** 279.08 g/mol

^{1}H NMR (300 MHz, DMSO-*d*$_6$) δ 9.66 (dd, J = 1.6, 0.9 Hz, 1H), 9.02 (s, 1H), 7.59 (t, J = 1.4 Hz, 1H), 3.89 (d, J = 0.8 Hz, 3H), 3.52 – 3.43 (m, 2H), 3.02 (td, J = 6.6, 1.3 Hz, 2H) ppm.

^{13}C NMR (75 MHz, DMSO-*d*$_6$) δ 145.5, 135.7, 131.0, 119.7, 38.9, 36.8, 18.8 ppm.

The characteristic data corresponded with reported literature values.[2]

[2] Saulnier M. G., Frennesson D. B., Wittman M. D., Zimmermann K., Velaparthi U., Langley D. R., Greer A., *Bioorg. Med. Chem. Lett.*, **2008**, 18(5), 1702-1707.

Synthesis of 2-(1-methyl-1H-imidazol-4-yl)ethan-1-amine (3.018)

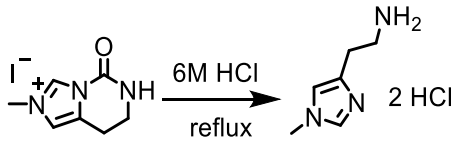

3.040 **3.018**

A solution of **3.040** (1 g, 3.6 mmol) in 6 M HCl was refluxed for 24 h. The solvent was evaporated in vacuo to afford the dihydrochloride of 1-methylhistamine as a gray solid (0.57 g, 89%).

Formula: $C_6H_{11}N_3$•2HCl **Molecular Weight:** 198.1 g/mol

^{1}H NMR (300 MHz, DMSO-d_6) δ 9.04 (d, *J* = 1.5 Hz, 1H), 8.18 (s, 2H), 7.54 (d, *J* = 1.4 Hz, 1H), 3.81 (s, 3H), 3.09 (dd, *J* = 12.0, 6.0 Hz, 2H), 2.98 (t, *J* = 7.2 Hz, 2H) ppm.

The characteristic data corresponded with reported literature values. [2]

Synthesis of N-(2-(1H-imidazol-4-yl)ethyl)-2-(1H-imidazol-4-yl)acetamide (3.009)

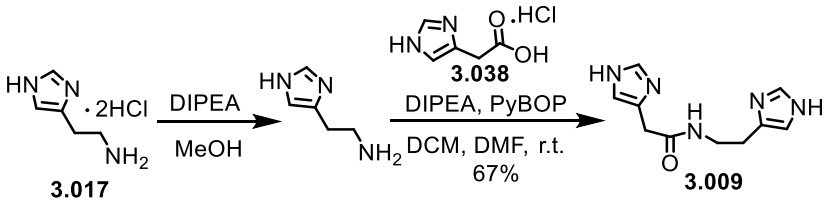

Histamine dihydrochloride **3.017**(0.1132 g, 0.615 mmol) was added to MeOH and two equiv. of diisopropylethylamine (DIPEA, 0.214 mL, 1.23 mmol) were added to yield a clear solution. MeOH was removed under reduced pressure and the residue dissolved in anhydrous DMF. To this solution at 0 °C were added the 4-imidazoleacetic acid hydrochloride **3.038** (0.1 g, 0.615 mmol), DIPEA (0.535 mL, 3.075 mmol), and PyBOP (0.32 g, 0.615 mmol) all dissolved in DCM. The resulting slurry was stirred for 48h at room temperature before removal of the solvent under reduced pressure. The resulting residue was purified by column chromatography on SiO_2 with DCM/MeOH (9:1; Et_3N = 1%) as the eluant to afford an off-red solid (91.1 mg, 67%).

Formula: $C_{10}H_{13}N_5O$ **Molecular Weight:** 219.25 g/mol

^{1}H NMR (300 MHz, Methanol-d_4) δ 7.66 – 7.61 (m, 1H), 7.60 (d, *J* = 1.2 Hz, 1H), 6.93 (s, 1H), 6.82 (d, *J* = 1.2 Hz, 1H), 3.50 (d, *J* = 0.8 Hz, 2H), 3.45 (t, *J* = 7.1 Hz, 2H), 2.78 (td, *J* = 7.1, 0.8 Hz, 2H) ppm.

^{13}C NMR (75 MHz, Methanol-d_4) δ 171.7, 135.1, 134.7, 134.3, 131.8, 116.9, 116.8, 39.2, 34.1, 26.2 ppm.

HRMS(ESI): m/z calculated for $C_{10}H_{14}N_5O$ $[M+H]^+$: 220.11929. found: 220.11926

Synthesis of 2-(1H-imidazol-4-yl)-N-(2-(1-methyl-1H-imidazol-4-yl)ethyl)acetamide (3.010)

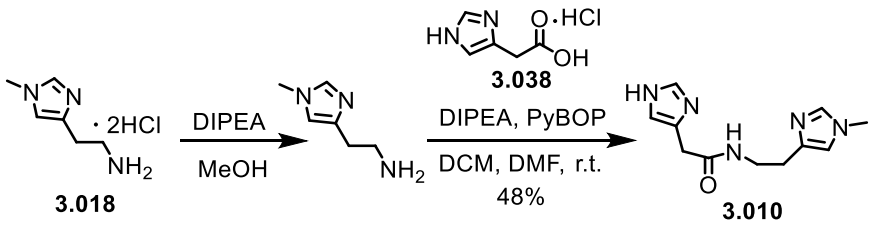

1-Methylhistamine dihydrochloride **3.018** (0.0975 g, 0.492 mmol) was added to MeOH and two equiv. Diisopropylethylamine (DIPEA, 0.171 mL, 0.9842 mmol) was added to yield a clear solution. The MeOH was removed under reduced pressure and the residue dissolved in anhydrous DMF. To this solution was added the 4-imidazoleacetic acid hydrochloride **3.038** (0.08 g, 0.492 mmol), DIPEA (0..429 mL, 2.46 mmol), and PyBOP (0.256 g, 0.492 mmol) all dissolved in DCM at 0 °C. The resulting slurry was stirred for 48h at room temperature before removal of the solvent under reduced pressure. The resulting residue was purified by column chromatography on SiO_2 with DCM/MeOH (9:1; Et_3N = 1%) as the eluant to afford an off-white solid (55.5 mg, 48%).

Formula: $C_{11}H_{15}N_5O$ **Molecular Weight:** 233.28 g/mol

^{1}H NMR (300 MHz, Methanol-d_4) δ 7.63 (d, *J* = 1.2 Hz, 1H), 7.49 (d, *J* = 1.4 Hz, 1H), 6.93 (d, *J* = 1.2 Hz, 1H), 6.80 (d, *J* = 1.3 Hz, 1H), 3.67 (s, 3H), 3.49 (d, *J* = 0.8 Hz, 2H), 3.43 (t, *J* = 7.1 Hz, 2H), 2.75 – 2.68 (m, 2H) ppm.

^{13}C NMR (75 MHz, Methanol-d_4) δ 172.4, 139.5, 138.1, 135.8, 132.5, 118.3, 117.9, 40.0, 34.9, 33.0, 28.1 ppm.

HRMS(ESI): m/z calculated for $C_{11}H_{16}N_5O$ $[M+H]^+$: 234.13494. found: 234.13493.

Synthesis of H-imidazole-4-carboxamide (3.011)

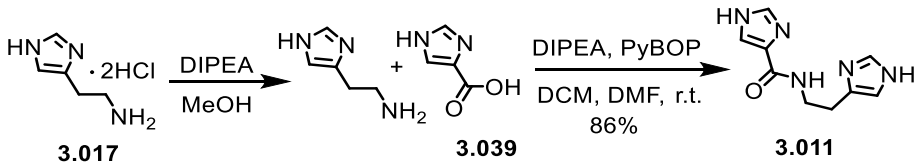

3.017 **3.039** **3.011**

Histamine dihydrochloride **3.017**(0.821 g, 4.46 mmol) was added to MeOH and two equiv. diisopropylethylamine (DIPEA, 1.554 mL, 8.92 mmol) was added to yield a clear solution. The MeOH was removed under reduced pressure and the residue dissolved in anhydrous DMF. To this solution at 0 °C was added the 4-Imidazolecarboxylic acid **3.039** (0.5 g, 4.46 mmol), DIPEA (2.33 mL, 13.38 mmol), and PyBOP (2.32 g, 4.46 mmol) all dissolved in DCM. The resulting slurry was stirred for 48h at room temperature before removal of the solvent under reduced pressure. The resulting residue was purified by column chromatography on SiO_2 with DCM/MeOH (9:1; Et_3N = 1%) as the eluant to afford an off-red solid (79 mg, 86%).

Formula: $C_9H_{11}N_5O$ **Molecular Weight:** 205.22 g/mol

1H NMR (300 MHz, Methanol-*d*$_4$) δ 7.69 (d, J = 1.2 Hz, 1H), 7.65 (d, J = 1.2 Hz, 1H), 7.63 (d, J = 1.2 Hz, 1H), 6.90 (s, 1H), 3.62 (t, J = 7.1 Hz, 2H), 2.89 (t, J = 7.1 Hz, 2H) ppm**.**

^{13}C NMR (75 MHz, Methanol-*d*$_4$) δ 164.9, 137.3, 136.0, 135.6, 121.77, 118.1, 39.9, 27.8 ppm.

HRMS(ESI): m/z calculated for $C_9H_{12}N_5O$ $[M+H]^+$: 206.10364. found: 206.10362.

Synthesis of N-(2-(1-methyl-1H-imidazol-4-yl)ethyl)-1H-imidazole-4-carboxamide (3.012)

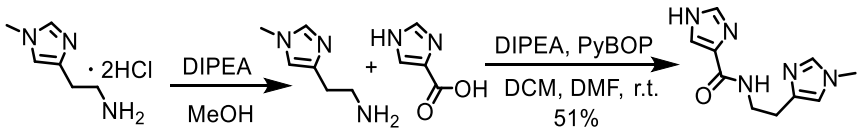

1-Methylhistamine dihydrochloride **3.018** (0.1 g, 0.5 mmol) was added to MeOH and two equiv. diisopropylethylamine (DIPEA, 0.234 mL, 1 mmol) was added to yield a clear solution. The MeOH was removed under reduced pressure and the residue dissolved in anhydrous DMF. To this solution at 0 °C was added the 4-Imidazolecarboxylic acid **3.039** (0.0567 g, 0.5 mmol), DIPEA (0.261 mL, 1.5 mmol), and PyBOP (0.263 g, 0.5 mmol) all dissolved in DCM. The resulting slurry was stirred for 48h at room temperature before removal of the solvent under reduced pressure. The resulting residue was purified by column chromatography on SiO_2 with DCM/MeOH (9:1; Et_3N = 1%) as the eluant to afford an off-red solid (51 mg, 51%).

Formula: $C_{10}H_{13}N_5O$ **Molecular Weight:** 219.25 g/mol

^{1}H NMR (300 MHz, Methanol-d_4) δ 7.68 (d, *J* = 1.2 Hz, 1H), 7.63 (d, *J* = 1.2 Hz, 1H), 7.53 – 7.48 (m, 1H), 6.89 (d, *J* = 1.3 Hz, 1H), 3.67 (s, 3H), 3.61 (t, *J* = 7.1 Hz, 2H), 2.82 (td, *J* = 7.2, 0.8 Hz, 2H) ppm.

^{13}C NMR (75 MHz, Methanol-d_4) δ 163.4, 138.7, 137.3, 135.9, 120.5 – 120.1 (m), 117.5, 38.6, 32.2, 27.6 ppm.

HRMS(ESI): m/z calculated for $C_{10}H_{14}N_5O$ $[M+H]^+$: 220.11929. found: 220.11936.

Synthesis of tert-butyl (2-(1-methyl-1H-imidazol-4-yl)ethyl)carbamate (3.030)

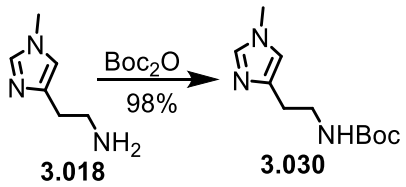

3.018 **3.030**

To a solution of 1-methylhistamine **3.018** (0.5 g, 3.99 mmol) in DCM were added saturated $NaHCO_3$ (10 mL) and $(Boc)_2O$ (1.74 g, 7.98 mmol). The solution was stirred for 120 h at room temperature and the aqueous phase was extracted with DCM. The combined organic phases were dried over Na_2SO_4, filtered and the volatiles were evaporated in vacuo. The product was afforded as white solid (0.88 g, 98%).

Formula: $C_{11}H_{19}N_3O_2$ **Molecular Weight:** 225.29 g/mol

1H NMR (300 MHz, Chloroform-*d*) δ 7.34 – 7.26 (m, 1H), 6.68 – 6.57 (m, 1H), 3.57 (s, 3H), 3.34 (q, J = 6.3 Hz, 2H), 2.66 (t, J = 6.5 Hz, 2H), 1.37 (s, 9H) ppm.

The characteristic data corresponded with reported literature values.[2]

Synthesis of tert-butyl 4-(2-((tert-butoxycarbonyl)amino)ethyl)-1H-imidazole-1-carboxylate (3.027)

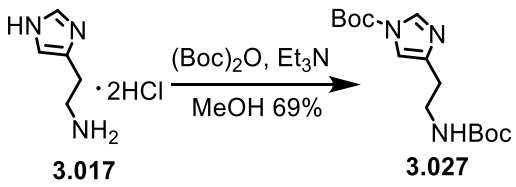

3.017 **3.027**

To a solution of histamine dihydrochloride **3.017** (5 g, 27 mmol) in methanol were added Et_3N (7.5 mL, 54 mmol) and $(Boc)_2O$ (1.36 g, 62.1 mmol). The reaction mixture was stirred overnight at room temperature until no starting material was detected as indicated by TLC. The reaction mixture was then extracted with ethyl acetate and washed with water. The resulting organic layer was dried over anhydrous Na_2SO_4 and concentrated under vacuum to afford the product as white solid (5.8 g, 69%) which was directly used for next step without purification.

Formula: $C_{15}H_{25}N_3O_4$ **Molecular Weight:** 311.38 g/mol

^{1}H NMR (300 MHz, DMSO-d_6) δ 8.09 (d, *J* = 1.3 Hz, 1H), 7.25 (d, *J* = 1.2 Hz, 1H), 6.83 (t, *J* = 5.8 Hz, 1H), 3.15 (q, *J* = 6.7 Hz, 2H), 2.57 (t, *J* = 7.2 Hz, 2H), 1.55 (s, 9H), 1.36 (s, 9H) ppm.

The characteristic data corresponded with reported literature values.[3]

[3] Saada M. C., Vullo D., Montero J. L., Scozzafava A., Winum J. Y., Supuran C. T., *Bioorg. Med. Chem. Lett.*, **2011**, 21(16), 4884-4887.

Synthesis of tert-butyl (2-(1H-imidazol-4-yl)ethyl)carbamate (3.028)

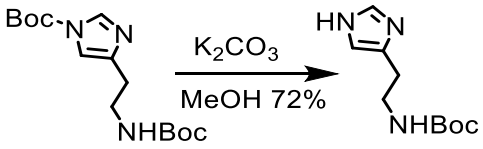

3.027 **3.028**

To a solution of **3.027** (6.9 g, 22.3 mmol) in MeOH, K_2CO_3 (30.7 g, 223 mmol) was added and the mixture was refluxed for 5 h. The mixture was extracted with EtOAc and washed with water. The organic layer was then dried over Na_2SO_4, and the solvent evaporated under reduced pressure to afford product as white solid (3.39 g, 72%).

Formula: $C_{10}H_{17}N_3O_2$ **Molecular Weight:** 211.27 g/mol

1H NMR (300 MHz, Chloroform-*d*) δ 7.52 (d, J = 1.1 Hz, 1H), 6.76 (d, J = 1.0 Hz, 1H), 4.92 (s, 1H), 3.36 (q, J = 6.4 Hz, 2H), 2.74 (t, J = 6.6 Hz, 2H), 1.37 (s, 9H) ppm.

The characteristic data corresponded with reported literature values.[4]

[4] Wang J., Liang Y. L., Qu J., *Chem. Comm.*, **2009**, (34), 5144-5146.

Synthesis of 2-Bromo (Chloro) ethyl-imidazole (3.029)

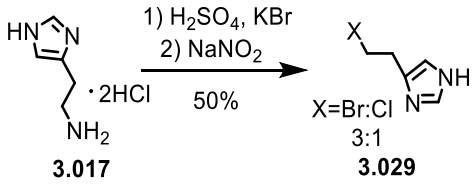

Histamine dihydrochloride **3.017** was stirred with roughly 3 equivalents of potassium bromide in 1.5 M sulfuric acid (8 mL/gram of histamine salt) and the solution was cooled to -15 °C. A saturated solution of sodium nitrite (0.7 mL/gram of histamine) was added all at once, causing the solution to change from colorless to orange-brown. The mixture was stirred cold for 30 minutes and then allowed to warm to room temperature. After ~2.5 hours, the mixture changed from orange-brown to pale yellow and was cooled again to -15 °C. The pH of the solution was brought to 10 with 5 M NaOH, and the basic solution was extracted with chloroform. A 0.5 N HCl/ethyl acetate solution was prepared (12 mL/gram of histamine) and the chloroform layer was added to this solution. The product was concentrated by rotary evaporation to yield a white-brown cake like solid in 50% yield.

1H NMR (300MHz, D_2O) δ (ppm) 8.46 (d, J = 1.2 Hz, 1 H), 7.21 (s, 1 H), 3.69 (t, J = 6.4 Hz, 1 H), 3.58- 3.52 (m, 3 H), 3.17 (t, J = 6.4 Hz, 3 H), 3.06 (t, J = 5.9 Hz, 1 H) ppm.

The characteristic data corresponded with reported literature values.[5]

[5] Shapiro J. A., Wencewicz, T. A., *ACS Infect. Dis.*, 2016, *2*(2), 157-168.

Synthesis of tert-butyl (2-(5-bromo-1-methyl-1H-imidazol-4-yl)ethyl)carbamate (4.014)

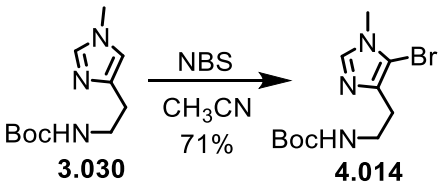

3.030 **4.014**

The **3.030** (54 mg, 0.24 mmol) was dissolved in 5 mL CH_3CN, under the argon atmosphere, NBS (42.72 mg, 0.24 mmol) in 5 mL of CH_3CN were added dropwise. The mixture was stirred in the dark for 12h at 45°C, then concentrated under vacuum. The residue was diluted with EtOAc and washed with 20mL saturated solution of Na_2CO_3. The organic layer was dried over Na_2SO_4 and concentrated under vacuum. The crude residue was purified by flash chromatography over silica column (5% MeOH in CH_2Cl_2) to yield yellow oil (51.8 mg, 71%).

Formula: $C_{11}H_{18}N_3O_2Br$ **Molecular Weight:** 304.19 g/mol

1H NMR (300 MHz, Chloroform-*d*) δ 7.49 (s, 1H), 5.10 (br s, 1H), 3.58 (s, 3H), 3.44-3.38 (m, 2H), 2.39 (t, *J* = 6.4 Hz, 2H), 1.43 (s, 9H) ppm.

^{13}C NMR (75 MHz, Chloroform-*d*) δ 156.1, 138.6, 137.5, 102.1, 79.0, 39.8, 33.1, 28.6, 27.7 ppm.

HRMS (ESI) m/z calculated for $C_{11}H_{19}{}^{79}BrN_3O_2$ $[M+H]^+$ 304.0655, found 304.0654.

The characteristic data corresponded with reported literature values.[6]

[6] Dubey R. K., Kumar N., Jain R., *Synth. Commun.*, **2012**, 42(15), 2207-2216.

Synthesis of 1-trityl-1H-imidazole (4.016)

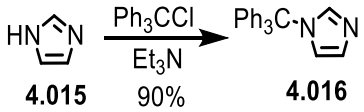

4.015 90% **4.016**

Imidazole (**4.015**) (5.1 g, 75 mmol) was dissolved in DCM (100 mL). Triphenylmethyl chloride (23.0 g, 82.5 mmol) was added over 20 min and the mixture was stirred until the dissolution was complete. Triethylamine (21 mL, 150 mmol) was added slowly to the stirred solution and the stirring was continued overnight at room temperature. The solution was evaporated to dryness and the residue was recrystallized from absolute ethanol and dried to give product as colorless needles (20.9 g, 90%).

Formula: $C_{22}H_{18}N_2$ **Molecular Weight:** 310.40 g/mol

^{1}H NMR (300 MHz, Chloroform-*d*) δ 7.48 (t, *J* = 1.2 Hz, 1H), 7.37 – 7.32 (m, 9H), 7.18 – 7.12 (m, 6H), 7.08 (t, *J* = 1.2 Hz, 1H), 6.84 (t, *J* = 1.4 Hz, 1H) ppm.

The characteristic data corresponded with reported literature values.[7]

[7] Wong F. F., Chen K. L., Lin C. M., Yeh M. Y., *J. Appl. Polym. Sci.*, **2007**, 104(5), 3292-3300.

Synthesis of 4-bromo-1-trityl-1H-imidazole (4.017)

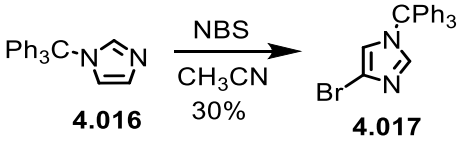

4.016 **4.017**

NBS (0.689 mg, 3.87 mmol) was added to a solution of **4.016** (1 g, 3.23 mmol) in DMF, and the mixture was stirred at 20 °C for 20 h and then poured into water. The resulting solution was extracted with EtOAc and the volatiles were removed *in vacuo*. The product was afforded as a colorless solid by recrystallizing from 99% EtOH (0.377 g, 30%).

Formula: $C_{22}H_{18}BrN_2$ **Molecular Weight:** 389.30 g/mol

^{1}H NMR (300 MHz, Chloroform-*d*) δ 7.40 – 7.34 (m, 9H), 7.33 (d, *J* = 1.6 Hz, 1H), 7.18 – 7.09 (m, 6H), 6.81 (d, *J* = 1.6 Hz, 1H) ppm.

The characteristic data corresponded with reported literature values.[8]

[8] Palmer B. D., Denny W. A., *J. Chem. Soc. Perkin Trans. I*, **1989**, (1), 95-99.

Synthesis of 4-iodo-1H-imidazole (4.019)

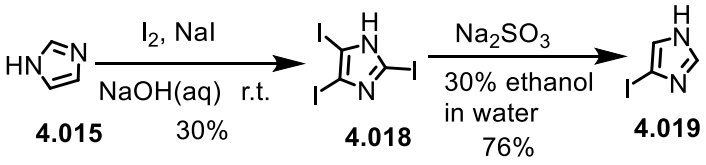

A solution of I_2 (11 g, 44 mmol) in 20% aqueous NaI (50 mL) was added dropwise to a solution of imidazole (**4.015**) in 2 M NaOH (150 mL) at room temperature and the resulting mixture was stirred overnight. Acetic acid was added until the mixture was neutral to give a white precipitate, which was filtered off, washed with water, and air dried to give the crude product.

A solution of 2,4,5-Tri-iodoimidazole (3 g, 6.73 mmol) and Na_2SO_3 (10 g) in 30% EtOH in water (150 mL) was heated at 85 °C for 72 h. The ethanol was removed under reduced pressure. The remaining solution was filtered, and the filtrate extracted with diethyl ether. The organic extracts were combined, dried (Na_2SO_4) and concentrated under reduced pressure to afford the pure product as a white solid (1.03 g, 76%).

Formula: $C_3H_3IN_2$ **Molecular Weight:** 193.98 g/mol

^{1}H NMR (300 MHz, Chloroform-*d*) δ 7.57 (s, 1H), 7.11 (s, 1H).

The characteristic data corresponded with reported literature values.[9]

[9] Sandtorv A. H., Bjørsvik H. R., *Eur. J. Org. Chem.*, **2015**, 2015(*21*), 4658-4666.

Synthesis of 4-iodo-1-trityl-1H-imidazole (4.020)

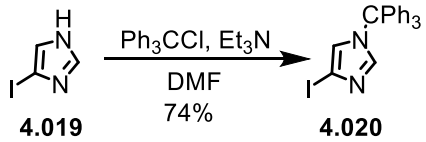

4.019 **4.020**

To a solution of **4.019** (3.38 g, 17 mmol) in 15 mL of DMF was added triphenylmethyl chloride (5.56 g, 20 mmol) and 1.5 ml Et_3N. The solution was stirred at room temperature overnight and was then poured into 200 mL ice water. The solid was filtered and recrystallized from ethyl actate/cyclohexane to give product 5.48 g (74%).

Formula: $C_{22}H_{17}IN_2$ **Molecular Weight:** 436.30 g/mol

1H NMR (300 MHz, Chloroform-*d*) δ 7.31 – 7.24 (m, 10H), 7.09 – 6.99 (m, 6H), 6.85 (d, J = 1.5 Hz, 1H) ppm.

The characteristic data corresponded with reported literature values.[10]

[10] Kirk K. L., *J. Heterocycl. Chem.*, **1985**, 22(1), 57-59.

Synthesis of (E)-2-((2-bromophenyl)amino)-4-methoxy-4-oxobut-2-enoic acid (4.022)

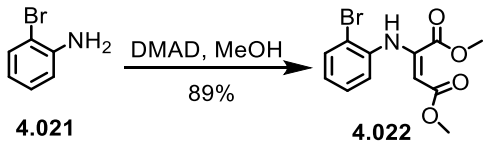

4.021 **4.022**

To a solution of 2-bromoaniline (10.0 g, 58 mmol) in 100 mL of methanol was added dimethyl acetylene dicarboxylate (8.5 mL, 69.6 mmol) dropwise at 0 °C. The mixture was stirred at room temperature overnight. The product was afforded by filtering and washing the residue with diethyl ether to give a yellow solid (16.2 g, 89%).

Formula: $C_{12}H_{12}BrNO_4$ **Molecular Weight:** 314.14 g/mol

^{1}H NMR (300 MHz, Chloroform-*d*) δ 9.76 (s, 1H), 7.58 (dd, *J* = 8.0, 1.5 Hz, 1H), 7.21 (td, *J* = 7.6, 1.3 Hz, 1H), 6.95 (td, *J* = 7.7, 1.5 Hz, 1H), 6.82 – 6.73 (m, 1H), 5.56 (s, 1H), 3.78 (s, 3H), 3.73 (s, 3H) ppm.

The characteristic data corresponded with reported literature values.[11]

[11] Zewge D., Chen C. Y., Deer C., Dormer P. G., Hughes D. L. *J. Org. Chem.*, **2007**, *72*(11), 4276-4279.

Synthesis of methyl 8-bromo-4-oxo-1,4-dihydroquinoline-2-carboxylate (4.023)

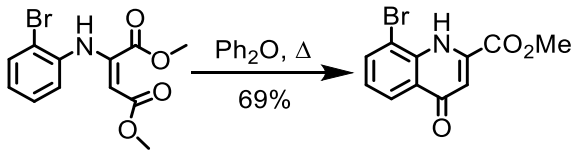

4.022 **4.023**

Then the **4.022** (10 g, 31.8 mmol) was added at once to the boiling diphenyl ether (at 260 °C). The mixture was heated for 7 min and cooled to room temperature. Petroleum ether was added to the solution and the solid was filtered, washed with petroleum ether and dried under vacuum to afford product as off-white solid (6.2 g, 89%).

Formula: $C_{11}H_8BrNO_3$ **Molecular Weight:** 282.09 g/mol

^{1}H NMR (300 MHz, Chloroform-*d*) δ 9.39 (s, 1H), 8.31 (ddd, *J* = 8.2, 1.4, 0.7 Hz, 1H), 7.90 (dd, *J* = 7.7, 1.4 Hz, 1H), 7.34 – 7.21 (m, 1H), 6.99 (d, *J* = 1.9 Hz, 1H), 4.07 (s, 3H) ppm.

The characteristic data corresponded with reported literature values.[11]

Synthesis of methyl 8-bromo-4-isobutoxyquinoline-2-carboxylate (4.024)

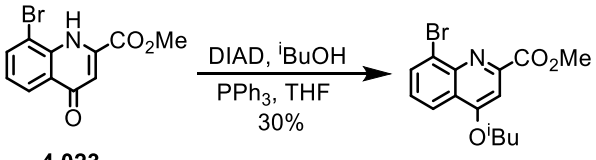

4.023 **4.024**

To a solution of **4.023** (15.0 g, 54.4 mmol), triphenylphosphine (17 g, 65 mmol) and isobutyl alcohol (6 mL, 65 mmol) in THF was added diisopropyl azodicarboxylate (DIAD) (12.9 mL, 65.0 mmol) at 0 °C. The reaction mixture was stirred at 0 °C for 30 min and then warmed up to room temperature and stirred overnight. The volatiles were removed *in vacuo*. The crude product was purified by flash chromatography over silica column (petroleum ether: EtOAc = 9:1) to yield a white solid (5.5 g, 30%).

Formula: $C_{15}H_{16}BrNO_3$ **Molecular Weight:** 338.20 g/mol

^{1}H NMR (300 MHz, Chloroform-*d*) δ 8.26 (dd, *J* = 8.4, 1.4 Hz, 1H), 8.10 (dd, *J* = 7.5, 1.3 Hz, 1H), 7.62 (s, 1H), 7.44 (dd, *J* = 8.4, 7.5 Hz, 1H), 4.08 (d, *J* = 0.8 Hz, 3H), 4.06 (s, 2H), 2.31 (dq, *J* = 13.3, 6.7 Hz, 1H), 1.15 (d, *J* = 6.7 Hz, 6H) ppm.

^{13}C NMR (75 MHz, Chloroform-*d*) δ 166.1, 163.1, 149.7, 145.6, 134.2, 127.7, 125.6, 123.7, 121.7, 101.4, 75.4, 53.3, 28.1, 19.2 ppm.

HRMS(ESI): m/z calculated for $C_{15}H_{17}NO_3{}^{79}Br$ $[M+H]^+$: 338.03863. found: 338.03835.

Synthesis of tetramethyl 2,2'-((2-methyl-1,3-phenylene)bis(azanediyl))dimaleate (4.008)

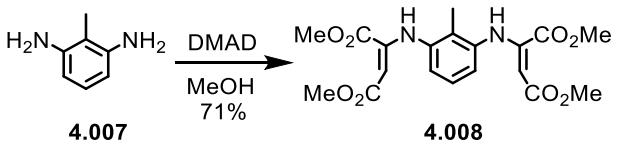

4.007 **4.008**

To a solution of 2,6-diaminotoluene (2 g, 16.37 mmol) in 30 mL of methanol was added dimethyl acetylene dicarboxylate (4.25 mL, 34.38 mmol) dropwise at 0 °C. The mixture was stirred at room temperature for overnight. The product was afforded by flitering and washing with diethyl ether as yellow solid (4.7 g, 71%).

Formula: $C_{19}H_{22}N_2O_8$ **Molecular Weight:** 406.39 g/mol

^{1}H NMR (300 MHz, Chloroform-*d*) δ 9.53 (s, 2H), 6.99 (t, *J* = 8.0 Hz, 1H), 6.58 (d, *J* = 8.0 Hz, 2H), 5.43 (s, 2H), 3.75 (s, 6H), 3.64 (s, 6H), 2.32 (s, 3H) ppm.

The characteristic data corresponded with reported literature values.[12]

[12] Molock F. F., Boykin D. W., *J. Heterocycl. Chem.*, **1983**, 20(3), 681-686.

Synthesis of dimethyl 4,6-diisobutoxy-10-methylpyrido[3,2-g]quinoline-2,8-dicarboxylate (4.010)

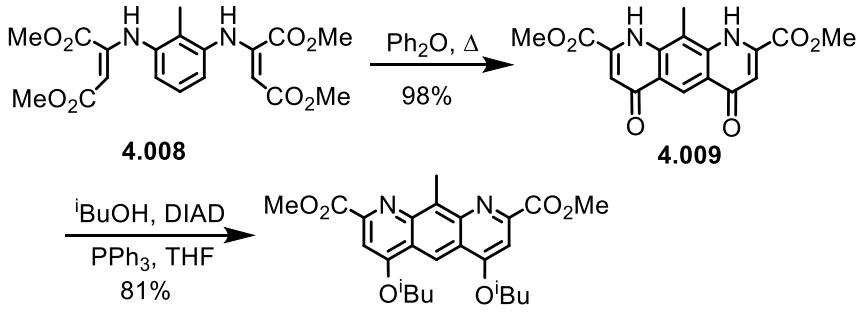

The tetramethyl **4.008** (5.0 g, 12.3 mmol) was added at once to the boiling diphenyl ether (at 260 °C). The mixture was heated for 15 min and cooled to room temperature. DCM was added to the solution and the solid was filtered, washed with DCM and dried under vacuum to afford product as off-white solid (4.13 g, 98%), which was directly used for next step without purification.

Then to a solution of **4.009** (3.88 g, 11.4 mmol), triphenylphosphine (6.87 g, 26.2 mmol) and isobutyl alcohol (2.42 mL, 26.2 mmol) in THF was added diisopropyl azodicarboxylate (DIAD) (5.18 mL, 26.2 mmol) at 0 °C. The reaction mixture was stirred at 0 °C for 30 min and then warmed up to room temperature and stirred overnight. The volatiles were removed in vacuo. The mixture was recrystallized by slow evaporation of DCM from a 2/1 mixture of DCM and MeOH to give the product as a yellow solid (4.2 g, 81%).

Formula: $C_{25}H_{30}N_2O_6$ **Molecular Weight:** 454.52 g/mol

^{1}H NMR (300 MHz, Chloroform-*d*) δ 9.14 (d, *J* = 1.1 Hz, 1H), 7.50 (s, 2H), 4.13 (d, *J* = 6.4 Hz, 4H), 4.10 (s, 6H), 3.50 (s, 3H), 2.36 (hept, *J* = 6.7 Hz, 2H), 1.20 (d, *J* = 6.7 Hz, 12H) ppm.

The characteristic data corresponded with reported literature values.[13]

[13] Berni E., Kauffmann B., Bao C., Lefeuvre J., Bassani D. M., Huc I., *Chem. Eur. J.*, **2007**, 13(30), 8463-8469.

Synthesis of 4,6-diisobutoxy-10-methylpyrido[3,2-g]quinoline-2,8-dicarbohydrazide (4.011)

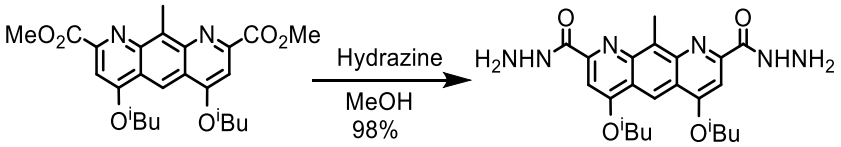

4.010 **4.011**

4.010 (2.0 g, 4.40 mmol) was placed in a round-bottomed flask and dissolved in 50 mL of MeOH. Hydrazine 64% (7.05 g, 140.8 mmol, 6.1 mL) was added to this mixture. The reaction mixture was then stirred and refluxed for 3 days. Solvent was removed on a rotary evaporator and the yellow residue was then recrystallized in THF, filtered and dried under vacuum to give product as a yellow solid (1.97g, 98%).

Formula: $C_{23}H_{30}N_6O_4$ **Molecular Weight:** 454.52 g/mol

^{1}H NMR (300 MHz, Chloroform-*d*) δ 9.30 (s, 2H), 9.13 (s, 1H), 7.58 (s, 2H), 4.15 (d, J = 6.4 Hz, 4H), 3.30 (d, J = 0.9 Hz, 3H), 2.36 (dt, J = 13.3, 6.6 Hz, 2H), 1.19 (d, J = 6.7 Hz, 12H) ppm.

^{13}C NMR (75 MHz, Chloroform-*d*) δ 165.3, 164.0, 151.1, 145.1, 136.2, 121.4, 114.1, 96.6, 75.4, 28.4, 19.3, 12.9 ppm.

HRMS(ESI): m/z calculated for $C_{23}H_{31}N_6O_4$ $[M+H]^+$: 455.24013. found: 455.23996.

Synthesis of di-tert-butyl (4,6-diisobutoxy-10-methylpyrido[3,2-g]quinoline-2,8-diyl)dicarbamate (4.013)

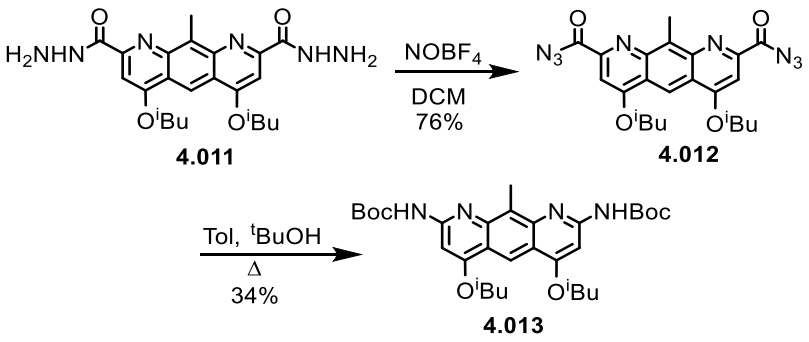

4.011 (0.5 g, 1.10 mmol) was placed in a round-bottomed flask and dissolved in 40 mL of DCM. The reaction mixture was cooled to 0 °C (ice bath). $NOBF_4$ (0.771 g, 6.60 mmol) was then added to this mixture, and the resulting mixture was stirred at room temperature for one night. The solvent was evaporated and $CHCl_3$ was added (150 mL) to the residue. The organic layer was washed with $NaHCO_3$ (2 x 150 mL), water (1 x 150 mL), dried over Na_2SO_4, filtered and the volatiles were removed in vacuo to yield product as a yellow solid (0.52 g, 76%) This product was directly used to do the next step without further purification.

This azide **4.012** (0.4 g, 0.84 mmol) was added to a 1:1 toluene (15 mL) and t-BuOH (15 ml) mixture. The mixture was stirred at 90 °C overnight. Solvent was removed on a rotary evaporator, and the crude material was purified by flash chromatography over silica column (petroleum ether: EtOAc=9:1) to yield product as a light yellow solid(0.16 g, 34%).

Formula: $C_{31}H_{44}N_4O_6$ **Molecular Weight:** 568.72 g/mol

^{1}H NMR (300 MHz, Chloroform-*d*) δ 8.85 (s, 1H), 7.55 (s, 2H), 4.07 (d, *J* =

6.3 Hz, 4H), 2.95 (s, 3H), 2.31 (dt, *J* = 13.2, 6.6 Hz, 2H), 1.56 (s, 18H), 1.16 (d, *J* = 6.8 Hz, 12H) ppm.

^{13}C NMR (75 MHz, Chloroform-*d*) δ 164.0, 152.8, 145.5, 128.7, 117.1, 113.6, 90.6, 80.9, 74.6, 28.4, 28.3, 19.3, 11.9 ppm.

HRMS(ESI): m/z calculated for $C_{31}H_{45}N_4O_6$ $[M+H]^+$: 569.33336. found: 569.33347.

Synthesis of 4,6-diisobutoxy-10-methylpyrido[3,2-g]quinoline-2,8-diamine (4.003)

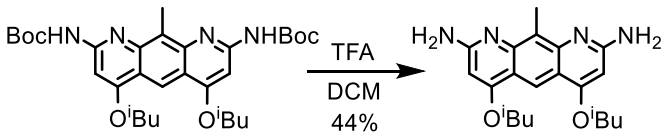

4.013 **4.003**

In a 20 mL round bottom flask, **4.013** (0.5 g, 0.88 mmol) was dissolved in 15 mL of 1:1 DCM: TFA. The reaction was stirred overnight at room temperature and then solvent was removed on the rotary evaporator. The crude yellow oil was partitioned between $CHCl_3$ and saturated $NaHCO_3$ solution. The organic layer was washed with water and brine and then dried over Na_2SO_4. After removal of solvent, the product was dried overnight on the vacuum line to give product as a yellow solid (0.33 g, 44%).

Formula: $C_{21}H_{28}N_4O_2$ **Molecular Weight:** 368.48 g/mol

^{1}H NMR (300 MHz, DMSO-d_6) δ 8.40 (s, 1H), 6.34 (s, 4H), 6.09 (s, 2H), 3.90 (d, *J* = 6.1 Hz, 4H), 2.69 (s, 3H), 2.17 (dt, *J* = 13.1, 6.6 Hz, 2H), 1.09 (d, *J* = 6.7 Hz, 12H) ppm.

^{13}C NMR (75 MHz, DMSO-d_6) δ 161.7, 158.7, 146.8, 122.1, 112.8, 111.7, 89.1, 73.4, 27.8, 18.8, 12.1 ppm.

HRMS(ESI): m/z calculated for $C_{21}H_{29}N_4O_2$ $[M+H]^+$: 369.22850. found: 369.22849.

Synthesis of 2-(1-trityl-1H-imidazol-4-yl)aniline (4.033)

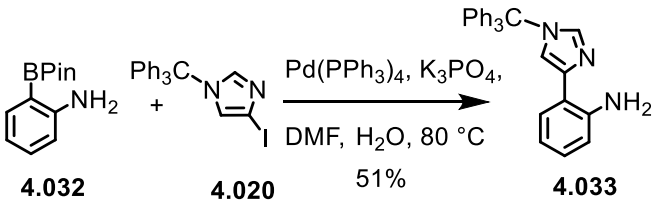

4.032 **4.020** **4.033**

A mixture of **4.020** (87.3 mg, 0.2 mmol), **4.032** (43.8 mg, 0.2 mmol) and K_3PO_4 (81.7 mg, 0.6 mmol) in DMF (5 mL) and H_2O (1 mL) solvent under nitrogen was added $Pd(PPh_3)_4$ (11.6 mg, 0.01 mmol) after purging with nitrogen 15 min. The reaction mixture was stirred at 80 °C for 14 hours. After cooling to room temperature, the solution was filtered through a pad of Celite. The crude mixture was purified by flash column chromatography using 5% EtOAc in petroleum ether to afford the product (41 mg, 51%) as white solid.

Formula: $C_{28}H_{23}N_3$ **Molecular Weight:** 401.51 g/mol

^{1}H NMR (300 MHz, Chloroform-*d*) δ 7.56 (s, 1 H), 7.40-7.34 (m, 9 H), 7.28 (d, 1 H), 7.23-7.18 (m, 6 H), 7.08 (s, 1 H), 7.04 (t, 1 H), 6.73 (d, 1 H), 6.66 (t, 1 H).

The characteristic data corresponded with reported literature values.[14]

[14] Peng Y. H., Ueng S. H., Tseng C. T., Hung M. S., Song J. S., Wu, J. S., Hsueh C. C., *J. Med. Chem.*, **2016**, 59(1), 282-293.

Synthesis of dimethyl 2-((2-(1-trityl-1H-imidazol-4-yl)phenyl)amino)maleate (4.034)

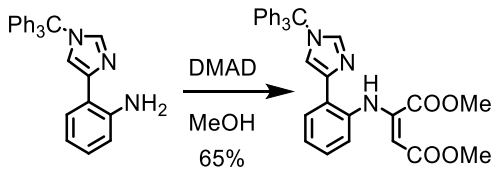

4.033 **4.034**

To a solution of **4.033** (4.639 g, 11.55 mmol) in MeOH (120 mL) was added DMAD (1.7 mL, 13.8 mmol) at 0 °C. The resulting solution was stirred at room temperature overnight. The volatiles were removed *in vacuo* and the residue was purified by flash column chromatography using 5% EtOAc in petroleum ether to afford a yellowish oil product (4.074 g, 65%).

Formula: $C_{34}H_{29}N_3O_4$ **Molecular Weight:** 543.62 g/mol

^{1}H NMR (300 MHz, Chloroform-*d*) δ 10.97 (br s, 1H), 7.60-7.56 (m, 2H), 7.34-7.32 (m, 9H), 7.21-7.16 (m, 7H), 7.09 (ddd, *J* = 7.5, 7.5, 1.6 Hz, 1H), 7.01 (ddd, *J* = 7.6, 7.6, 1.5 Hz, 1H), 6.73 (dd, *J* = 7.9, 1.2 Hz, 1H), 5.37 (s, 1H), 3.69 (s, 3H), 3.63 (s, 3H) ppm.

^{13}C NMR (75 MHz, Chloroform-*d*) δ 168.9, 165.7, 147.0, 146.9, 142.4, 139.0, 138.7, 137.9, 130.0, 128.2, 128.0, 127.4, 127.1, 124.9, 123.7, 120.9, 119.3, 90.1, 52.8, 51.2 ppm.

HRMS (ESI) m/z calculated for $C_{34}H_{30}N_3O_4$ $[M+H]^+$ 544.2231, found 544.2233.

Synthesis of methyl 4-isobutoxy-8-(1-trityl-1H-imidazol-4-yl)quinoline-2-carboxylate (4.036)

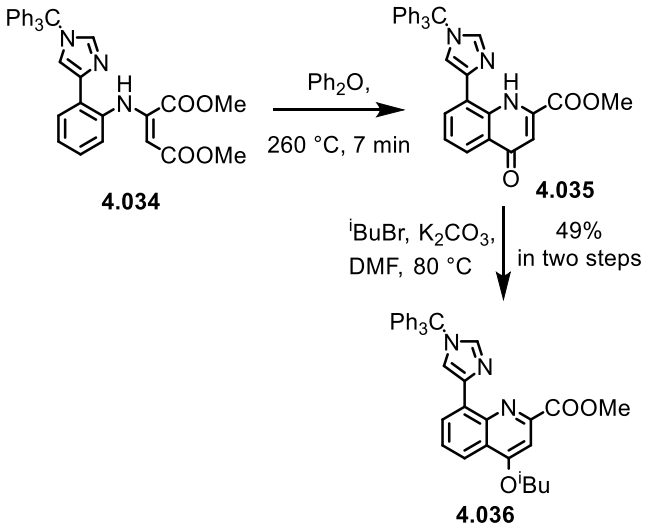

In a 500 mL round-bottomed flask, 100 ml of diphenylether was heated to 260°C (without stirrer) using a heating mantel. Compound **4.034** (3.633 g, 6.683 mmol) was added all at once. The mixture was heated for 7 min. The flask was removed from the heating mantel and allowed to cool down for ~30 minutes. 50 mL petroleum ether was first added to the flask, and then the still hot mixture was carefully poured into to an Erlenmeyer flask containing 200 mL petroleum ether. The precipitate was collected by filtration and washed with petroleum ether. After drying under reduced pressure, methyl 4-oxo-8-(1-trityl-1H-imidazol-4-yl)-1,4-dihydroquinoline-2-carboxylate was obtained as a sandy yellow solid and was subjected to the subsequent reaction without further purification.

To a solution of **4.035** in DMF (43 mL) was added K_2CO_3 (1.467 g, 10.61 mmol) and ^{i}BuBr (0.9 mL, 8.28 mmol) and the resulting solution was heated at 80 ^{o}C overnight. After the mixture was cooled to room temperature, water was added

and the mixture was extracted with EtOAc. The combined organic layers were dried over anhydrous Na_2SO_4 and the volatiles were removed *in vacuo*. The residue was purified by flash column chromatography using 5% EtOAc in petroleum ether to afford the final product with yellow solid (1.870 g, 49% yield over 2 steps).

Formula: $C_{37}H_{33}N_3O_3$ **Molecular Weight:** 567.69 g/mol

^{1}H NMR (300 MHz, Chloroform-*d*) δ 8.80 (d, *J* = 1.5 Hz, 1H), 8.69 (dd, *J* = 7.5, 1.5 Hz, 1H), 8.11 (dd, *J* = 8.2, 1.5 Hz, 1H), 7.64 (dd, *J* = 8.2, 7.6 Hz, 1H), 7.56 (d, *J* = 1.5 Hz, 1H), 7.47 (s, 1H), 7.37-7.29 (m, 15H), 4.01 (d, *J* = 6.6 Hz, 2H), 3.58 (s, 3H), 2.34-2.20 (m, 1H), 1.13 (d, J = 6.7 Hz, 6H) ppm.

^{13}C NMR (75 MHz, Chloroform-*d*) δ 166.9, 162.9, 147.5, 145.0. 142.9, 138.2, 137.4, 133.3, 130.0, 128.2, 128.0, 127.9, 127.6, 125.4, 122.8, 119.8, 100.2, 75.7, 75.1, 52.7, 28.3, 19.4 ppm.

HRMS (ESI) m/z calculated for $C_{37}H_{34}N_3O_3$ $[M+H]^+$ 568.2595, found 568.2596.

Synthesis of *tert*-Butyl (2-(5-(2-aminophenyl)-1-methyl-1H-imidazol-4-yl)ethyl)carbamate (4.038)

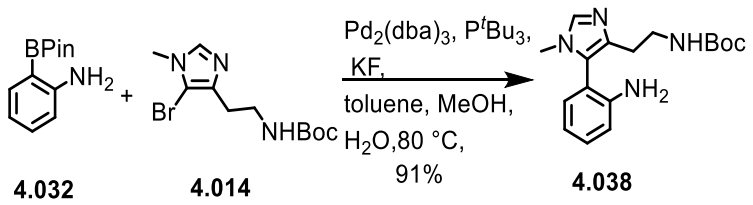

4.032 **4.014** **4.038**

A solution of **4.014** (5.024 g, 16.52 mmol), **4.032** (4.347 g, 19.83 mmol), P^tBu_3 (0.800 mL, 3.30 mmol) and KF (2.0 M in H_2O, 16.5 mL, 33.0 mmol) in toluene (247 mL) and MeOH (165 mL) was degassed for 30 min. $Pd_2(dba)_3$ (0.764 g, 0.835 mmol) was added. The resulting solution was heated at 80 °C overnight and then cooled to room temperature. Water was added and the mixture was extracted with EtOAc. The combined organic layers were dried over anhydrous Na_2SO_4 and the volatiles were removed *in vacuo*. The residue was purified by flash column chromatography using 5% MeOH in CH_2Cl_2 to afford yellow oil (4.734 g, 91%).

Formula: $C_{17}H_{24}N_4O_2$ **Molecular Weight:** 316.41 g/mol

^{1}H NMR (300 MHz, Chloroform-*d*) d 7.50 (s, 1H), 7.22 (ddd, J = 8.0, 7.6, 0.5 Hz, 1H), 7.01 (dd, J = 7.4, 1.4 Hz, 1H), 6.81-6.75 (m, 2H), 5.29 (s, 1H), 3.65 (br s, 2H), 3.42 (s, 3H), 3.39-3.28 (m, 2H), 2.61-2.56 (m, 2H), 1.39 (s, 9H) ppm.

^{13}C NMR (75 MHz, Chloroform-*d*) d 156.1, 146.4, 138.3, 137.6, 132.3, 130.4, 126.3, 118.5, 115.5, 114.4, 78.9, 40.6, 31.9, 28.6, 27.6 ppm.

HRMS (ESI) m/z calculated for $C_{17}H_{25}N_4O_2$ $[M+H]^+$ 317.1972, found 317.1972.

Synthesis of Dimethyl 2-((2-(4-(2-((tert-butoxycarbonyl)amino)ethyl)-1-methyl-1H-imidazol-5-yl)phenyl)amino)maleate (4.039)

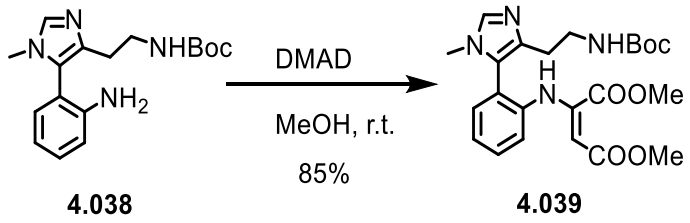

4.038 **4.039**

To a solution of **4.038** (2.454 g, 7.756 mmol) in MeOH (80 mL) was added DMAD (1.15 mL, 9.31 mmol) at 0 °C. The resulting solution was stirred at room temperature overnight. The volatiles were removed in vacuo and the residue was purified by flash column chromatography using 5% MeOH in CH_2Cl_2 to afford product (3.025 g, 85% yield).

Formula: $C_{23}H_{30}N_4O_6$ **Molecular Weight:** 458.52 g/mol

^{1}H NMR (300 MHz, Chloroform-*d*) δ 9.18 (s, 1H), 7.52 (s, 1H), 7.30 (ddd, *J* = 7.8, 7.8, 1.6 Hz, 1H), 7.19 (dd, *J* = 7.6, 1.4 Hz, 1H), 7.14-7.09 (m, 1H), 6.75 (d, *J* = 8.0 Hz, 1H), 5.56-5.52 (m, 1H), 5.42 (s, 1H), 3.76 (s, 3H), 3.64 (s, 3H), 3.43 (s, 3H), 3.41-3.27 (m, 2H), 2.60 (t, *J* = 5.9 Hz, 2H), 1.32 (s, 9H) ppm.

^{13}C NMR (75 MHz, Chloroform-*d*) δ 169.4, 164.7, 156.1, 146.4, 140.5, 139.3, 138.1, 132.6, 129.9, 125.5, 124.0, 121.1, 119.5, 96.1, 78.5, 53.0, 51.6, 40.4, 31.9, 28.5, 27.6 ppm.

HRMS (ESI) m/z calculated for $C_{23}H_{31}N_4O_6$ $[M+H]^+$ 459.2238, found 459.2238.

Synthesis of methyl 8-(4-(2-((*tert*-butoxycarbonyl)amino)ethyl)-1-methyl-1H-imidazol-5-yl)-4-oxo-1,4-dihydroquinoline-2-carboxylate (4.040)

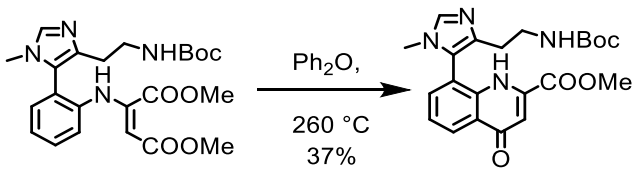

4.039 **4.040**

This reaction has to be performed in small batches (~100 mg) with well-controlled reaction time and temperature in order to minimize decomposition and maximize product yield and starting material recovery. In each batch, in a boiling tube, 20 mL of diphenylether was heated to boiling 260°C (without stirrer) using a heating mantel. The starting material **4.039** (0.533 g, 1.09 mmol) was added all at once. The mixture was heated for 5 min. The flask was removed from the heating mantel and allowed to cool to room temperature. The combined cooled reaction mixture were purified by flash column chromatography using 5% MeOH in CH_2Cl_2 to afford yellow oil product (0.266 g, 37% yield) and recovered starting material (0.423 g, 55%).

Formula: $C_{22}H_{26}N_4O_5$ **Molecular Weight:** 426.47 g/mol

^{1}H NMR (300 MHz, Chloroform-*d*) δ 8.79 (br s, 1H), 8.42 (dd, *J* = 8.2, 1.4 Hz, 1H), 7.66 (s, 1H), 7.55 (dd, *J* = 7.3, 1.4 Hz, 1H), 7.45 (dd, *J* = 8.0, 8.0 Hz, 1H), 6.96 (s, 1H), 5.23 (br s, 1H), 3.97 (s, 3H), 3.41 (s, 3H), 3.40-3.29 (m, 2H), 2.66-2.57 (m, 1H), 2.54-2.45 (m, 1H), 1.34 (s, 9H) ppm.

^{13}C NMR (75 MHz, Chloroform-*d*) δ 179.5, 163.2, 155.9, 140.4, 139.4, 138.2, 136.5, 135.9, 127.7, 126.9, 124.3, 122.4, 118.7, 112.0, 79.1, 54.0, 40.3, 32.3, 28.4, 27.9 ppm.

HRMS (ESI) m/z calculated for $C_{22}H_{26}N_4O_5$ $[M+H]^+$ 427.1976, found

427.1976.

Synthesis of methyl 8-(4-(2-((tert-butoxycarbonyl)amino)ethyl)-1-methyl-1H-imidazol-5-yl)-4-isobutoxyquinoline-2-carboxylate (4.041)

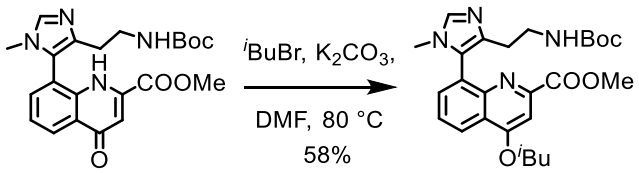

4.040 **4.041**

To a solution of **4.040** (1.180 g, 2.767 mmol) in DMF (50 mL) was added K_2CO_3 (0.770 g, 5.57 mmol) and ^{i}BuBr (0.360 mL, 3.31 mmol) and the resulting solution was heated at 80 °C overnight. After the mixture was cooled to room temperature, water was added and the mixture was extracted with EtOAc. The combined organic layers were dried over anhydrous Na_2SO_4 and the volatiles were removed *in vacuo*. The residue was purified by flash column chromatography using 5% MeOH in EtOAc to afford the desired product as yellow solid (0.779 g, 58%).

Formula: $C_{26}H_{34}N_4O_5$ **Molecular Weight:** 482.58 g/mol

^{1}H NMR (300 MHz, Chloroform-*d*) δ 8.34 (dd, *J* = 7.9, 2.1 Hz, 1H), 7.70-7.61 (m, 2H), 7.57 (s, 1H), 7.53 (s, 1H), 5.38 (br s, 1H), 4.05 (d, *J* = 6.4 Hz, 2H), 3.95 (s, 3H), 3.47 (s, 3H), 3.42-3.29 (m, 2H), 2.74-2.58 (m, 2H), 2.37-2.24 (m, 1H), 1.30 (s, 9H), 1.15 (d, *J* = 6.7 Hz, 6H) ppm.

^{13}C NMR (75 MHz, Chloroform-*d*) δ 166.4, 163.0, 156.1, 149.2, 147.3, 139.0, 137.8, 133.8, 130.0, 127.8, 127.2, 123.0, 122.9, 101.1, 78.5, 75.3, 53.0, 40.6, 33.2, 28.5, 28.3, 27.8, 19.4 ppm.

HRMS (ESI) m/z calculated for $C_{26}H_{35}N_4O_5$ $[M+H]^+$ 483.2602, found

483.2603.

Synthesis of *N*-(8-amino-4,6-diisobutoxy-10-methylpyrido[3,2-g]quinolin-2-yl)-4-isobutoxy-8-(1-trityl-1H-imidazol-4-yl)quinoline-2-carboxamide (4.043)

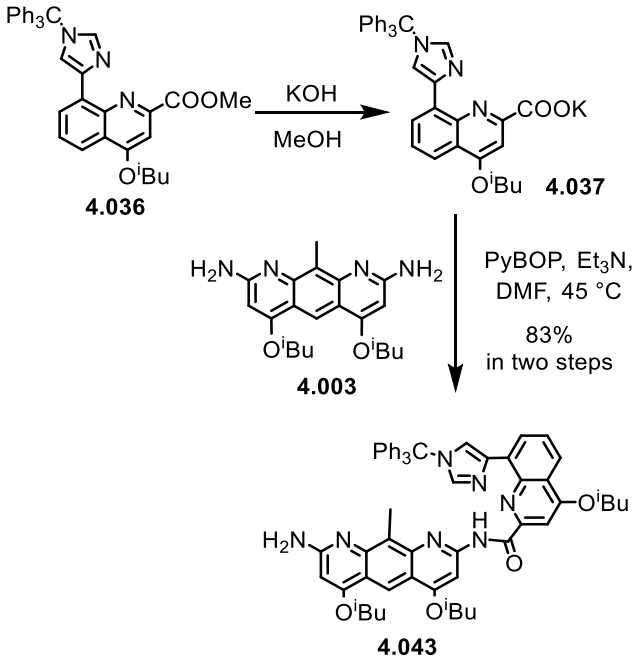

To a solution of **4.036** (0.193 g, 0.340 mmol) in MeOH (3.4 mL) was added KOH (0.1 M in MeOH, 3.4 mL, 0.34 mmol). The resulting solution was heated at 50 °C overnight and then cooled to room temperature. The volatiles were removed *in vacuo* and the crude product of **4.037** was subjected to the subsequent reaction without further purification.

To a solution of **4.037**, **4.003** (0.151 g, 0.410 mmol) and PyBOP (0.252 g, 0.484 mmol) in DMF (3.4 mL) was added Et_3N (0.180 mL, 1.29 mmol). The resulting solution was heated at 45 °C overnight and cooled to room

temperature. Water was added and the suspension was filtered through a short pad of Celite®. The residue was redissolved in CH_2Cl_2 and purified by flash column chromatography using 5% MeOH in CH_2Cl_2 to afford yellow solid (0.256 g, 83% yield over 2 steps).

Formula: $C_{57}H_{57}N_7O_4$ **Molecular Weight:** 904.13 g/mol

^{1}H NMR (500 MHz, Chloroform-*d*) δ ^{1}H NMR (500 MHz, $CDCl_3$) δ 10.19 (s, 1H), 8.78 (s, 1H), 8.57 (dd, *J* = 7.3, 1.1 Hz, 1H), 8.19 (dd, *J* = 8.2, 1.4 Hz, 1H), 8.12-8.10 (m, 2H), 7.69 (s, 1H), 7.67 (dd, *J* = 7.9, 7.9 Hz, 1H), 7.55 (d, *J* = 1.0 Hz, 1H), 7.25-7.20 (m, 9H), 7.15-7.12 (m, 6H), 6.59 (s, 1H), 4.14 (d, *J* = 6.4 Hz, 2H), 4.08-4.06 (m, 4H), 2.51 (s, 3H), 2.38-2.22 (m, 3H), 1.18 (d, *J* = 6.7 Hz, 6H), 1.15 (d, *J* = 6.7 Hz, 6H), 1.12 (d, *J* = 6.7 Hz, 6H) ppm.

^{13}C NMR (125 MHz, Chloroform-*d*) δ 165.3, 165.2, 164.0, 163.6, 158.3, 153.4, 150.3, 147.1, 144.6, 142.7, 139.9, 136.8, 133.1, 129.9, 129.5, 128.4, 128.2, 127.7, 123.1, 122.7, 120.3, 117.2, 115.5, 114.3, 98.4, 93.6, 89.5, 77.7, 75.9, 75.7, 75.3, 75.1, 28.5, 28.3, 28.3, 19.4, 19.3, 19.2, 11.9 ppm.

HRMS (ESI) m/z calculated for $C_{57}H_{58}N_7O_4$ $[M+H]^+$ 904.4545, found 904.4543.

Synthesis of *tert*-Butyl (2-(5-(2-((4,6-diisobutoxy-8-(4-isobutoxy-8-(1-trityl-1H-imidazol-4-yl)quinoline-2-carboxamido)-10-methylpyrido[3,2-g]quinolin-2-yl)carbamoyl)-4-isobutoxyquinolin-8-yl)-1-methyl-1H-imidazol-4-yl)ethyl)carbamate (4.044)

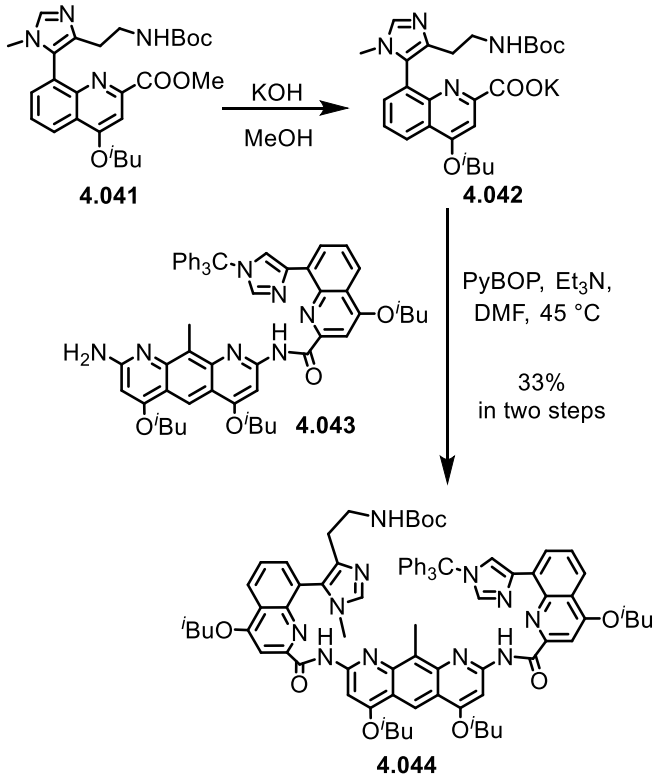

To a solution of **4.041** (0.0976 g, 0.202 mmol) in MeOH (2.1 mL) was added KOH (0.1 M in MeOH, 2.1 mL, 0.21 mmol). The resulting solution was heated at 50 °C overnight and then cooled to room temperature. The volatiles were removed *in vacuo* and the crude product of **4.042** was subjected to the subsequent reaction without further purification.

To a solution of **4.042**, **4.043** (0.1772 g, 0.1960 mmol) and PyBOP (0.319 g, 0.613 mmol) in DMF (2.1 mL) was added DIPEA (0.140 mL, 0.804 mmol). The

resulting solution was heated at 45 °C overnight and cooled to room temperature. Water was added and the suspension was filtered through a short pad of Celite®. The residue was redissolved in CH_2Cl_2 and purified by flash column chromatography using 5% MeOH in CH_2Cl_2 to afford product as yellow solid (0.0877 g, 33% yield over 2 steps) and recovered starting material dimer (0.1036 g, 58%).

Formula: $C_{82}H_{87}N_{11}O_8$ **Molecular Weight:** 1354.67 g/mol

^{1}H NMR (500 MHz, Chloroform-*d*) δ 10.65 (s, 1H), 9.93 (s, 1H), 9.02 (s, 1H), 8.65 (d, *J* = 7.0 Hz, 1H), 8.42 (dd, *J* = 8.5, 0.8 Hz, 1H), 8.28 (s, 1H), 8.21 (dd, *J* = 8.2, 1.1 Hz, 1H), 8.05 (s, 1H), 7.94 (s, 1H), 7.85-7.80 (m, 3H), 7.73-7.68 (m, 3H), 7.57 (s, 1H), 7.24-7.22 (m, 6H), 7.15-7.12 (m, 9H), 5.68 (br s, 1H), 4.20 (d, *J* = 6.5 Hz, 2H), 4.16-4.13 (m, 4H), 4.09 (d, *J* = 6.5 Hz, 2H), 3.65 (s, 3H), 3.54-3.48 (m, 1H), 3.47-3.41 (m, 1H), 2.88 (s, 3H), 2.76-2.70 (m, 2H), 2.46-2.29 (m, 4H), 1.26 (s, 9H), 1.24 (d, *J* = 6.8 Hz, 6H), 1.22 (d, *J* = 6.8 Hz, 6H), 1.18 (d, *J* = 6.8 Hz, 6H), 1.15 (d, *J* = 6.8 Hz, 6H) ppm.

^{13}C NMR (125 MHz, Chloroform-*d*) δ 165.3, 165.3, 164.2, 164.1, 163.8, 163.6, 163.2, 156.2, 151.9, 151.6, 150.7, 150.5, 146.3, 145.6, 145.5, 144.6, 142.8, 139.7, 137.9, 136.8, 134.0, 133.0, 130.8, 129.9, 129.1, 128.2, 128.1, 127.6, 127.4, 123.3, 123.1, 126.1, 122.9, 120.2, 118.3, 118.1, 113.5, 98.6, 98.5, 93.5, 92.2, 78.6, 77.7, 75.7, 75.7, 75.3, 75.0, 75.0, 40.8, 33.2, 28.6, 28.5, 28.5, 28.3, 28.3, 19.4, 19.4, 19.4, 12.3 ppm.

HRMS (ESI) m/z calculated for $C_{82}H_{88}N_{11}O_8$ $[M+H]^+$ 1354.6812, found 1354.6807.

Synthesis of *tert*-Butyl (2-(5-(2-((8-(8-(1H-imidazol-5-yl)-4-isobutoxyquinoline-2-carboxamido)-4,6-diisobutoxy-10-methylpyrido[3,2-g]quinolin-2-yl) carbamoyl) -4-isobutoxyquinolin-8-yl)-1-methyl-1H-imidazol-4-yl)ethyl)carbamate (4.045)

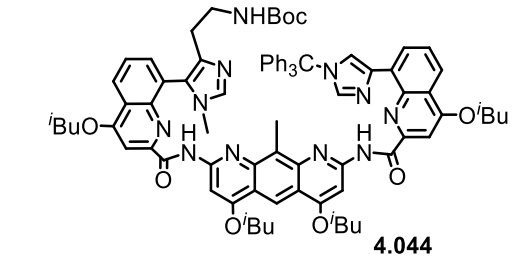

4.044

1. TFA, $^{i}Pr_3SiH$, DCM, r.t.
2. $(Boc)_2O$, Et_3N, DMAP, DCM, r.t.

33% in two step

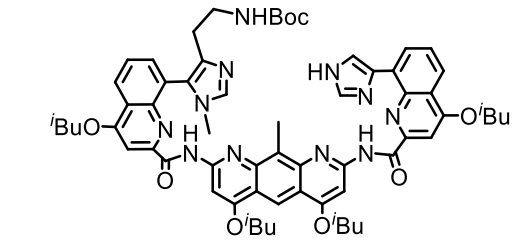

4.045

To a solution of **4.044** (0.1188 g, 0.08770 mmol) and $^{i}Pr_3SiH$ (0.080 mL, 0.39 mmol) in CH_2Cl_2 (5.0 mL) was added TFA (1.0 mL). The resulting solution was stirred at room temperature overnight. The volatiles were removed *in vacuo* and the residue was redissolved in CH_2Cl_2 (5.0 mL). $(Boc)_2O$ (0.0574 g, 0.263 mmol), DMAP (0.0054 g, 0.044 mmol) and Et_3N (0.060 mL, 0.430 mmol) was added. The resulting solution was stirred at room temperature overnight. The volatiles were removed *in vacuo* and the residue was directly purified by flash

column chromatography using 5% MeOH in CH_2Cl_2 to afford the desired product as yellow solid (0.0877 g, 33% yield over 2 steps).

Formula: $C_{67}H_{73}N_{11}O_8$ **Molecular Weight:** 1112.35 g/mol

^{1}H NMR (500 MHz, Chloroform-*d*) δ 10.68 (s, 1H), 10.67 (s, 1H), 8.99 (s, 1H), 8.61 (dd, *J* = 7.3, 1.3 Hz, 1H), 8.59 (s, 1H), 8.42-8.40 (m, 2H), 8.29 (s, *J* = 8.3, 1.3 Hz, 1H), 8.10 (s, 1H), 8.04 (s, 1H), 7.82-7.78 (m, 4H), 7.73-7.69 (m, 2H), 5.43-5.41 (m, 1H), 4.19-4.13 (m, 8H), 3.63 (s, 3H), 3.50-3.37 (m, 2H), 3.20 (s, 3H), 2.75-2.64 (m, 2H), 2.43-2.30 (m, 4H), 1.48 (s, 9H), 1.22-1.20 (m, 12H), 1.18-1.17 (m, 12H) ppm.

^{13}C NMR (125 MHz, Chloroform-*d*) δ 164.7, 164.2, 164.1, 163.8, 163.2, 156.1, 152.0, 151.5, 150.7, 150.5, 147.3, 146.3, 145.8, 145.6, 144.7, 139.5, 138.0, 137.0, 134.1, 131.7, 130.7, 129.9, 129.4, 127.6, 127.5, 127.3, 123.3, 123.1, 123.1, 121.5, 118.3, 118.0, 118.0, 113.6, 98.6, 98.5, 92.7, 92.1, 85.6, 78.6, 75.6, 75.4, 74.9, 40.7, 33.0, 29.9, 28.5, 28.5, 28.5, 28.3, 28.3, 27.9, 27.6, 19.4, 19.4, 12.4 ppm.

HRMS (ESI) m/z calculated for $C_{63}H_{74}N_{11}O_8$ $[M+H]^+$ 1112.5722, found 1112.5712.

Synthesis of *N*-(8-(8-(1H-imidazol-5-yl)-4-isobutoxyquinoline-2-carboxamido)-4,6-diisobutoxy-10-methylpyrido[3,2-g]quinolin-2-yl)-8-(4-(2-aminoethyl)-1-methyl-1H-imidazol-5-yl)-4-isobutoxyquinoline-2-carboxamide (4.046)

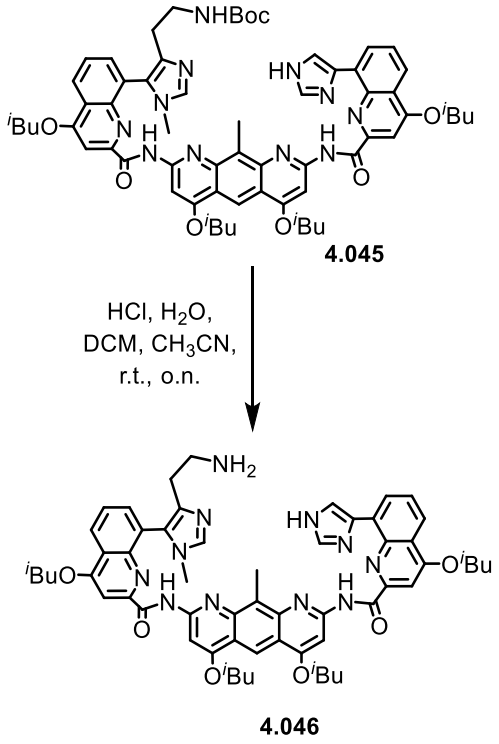

In a round bottom flask, **4.045** (5.4 mg, 0.44 mmol) was dissolved in 2 mL CH_2Cl_2 and 2 ml and 0.1 ml 1 M HCl was added. The mixture was stirred overnight at room temperature and then solvent was removed on the rotary evaporator. The crude yellow oil was partitioned between CH_2Cl_2 and saturated $NaHCO_3$ solution. The organic layer was washed with water and brine and then dried over Na_2SO_4. After removal of solvent, the product was dried on the vacuum line to give product as a yellow solid.

Formula: $C_{58}H_{65}N_{11}O_6$ **Molecular Weight:** 1012.23 g/mol

^{1}H NMR (500 MHz, 9:1 CD_2Cl_2:CD_3OD) δ 8.92-8.91 (m, 1H), 8.44-8.42 (m, 1H), 8.37-8.33 (m, 1H), 8.25-8.23 (m, 1H), 8.18-8.16 (m, 1H), 8.02-8.00 (m, 2H), 7.93-7.90 (m, 2H), 7.84-7.81 (m, 1H), 7.80-7.77 (m, 2H), 7.73-7.65 (m, 2H), 4.20-4.12 (m, 8H), 3.46 (s, 3H), 3.37-3.34 (m, 2H), 3.20 (s, 3H), 2.79-2.70 (m, 2H), 2.38-2.30 (m, 4H), 1.21-1.15 (m, 24H) ppm.

^{13}C NMR (125 MHz, 9:1 CD_2Cl_2:CD_3OD) δ 164.8, 164.7, 164.3. 163.1, 163.0, 156.7, 151.9, 150.7, 146.7, 145.8, 144.6, 138.2, 136.5, 134.4, 130.4, 129.9, 129.2, 127.9, 127.6, 124.0, 123.5, 118.3, 114.0, 98.7, 98.5, 92.3, 91.8, 79.2, 76.1, 75.8, 75.4, 40.9, 33.0, 32.4, 29.8, 28.8, 28.7. 28.2, 19.3, 12.4 ppm.

Synthesis of dimethyl 2-(o-tolylamino)maleate

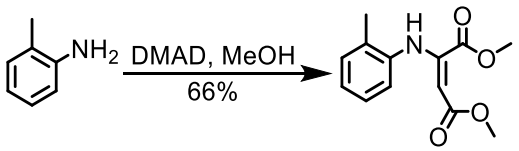

4.048 **4.060**

To a solution of o-toluidine **4.048** (5.0 g, 46.66 mmol) in 100 mL of methanol was added DMAD (6.9 mL, 56 mmol) dropwise at 0 °C. The mixture was stirred at room temperature for overnight. Solvent was removed on a rotary evaporator, and the crude material was purified by flash chromatography over silica column (petroleum ether: EtOAc=9:1) to yield product as a yellowish oil (7.6 g, 66%).

Formula: $C_{13}H_{15}NO_4$ **Molecular Weight:** 249.27 g/mol

^{1}H NMR (300 MHz, Chloroform-*d*) δ 9.55 (s, 1H), 7.23 – 7.16 (m, 1H), 7.06 (ddd, *J* = 12.7, 7.4, 1.7 Hz, 2H), 6.81 – 6.67 (m, 1H), 5.39 (s, 1H), 3.75 (s, 3H), 3.66 (s, 3H), 2.35 (s, 3H) ppm.

^{13}C NMR (75 MHz, Chloroform-*d*) δ 170.35, 164.97, 149.00, 139.08, 130.87, 130.34, 126.58, 124.88, 121.30, 92.89, 52.82, 51.32, 17.99 ppm.

The characteristic data corresponded with reported literature values.[15]

[15] Thorwirth R., Stolle, A. *Synlett*, **2011**, 2011(15), 2200-2202.

Synthesis of methyl 8-methyl-4-oxo-1,4-dihydroquinoline-2-carboxylate (4.049)

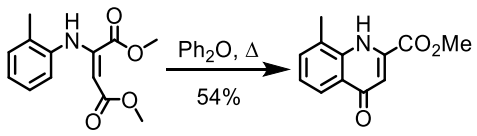

4.060 **4.049**

The oily **4.060** (2.6 g, 10.43 mmol) was added to the boiling diphenyl ether (about 260 °C). After refluxing for 7 minutes, move away the heating jacket and cool down to 50°C at room temperature. And then pour the liquid mixture into petroleum ether (100 mL) in a beaker. There will appear precipitant (our product) and then filter it with a big Buchner funnel. Product was obtained as gray solid after drying under reduced pressure (1.23 g, 54%).

Formula: $C_{12}H_{11}NO_3$ **Molecular Weight:** 217.22 g/mol

^{1}H NMR (300 MHz, Chloroform-*d*) δ 8.87 (s, 1H), 8.22 (ddt, *J* = 8.2, 1.5, 0.7 Hz, 1H), 7.51 (ddq, *J* = 7.2, 1.8, 0.9 Hz, 1H), 7.33 – 7.26 (m, 1H), 6.98 (d, *J* = 1.8 Hz, 1H), 4.05 (s, 3H), 2.56 (s, 3H) ppm.

^{13}C NMR (75 MHz, Chloroform-*d*) δ 179.9, 163.6, 137.8, 135.6, 133.8, 126.4, 125.3, 124.3, 124.1, 111.6, 53.9, 16.6 ppm.

The characteristic data corresponded with reported literature values.[16]

[16] Yan T., Li F., Tian J., Wang L., Luo Q., Hou C., Liu J., *ACS Appl. Mater. Inter.*, **2019**, 11(34), 30566-30574.

Synthesis of methyl 4-isobutoxy-8-methylquinoline-2-carboxylate (4.050)

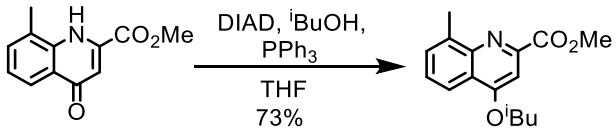

4.049 **4.050**

To a solution of **4.049** (1.23 g, 5.66 mmol), PPh_3 (11.2 g, 6.80 mmol), isobutanol (4.16 mL, 6.80 mmol) in 30 mL anhydrous THF were added DIAD dropwise at 0 °C. The reaction mixture was stirred at 0 °C for 30 min and then warmed up to room temperature and stirred overnight. The volatiles were removed *in vacuo*. The crude product was purified by flash chromatography over silica column (petroleum ether: EtOAc = 9:1) to yield the product as a white solid (1.13 g, 73%)

Formula: $C_{16}H_{19}NO_3$ **Molecular Weight:** 273.33 g/mol

^{1}H NMR (300 MHz, Chloroform-*d*) δ 8.12 (ddd, *J* = 8.3, 1.6, 0.8 Hz, 1H), 7.60 (ddd, *J* = 7.0, 1.6, 0.9 Hz, 1H), 7.54 (s, 1H), 7.48 (dd, *J* = 8.3, 7.0 Hz, 1H), 4.05 (s, 3H), 4.04 (d, *J*=6.5 Hz 1H), 2.87 (s, 3H), 2.29 (dp, *J* = 13.3, 6.7 Hz, 1H), 1.14 (d, *J* = 6.7 Hz, 6H) ppm.

^{13}C NMR (75 MHz, Chloroform-*d*) δ 166.7, 162.9, 147.9, 147.7, 138.2, 130.6, 127.2, 122.4, 119.6, 100.6, 75.0, 53.1, 28.3, 19.4, 18.2 ppm.

HRMS(ESI): m/z calculated for $C_{16}H_{20}NO_3$ $[M+H]^+$: 274.14377. found: 274.14376.

The characteristic data corresponded with reported literature values.[15]

Synthesis of methyl 8-(bromomethyl)-4-isobutoxyquinoline-2-carboxylate (4.047)

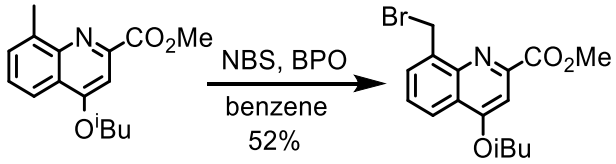

4.050 **4.047**

In a 10 mL round bottomed flask, **4.050** (50 mg, 0.138 mmol), NBS (35.8 mg, 0.2013 mmol), and BPO (22.16 mg, 0.0915 mmol) were stirred in benzene (10 mL). The mixture was heated to 75 °C and stirred overnight. Solvent was removed by rotary evaporation, and the yellow residue was recrystallized from MeOH to yield the product as yellow crystals (25 mg, 52%).

Formula: $C_{16}H_{18}BrNO_3$ **Molecular Weight:** 352.23 g/mol

^{1}H NMR (300 MHz, Chloroform-*d*) δ 8.24 (dd, *J* = 8.4, 1.5 Hz, 1H), 7.91 (dd, *J* = 7.1, 1.5 Hz, 1H), 7.61 – 7.52 (m, 2H), 5.31 (s, 2H), 4.05 (d, *J* = 7.5 Hz, 5H), 2.38 – 2.16 (m, 1H), 1.14 (d, *J* = 6.7 Hz, 6H) ppm.

^{13}C NMR (75 MHz, Chloroform-*d*) δ 166.4, 162.9, 148.7, 146.0, 136.9, 131.7, 127.2, 122.6, 122.5, 101.1, 75.2, 53.1, 29.4, 28.2, 19.2 ppm.

HRMS(ESI): m/z calculated for $C_{16}H_{19}{}^{79}BrNO_3$ $[M+H]^+$: 352.05428. found: 352.05417.

The characteristic data corresponded with reported literature values.[15]

Synthesis of 8-((1H-imidazol-1-yl) methyl)-4-isobutoxyquinoline-2-carboxylic acid sodium (4.051)

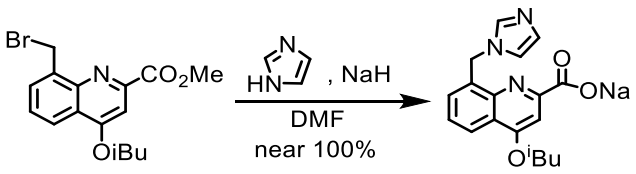

4.047 **4.051**

The **4.047** (1.0 g, 2.86 mmol) and imidazole (0.19 g, 2.86 mmol) were dissolved in DMF (10ml). The mixture was stirred at room temperature overnight. The solvent was removed under vacuum to afford the product (0.99 g, near 100%).

Formula: $C_{18}H_{18}N_3O_3^-Na^+$ **Molecular Weight:** 347.35 g/mol

^{1}H NMR (300 MHz, DMSO-*d*$_6$) δ 8.10 – 8.03 (m, 1H), 8.01 (s, 1H), 7.46 (dd, J = 9.7, 6.7 Hz, 4H), 6.81 (s, 1H), 5.73 (s, 2H), 4.01 (d, J = 6.4 Hz, 2H), 2.26 – 2.08 (m, 1H), 1.07 (d, J = 6.7 Hz, 6H) ppm.

^{13}C NMR (75 MHz, DMSO-*d*$_6$) δ 169.3, 161.1, 159.2, 145.4, 138.3, 136.1, 128.0, 125.3, 121.2, 120.6, 101.4, 79.3, 74.1, 46.4, 27.7, 19.0 ppm.

HRMS(ESI): m/z calculated for $C_{18}H_{20}N_3O_3$ $[M\text{-}Na^+\text{+}2H]^+$: 326.14992. found: 326.14977.

Synthesis of Compound 4.054

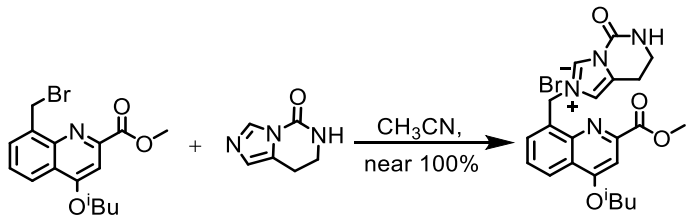

4.047 **3.022** **4.054**

To a suspension **3.022** (5 g, 36.5 mmol) in acetonitrile was added 1 equivalent of **4.047**(12.77 g, 36.5 mmol). The reaction mixture was heated at reflux for 24 h, at which point TLC showed the absence of starting material. The solution was cooled, evaporated to dryness under vacuum to afford the product as a yellow solid (17.8 g, near 100%).

Formula: $C_{22}H_{25}N_4O_4^+Br^-$ **Molecular Weight:** 489.37 g/mol

^{1}H NMR (300 MHz, DMSO-d_6) δ 9.98 (d, *J* = 1.6 Hz, 1H), 9.03 (s, 1H), 8.30 (dd, *J* = 8.5, 1.4 Hz, 1H), 8.06 (dd, *J* = 7.1, 1.4 Hz, 1H), 7.85 – 7.67 (m, 2H), 7.63 (s, 1H), 6.01 (s, 2H), 4.17 (d, *J* = 6.4 Hz, 2H), 4.04 (s, 3H), 3.42 (td, *J* = 6.5, 2.7 Hz, 2H), 2.95 (t, *J* = 6.4 Hz, 2H), 2.29 – 2.12 (m, 1H), 1.09 (d, *J* = 6.7 Hz, 6H) ppm.

^{13}C NMR (75 MHz, DMSO-d_6) δ 165.3, 162.7, 148.4, 145.6, 144.9, 135.9, 132.2, 131.9, 130.5, 127.7, 123.1, 121.7, 118.3, 101.4, 74.9, 53.0, 49.7, 38.11, 27.6, 18.9, 18.3 ppm.

HRMS(ESI): m/z calculated for $C_{22}H_{25}N_4O_4$ [M-Br$^-$]$^+$: 409.18703. found: 409.18689.

Synthesis of methyl 8-((4-(2-((tert-butoxycarbonyl)amino)ethyl)-1H-imidazol-1-yl)methyl)-4-isobutoxyquinoline-2-carboxylate (4.055)

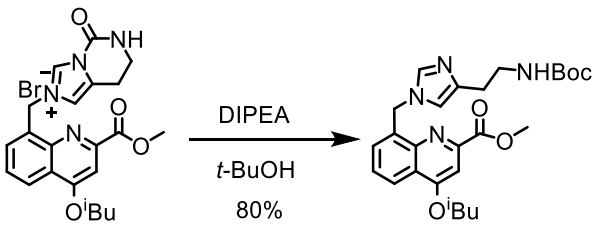

4.054 **4.055**

To a suspension **4.054** (1.78 g, 3.65 mmol) in *t*-BuOH (20 mL) was added DIPEA (1.28 mL, 7.3 mmol). The mixture was heated under reflux for 6 days. The volatile components were removed under vacuum and the residue was dissolved in DCM. The DCM solution was washed with water and dried over Na_2SO_4. Removing the solvent, the product was obtained as an off-white solide (1.41 g, 80%).

Formula: $C_{26}H_{34}N_4O_5$ **Molecular Weight:** 482.58 g/mol

^{1}H NMR (300 MHz, Chloroform-*d*) δ 8.24 (dd, *J* = 8.3, 1.6 Hz, 1H), 7.78 (s, 1H), 7.56 (s, 1H), 7.53 (dd, *J* = 8.3, 7.1 Hz, 1H), 7.45 (d, *J* = 7.0 Hz, 1H), 6.88 (s, 1H), 5.74 (s, 2H), 5.12 (s, 1H), 4.08 (s, 3H), 4.04 (d, *J* = 6.5 Hz, 2H), 3.39 (q, *J* = 6.2 Hz, 2H), 2.70 (t, *J* = 6.5 Hz, 2H), 2.28 (dt, *J* = 13.2, 6.6 Hz, 1H), 1.41 (s, 9H), 1.13 (d, *J* = 6.7 Hz, 6H) ppm.

^{13}C NMR (75 MHz, Chloroform-*d*) δ 166.3, 163.0, 156.1, 148.5, 146.1, 140.0, 137.99, 135.9, 129.3, 127.2, 122.5, 116.7, 101.2, 78.9, 75.2, 53.2, 47.4, 40.4, 28.5, 28.2, 19.3 ppm.

HRMS(ESI): m/z calculated for $C_{26}H_{35}N_4O_5$ $[M+H]^+$: 483.26020. found: 483.26018.

Synthesis of 8-((4-(2-((tert-butoxycarbonyl)amino)ethyl)-1H-imidazol-1-yl)methyl)-4-isobutoxyquinoline-2-carboxylic acid (4.056)

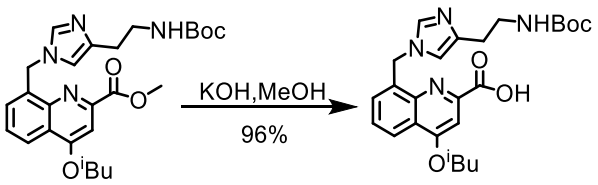

4.055 **4.056**

The **4.055** (1.4 g, 2.9 mmol) was dissolved in MeOH, and KOH (0.2 g, 3.48 mmol) was added. The reaction mixture was stirred overnight at room temperature and then solvent was removed on the rotary evaporator. The residue was dissolved in H_2O, acidified using AcOH to pH=3~4. Then the solution was extracted with EtOAc. The organic layer was then dried over Na_2SO_4, and the solvent was evaporated under reduced pressure to afford the product as a white solide (1.35 g, 90%), which is directly used for next step without more purification.

Formula: $C_{25}H_{32}N_4O_5$ **Molecular Weight:** 468.55 g/mol

^{1}H NMR (300 MHz, Chloroform-*d*) δ 9.98 (s, 1H), 8.27 (dd, *J* = 8.3, 2.6 Hz, 1H), 7.75 (d, *J* = 6.9 Hz, 1H), 7.68 (s, 1H), 7.56 – 7.41 (m, 1H), 6.88 (s, 1H), 5.92 (s, 1H), 5.76 (s, 2H), 4.08 – 3.95 (m, 2H), 3.66 – 3.40 (m, 2H), 3.02 (t, *J* = 6.8 Hz, 2H), 2.38 – 2.11 (m, 1H), 1.32 (s, 9H), 1.08 (dd, *J* = 6.7, 2.0 Hz, 6H) ppm.

^{13}C NMR (75 MHz, Chloroform-*d*) δ 170.4, 162.9, 156.5, 154.2, 146.4, 138.8, 133.9, 132.6, 130.2, 125.8, 124.1, 122.4, 117.3, 101.6, 78.8, 75.1, 50.4, 39.8, 28.4, 28.2, 19.3 ppm.

Synthesis of 8-((1H-imidazol-1-yl)methyl)-N-(8-amino-4,6-diisobutoxy-10-methylpyrido [3,2-g]quinolin-2-yl)-4-isobutoxyquinoline-2-carboxamide (4.057)

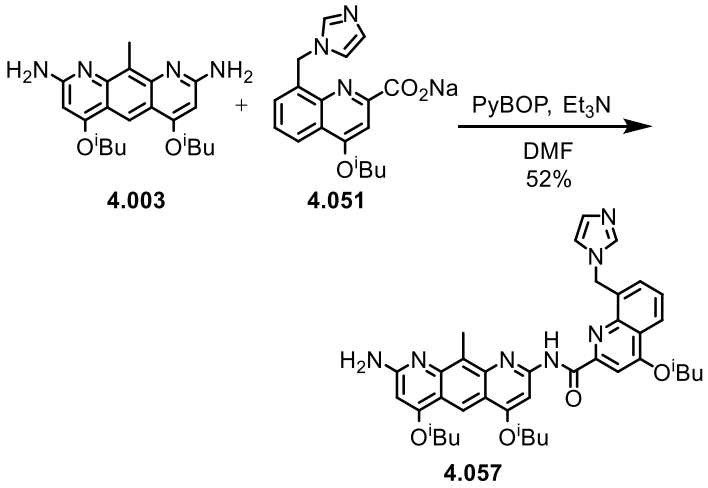

4.003 **4.051** **4.057**

In a 50 mL round bottom flash, under a argon atmosphere, monomer **4.003** (2.78 g, 7.57 mmol), **4.051** (2.46 g, 7.57 mmol), and PyBOP (5.12 g, 9.84 mmol) were dissolved in 20 mL of DMF. Et_3N (4 mL, 28.8 mmol) was added and the reaction was stirred at 45 °C overnight. Water was added to the mixture solution, the solid was filtered and dried at vacuum. The crude material was purified by flash chromatography over silica column (DCM: MeOH = 9:1, Et_3N: 0.5%) to yield the product as a light-yellow solid (2.66 g, 52%).

Formula: $C_{39}H_{45}N_7O_4$ **Molecular Weight:** 675.83

^{1}H NMR (300 MHz, Chloroform-*d*) δ 10.82 (s, 1H), 8.81 (s, 1H), 8.31 (dd, *J* = 8.3, 1.5 Hz, 1H), 8.05 (s, 1H), 7.82 (s, 1H), 7.78 (s, 1H), 7.62 – 7.55 (m, 1H), 7.51 (d, *J* = 7.0 Hz, 1H), 7.32 (d, *J* = 1.4 Hz, 1H), 7.12 (d, *J* = 1.2 Hz, 1H), 6.08 (s, 2H), 5.95 (s, 2H), 5.65 (s, 1H), 4.13 (dd, *J* = 8.8, 6.5 Hz, 4H), 3.95 (d, *J* = 6.3 Hz, 2H), 3.13 (s, 3H), 2.39 – 2.26 (m, 3H), 1.22 – 1.13 (m, 18H) ppm.

^{13}C NMR (75 MHz, Chloroform-*d*) δ 164.3, 163.9, 163.5, 163.0, 158.3, 156.4, 155.2, 154.5, 151.7, 150.5, 146.1, 145.1, 137.9, 134.8, 129.9, 129.7, 127.0, 122.9, 122.8, 120.2, 116.3, 113.6, 98.9, 91.6, 89.5, 75.5, 74.8, 74.6, 47.8, 28.2, 28.4, 28.2, 19.3, 12.3 ppm.

HRMS(ESI): m/z calculated for $C_{39}H_{46}N_7O_4$ $[M+H]^+$: 676.36113. found: 676.36007.

Synthesis of tert-butyl (2-(1-((2-((8-(8-((1H-imidazol-1-yl)methyl)-4-isobutoxyquinoline-2-carboxamido)-4,6-diisobutoxy-10-methylpyrido[3,2-g]quinolin-2 yl) carbamoyl) -4-isobutoxyquinolin-8-yl)methyl)-1H-imidazol-4-yl)ethyl)carbamate (4.058)

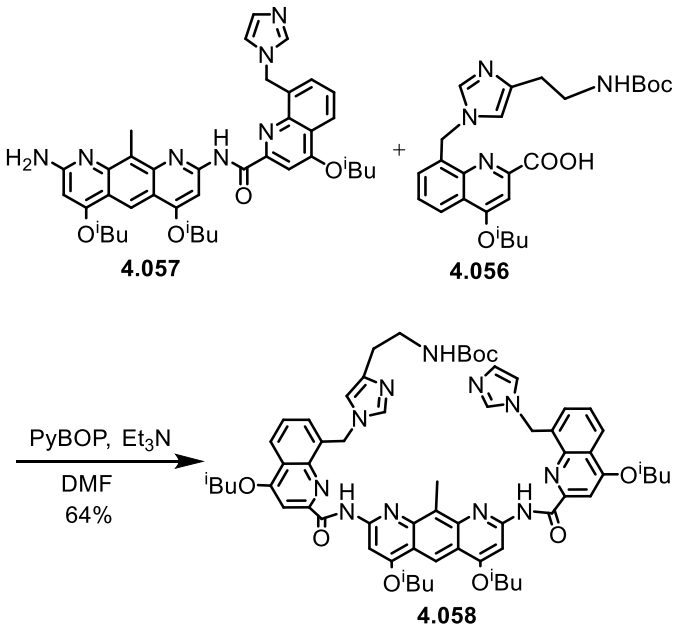

In a 20 mL round bottom flash, under a argon atmosphere, **4.057** (0.564 g, 0.835 mmol), **4.056** (0.43 g, 0.918 mmol), and PyBOP (1.3 g, 2.5 mmol) were dissolved in 15 mL of DMF. Et_3N (0.44 mL, 3.17 mmol) was added and the reaction was stirred at 45 °C overnight. Water was added to the mixture solution, the solid was filtered and dried at vacuum. The crude material was purified by flash chromatography over silica column (DCM: MeOH = 9:1, Et_3N: 0.5%) to yield the product as a light-yellow solid (0.606 g, 64%).

Formula: $C_{64}H_{75}N_{11}O_8$ **Molecular Weight:** 1126.37 g/mol

^{1}H NMR (300 MHz, Chloroform-*d*) δ 10.90 (d, *J* = 5.8 Hz, 2H), 8.97 (s, 1H),

8.30 (d, *J* = 8.2 Hz, 2H), 8.09 (s, 2H), 7.87 – 7.72 (m, 4H), 7.57 (d, *J* = 8.0 Hz, 2H), 7.54 – 7.43 (m, 2H), 7.30 (d, *J* = 1.3 Hz, 1H), 7.11 (s, 1H), 7.00 (s, 1H), 5.94 (s, 2H), 5.88 (s, 2H), 5.21 (s, 1H), 4.17 (d, *J* = 6.5 Hz, 4H), 4.11 (d, *J* = 6.5 Hz, 4H), 3.35 (t, *J* = 6.5 Hz, 2H), 3.31 (s, 3H), 2.68 (t, *J* = 6.5 Hz, 2H), 2.49 – 2.21 (m, 4H), 1.36 (s, 9H), 1.22 (d, *J* = 6.7 Hz, 12H), 1.15 (d, *J* = 6.7 Hz, 12H) ppm.

^{13}C NMR (75 MHz, Chloroform-*d*) δ 163.9, 163.7, 162.8, 156.1, 151.5, 150.1, 145.3, 144.9, 137.9, 137.4, 134.7, 130.2, 129.8, 129.6, 127.0, 122.6, 120.1, 117.8, 116.7, 113.4, 98.6, 91.9, 78.8, 75.4, 74.7, 47.6, 40.4, 28.5, 28.2, 19.4, 19.3, 12.7 ppm.

HRMS(ESI): m/z calculated for $C_{64}H_{76}N_{11}O_8$ $[M+H]^+$: 1126.58728. found: 1126.58740.

Synthesis of 8-((1H-imidazol-1-yl)methyl)-N-(8-(8-((4-(2-aminoethyl)-1H-imidazol-1-yl) methyl)-4-isobutoxyquinoline-2-carboxamido)-4,6-diisobutoxy-10-methylpyrido[3,2-g]quinolin-2-yl)-4-isobutoxyquinoline-2-carboxamide (4.005)

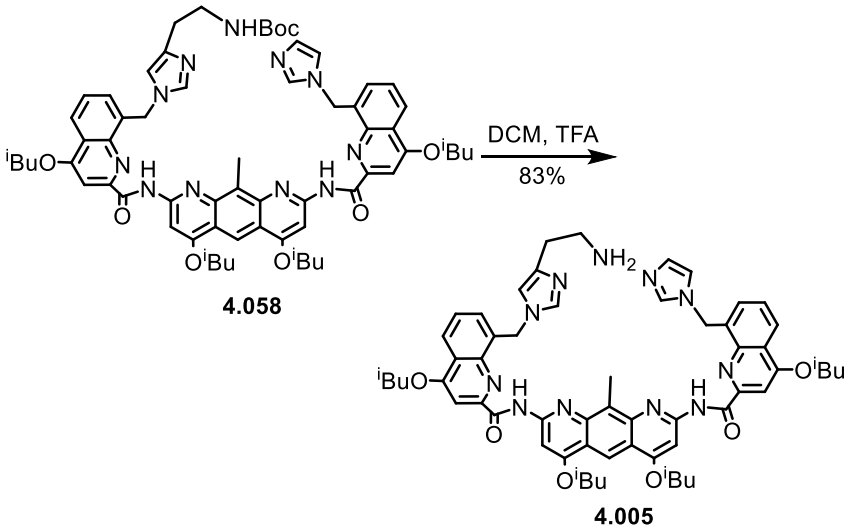

4.058 **4.005**

In a 50 mL round bottom flask, **4.058** (0.5 g, 0.44 mmol) was dissolved in 25 mL of 1:1 CH_2Cl_2: TFA. The reaction was stirred overnight at room temperature and then solvent was removed on the rotary evaporator. The crude yellow oil was partitioned between $CHCl_3$ and saturated $NaHCO_3$ solution. The organic layer was washed with water and brine and then dried over Na_2SO_4. After removal of solvent, the product was dried overnight on the vacuum line to give the product as a yellow solid (0.38 g, 83%).

Formula: $C_{59}H_{67}N_{11}O_6$ **Molecular Weight:** 1026.26 g/mol

^{1}H NMR (300 MHz, Chloroform-*d*) δ 10.80 (s, 2H), 8.87 (s, 1H), 8.21 (t, J = 9.1 Hz, 2H), 8.00 (s, 1H), 7.74 (t, J = 13.5 Hz, 4H), 7.48 (dt, J = 16.9, 9.5 Hz, 4H), 7.24 (s, 1H), 7.03 (d, J = 6.3 Hz, 2H), 5.87 (dd, J = 19.9, 14.3 Hz, 4H),

4.06 (dd, J = 16.3, 7.1 Hz, 8H), 3.29 – 3.14 (m, 5H), 2.62 (d, J = 7.9 Hz, 2H), 2.41 – 2.16 (m, 4H), 1.16 (t, J = 6.5 Hz, 12H), 1.09 (dd, J = 6.6, 2.8 Hz, 12H) ppm.

^{13}C NMR (75 MHz, Chloroform-*d*) δ 164.1, 163.7, 163.2, 162.8, 151.6, 150.1, 145.0, 137.7, 134.5, 130.1, 128.2, 126.9, 122.7, 119.9, 117.7, 113.6, 109.1, 98.6, 91.9, 75.3, 74.7, 47.6, 36.3, 29.7, 28.2, 19.2, 12.6 ppm.

HRMS(ESI): m/z calculated for $C_{59}H_{68}N_{11}O_6$ $[M+H]^+$: 1026.53486. found: 1026.53458.

Synthesis of N,N'-(4,6-diisobutoxy-10-methylpyrido[3,2-g]quinoline-2,8-diyl)bis(8-((1H-imidazol-1-yl)methyl)-4-isobutoxyquinoline-2-carboxamide) (4.059)

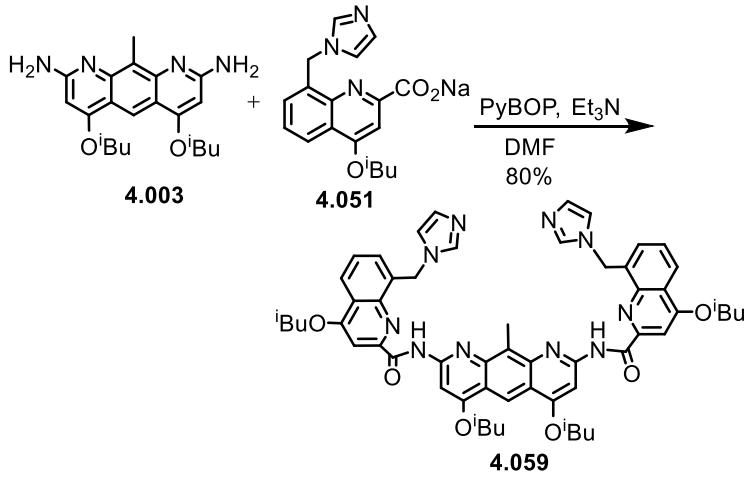

4.003 **4.051** **4.059**

In a 25 mL round bottom flash, under a argon atmosphere, **4.003** (0.1 g, 0.272 mmol), **4.051** (0.221 g, 0.679 mmol), and PyBOP (0.425 g, 0.816 mmol) were dissolved in 20 mL of DMF. Et_3N (0.143 mL, 1.0336 mmol) was added and the reaction was stirred at 45 °C overnight. Water was added to the mixture, the solid was filtered and dried under vacuum, and the product recrystallized from CH_3CN to give the product as a yellow solid (0.21 g, 80%).

Formula: $C_{57}H_{62}N_{10}O_6$ **Molecular Weight:** 983.19 g/mol

^{1}H NMR (300 MHz, Chloroform-d) δ 10.91 (s, 2H), 8.98 (s, 1H), 8.32 (d, J = 8.2 Hz, 2H), 8.10 (s, 2H), 7.85 (d, J = 14.2 Hz, 4H), 7.58 (dt, J = 14.4, 7.1 Hz, 4H), 7.34 (s, 2H), 7.14 (s, 2H), 5.97 (s, 4H), 4.19 (d, J = 6.5 Hz, 4H), 4.13 (d, J = 6.5 Hz, 4H), 3.34 (s, 2H), 2.38 (dp, J = 20.4, 6.7 Hz, 4H), 1.24 (d, J = 6.7 Hz, 12H), 1.18 (d, J = 6.7 Hz, 12H) ppm.

^{13}C NMR (75 MHz, Chloroform-*d*) δ 164.1, 163.8, 162.9, 151.6, 150.2, 145.5,

145.1, 137.8, 134.7, 129.9, 129.5, 127.0, 122.8, 122.7, 120.2, 118.0, 113.5, 98.8, 92.0, 75.5, 74.8, 47.8, 28.5, 28.2, 19.4, 19.3, 12.7 ppm.

HRMS(ESI): m/z calculated for $C_{57}H_{63}N_{10}O_6$ $[M+H]^+$: 983.49320. found: 983.49168.

Synthesis of Cu(II) complexes

Cu(II) complex **1**: To a stirred solution of methanol (2 mL) containing the ligand **L1** (20 mg, 0.0912 mmol) and Et_3N (12.7 µL, 0.0912 mmol), a solution of $CuCl_2•2H_2O$ (15.5 mg, 0.0912 mmol) in methanol (1 mL) was added. The resulting solution was stirred for 3h at room temperature. The color changed to a dark green color. The solvent removal under reduced pressure gave the same color product.

Cu(II) complex **2**, **3**, **4** were formed by the same procedure as above described.

$Cu_2(L1)_2$: To the solution of ligand **L1** (20 mg, 0.0912 mmol) in methanol (2 ml) and $CuCl_2•2H_2O$ (15.5 mg, 0.0912 mmol) in methanol (1 mL) was added at room temperature for overnight and the color changed to a dark green color. Et_2O was diffused to the mixture solution directly to get a green colored crystal suitable for X-ray crystallography analysis.

Oxidation of p-nitrophenyl-β-D-glucopyranoside

The catalytic activity of the Cu(II) complexes **1**-**4** was assessed using the oxidation of p-nitrophenyl-β-D-glucopyranoside by H_2O_2 in carbonate buffer solution (100 mM, pH = 10.5) or H_2O (with 20 mM Et_3N). Reaction conditions: 20 mM model substrate, 0.05 mM complex, 20 mM H_2O_2 were dissolved in carbonate buffer solution or H_2O at room temperature for 24h. Then the mixture was diluted 10 times and the product (4-nitorophenolate) was monitored by using UV-Vis spectroscopy. The concentration of the product was calculated based on the absorbance at 400 nm. Controls were performed using the same conditions in the presence of $CuSO_4•5H_2O$/ $CuCl_2•2H_2O$, or in the absence of complexes or H_2O_2.

3. X-ray crystallography

X-ray iffraction data for **3.012** and **4.005** were recorded on a MAR345 image plate using Mo-Kα radiation generated by a Rigaku UltraX 18S rotating anode (Xenocs Fox3d mirrors). Prior to data collection the crystals were flash frozen to 150 K. Data integration and reduction was performed by CrysAlisPRO,[17] and the implemented absorption correction was applied. The structures were solved by SHELXT[18] and refined against F^2 by SHELXL-2014/7.[19] All non-hydrogen atoms were re-fined anisotropically, hydrogen atoms were added in calculated positions and refined in riding mode, with temperature factors 1.2 times higher than their parent atoms. At the time of writing of this thesis the data for **$Cu_2(L1)_2$** were not finalized. The structures described in the text for this compound should be considered preliminary.

Molecular No.	**3.012 (L4)**	**4.005 (L6)**
CCDC code	UCL1142_ms_xiaoMU3	UCL1139_kr525_ms_xiao
Empirical formula	C10 H13 N5 O	C64 H75 N11 O8
Formula weight	219.25	1126.35
Temperature	297(2) K	100(2) K
Wavelength	0.71073 Å	1.54184 Å

[17] CrysAlisPRO Software System, Vol. Rigaku Corporation : Oxford, UK, **2015**.

[18] G. M. Sheldrick, *Acta Crystallogr., Sect. C: Struct. Chem.,* **2015**, 71, 3-8.

[19] G. M. Sheldrick, *Acta Crystallogr., Sect. A: Found. Adv.*, **2015**, 71, 3-8.

Crystal system	monoclinic	Monoclinic
Space group	P 21	I a
Unit cell dimensions	a = 5.3607(2) Å	a = 17.3028(2) Å
	b = 11.6230(6) Å	b = 21.3983(17) Å
	c = 9.0790(4) Å	c = 17.8756(4) Å
	α = 90°	α = 90°
	β = 93.431(4)°	β = 94.017 (2)°
	γ = 90	γ = 90°
Volume	564.68(5) Å3	6602.2(3) Å3
Z	2	4
Density (calculated)	1.290 Mg/m^3	1.133 Mg/m3
Absorption coefficient	0.090 mm^{-1}	0.614 mm^{-1}
F(000)	232	2400
Crystal size	0.50 x 0.3 x 0.18 mm^3	0.500 x 0.186 x 0.139 mm^3
θ range	3.506 to 25.335°.	4.132 to 66.963°.

Reflections collected	2050	13094
Independent reflections	2050 [$R_{(int)}$ = ?]	8341 [$R_{(int)}$ = 0.0274]
Compl. to θ = 25.242°	0.996	0.977
Absorption correction	Semi-empirical from equivalents	Semi-empirical from equivalents
Max. and min. transm.	1.00000 and 0.69563	1.00000 and 0.83929
Refinement method	Full-matrix least-squares on F2	Full-matrix least-squares on F2
Data / restr. / param.	2050 / 86 / 206	8341 / 686 / 1011
Goodness-of-fit on F2	1.070	1.301
Final R indices [I>2σ(I)]	R_1 = 0.0625, wR_2 = 0.1425	R_1 = 0.1487, wR_2 = 0.3367
R indices (all data)	R_1 = 0.1057, wR_2 = 0.1752	R_1 = 0.1764, wR_2 = 0.3530
ρ min and max	0.284 and -0.232 e.Å^{-3}	1.227 and -0.658 e.Å-3